Orchestration of the self-assembly and molecular motion of helical pseudorotaxanes

Xiang Wang

université de BORDEAUX

THÈSE PRÉSENTÉE

POUR OBTENIR LE GRADE DE

DOCTEUR DE

L'UNIVERSITÉ DE BORDEAUX

ÉCOLE DOCTORALE DES SCIENCES CHIMIQUES

SPÉCIALITÉ : CHIMIE ORGANIQUE

Par Xiang WANG

Orchestration de l'auto-assemblage et des mouvements moléculaires de pseudo-rotaxanes helicoïdaux

Sous la direction de : Dr. Ivan HUC
(co-directeur : Dr. Yann FERRAND)

Soutenue le 28 Juin 2016

Membres du jury :

M. RAPENNE, Gwénaël	Professeur, Université Toulouse III	Président
M. CREDI, Alberto	Professeur, Università di Bologna	Rapporteur
M. COUTROT, Frédéric	Maître de Conférences, Université Montpellier 2	Rapporteur
M. HUC, Ivan	Directeur de recherche, CNRS	Examinateur
M. FERRAND, Yann	Chargé de recherche, CNRS	Examinateur

Orchestration de l'auto-assemblage et des mouvements moléculaires de pseudo-rotaxanes helicoïdaux

L'orchestration des mouvements directionnels d'architectures supramoléculaires s'avère cruciale pour la préparation de machines moléculaires artificielles. Les oligomères d'amides aromatiques (i.e. foldamères) peuvent adopter des conformations stables capables de se complexer à des tiges moléculaires pour former des (pseudo)-rotaxanes. Un contrôle fin des cinétiques d'association et de dissociation de l'hélice autour de la tige permet à l'oligomère hélicoïdal de glisser le long de celle-ci sans dissociation. Des études RMN et cristallographiques ont montré que des tiges moléculaires possédant plusieurs sites de reconnaissance pour des hélices permettaient l'élaboration d'architectures supramoléculaires hélicoïdales chirales avec une haute-fidélité. Chaque station possédant une longueur et une chiralité définie peut induire la complexation de foldamères de taille et d'hélicité concordante. Le glissement directionnel d'une double hélice le long d'une tige possédant plusieurs stations a également été investigué. Insérer un espaceur encombrant (i.e. plus large que la cavité de l'hélice) sur le chemin du foldamère le force à se déplier et se replier pour atteindre le site le plus favorable thermodynamiquement. Un oligomère asymétrique montrant de hautes affinités et de fortes sélectivités pour des tiges asymétriques a été préparé. L'enfilement de cet oligomère sur des tiges asymétriques a été étudié. Des données cinétiques (RMN) indiquent que l'enfilement de celui-ci s'effectue de façon polarisée en fonction de la nature de la tige.

Mots clés: foldamère, hélice, pseudo-rotaxane, auto-assemblage, mouvement directionnel, chimie hôte-invité, reconnaissance moléculaire, machine moléculaire, cristallographie, RMN

Orchestration of the self-assembly and molecular motion of helical pseudorotaxanes

The directional motion orchestration of supramolecular architectures is crucial for the construction of artificial molecular machines. Aromatic amide oligomers (i.e. foldamers) can adopt stable helical conformations able to wind around dumbbell-like guests to form (pseudo)-rotaxanes. A fine control of the association-dissociation kinetics allows the oligomers to slide along the rods without dissociation. In this thesis, based on the segregation of the kinetics of association-dissociation and sliding, helical oligomer motions were orchestrated to form complex self-assemblies and to perform directional motion. NMR and crystallographic studies showed that multistation rod guests can template the formation of well-defined multi-helical supramolecular polymers with high fidelity. Each station possessing a defined length and chirality can induce the complexation of oligomers presenting matching length and chirality. Directional sliding of a double helical oligomer along linear multistation rod guests was investigated. Placing a bulky spacer on the rod prohibits the sliding process, forcing the oligomer to dissociate and reassociate onto the thermodynamically favored station. An asymmetrical oligomer was prepared showing highly selective binding toward asymmetrical rod guests. The threading of this oligomer onto linear asymmetrical guests was investigated. Kinetic data indicated that the threading orientation of this asymmetrical oligomer was polarized by its passage along guest molecules.

Keywords: foldamer, helix, pseudorotaxane, self-assembly, directional motion, host-guest chemistry, molecular recognition, molecular machine, crystallography, NMR

UMR 5248 Chimie et Biologie des Membranes et Nanoobjets (CBMN)

Institut Européen de Chimie et Biologie (IECB)

2 rue Robert Escarpit 33607 PESSAC CEDEX

ACKNOWLEDGEMENT

First and foremost, I thank my supervisor Dr. Ivan Huc for giving me the chance to study in France. I would like to thank him for his support, guidance and insightful discussions throughout the past four years. I am also very grateful to my co-supervisor Dr. Yann Ferrand for many insightful discussions, for his patience and tolerance of my mistakes, for his invaluable encouragement. It would not be possible to finish this thesis without his efficiency. I also thank Dr. Victor Maurizot, Dr. Lucile Fischer (these delicious snacks!) and Eric Merlet for their friendliness and help.

I thank Dr. Brice Kauffmann and Dr. Barbara Wicher for their expertise in crystallography. Many thanks to Axelle Grélard and Estelle Morvan for their assistance with NMR measurements. I also thank Dr. Frédéric Rosu and Loïc Klinger for the mass measurements. It would not be possible to conduct my research without their help.

I thank Quan and Guillaume for their guidance on foldamer synthesis at the beginning of my PhD study. Thanks to Bo for so many useful tips, without his help living in France would be much harder at the beginning. There cannot be more gratitude to Xuesong for the sharing of happiness and complaints in the past four years. He is always there for help. His sincerity, friendliness, advises and wonderful cuisine will always be remembered.

I thank all of the Huc Group members, past and present, for the fun times we spent together: Jie, Simon, Michael, Christos, Krzysztof, Nan, Xiaobo, Markendeya, Panchami, Pradeep, Daniel, Soumen, Maëlle, Michal, Antoine M., Antoine J., Subrata, Arthur, Sunbum, Jinhua, Albano, Joan, Valentina, Pedro and many others.

Life in a foreign country would be like hell without so many Chinese friends. Many gratitude to them, for the help and happiness which will all be treasured. More than words can ever express, I thank my parents and brother for their support in everything I do. Their appreciation and encouragement has always been the solidest ground during my study.

List of abbreviations

AcOH : acetic acid

Boc : *tert*-butyloxycarbonyl

CD : circular dichroism

CPK : Corey, Pauling, Koltune space filling

DCM : dichloromethane

DIEA : diisopropylethylamine

DMF : *N*,*N*-dimethylformamide

EDC : N-(3-Dimethylaminopropyl)-N'-ethylcarbodiimide hydrochloride

ESI : electrospray ionization

Fmoc : Fluorenylmethyloxycarbonyl

Ghosez reagent : 1-chloro-*N*,*N*,2-trimethyl propenylamine

HBTU : N,N,N',N'-Tetramethyl-O-(1H-benzotriazol-1-yl)uronium hexafluorophosphate

HOBt : 1-Hydroxybenzotriazole hydrate

HRMS : high resolution mass spectroscopy

MALDI : matrix-assisted laser desorption/ionization

Me : methyl

MeOH : methanol

MMFFs : Merck Molecular Force Field static

NaH : sodium hydride

NaOH : sodium hydroxide

NMR : nuclear magnetic resonance

NOESY : Nuclear Overhauser Effect SpectroscopY

ppm : parts per million

PyBOP : benzotriazol-1-yl-oxytripyrrolidinophosphonium hexafluorophosphate

TFA : trifluoroacetic acid

THF : tetrahydrofuran

TLC : thin layer chromatography

Abbreviations of the aromatic amino acid building blocks

P : 2,6-diaminopyridine and 2,6-pyridinedicarboxylic acid

Q^F : 7-amino-8-fluoro-2-quinolinecarboxylic acid

N : 2-amino-1,8-naphthyridine-7-carboxylic acid

A^F : 1,8-diaza-9-fluoro-2,7-anthracene-dicaboxylic acid

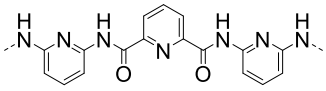

"P_3"

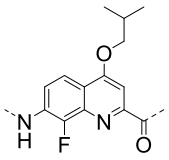

"Q^F"

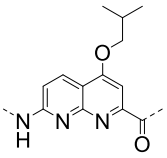

"N"

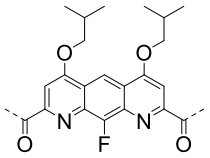

"A^F"

CONTENTS

INTRODUCTION

Oligomer folding is the methodology nature choose to construct biomolecules crucial for cells. Folded proteins and nucleic acids composed of linear sequence of amino acids and nucleotides further assemble into biological machines. Functions in cells, such as DNA translation, photosynthesis, and material transportation, are all performed by such biological machines. Folding and self-assembly allow the creation of numerous biological machines carrying out different functions from a set of only 20 amino acids and 8 nucleotides.

Foldamers, defined as "artificially folded architectures", are investigated to construct artificial systems with properties comparable to biological proteins. Foldamers with various backbones have been shown to adopt helical conformation, to form tertiary and even quaternary structures, and to interact with proteins. Moreover, the research in foldamer chemistry is not limited to only mimic the structure and function of natural peptide. As investigation evolves, unprecedented applications in fields such as molecular recognition, catalysis, and material science have emerged.

The aromatic amide oligomers developed by our group can adopt very stable and well-defined helical conformation disregarding the relative orientation of the acid and the amine group, the size, and the side chain of each monomer. Through two decades of iterative evolution novel properties of these foldamers have been established: i) Multiple helical structures (double, triple and even quadruple helix) were obtained by tuning the curvature; ii) β-sheet like structure was achieved by introducing rigid turns; iii) Molecular capsules were synthesized with high selectivity for different molecules; iv) Water soluble foldamers exhibiting specific interaction with proteins were developed by using proteinaceous side chains; v) Shuttling and screwing motion were realized by foldamers winding around rod like guests.

Among all the molecular machines operated by nature, proteins like ribosome and kinesin have drawn particular interest due to the processive and progressive work performed by them. By encircling around RNA, ribosome translates encoded genetic information into defined order of amino acids. This process is performed with high accuracy and efficiency. Kinesin transports molecules directionally along polarized filament without dissociation from the track. One remarkable property of biological machine is that they operate by fast local conformational change with microscopic reversibility. This endows biological molecular machine high efficiency by avoiding the slow disassembly and re-assembly of the whole folded structure. Although artificial molecular machines like their natural counterparts are still unseen, artificial molecular machines performing work have been envisaged and sought for more than half a

century. Controlling motion at molecular scale will not only enhance our understanding and control of biological process, but also surely have great impact on the way molecules are produced and manipulated.

Aromatic oligoamide foldamers with a cylindrical cavity have been shown to wind around dumbbell like dicarbamate guests derived from α,ω-diamine to form stable pseudorotaxane. The binding affinities vary according to the length of the α,ω-diamine. Since the unfolding-refolding is slow, foldamer can shuttle/screw fast along the guest without dissociation. In this thesis, the kinetic difference between the unfolding-refolding process and shuttling/screwing process was exploited to construct complex self-assemblies and to force foldamers to move directionally.

Chapter 1 includes two parts. In the first part, a brief introduction of different backbones that can adopt folded conformation is presented. Recent achievements of foldamers in protein mimics, protein interaction, molecular recognition, and material science are highlighted. Following this, in the second part, a non-exhaustive review of research in threading behavior of macrocycles onto polymers, processive molecular machines, and artificial molecular walkers along linear track is presented.

In chapter 2, foldamers with different length were synthesized and characterized. The binding affinities of these foldamers towards a series of dicarbamate rods were measured. The chiral induction efficiency of different stereogenic centers on the rods was also investigated. Relying on error correction via unfolding-refolding mechanism, multistation rod guests templated the formation of well-defined multi-helical supramolecular polymer with high fidelity. Each station, possessing a defined length and chirality, induced the complexation and folding of oligomers presenting specific sequences and chirality.

In chapter 3, it was shown that the structure of a linear rod can dictate the supramolecular pathways of the directional motion of a double helical foldamer. This foldamer could slide along linear guest molecules with varying rates accordingly to the lengthscale of the rod. Placing a bulky spacer in the way of the foldamer forced it to dissociate from the molecular thread, to slowly unfold and refold further than obstacle.

In chapter 4, the host-guest chemistry of an asymmetrical foldamer with two different binding groups at each extremity was investigated. This foldamer exhibited high selectivity binding toward asymmetrical rod guests, forming only one thermodynamically favored isomer. Kinetic studies indicated that the threading of this asymmetrical foldamer was polarized by its passage along linear guest molecules.

Chapter 1

Introduction

1. Introduction

Cellular metabolism is performed by biological machines composed of assemblies of biopolymers, such as proteins and nucleic acids. Through folding and non-covalent interaction, these biopolymers adopt well-defined conformation to allow specific interaction with their substrates to perform for example catalysis or signal transduction. This strategy allows nature to fulfill different functions with a limited range of amino acids and nucleotides.

Inspired by nature's design, artificially folded architectures, termed foldamers, have been extensively studied to understand and mimic the structures and functions of biopolymers. Synthetic molecules with biotic or abiotic backbones have been shown to adopt folded conformation. The folding behavior is facilitated not only by hydrogen bonding but also by other different non-covalent interactions. As mimics of natural peptides, foldamers have been shown to form tertiary and quaternary structures, and to interact with proteins. Unlimited to this, foldamers have shown applications, unprecedented for natural peptide, in fields such as molecular recognition and material science.

One fascinating feature of biological molecular machines is their processivity and progressivity. To fulfill these two requisites, biological machines usually operate along one dimensional track in a confined manner. One typical biological machine with this feature is ribosome. Encircling around RNA, ribosome recognizes the genetic code and adds corresponding amino acid to a peptide sequence. This process is performed stepwise with high accuracy and efficiency. Another example is the transporting of cargo by kinesin. With local conformational change caused by ATP binding and hydrolysis, kinesin can walk directionally along polarized microtube filament with loaded cargo. Over the past two decades, artificial molecular systems that can perform controlled motion on one dimensional track were extensively investigated. Rotaxanes and pseudorotaxanes, in which a macrocycle threads onto an axle molecule, are ideal candidate for the construction of processive and progressive molecular machine. Synthetic molecules walking along a track were also reported.

In this chapter, selected examples highlighting important advancement in foldamer chemistry and unidirectional motion on unidimensional track was reviewed, with the prospect of constructing directional motion molecular systems based on foldamer.

2. Synthetic foldamers

Molecular machines carry out biological processes, such as information translation, energy transfer, and material transportation, hierarchically to drive living system out of equilibrium. These distinct functions of molecular machine can mostly be attributed to the diverse structures of proteins derivate from sequential peptides. A versatile methodology is applied by nature to create miscellaneous proteins. Firstly, ribosome translates genetic information encoded in nucleic acids into corresponding sequence of peptides. Secondly, a sequence of peptides folds into helical or sheet-like secondary structures. Then, together with the interplay of non-covalent interaction, these secondary structures of peptides further assemble into tertiary and quaternary functional entities. Inspired by this, a new research field, namely foldamer, emerges to employ artificial molecules for the construction of folded structure with potential functions comparable to nature. In the following sections, a non-exhaustive review of structural basis and striking applications of foldamers is carried out.

2.1 Folded structures from diverse backbones

By definition, foldamers are "artificial folded molecular architectures".[1] Pioneer works are the investigation of peptide nucleic acids (PNAs) and peptoids in mimicking the structure and biological functionality of nucleic acid and peptide. In 1996, Seebach and Gellman et al. separately reported the higher stability of helix formed by β-peptides than those of α-peptides.[2,3] Since then, extensive research of β-peptides, incorporating cyclic or non-cyclic side chains, was carried out. Helical conformation adopted by aliphatic γ peptides, and δ peptides were reported. Using urea,[4] hydrazide[5] or hydroxyamide[6] bond instead of the amide bond can also give folded structures.

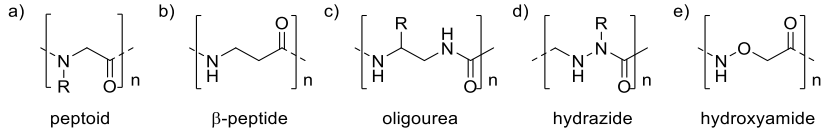

Figure 1. Examples of aliphatic foldamer backbones

1. S. Hecht, I. Huc. Foldamers: structure, properties and applications. Wiley-VCH, Weinheim, **2007**.
2. D. H. Appella, L. A. Christianson, I. L. Karle, D. R. Powell, S. H. Gellman, β-Peptide foldamers: robust helix formation in a new family of β-amino acid oligomers. *J. Am. Chem. Soc.* **1996**, *118*, 13071–13072.
3. D. Seebach, M. Overhand, F. N. M. Kühnle, B. Martinoni, L. Oberer, U. Hommel, H. Widmer, β-Peptides: Synthesis by Arndt-Eistert homologation with concomitant peptide coupling. Structure determination by NMR and CD spectroscopy and by X-ray crystallography. Helical secondary structure of a β-hexapeptide in solution and its stability towards pepsin." *Helv. Chim. Acta*, **1996**, *79*, 913–941.
4. V. Semetey, D. Rognan, C. Hemmerlin, R. Graff, J.-P. Briand, M. Marraud, G. Guichard. Stable helical secondary structure in short-chain N, N'-linked oligoureas bearing proteinogenic side chains. *Angew. Chem. Int. Ed.* **2002**, *114*, 1973-1975.
5. A. Salaun, M. Potel, T. Roisnel, P. Gall, P. Le Grel. Crystal structures of aza-β_3-peptides, a new class of foldamers relying on a framework of hydrazinoturns. *J. Org. Chem.* **2005***, 70,* 6499–6502.
6. X. Li, D. Yang. Peptides of aminoxy acids as foldamers. *Chem. Commun.* **2006**, *32*, 3367–3379.

Beside foldamers based on aliphatic backbones, aromatic segments with no structure reminiscence to natural peptide can also adopt folded structure. Following Hamilton et al's first report of foldamer with aromatic backbone in 1996,[7] folded structure has been shown to form based on solvophobic interaction between oligo-phenylene-ethynylenes,[8,9] electrostatic repulsion between aza-heterocycles,[10] donor-acceptor interaction,[11] and aromatic oligoamide.[12] (Fig. 2a-d) The later one is stabilized by hydrogen bonding, local conformational preferences at aryl–amide linkages and intramolecular π−π interactions between aromatic monomers. For example, an oligoamide octamer **4** based on quinoline unit can adopt very stable folded conformation.[13] Investigation on aromatic oligoamides has undergone a rapid growth in the last decade due to their high stability and predictability of the folded conformation.

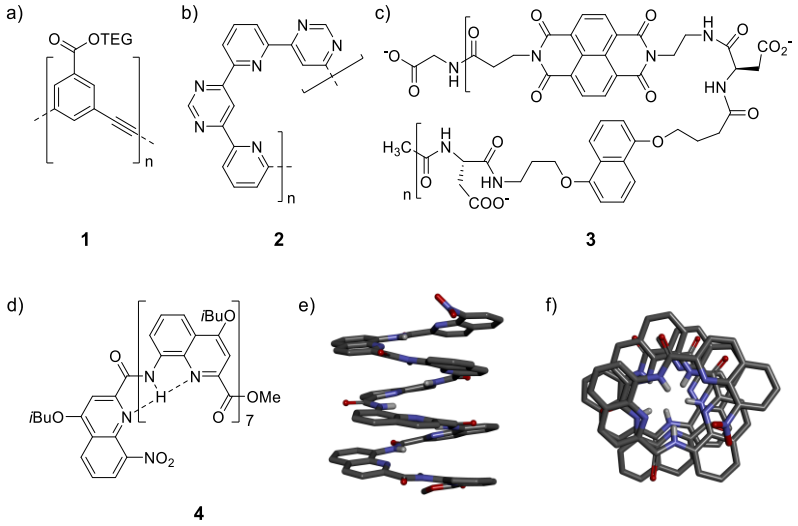

Figure 2. Examples of foldamers with aromatic backbones. a) Oligo-phenylene-ethynylenes. b) Aza-heterocycle oligomer. c) Donor-acceptor oligomer. d) Aromatic oligoamide. e) Side view and f) top view of the solid state crystal structure of **4**. Side chains (O*i*Bu groups) and included solvent molecules have been removed for clarity.

Recently, the Huc group demonstrated that, unlimited to the commonly seen helical structures, β-sheet structures were also accessible for aromatic oligoamides (Fig. 3).[14] NMR studies suggested that rigid turns force the five aromatic segments to fold face to face in solution,

7. Y. Hamuro, S.J. Geib, A. D. Hamilton. Oligoanthranilamides. Non-peptide subunits that show formation of specific secondary structure. *J. Am. Chem. Soc.* **1996**, *118*, 7529–7541.
8. D. J. Williams, H. M. Colquhoun, C.A. O'Mahoney. The structure of poly(m-phenylene): a prediction from single-crystal X-ray studies of m-deciphenyl and m-undeciphenyl. *J. Chem. Soc., Chem. Commun.* **1994**, *14*, 1643-1644
9. J. C. Nelson, J. G. Saven, J. S. Moore, P. G. Wolynes. Solvophobically driven folding of nonbiological oligomers. *Science*, **1997**, *277*, 1793–1796.
10. D. M. Bassani, J.-M. Lehn, G. Baum, D. Fenske. Designed self-generation of an extended helical structure from an achiral polyheterocylic strand. *Angew. Chem. Int. Ed.* **1997**, 36, 1845-1847.
11. R. S. Lockey, B. L. Iverson. Synthetic molecules that fold into a pleated secondary structure in solution. *Nature*, **1994**, *375*, 303-305.
12. D.-W.Zhang, X, Zhao, J,-L. Hou, Z.-T. Li. Aromatic amide foldamers: structures, properties, and functions. *Chem. Rev.* **2012**, *112*, 5271–5316.
13. H. Jiang, J.-M. Léger, I. Huc. Aromatic δ-peptides. *J. Am. Chem. Soc.* **2003**, *125*, 3448-3449.
14. L. Sebaoun, V. Maurizot, T. Granier, B. Kauffmann, I. Huc. Aromatic oligoamide β-sheet foldamers. *J. Am. Chem. Soc.* **2014**, *136*, 2168-2174.

with no apparent aggregation. The sheet structure was unambiguously proved by X-ray crystallography. This sheet structure was mainly stabilized by π-π interactions between the aromatic segments instead of hydrogen bonding.

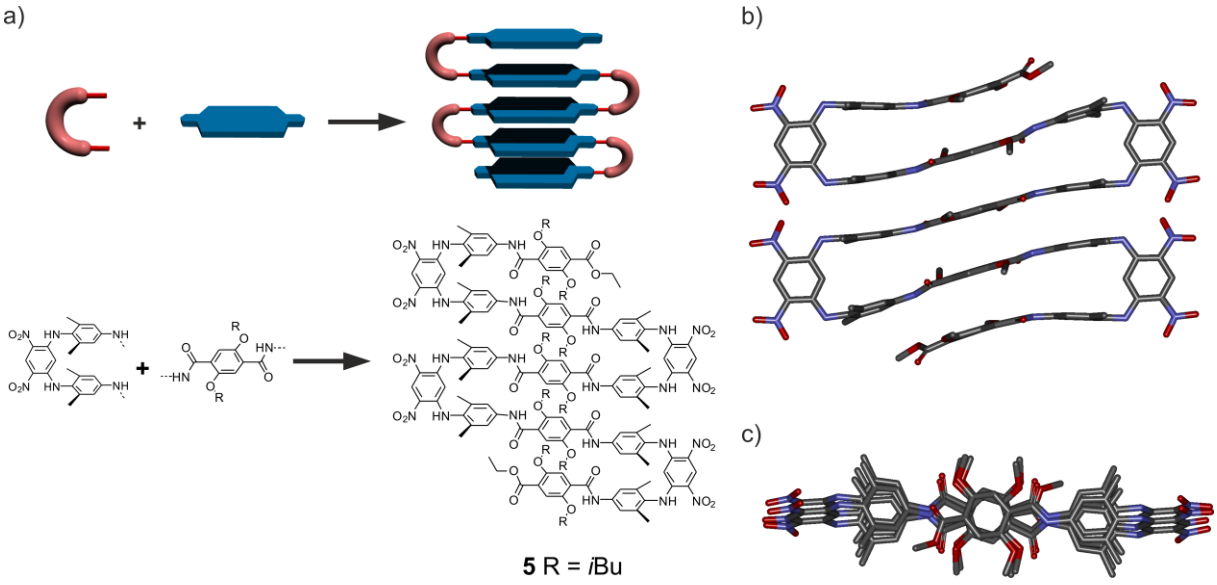

Figure 3. a) Schematic representation and molecular structure of the five-stranded artificial β-sheet **5**. b) Side view and c) top view of the crystal structure of **5**. Included solvent molecules have been removed for clarity.

2.2 Toward tertiary and quaternary structures

The functions of biopolymers depend above all on their tertiary or quaternary structures. Although the construction of artificial system with equivalent complexity and function remains a challenge, artificial tertiary and quaternary structures have been successfully designed and constructed.

Ethylene glycol tethered aromatic oligoamide foldamers **6**-**8** with size and complexity comparable to modest size proteins were synthesized in 2011 by the Huc group.[15] The short ethylene glycol maintained the tight interaction between the two helices, allowing intramolecular communication via the side chains. Solution studies and crystal structures gave a panorama of the conformation equilibria between *P* vs *M* conformer, parallel vs perpendicular orientation and *gauche* vs *anti* conformation of the ethylene glycol spacer. It is also worth mentioning that the structure of **8** remains the largest crystal structure of synthetic molecules solved by direct methods up to date.

15. N. Delsuc, S. Massip, J.-M. Léger, B. Kauffmann, I. Huc. Relative helix-helix conformations in branched aromatic oligoamide foldamers. *J. Am. Chem. Soc.* **2011**, *133*, 3165-3172.

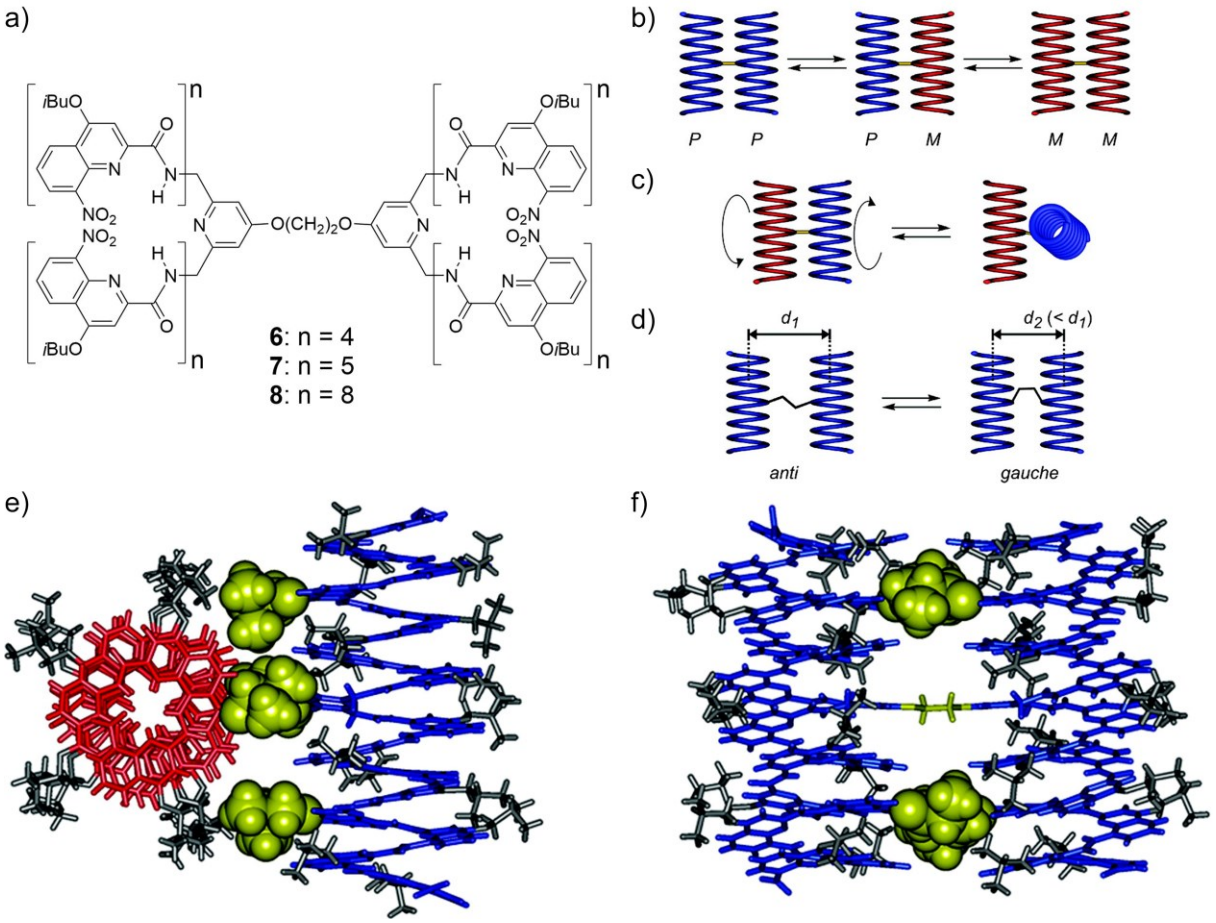

Figure 4. a) Formulas of ethylene glycol tethered foldamer **6**-**8**. b) *P* and *M* helix handedness inversion; c) Rotation about the ethylene glycol spacer. d) Helix-helix distance change caused by anti or gauche conformation of the spacer. e) Crystal structure of the *PM* isomer of **8** shown as front views; f) Crystal structure of the *PP* isomer of **8** shown as front views. Right-handed and left-handed helices are shown in blue and red, respectively. Most isobutoxy side chains are shown in gray. The ethylene spacer and the four isobutoxy chains in contact are shown in CPK colored in yellow. Included solvent molecules are removed for clarity.

Recently, Guichard et al. reported quaternary structures assembled from oligourea foldamers with proteinaceous side chains.[16] Based on the canonical 2.5-helices of the oligourea foldamer, two sequences with alternative charged and uncharged side chains were designed and synthesized. In both cases, crystal structures elucidated the origin for their distinct quaternary arrangement. Oligourea **9** formed anti-parallel dimer, which, through hydrophobic Leu^{u}-Leu^{u} interactions, further assembled into unprecedented hexameric helical bundle with an isolated hydrophobic inner cavity. This hexameric structure was also confirmed by NMR and mass spectroscopy studies. Individual oligourea helices **10** packed together to form a superhelix, two of which intertwined to assemble into a highly charged channel-type

16. G. W. Collie, K. Pulka-Ziach, C. M. Lombardo, J. Fremaux, F. Rosu, M. Decossas, L. Mauran, O. Lambert, V. Gabelica, C. D. Mackereth, G. Guichard. Shaping quaternary assemblies of water-soluble non-peptide helical foldamers by sequence manipulation. *Nat. Chem.* **2015**, *7*, 871–878.

structure filled with water. The channel was also evidenced by electron microscopy and cryo-electron microscopy. The whole assembly was stabilized by hydrophobic interactions and interhelical salt bridges.

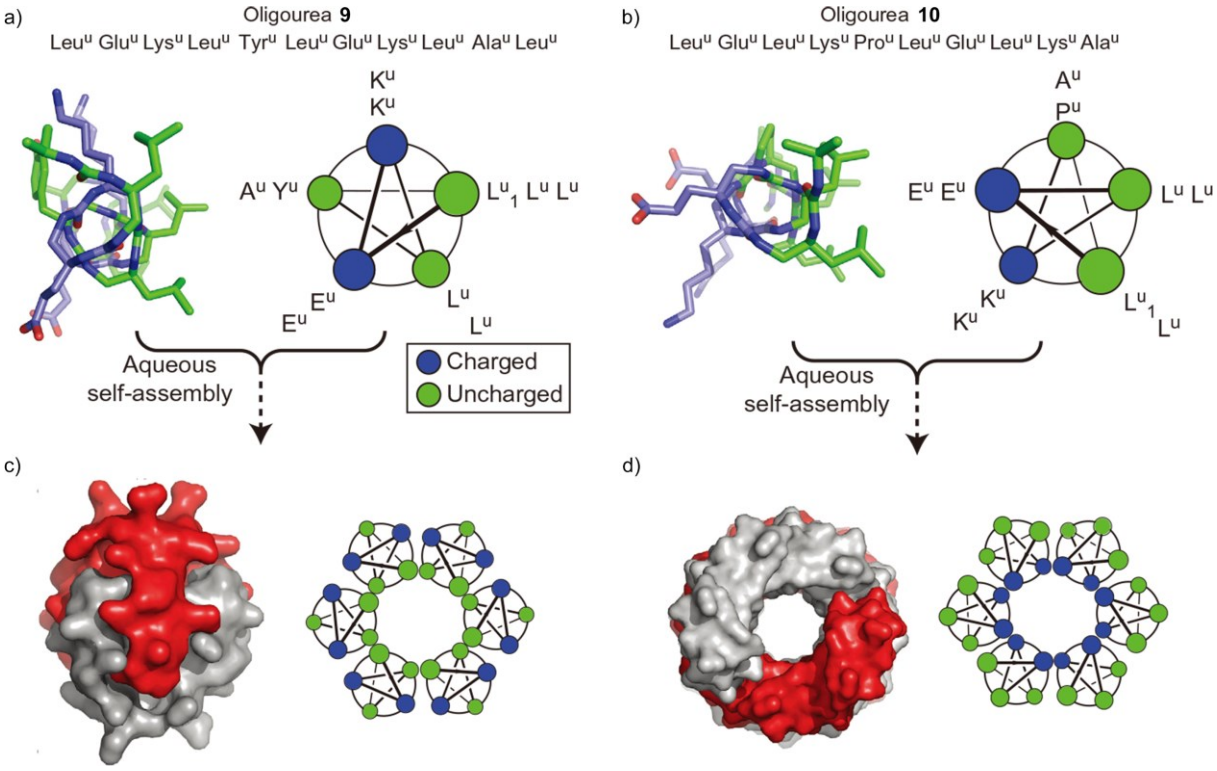

Figure 5. a) Primary sequence (top), top view of the crystal structure (bottom left), and helical wheel with side chain distribution (bottom right) of oligourea **9**. b) Equivalent information to that for oligourea **10**. c) Crystal structure of the hexameric helical bundle formed by **9**. Helices colored according to the common chain orientation. d) Crystal structure of the channel-type assembly formed by **10**. The two individual super helix chains of the channel are colored separately.

2.3 Emerging application of foldamer

2.3.1 Exorecognition of biomolecules by foldamers

Foldamers are ideal candidates for the study of protein-protein interactions for the following reasons: medium size, stable helicity, tunable backbone and side chains, and reduced susceptibility to proteolysis. Recently, the group of Gellman synthesized a series of α/β-peptides (Fig. 6a) via the combination of amino acid replacement and side chain cross linking. [17] The interactions of these α/β-peptides with anti-apoptotic proteins were investigated. Surface plasmon resonance experiments showed that cross-linked and unlinked **12** and **13** bound to anti-apoptotic proteins (Bcl-x_L, Mcl-1, and Bcl-2) with similar or even

17. J. W. Checco, E. F. Lee, M. Evangelista, N. J. Sleebs, K. Rogers, A. Pettikiriarachchi, N. J. Kershaw, G. A. Eddinger, D. G. Belair, J. L. Wilson, C. H. Eller, R. T. Raines, W. L. Murphy, B. J. Smith, S. H. Gellman, D. Fairlie. α/β-Peptide foldamers targeting intracellular protein–protein interactions with activity in living cells. *J. Am. Chem. Soc.* **2015**, *137*, 11365–11375.

higher affinity compared to natural peptide **11**-α. Crystal structures of complexes of **13**-α/β and **13**-α/β-LIN (unlinked) with Bcl-2 revealed the interaction of hydrophobic residues with Bcl-2 protein groove. The salt bridge between Asp12 of the α/β-peptides and Arg146 from the BH1 domain of Bcl-2 also contributed to the binding. Experiments with permeabilized wild-type mouse embryonic fibroblast showed that **13**-α/β can induce the release of cytochrome *c*, a sign of apoptosis. Also, Fluorescein-labeled **13**-α/β analogues verified the cell permeability of this peptide.

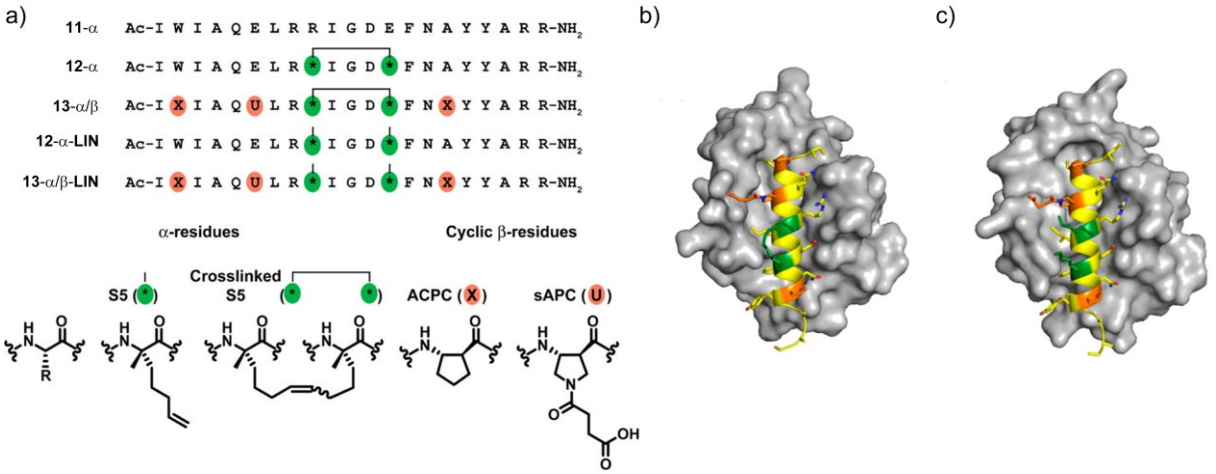

Figure 6. a) Primary sequences of α- and α/β-peptides. Non-natural amino acid residues are indicated by colored circles: green for S5 residue used for cross-linking, and orange for cyclic β-residues. Cross-linked residues are marked with a horizon line. Bottom, molecular formulas of a generic α-residue, the S5 residue (*), two cross-linked S5 residues, and the cyclic β-residues ACPC (X) and sAPC (U). b) Crystal structure of **13**-α/β bound to Bcl-2. c) Crystal structure of **13**-α/β-LIN bound to Bcl-2. Natural α-residues, S5 residues, and cyclic β-residues are shown in yellow, green, and orange, respectively. The Bcl-2 surface is shown in gray.

2.3.2 Endorecognition of biologically relevant molecules using foldamers

A folded helical structure creates an internal cavity, which is ample enough for molecular recognition. The Moore group found that *m*-phenylene ethynylene oligomers **14** can adopt a helical structure in polar solvent.[18] The internal cavity can bind a hydrophobic pinene molecule with an affinity constant of 6830 M^{-1} in water/acetonitrile (40:60 vol/vol). Inouye et al. reported that, by replacing the phenyl group with pyridine, the oligomer **15** adopted linear conformation in dichloromethane due to dipole-dipole repulsion between pyridines.[19] However, it was found that **15** could fold around n-octyl β-glucopyranoside to form stable complex through hydrogen bonding between pyridine nitrogen atoms and hydroxyl groups of β-glucose.

18. R. B. Prince, S. A. Barnes, J. S. Moore, Foldamer-based molecular recognition. *J. Am. Chem. Soc*. **2000**, *122*, 2758–2762.
19. M. Inouye, M. Waki, H. Abe, Saccharide-dependent induction of chiral helicity in achiral synthetic hydrogen-bonding oligomers. *J. Am. Chem. Soc*. **2004**, *126*, 2022–2027.

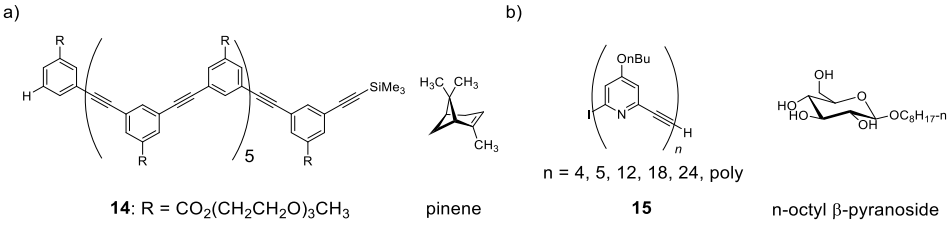

Figure 7. Formulas of a) foldamer **14** and b) **15** with their guest molecules.

The high helical stability and predictability of aromatic oligoamide foldamer allows the manipulation of building units at any position without losing the overall topology. Each monomer has a unique structure and contributes to the overall size and shape of the inner cavity whilst the helicity of the foldamer remains. Based on this principle, the Huc group developed an iterative strategy to construct a foldamer with high selectivity toward D-fructose.[20] First generation foldamer **16** could encapsulate sugar guests into its cavity with low discrimination between D-fructose and D-mannose. Thanks to the high crystallization tendency of the foldamer-guest complex, solid state structure was obtained, which provides information about the interactions between the foldamer and sugar guests at atomic scale. Based on this, new generations of sequence **17**-**21** were designed and synthesized through mutation, addition, or deletion of monomers of the initial sequence (Fig. 8b). Sequence **20** achieved precise shape complementary with D-fructose, leading to much favored affinity toward it. Crystal structure showed that the fluoride atoms of F4 and Q^F11 filled the void between **20** and D-fructose (Fig. 8c), whilst other monomers form hydrogen bonds around D-fructose (Fig. 8d).

20. N. Chandramouli, Y. Ferrand, G. Lautrette, B. Kauffmann, C. D.Mackereth, M. Laguerre, D. Dubreuil, I. Huc. Iterative design of a helically folded aromatic oligoamide sequence for the selective encapsulation of fructose. *Nat. Chem.* **2015**, *7*, 334-341.

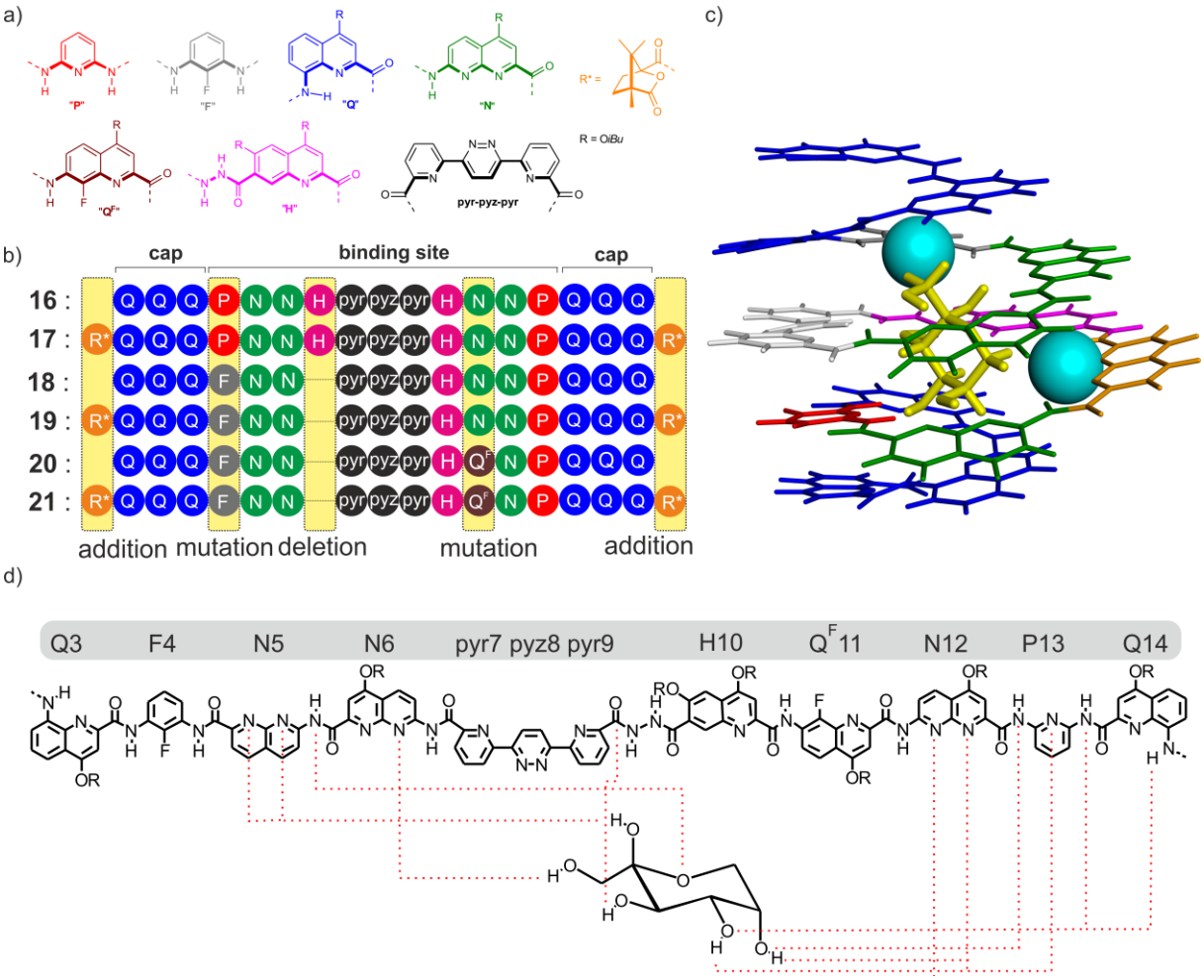

Figure 8. a) Color-coded formulas and associated letters of amino acid, diamino and diacid monomers. The inner rim of the helix is marked by thick bonds. b) Primary sequences of six generations of capsules. c) Crystal structures of capsule *P*-**20** with β-$^{2}C_{5}$-D-fructopyranose with tube and CPK representation for the helix and the guest, respectively. Fluorine atoms are represented as spheres. d) Hydrogen bonds between **20** and β -D-fructopyranose shown in red dashed lines. Two terminal quinoline monomers have been removed for clarity.

2.3.3 Self-assembled material

Lee et al. reported that t*rans*-(*S*,*S*)-2-aminocyclopentanecarboxylic acid oligomers could form unprecedented three-dimensional structures (foldectures) in aqueous environment. These foldectures varied according to the number of amino acid units and the end groups. More interestingly, when surfactant P123 ((ethylene glycol)$_{20}$-(propylene glycol)$_{70}$-(ethylene glycol)$_{20}$) was added at the initial state of self-assembly process, the foldecture can be altered to a different shape.[21] Recently, the same group showed that the alignment of foldectures formed by **22** and **23** can be modulated by exterior static magnetic field.[22] This is attributed to

21. S. H. Yoo, T. Eom, S. Kwon, J. Gong, J. Kim, S. J. Cho, R. W. Driver, Y. Lee, H. Kim, H.-S. Lee. Foldecture as a core material with anisotropic surface characteristics. *J. Am. Chem. Soc.* **2015**, *137*, 2159–2162.
22. S. Kwon, B. J. Kim, H.-K. Lim, K. Kang, S. H. Yoo, J. Gong, E. Yoon, J. Lee, I. S. Choi, H. Kim, H.-S. Lee. Magnetotactic molecular architectures from self-assembly of β-peptide foldamers. *Nat. Commun.* **2015**, *6*, 8747.

the well-arranged order of foldamer within the foldecture, which amplifies the diamagnetic anisotropy of the self-assembly. Moreover, when a dynamic magnetic field is applied, the foldecture of **22** could perform directional motion with loaded gel.

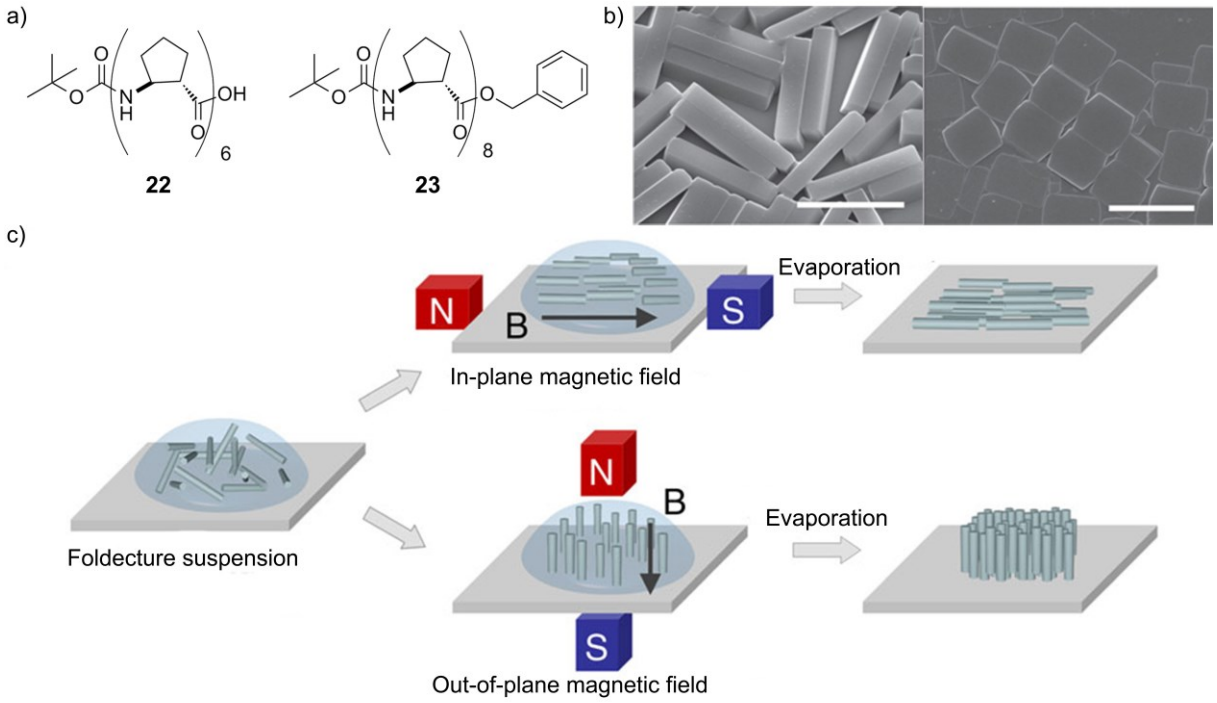

Figure 9. a) Formulas of the peptide sequences **22** and **23**. b) SEM images of the foldectures formed by **22** (left) and **23** (right). Scale bars, 5μm. c) Schematic representation of the operation of foldecture alignment under static magnetic field.

2.3.4 Foldamer as scaffold for photoelectronics

The folded structure of foldamers allows delicate control of the distance between the donor and acceptor and their relative spatial orientation. The Huc group investigated the effects of bridging aromatic oligoamide foldamers on photoinduced electron transfer process.[23] A well-defined array of distances and orientations between oligo(*p*-phenylene vinylene) (OPV) and perylene bisamide (PB) was obtained with foldamer of different length as bridge. Foldamer bridge ensures that the distance between OPV and PB is different through space and through the bridge. Fast charge separation reaction between OPV and PB was observed. The charge recombination mainly depended on the formation of triplet states. Calculations indicated that the fast charge separation could be explained by the foldamer mediate charge transfer from donor to acceptor via superexchange mechanism. However, the attenuation factors of **24a-d** indicated the complexity of this system, since the attenuation factors could not be explained solely by either charge separation through space or through the bridge.

23. M. Wolffs, N. Delsuc, D. Veldman, N. Vân Anh, R. M. Williams, S. C. J. Meskers, R. A. J. Janssen, I. Huc, A. P. H. J. Schenning. Helical aromatic oligoamide foldamers as organizational scaffolds for photoinduced charge transfer. *J. Am. Chem. Soc.* **2009**, *131*, 4819-4829.

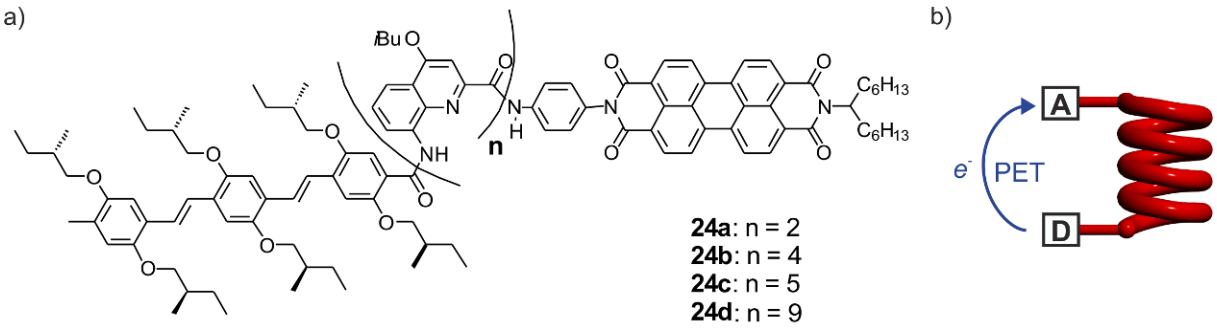

Figure 10. a) Formulas of donor-acceptor molecules **24a-d** with foldamer as bridge. b) Schematic representation of the photoinduced electron transfer.

3. Unidirectional motion on one dimensional track

To maintain the non-equilibrium biological system, biological machineries need to perform work processively and progressively. One way to fulfill these prerequisites is confining the motion of the molecular machine to its substrate to limit Brownian diffusion. Since the molecular machine cannot detach from or exchange its substrate, the efficiency is enhanced. This confinement of molecular machine can be achieved in two ways: a) the molecular machine adopts a cyclic conformation around its substrate and slides along the biopolymer; b) the molecular machine interacts with its substrate non-covalently, and walks along the substrate. An example of the former is protein synthesis by ribosome. Whilst sliding along a DNA sequence, ribosome translate the genetic code and adds the corresponding amino acid to a peptide sequentially. Meanwhile, the transportation of a cargo by kinesin and myosin belongs to the latter. With ATP as fuel, kinesin can move along a filament track without dissociation whilst transporting a cargo.

Inspired by nature's design, artificial molecular machines have been widely investigated in the past decades.[24,25] One typical category of artificial molecular machines is molecular rotor, which can rotate directionally and continuously under the stimulus of light[26,27] or STM tip.[28,29,30] Light controlled molecular rotors have been reported to drive the rotation of glass rods[31] or contract the size of gel.[32] The majority of artificial molecular machines are based on rotaxanes and pseudorotaxanes, which have been shown to perform translational motion to bend gold,[33] or to synthesize peptide.[34] Despite all these achievements, synthetic system that can perform work in a processive and progressive manner remains a challenge. Herein, a non-exhaustive review of state-of-the-art synthetic systems with processivity and progressivity is carried out.

24. A. Credi, S. Silvi, M. Venturi (Eds.). Molecular machines and motors: recent advances and perspectives. *Top. Curr. Chem.* Springer, Berlin, **2014**.
25. S. Erbas-Cakmak, D. A. Leigh, C. T. McTernan, A. L. Nussbaumer. Artificial molecular machines. *Chem. Rev.* **2015**, *115*, 10081–10206.
26. N. Ruangsupapichat, M. M. Pollard, S. R. Harutyunyan, B. L. Feringa. Reversing the direction in a light-driven rotary molecular motor. *Nat. Chem.* **2011**, *3*, 53–60.
27. J. C. M. Kistemaker, P. Štacko, J. Visser, B. L. Feringa. Unidirectional rotary motion in achiral molecular motors. *Nat. Chem.* **2015**, *7*, 890–896.
28. L. Grill, K.-H. Rieder, F. Moresco, G. Rapenne, S. Stojkovic, X. Bouju, C. Joachim. Rolling a single molecular wheel at the atomic scale. *Nat. Nanotechnol.* **2007**, *2*, 95–98.
29. T. Kudernac, N. Ruangsupapichat, M. Parschau, B. Maciá, N. Katsonis, S. R. Harutyunyan, K.-H. Ernst, B. L. Feringa. Electrically driven directional motion of a four-wheeled molecule on a metal surface. *Nature* **2011**, *479*, 208–211.
30. U. G. E Perera, F. Ample, H. Kersell, Y. Zhang, G. Vives, J. Echeverria, M. Grisolia, G. Rapenne, C. Joachim, S.-W. Hla. Controlled clockwise and anticlockwise rotational switching of a molecular motor. *Nat. Nanotechnol.* **2012**, *8*, 46–51.
31. R. Eelkema, M. Pollard, J. Vicario, N. Katsonis, B. Ramon, C. W. M. Bastiaansen, D. J. Broer, B. L. Feringa. Nanomotor rotates microscale objects. *Nature* **2006**, *440*, 163−163.
32. Q. Li, G. Fuks, E. Moulin, M. Maaloum, M. Rawiso, I. Kulic, J. T. Foy, N. Giuseppone. Macroscopic contraction of a gel induced by the integrated motion of light-driven molecular motors. *Nat. Nanotechnol.* **2015**, *10*, 161–165.
33. Y. Liu, A. H. Flood, P. A. Bonvallet, S. A. Vignon, B. H. Northrop, H.-R. Tseng, J. O. Jeppesen, T. J. Huang, B. Brough, M. Baller, S. Magonov, S. D. Solares, W. A. Goddard, C.-M. Ho, J. F. Stoddart. Linear artificial molecular muscles. *J. Am. Chem. Soc.* **2005**, *127*, 9745–9759.
34. B. Lewandowski, G. De Bo, J. W. Ward, M. Papmeyer, S.Kuschel, M. J. Aldegunde, P. M. E. Gramlich, D. Heckmann, S. M. Goldup, D. M. D'Souza, A. E. Fernandes, D. A. Leigh. Sequence-specific peptide synthesis by an artificial small-molecule machine. *Science*, **2013**, *339*, 189–193.

3.1 Unidirectional sliding along polymer tracks

Over the decades, many progress has been made in the construction of unidirectional motion along axle molecules.[35,36,37] However, in most cases, less than three stations are integrated. In order to design artificial molecular machines that can perform work processively, thorough understanding and control of the sliding process of synthetic macrocycles along polymers is prerequisite. Cyclodextrins can form polyrotaxanes by sliding onto polymer chains, the thermodynamics and kinetics of which was studied by Harada and Wenz et al.[38,39] However, the sliding process of such systems lacks the directionality required for molecular machine.

The group of Nolte investigated the unidirectional sliding of macrocycles along a series of polymer chains.[40,41] Toroidal shaped macrocycles with a porphyrin roof (**25-H**$_2$, **25-Zn**, **26-H**$_2$, and **26-Zn**) were synthesized, together with a series of viologen derivatives **28a-g** as guest molecules. NMR and mass studies confirmed the formation of stable 1:1 host-guest complex, with the viologen group stays inside the macrocyclic cavity. However, due to the large size of the 3,5-di-tert-butylphenoxyl stopper at one terminal of the viologen, the macrocycle must slide along the polymer chain to reach its binding site. When the macrocycle reached to the viologen group, the fluorescence of the porphyrin was quenched. Thus, fluorescence spectroscopy was applied for the study of the sliding kinetics. Investigation indicated that the motion of these macrocycles along the polymers can be explained by a consecutive-hopping mechanism. This means that the overall threading rate k depends on the rate of the initial binding (k_{initial}) and the chain length. The initial binding rate is irrelevant to the chain length. Once the macrocycle binds to the polymer, it hops through local energy minimum until reaching to the viologen group. Kinetic studies at varied temperatures indicated that the threading process of **25-H**$_2$ has a constant positive activation enthalpy, and the activation entropy is negative and decreases as chain length increases.

35. C. Romuald, A. Ardá, C. Clavel, J. Jiménez-Barbero, F. Coutrot. Tightening or loosening a ph-sensitive double-lasso molecular machine readily synthesized from an ends-activated [c2]daisy chain. *Chem. Sci.* **2012**, *3*, 1851–1857.
36. H. Li, C. Cheng, P. R. McGonigal, A. C. Fahrenbach, M. Frasconi, W.-G. Liu, Z. Zhu, Y. Zhao, C. Ke, J. Lei, R. M. Young, S. M. Dyar, D. T. Co, Y.-W. Yang, Y. Y. Botros, W. A. Goddard, M. R. Wasielewski, R. D. Astumian, J. F. Stoddart. Relative unidirectional translation in an artificial molecular assembly fueled by light. *J. Am. Chem. Soc.* **2013**, *135*, 18609–18620.
37. G. Ragazzon, M. Baroncini, S. Silvi, M. Venturi, A. Credi. Light-powered autonomous and directional molecular motion of a dissipative self-assembling system. *Nat. Nanotechnol.* **2014**, *10*, 70–75.
38. W. Herrmann. B. Keller, G. Wenz. Kinetics and thermodynamics of the inclusion of ionene-6, 10 in α-cyclodextrin in an aqueous solution. *Macromolecules*, **1997**, *30*, 4966–4972.
39. A. Harada, J. Li, M. Kamachi. The molecular necklace: a rotaxane containing many threaded α-cyclodextrins. *Nature*, **1992**, *356*, 325–327.
40. R. G. E. Coumans, J. A. A. W. Elemans, R. J. M. Nolte, A. E. Rowan. Processive enzyme mimic: kinetics and thermodynamics of the threading and sliding process. *Proc. Natl. Acad. Sci. U.S.A.* **2006**, *103*, 19647–19651.
41. A. B. C. Deutman, C. Monnereau, J. A. A. W. Elemans, G. Ercolani, R. J. M. Nolte, A. E. Rowan. Mechanism of threading a polymer through a macrocyclic ring. *Science*, **2008**, *322*, 1668–1671.

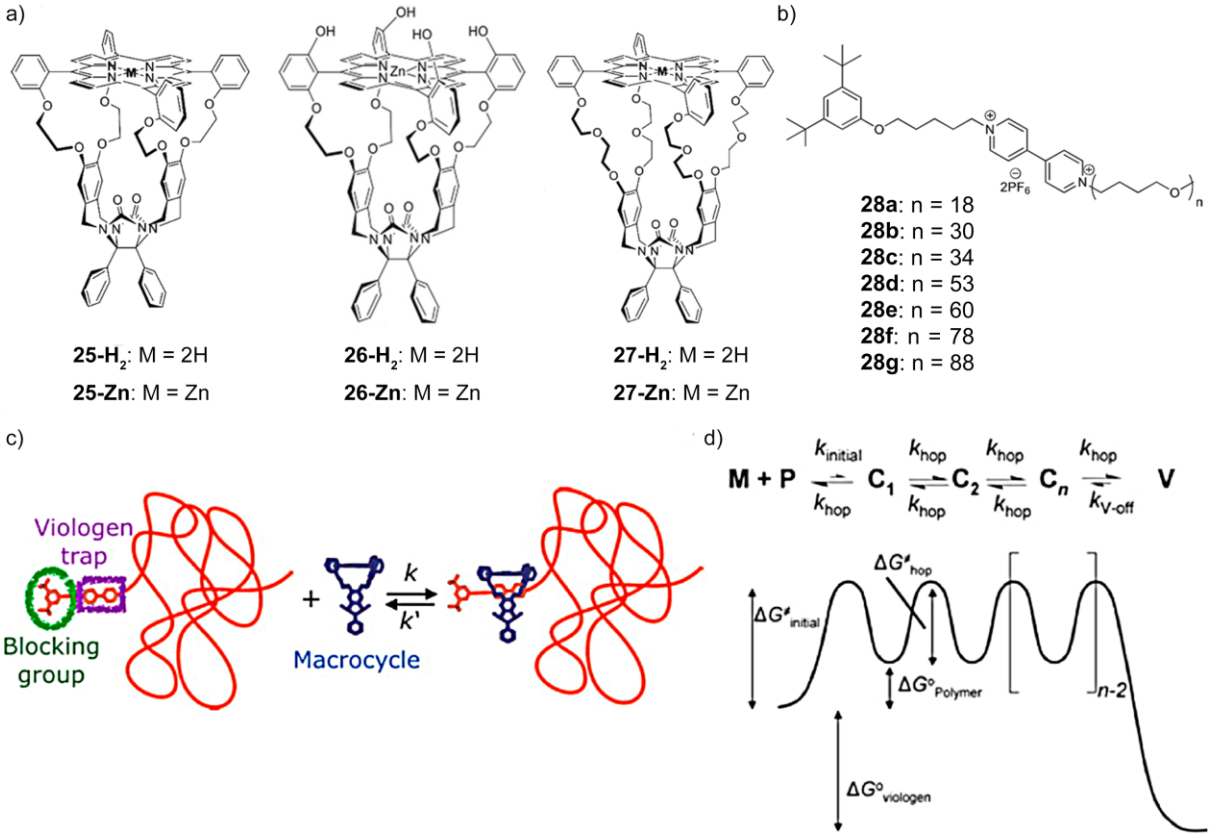

Figure 11. Formulas of a) porphyrin macrocycles and b) viologen functionalized polymer chains with different number of repeating units. c) Schematic representation of the threading of the polymer chain through the macrocycle. d) Energy diagram of the consecutive hopping mechanism with the rate constants (k) and energy levels of all the individual processes (M: macrocycle, P: polymer, V: viologen trap, C: local energy minimum).

It was found that threading through more flexible hosts **27-H$_2$** and **27-Zn** is relatively slower.[42] When the chain length of the polymer doubles, the rate of threading decrease by a factor of 4 instead of an expected factor of 2 derived from studies of macrocycle **25** and **26**. This indicated a threading mechanism more complex than consecutive-hopping, which could be attributed to the strong interaction of the macrocycle with the polymer chain. Detailed investigations suggested that the initial binding of macrocycle to the open end of polymer resulted in a large entropy loss due to the loss of the conformational freedom of both the macrocycle and the polymer chain upon binding. This is compensated by a negative enthalpy, which probably originates from the conformation change of the macrocycle. However, the translocation process is enthalpically unfavorable but entropically favorable, because the macrocycle need to release the interaction and adopt more flexible conformation to hop along the polymer chain.

42. A. B. C. Deutman, S. Cantekin, J. A. A. W. Elemans, A. E. Rowan, R. J. M. Nolte. Designing processive catalytic systems. threading polymers through a flexible macrocycle ring. *J. Am. Chem. Soc.* **2014**, *136*, 9165-9172.

Furthermore, the threading process can be controlled allosterically.[43] Through hydrogen bonding and metal ligation, very stable 2:1 complex can form between the macrocycle **26-Zn** and a bidentate ligand 1,4-diazabicyclo[2.2.2]octane **29**. Due to the allosteric interactions between the macrocycle, the ligand and the polymer, this trimeric complex has enhanced affinity toward polymer **30** to form pentameric complex (**26-Zn**)$_2$·**29**·(**30**)$_2$. As a consequence, very slow dethreading rate of the polymer chain out of this pentameric complex is observed. It is also worth mentioning that the threading of a second polymer **29** possessed a slow rate. This is probably because the macrocyclic cavity was occupied by the open end of the polymer residing in the first macrocycle.

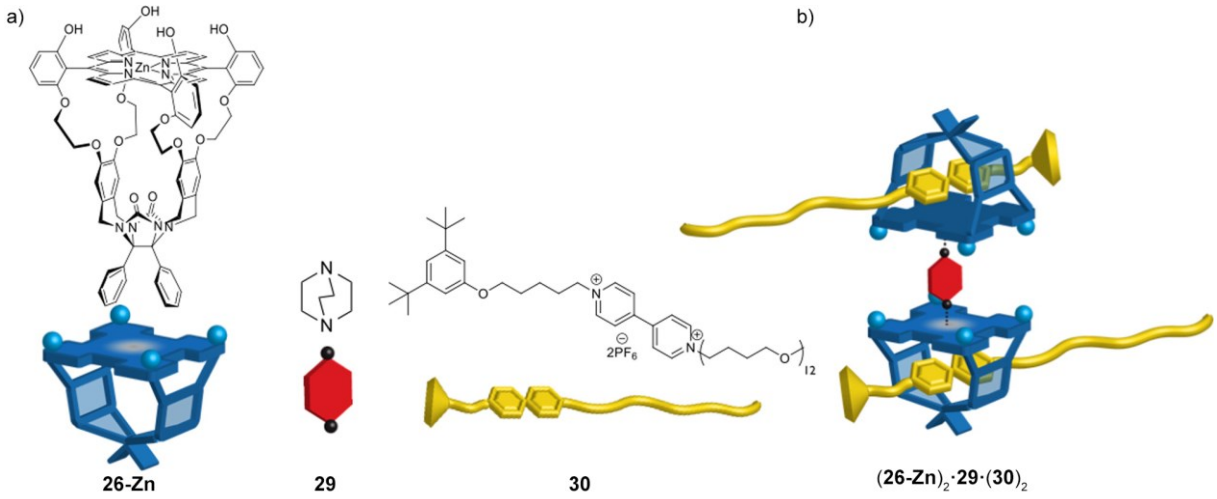

Figure 12. a) Formulas of the porphyrin macrocycle **26-Zn**, ligand **29**, and viologen functionalized polymer chain **30**. b) Schematic representation of the pentameric complex (**26-Zn**)$_2$·**29**·(**30**)$_2$.

Recently, B. D. Smith et al. reported a threading process in aqueous environment.[44] By exploiting both hydrogen bond and hydrophobic interaction, a macrocycle host **31** could bind squaraine dyes with nanomolar dissociation constant. The threading of a polyethylene glycol (PEG) chain through **31** was studied. It was found that the threading rate of **32a** is only three times lower than that of **33a**, which had 20 times shorter ethylene glycol chain than the former. Further investigation showed that changing the N-alkyl substituents will dramatically influence the threading kinetics. The threading of **33c** with a propyl group is 30 000 times slower in aqueous solution, thus acting as a "bumper" for the macrocycle.[45]

43. S. Cantekin, A. J. Markvoort, J. A. A. W. Elemans, A. E. Rowan, R. J. M. Nolte. Allosterically controlled threading of polymers through macrocyclic dimers. *J. Am. Chem. Soc.* **2015**, *137*, 3915–3923.
44. E. M. Peck, W. Liu, G. T. Spence, S. K. Shaw, A. P. Davis, H. Destecroix, B. D. Smith. Rapid macrocycle threading by a fluorescent dye-polymer conjugate in water with nanomolar affinity. *J. Am. Chem. Soc.* **2015**, *137*, 8668–8671.
45. W. Liu, E. M. Peck, K. D. Hendzel, B. D. Smith. Sensitive structural control of macrocycle threading by a fluorescent squaraine dye flanked by polymer chains. *Org. Lett.* **2015**, *17*, 5268–5271.

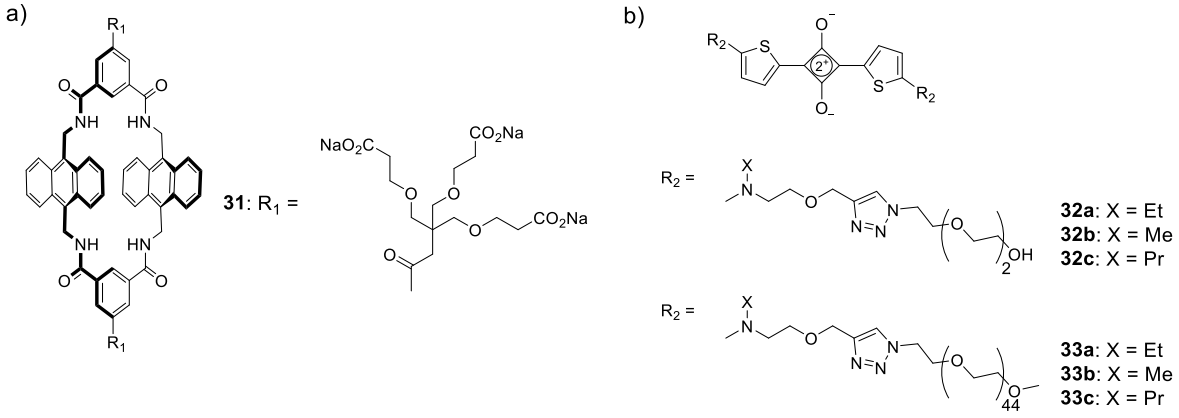

Figure 13. Formulas of a) the macrocycle **31**; b) guest molecules **32a-c** and **33a-c**.

3.2 Processive synthesis

In 2003, the first artificial catalyst mimicking biological processivity was reported by the Nolte group.[46] The U-shaped cavity of macrocycle **34** was large enough to allow the threading of polybutadiene **36**. With the presence of an oxygen donor, the manganese (III) porphyrin group carried out epoxidation reaction to convert polybutadiene into polybutadineepoxide. A bulky ligand 4-*tert*-butylpyridine **35** coordinated to the outside of the manganese center, ensuring that the epoxidation reaction happened only inside the macrocycle. Whilst sliding along **36**, the macrocycle could efficiently convert **36** into its corresponding polyepoxide. The domination of *trans* product also indicated that the epoxidation is performed inside the cavity.

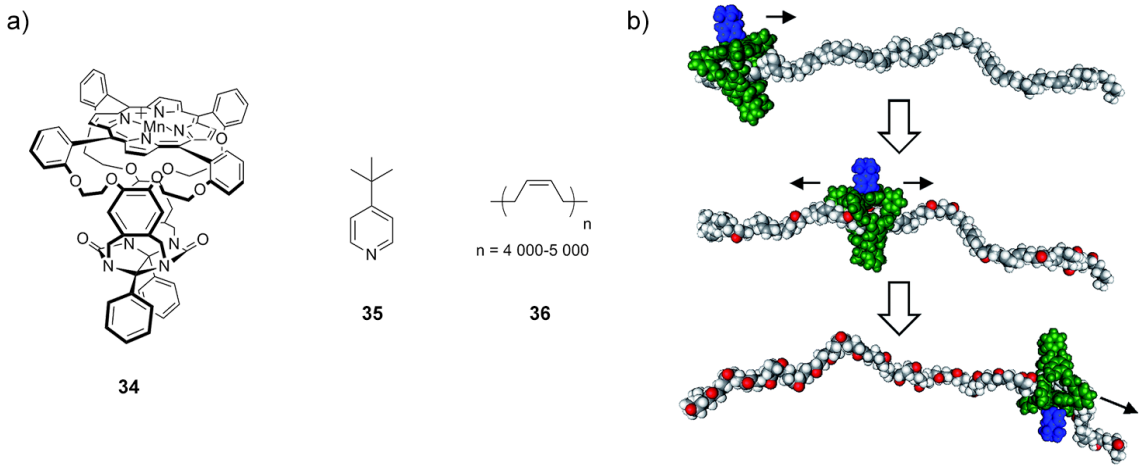

Figure 14. a) Formulas of the catalytic macrocycle **34**, the bulky axial ligand **35**, and polybutiene **36**. b) Schematic representation of sliding of the macrocycle complex along the polybutadiene and performing epoxidation.

46. P. Thordarson, E. J. A. Bijsterveld, A. E. Rowan, R. J. M. Nolte. Epoxidation of polybutadiene by a topologically linked catalyst. *Nature*, **2003**, *424*, 915–918.

Harada et al. dedicatedly designed a rotaxane-based catalyst **37** resembling to molecular clamp.[47] A smaller α-cyclodextrin (α-CD) was conjugated with a relatively larger β-cyclodextrin (β-CD). The β-CD activated δ-valerolactone, performing the ring opening reaction for the polymerization. The tethered α-CD allowed the threading of the growing polymer chain. This molecular clamp leaded up to a conversion of 95% of δ-valerolactone, affording polylactones with an M_n value of 16 500. In contrast, without the molecular clamp, the polymerization only resulted in oligomers. Detailed studies suggested that the length of linker is crucial for the performance of the molecular clamp: too short linker hinders the recognition of monomer into the CD cavity, whilst too long linker fails to clamp the growing polymer chain.

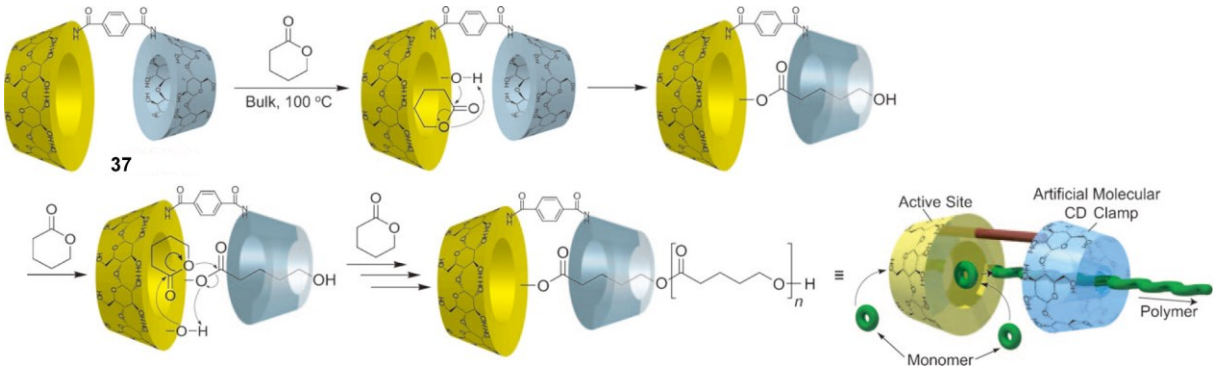

Figure 15. Proposed mechanism for cyclodextrin dimer **37** initialed polymerization of δ-valerolactone.

More recently, the group of Leigh reported a ribosome like peptide synthesizing rotaxane system **38**.[48] Amino acids were arranged sequentially along a template axle, and the functionalized macrocycle was interlocked at one extremity of the axle. The thiol arm in the macrocycle can pick up the amino acid through the breakage of the weak phenolic ester linkage between the amino acid and the axle. Subsequently, through *S*-*N* acyl transfer, the amino acid is added to the free amine on the macrocycle arm. Moving along the axle, up to three different amino acids were coupled to the macrocycle arm processively. Mass spectrometry and HPLC-MS analysis of the product indicated that the coupling reaction only happens in the designed order and no byproduct with different sequences or missing/adding unit existed. An improved synthesis along with the addition of a fourth residue was reported.[49] This new design avoided the challenging step of coupling the precious sequence-bearing template with the macrocycle to form the final rotaxane. Instead, in the new design, the rotaxanes were synthesized with the first amino acid as stopper, following by the addition of the rest of the amino acid sequence.

47. Y. Takashima, M. Osaki, Y. Ishimaru, H. Yamaguchi, A. Harada. Artificial molecular clamp: a novel device for synthetic polymerases. *Angew. Chem. Int. Ed.* **2011**, *50*, 7524–7528.
48. B. Lewandowski, G. De Bo, J. W. Ward, M. Papmeyer, S.Kuschel, M. J. Aldegunde, P. M. E. Gramlich, D. Heckmann, S. M. Goldup, D. M. D'Souza, A. E. Fernandes, D. A. Leigh. Sequence-specific peptide synthesis by an artificial small-molecule machine. *Science*, **2013**, *339*, 189–193.
49. G. De Bo, S. Kuschel, D. A. Leigh, B. Lewandowski, M. Papmeyer , J. W. Ward. Efficient assembly of threaded molecular machines for sequence-specific synthesis. *J. Am. Chem. Soc.* **2014**, *136*, 5811−5814.

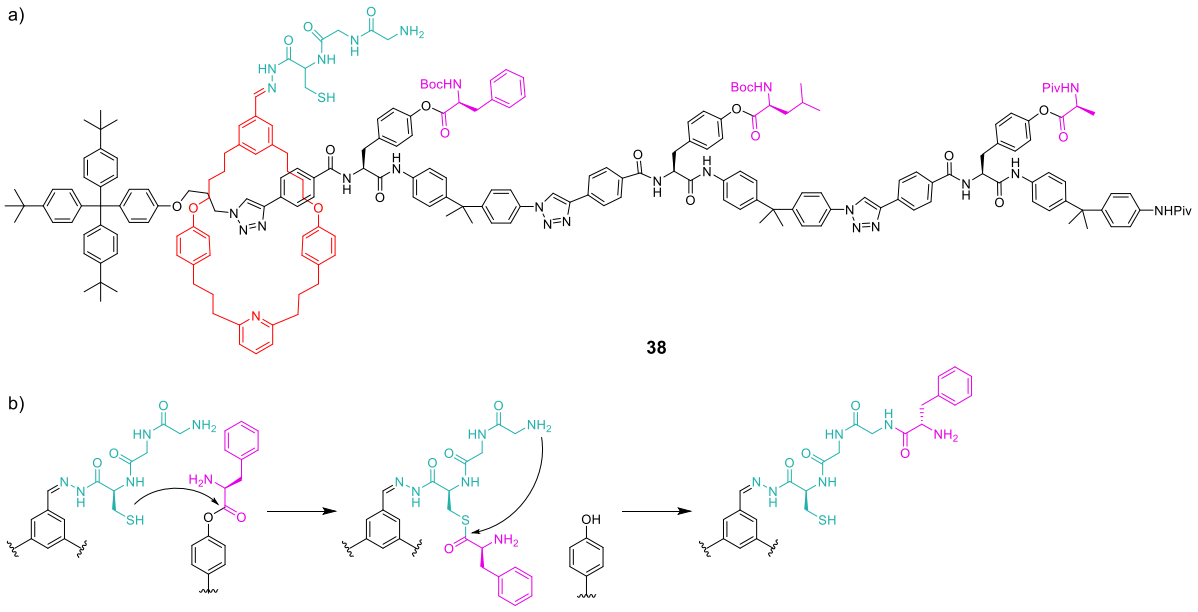

Figure 16. a) Formula of rotaxanes-based molecular machine **38**. b) Proposed mechanism for peptide synthesis by molecular machine **38**.

By integrating biological processive block with artificial systems, Nolte's group reported a biohybrid processive catalyst.[50] In this system, a DNA-nicking catalyst **39** (manganese tripyridyl porphyrin) was conjugated to a DNA-binding clamp protein. The clamp protein gp45 (Fig. 17b) could bind to double strand DNA and slide along it, while the porphyrin catalyst intercalates into AAA sequence to perform oxidation. By stamping the oxidized sites with biotin derivative **40**, streptavidin can be used as a marker for the reaction site. Therefore, the reaction site can be identified by AFM due to the large size difference of streptavidin and double strand DNA: clusters of streptavidin suggest processive catalysis. Moreover, with the guidance of engineered restriction enzymes, the sliding direction of the catalytic clamp could be controlled.

50. S. F. M. van Dongen, J. Clerx, K. Nørgaard, T. G. Bloemberg, J. J. L. Cornelissen, M. A. Trakselis, S. W. Nelson, S. J. Benkovic, A. E. Rowan, R. J. M. Nolte. A clamp-like biohybrid catalyst for DNA oxidation. *Nat. Chem.* **2013**, *5*, 945–951.

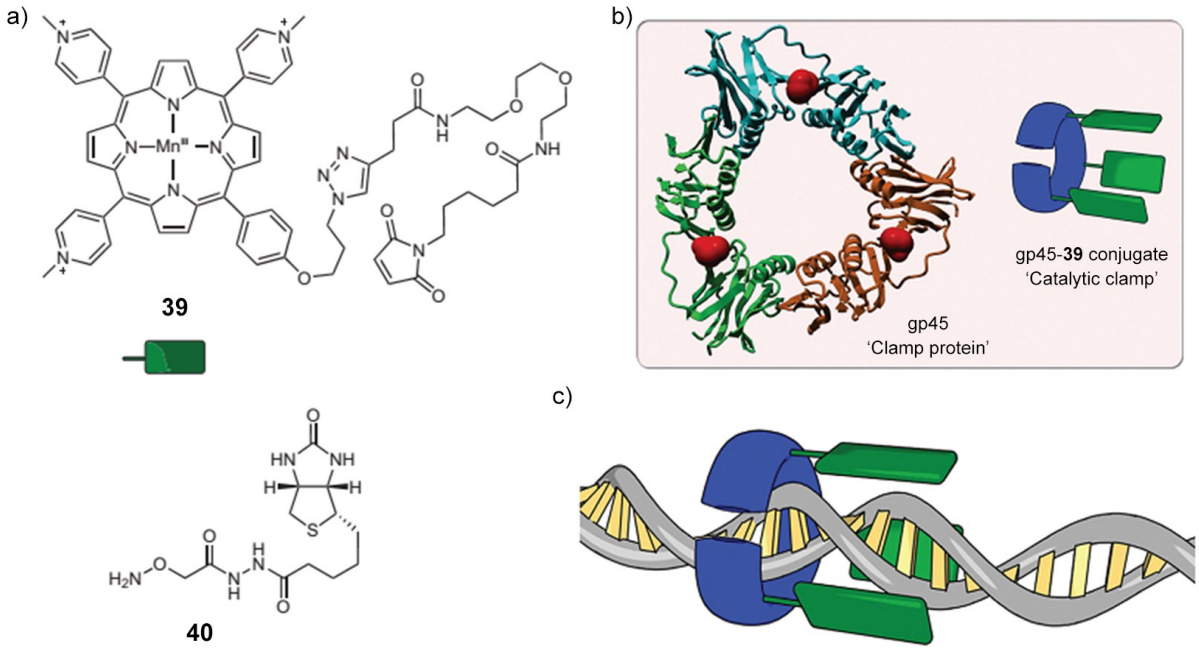

Figure 17. a) Formula and shape representations of manganese tripyridyl porphyrin **39** and biotin stamper **40**. b) Shape representations and colloquial names of proteins and protein conjugates. The E212C mutant of gp45 is shown with its cysteine residues (red) conjugated with **39** to afford the catalytic clamp. c) Schematic representation of the porphyrin conjugated clamp protein binding to DNA.

3.3 Molecular walkers

Principles and examples of molecular walkers were reviewed by Leigh and coworkers.[51] The Brownian walking of small molecules along the axis of a metal surface was reported, and the process could be visualized with STM.[52] Huskens et al. demonstrated the gradient-driven diffusion of molecules bearing two adamantine legs across α-cyclodextrin host covered surface.[53] Bayley's group showed that an organoarsenic molecule can walk within a protein nanoreactor via thiol ligand exchange.[54]

The precise and reversibility of base-pairing makes DNA a versatile candidate for designing molecular walkers. The general principle is strand displacement. Seeman et al. reported the first artificial DNA walker based on this principle.[55] Single strand DNA feet are connected via unreactive flexible single strand linker. Each foot can be attached to a single helix foothold by using an anchor strand complementary to both the foot and the foothold. This anchor strand has a free single strand toehold, which does not hybridize with either the foot or

51. D. A. Leigh, U. Lewandowska, B. Lewandowski, M. R. Wilson. Synthetic molecular walkers. *Top. Curr. Chem.* **2014**, *354*, 111–138.
52. K.-Y. Kwon, K. L. Wong, G. Pawin, L. Bartels, S.Stolbov, T. S. Rahman. Unidirectional adsorbate motion on a high-symmetry surface: "walking" molecules can stay the course. *Phys. Rev. Lett.* **2005**, *95*, 166101–116104.
53. A. Perl, A. Gomez-Casado, D. Thompson, H. H. Dam, P. Jonkheijm, D. N. Reinhoudt, J. Huskens. Gradient-driven motion of multivalent ligand molecules along a surface functionalized with multiple receptors. *Nat. Chem.* **2011**, *3*, 317−322.
54. G. S. Pulcu, E. Mikhailova, L. S. Choi, H. Bayley. Continuous observation of the stochastic motion of an individual small-molecule walker. *Nat. Nanotechnol.* **2014**, *10*,76−83
55. W. B. Sherman, N. C. Seeman. A precisely controlled DNA biped walking device. *Nano Letters* **2004**, *4*, 1203–1207.

the foothold. When an unset strand is added, the toehold can initiate the hybridization of this unset strand with the anchor strand, unsetting the foot to move forward. A thorough review on DNA walkers along complex tracks, carrying cargo or performing organic synthesis, in controlled manner or autonomously was carried out by Choi et al.[56]

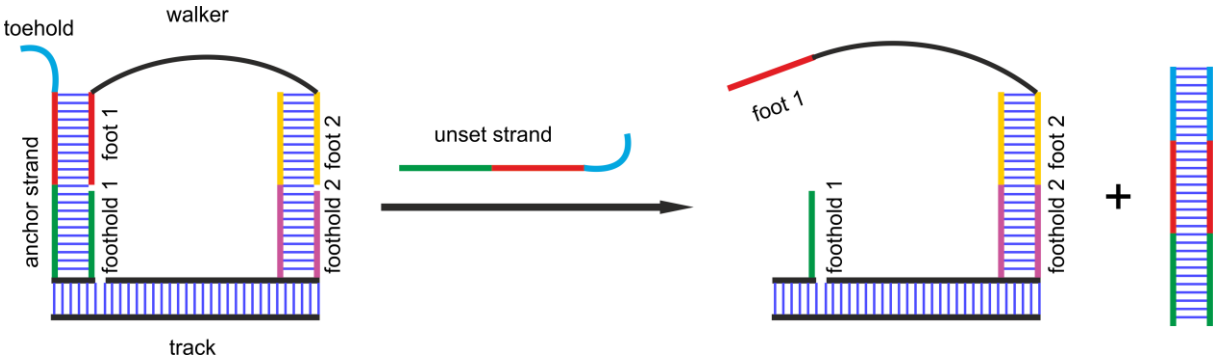

Figure 18. Schematic representation of the mechanism of DNA walker. Complementary strands are coded with the same color.

Lehn and coworkers found that the intramolecular dynamic exchange rate of imine formed by salicylaldehyde and aliphatic α,ω-diamines can be modulated by substitution, solvent composition, or temperature. [57] Furthermore, the salicylidene residue can move nondirectionally along a polyamine track without dissociation (Fig. 19a). When one equivalent methoxyamine trigger was added to a molecular walker **42**, one imine was set free, leaving a reactive amine. Thus, the central aminal moved intramolecularly to reach the free amine, forming thermodynamically favored imine. Recently, controlled directionality was achieved by using 2-carboxybenzaldehyde group as walker.[58] Under acid or basic conditions, the walker **43** could be trapped as lactone at one end, or imine at the other end (Fig. 19c).

56. J. Pan, F. Li, T. G. Cha, H. Chen, J. H. Choi, Recent progress on DNA based walkers. *Curr. Opin. Biotechnol.* **2015**, *34*, 56-64.
57. P. Kovaricek, J.-M. Lehn. Merging constitutional and motional covalent dynamics in reversible imine formation and exchange processes. *J. Am. Chem. Soc.* **2012**, *134*, 9446−9455.
58. P. Kovaricek, J.-M. Lehn, Directional dynamic covalent motion of a carbonyl walker on a polyamine track. *Chem. - Eur. J.* **2015**, *21*, 9380−9384.

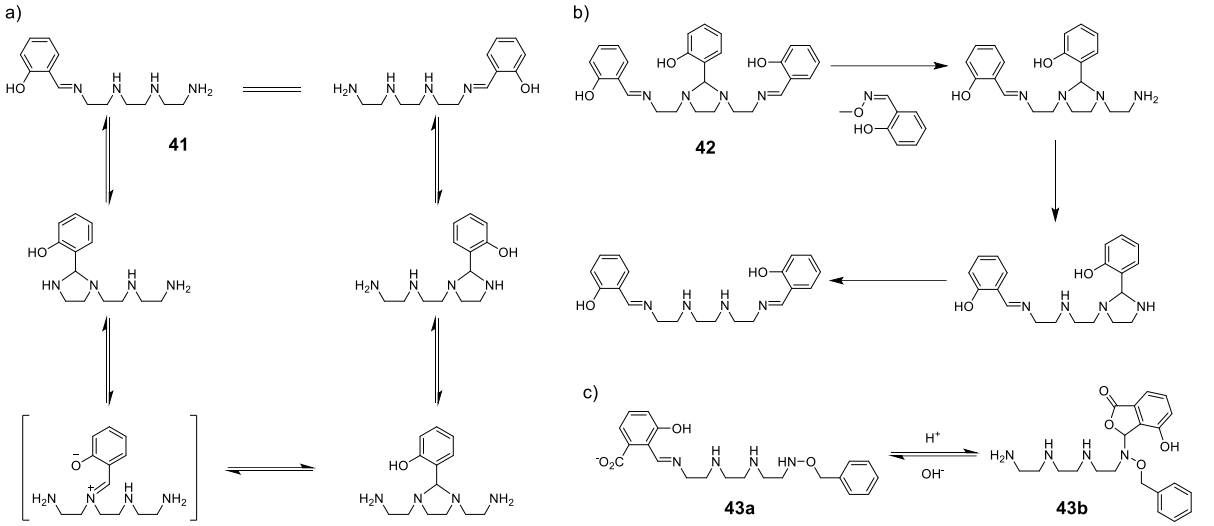

Figure 19. a) Formula and inchworm-type transportation of 2-carboxybenzaldehyde along a polyamine track. b) Formulas and operation of walker 40 via dynamic imine exchange chemistry. c) Controlled directional walker **43** on a polyamine track through the stabilization of imine **43a** or lactone **43b** under basic or acid conditions, respectively.

Another example of molecular walker along polyamine track was reported by Leigh et al., exploiting the Michael and retro-Michael reactions of α-methylene-4-nitrostyrene.[59] The walker **44** can walk randomly along the track without significant intermolecular exchange (Fig. 20a). NMR studies showed that the walker reached the most favored thermodynamic distribution through taking adjacent amine footholds progressively. By displacing one terminal phenyl group with anthracene, molecular walker **45** was synthesized. The walking process of **45** can be monitored by the fluorescent decrease of the anthracene group caused by the approaching of nitrophenyl group. Both NMR and fluorescent studies indicated that the steady state is reached after 6.5 hours with a biasing toward the anthracene end.

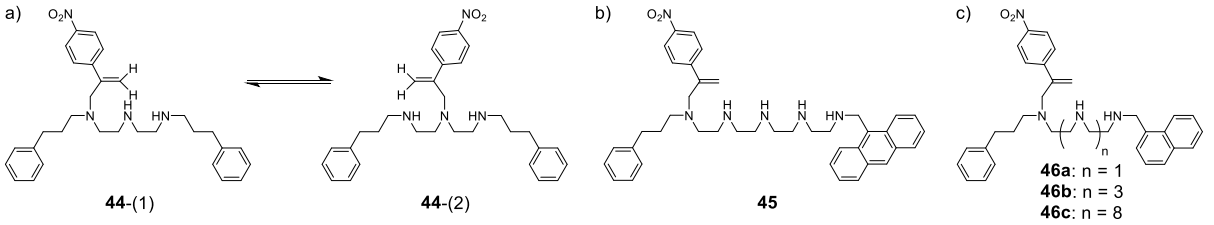

Figure 20. a) Formula and transportation of α-methylene-4-nitrostyrene between secondary amine groups. Attached footholds are shown as numbers in parentheses. b-c) Formulas of walker **45** and **46a-c** with their respective tracks.

59. A. G. Campana, A. Carlone, K. Chen, D. T. F. Dryden, D. A. Leigh, U. Lewandowska, K. M. Mullen. A small molecule that walks on-directionally along a track without external intervention. *Angew. chem. Int. Ed.* **2012**, *51*, 5480−5483.

The same group extensively studied the walking process along polyamine tracks of different length (Fig. 20c).[60] In the presence of excess base, naphthalene group at one terminal of these tracks served as a thermodynamic sink for the walker. Investigation showed that the walking process of **46a**-**b** was biased with a distribution of 67%, 46%, and 19% on the naphthalene sink.

In 2010, Leigh et al. reported a molecular walker incorporating two chemically orthogonal feet (Fig. 21).[61] The imine foot is labile under acidic condition, and can move forward or remain on the same foothold; under basic condition, the disulfide bond breaks, the foot can move one step forward or remain on the same foothold. ^{1}H NMR studies indicated that statistical thermodynamic distribution was reached after successive acid-basic cycles. A distribution of 39:36:19 on footholds **47**-(1,2), **47**-(2,3) and **47**-(3,4), respectively, was reached, with 6% isomer on foothold 1 and 4. When oxidation was used for breaking and reforming the disulfide bond, kinetically biased walking was achieved to give 43% of **47**-(3,4) isomer.[62] Reducing the length of the alkyl foot linker could bias the walker toward opposite directions due to chain strain of the (2,3) isomer.

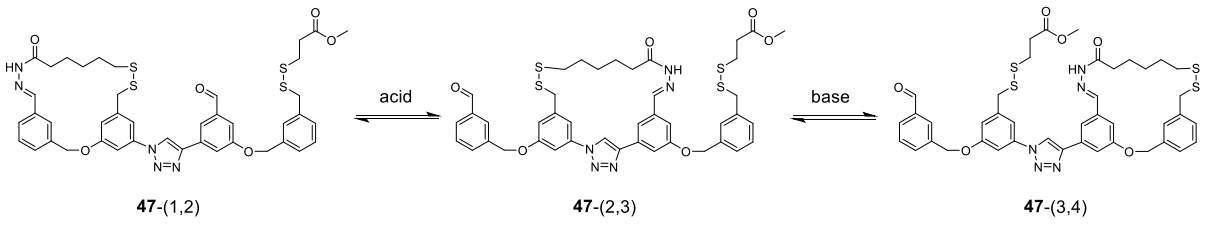

Figure 21. a) Formula and operation of the walking process of molecule walker **47** along a molecular track. Attached footholds are shown as numbers in parentheses.

Furthermore, by displacement of the central triazole track linker with a double bond, biased walking could be modulated by light.[63] *Z* conformation biased the system in favor of forward movement from *Z*-(1,2) to *Z*-(2,3) isomer. Consequent photoisomerization and acid treatment lead to the formation of *E*-3,4 isomer. A full cycle of reactions gave a distribution of 48:16:30 on foothold **48**-(3,4), **48**-(2,3), and **48**-(1,2), respectively.

60. A. G. Campana, D. A. Leigh, U. Lewandowska. One dimensional random walk of a synthetic small molecule toward a thermodynamic sink. *J. Am. Chem. Soc.* **2013**, *135*, 8639−8645.
61. M. von Delius, E. M. Geertsema, D. A. Leigh. A synthetic small molecule that can walk down a track. *Nat. Chem.* **2010**, *2*, 96−101.
62. M. von Delius,E. M. Geertsema, D. A. Leigh, D. T. D. Tang. Design, synthesis, and operation of small molecules that walk along tracks. *J. Am. Chem. Soc.* **2010**, *132*, 16134−16145.
63. M. J. Barrell, A. G. Campana, M. von Delius, E. M. Geertsema, D. A. Leigh. Light-driven transport of a molecular walker in either direction along a molecular track. *Angew. Chem. Int. Ed.* **2011**, *50*, 285−290.

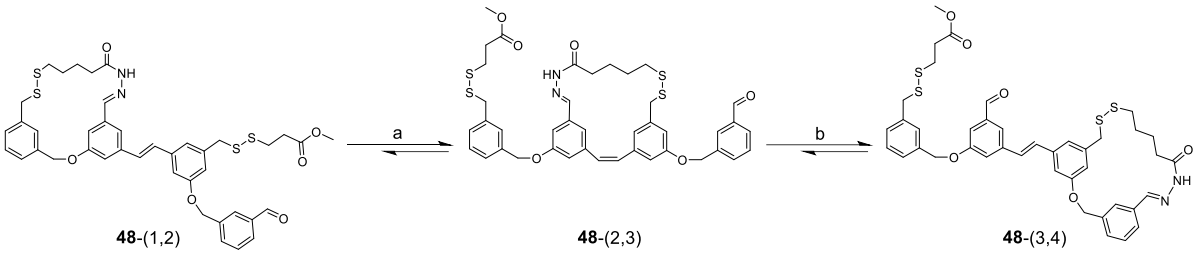

Figure 22. a) Formula and operation of the walking process of molecule walker **48** along a molecular track. Attached footholds are shown as numbers in parentheses. a) *hv* (356 nm), CD_2Cl_2; then DBU, DTT, $CHCl_3$. Equilibrium ratio: *Z*:*E* = 88:12; (2,3):(1,2) = 60:40. b) I_2, *hv* (500 nm), CD_2Cl_2; then TFA, $CHCl_3$. Equilibrium ratio: *Z*:*E* = 25:75; (3,4):(2,3) = 95:5.

Leigh et al. reported a biased motion based on dynamic metal ligand interaction.[64] 2,6-dialkyl-4-N,N-dimethylaminopyridine (foothold 1), 3,5-dialkylpyridine (foothold 2), and 2,6-dialkylpyridine (foothold 3) was sequentially integrated into a track. Initially, one foot was attached to foothold 1 through palladium(II) ligation, and the other foot to foothold 2 through platinum(II) ligation (Fig. 23a). Upon protonation with one equivalent of acid, the more basic foothold 1 was protonated at thermodynamic equilibrium. This was accompanied by the forward movement of Pd(II) foot to form complex with foothold 3 whilst the kinetically more stable Pt(II) complex remains locked. Due to the kinetic stability of metal-ligand complex, the diped distribution remained unchanged at room temperature after 30 hours. After heating at 65 ^{o}C for 48h, the diped distribution was shifted, with a ratio of 15:85 in favor of foothold 3. When deprotonation and heating was applied, the motion was reversed to go back to the initial state with a ratio of >95:5.

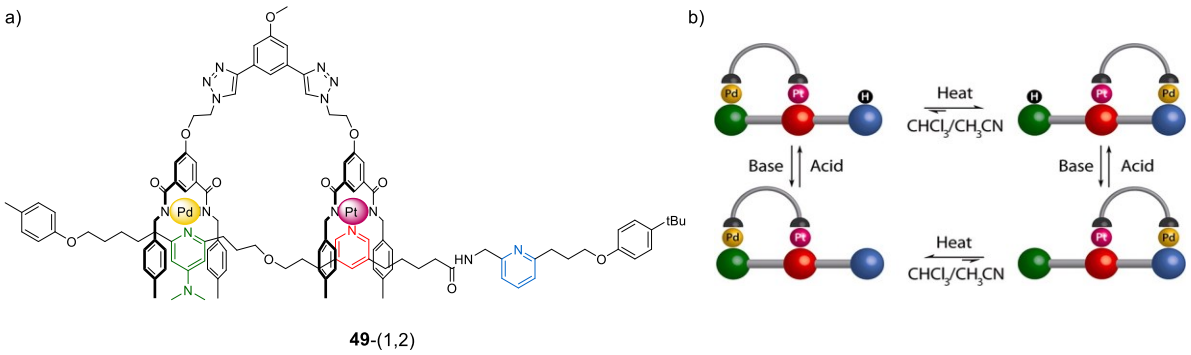

Figure 23. a) Formula and schematic representation of molecular walker **49** attached to foothold 1 (green) and foothold 2 (red). b) Schematic representation of the operation of walking process through successive acid−base addition and heating cycles.

64. J. E. Beves, V. Blanco, B. A. Blight, R. Carrillo, D. M. D'Souza, D. Howgego, D. A. Leigh, A. M. Z. Slawin, M. D. Symes. Toward metal complexes that can directionally walk along tracks: controlled stepping of a molecular biped with a palladium(II) foot. *J. Am. Chem. Soc.* **2014**, *136*, 2094−2100.

4. Conclusion

A variety of synthetic molecular machines have been reported by chemists in the past two decades. However, compared to biological system and macroscopic machines around us, these synthetic systems still lack autonomy and complexity. Most of the advanced synthetic molecular machines exploit irreversible interlocked mechanical bond to confine and drive its subcomponents towards desired direction. To unset such system after one cycle of operation requires the breakage and reconstruction of the mechanical bond, which remains synthetically inefficient (low yield, hard purification, etc.). In the meantime, integrating of multiple functional blocks into one synthetic molecular machine is still in imagination.

With these questions in mind, we propose that foldamer can be a novel tool for synthetic molecular machines. The stability of foldamer could allow it to wind around a guest to perform work in a manner resembling to macrocycles. However, to unset the system, only an unfolding/refolding process is required, avoiding synthetic effort. Moreover, due to the highly stable conformation, foldamers can tolerate a combination of functional segments without losing the overall helicity. This means that complexity can be achieved, by either chemical bond or supramolecular interaction, with relative ease and predictability.

Chapter 2

Translation of rod-like template sequences into well-defined homochiral assemblies of stacked helical oligomers

1. Introduction

At the molecular level, translation refers to the production of a new entity according to a template that has a completely different chemical composition. Just like languages, chemical information may be translated from one molecule into another. The process of translation is of utmost importance as it gives rise to structures and thus functions that may not be created otherwise. It reaches exquisite levels of efficiency in biological systems as illustrated by protein expression from mRNA templates,[1,2] or by the translation of the length of the tobacco mosaic virus RNA into the defined assembly of its protein capsid.[3] In synthetic systems, examples of molecules serving as a template to direct the synthesis of a completely different structure are numerous.[4,5,6] But general and versatile schemes in which a non-natural sequence actually encodes the information necessary to produce a completely different sequence are very few and far from being optimized.[7,8,9]

We reported previously that 7-amino-8-fluoro-2-quinolinecarboxylic acid (Q^F) based oligomers can adopt folded structures.[10] The folded structure was stabilized by electrostatic repulsions between carbonyl group and hetero atoms of the aromatic group (Fig. 1a), hydrogen bonding (Fig. 1b), and intramolecular π−π interactions between aromatic monomers. The cavity within the folded architecture was large enough for the penetration of rod like alkyl chain. By appending carbamate binding pyridine units (Fig. 1c) at the terminal of Q^F oligomer, helix-rod host-guest complexes have been shown to form upon mixing dicarbamate derived from α,ω-diaminoalkanes, and arylamide foldamers[9] that may be either single[11] or double[12] helical once wound around the rod (Fig. 2).

1. P. B. Moore, T. A. Steitz. The structural basis of large ribosomal subunit function. *Annu. Rev. Biochem.* **2003**, *72*, 813–850.
2. J. M. Ogle, V. Ramakrishnan. Structural insights into translational fidelity. *Annu. Rev. Biochem.* **2005**, *74*, 129–177.
3. K. Namba, G. Stubbs. Structure of tobacco mosaic virus at 3.6 Å resolution: implications for assembly. *Science*, **1986**, *231*, 1401–1406.
4. A. Petitjean, H. Nierengarten, A. van Dorsselaer, J.-M. Lehn. Self-organization of oligomeric helical stacks controlled by substrate binding in a tobacco mosaic virus like self-assembly process. *Angew. Chem. Int. Ed.* **2004**, *43,* 3695–3699.
5. K. Suzuki, S. Sato, M. Fujita. Template synthesis of precisely monodisperse silica nanoparticles within self-assembled organometallic spheres. *Nature Chem.* **2010**, *2*, 25–29.
6. B. Lewandowski, G. De Bo, J. W. Ward, M. Papmeyer, S. Kuschel, M. J. Aldegunde, P. M. E. Gramlich, D. Heckmann, S. M. Goldup, D. M. D'Souza, A. E. Fernandes, D. A. Leigh. Sequence-specific peptide synthesis by an artificial small-molecule machine. *Science*, **2013**,*339*, 189–193.
7. Y. He, D. R. Liu. Autonomous multistep organic synthesis in a single isothermal solution mediated by a DNA walker. *Nat. Nanotechnol.* **2010**, *5*, 778-782.
8. G. Guichard, I. Huc. Synthetic foldamers. *Chem. Commun.* **2011**, *47*, 5933–5941.
9. D.-W. Zhang, X. Zhao, J.-L. Hou, Z.-T. Li. Aromatic amide foldamers: structures, properties, and functions. *Chem. Rev.* **2012**, *112*, 5271–5316.
10. Q. Gan, C. Bao, B. Kauffmann, A. Grélard, J. Xiang, S. Liu, I. Huc, H. Jiang. Quadruple and double helices of 8-fluoroquinoline oligoamides. *Angew. Chem. Int. Ed.* **2008**, *47*, 1715–1718.
11. Q. Gan, Y. Ferrand, C. Bao, B. Kauffmann, A. Grélard, H. Jiang, I. Huc. Helix-rod host-guest complexes with shuttling rates much faster than disassembly. *Science*, **2011**, *331*, 1172–1175.
12. Y. Ferrand, Q. Gan, B. Kauffmann, H. Jiang, I. Huc. Template-induced screw motions within an aromatic amide foldamer double helix. *Angew. Chem. Int. Ed.* **2011**, *50*, 7572–7575.

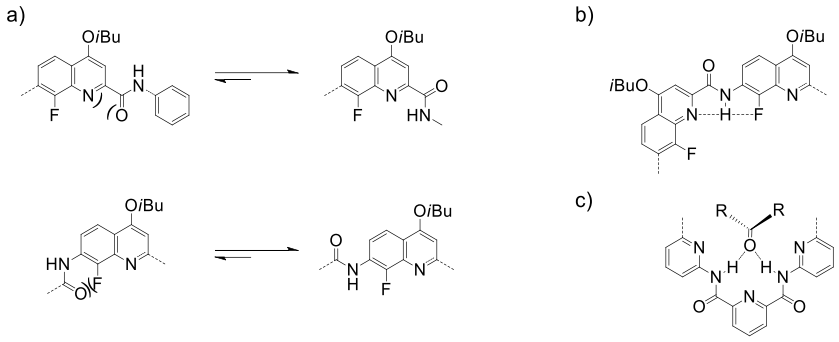

Figure 1. a) Electrostatic repulsion between carbonyl and hetero atoms of the aromatic group. b) Intramolecular hydrogen bonding between two Q^F monomer. c) Hydrogen bonding between carbonyl groups of the guest and amide protons of 2,6-pyridinedicarboxamide units.

Complex formation involves hydrogen bonding between carbonyl groups of the guest and amide protons of 2,6-pyridinedicarboxamide units of the host, located at the two ends of the single helices (Fig. 2a), or at one end of each strand of the double helices (Fig. 2b). Consequently, a strict match is required between on one hand the distance between hydrogen bond donors on the helices (*i.e.* the number of helix turns) and on the other hand the length of the alkyl chains connecting hydrogen bond acceptors on the rods.[11] In *single* helical complexes, shrinking the rod by a single CH_2 unit may result in a large or even complete loss of stability. In contrast, screw motions within the *double* helices (Fig. 2b) allow them to adjust their length and to bind to rods differing by 3 to 4 CH_2 units with comparable affinities.[12]

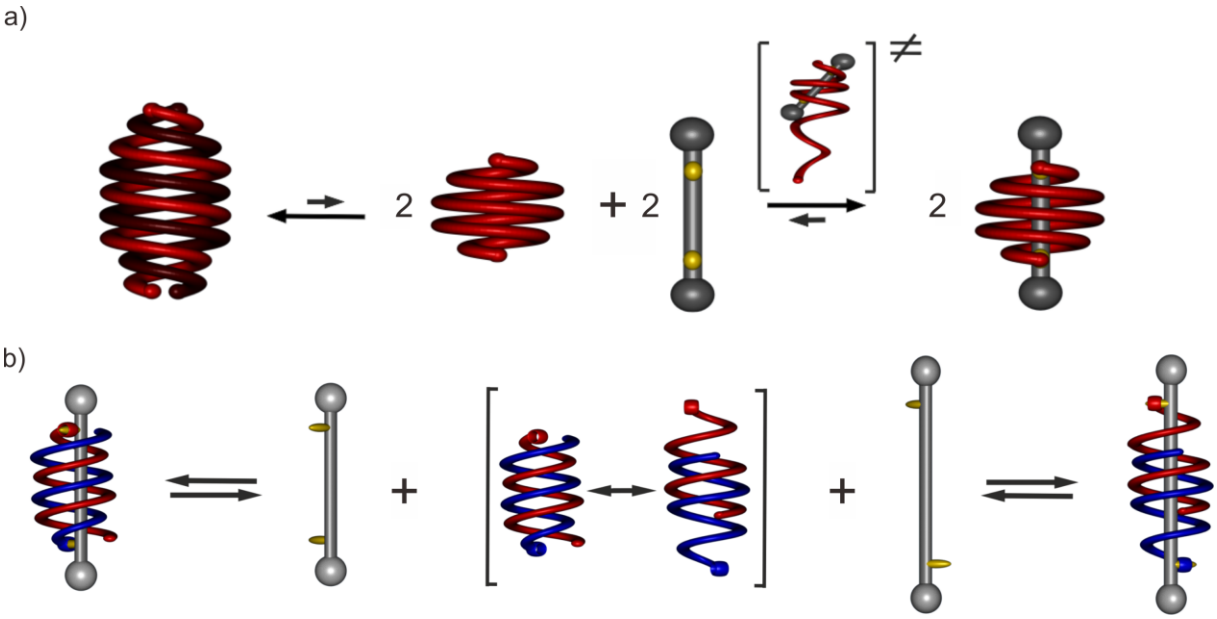

Figure 2. Schematic representation of a) the formation of single helix-rod complex through unfolding/refolding mechanism. b) screw motions of the double helices to bind different rods.

This prior knowledge hinted at the possibility to load numerous single and/or double helices, each having a defined length, on rods possessing the complementary binding stations arranged in an organized sequence, the sequence on the rods thus translating into the assembly of an organized multi-helical supramolecular polymer (Fig. 3). Translation would be facilitated by the facts that: (i) complex formation does not to require a threading mechanism, but also occurs via an unfolding of the helix and its refolding around the rod allowing error correction in the translation process. Thermodynamic products may thus form regardless of the order in which components are assembled; (ii) both single and double helices may slide along the rods and find their best binding station without dissociating.[11,12]

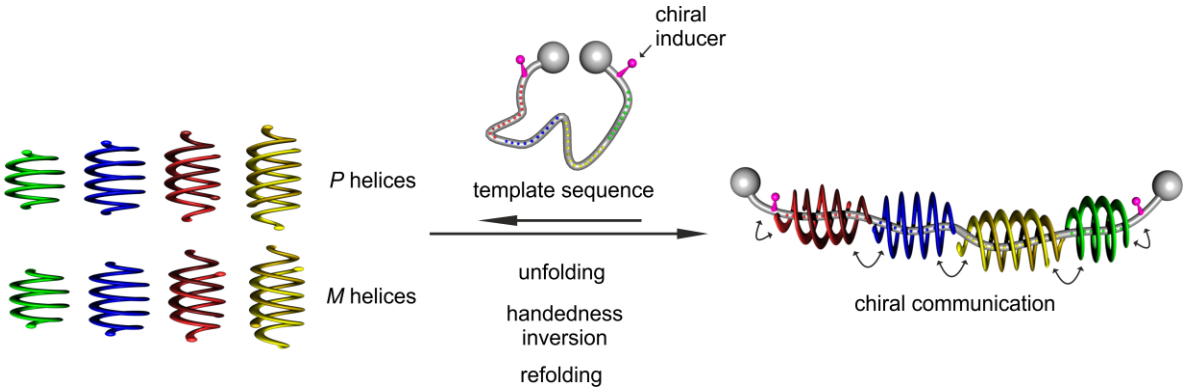

Figure 3. Schematic representation of the controlled homochiral assembly of single and double stranded helices of various length onto a long dumbbell shape template possessing complementary binding stations for each helix and terminal stereogenic centers.

In this chapter, together with the endeavor of former group member Dr. Quan Gan, previously described oligomers **1**, **2** and **4** along with longer oligomers **3**, **5**, **6** (Fig. 4) were synthesized. The stability of host-guest complexes as a function of guest length was firstly established using single station rods, followed by the investigation of handedness induction from stereogenic centers on the rod to the helical host.

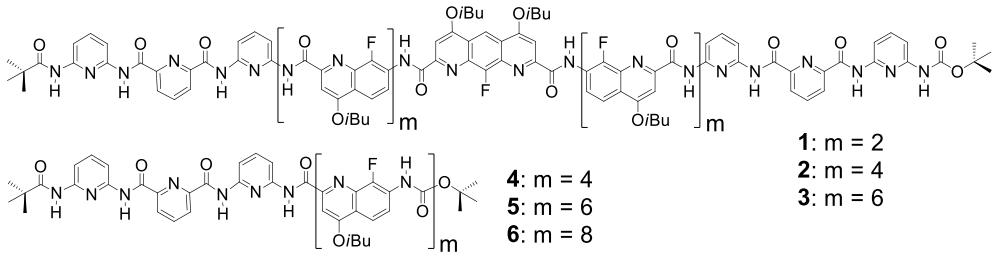

Figure 4. Formulas of aromatic oligoamides forming single helical **1-3** and double helical **4-6** host-guest helix-rod complexes.

Furthermore, we present the high-fidelity enzyme-free translation of long rod-like alkylcarbamate oligomers into well-defined sequences of stacked helical aromatic oligoamides each of which possibly differing by its length, its single or double helical state, and its right (*P*) or left (*M*) handedness (Fig. 3). This translation enables the production of very large (> 20 kDa) abiotic artificial folded architectures (i.e. foldamers[11]) that may, for example, serve as scaffolds to organize appended functional features at positions in space defined with atomic precision across nanometric distances.

2. Synthesis

2.1 Synthesis of foldamers

Four different units were used for the synthesis of all foldamers: 2,6-diaminopyridine and 2,6-pyridinedicarboxylic acid (P),[13,14,15] 7-amino-8-fluoro-2-quinolinecarboxylic acid (Q^F),[16] and 1,8-diaza-9-fluoro-2,7-anthracene-dicaboxylic acid (A^F)[17]. Local preferential conformation at aryl-amide linkages and intramolecular interaction between aromatic groups give rise to stable helical structures, and a void was formed by the fluoroaromatic units. This void allows the interpenetration of an alkyl chain, whilst each terminal 2,6-pyridinedicarboxamide units anchor a carbamate group via hydrogen bonding[11,12].

For double helix host-guest formation foldamers, the target compound can be obtained by simply coupling the amine precursor with the acid chloride of a $\mathbf{Q^F_2}$ dimer **28**, as the scheme for the synthesis of **6** shows (Scheme 1a).

Concerning the synthesis of the symmetrical single helical host-guest formation foldamers, convergent rules are followed to minimize the reaction steps. Foldamer **3**, for example, was synthesized by coupling amine **26** with $\mathbf{A^F}$ diacid chloride **27** (Scheme 1b).

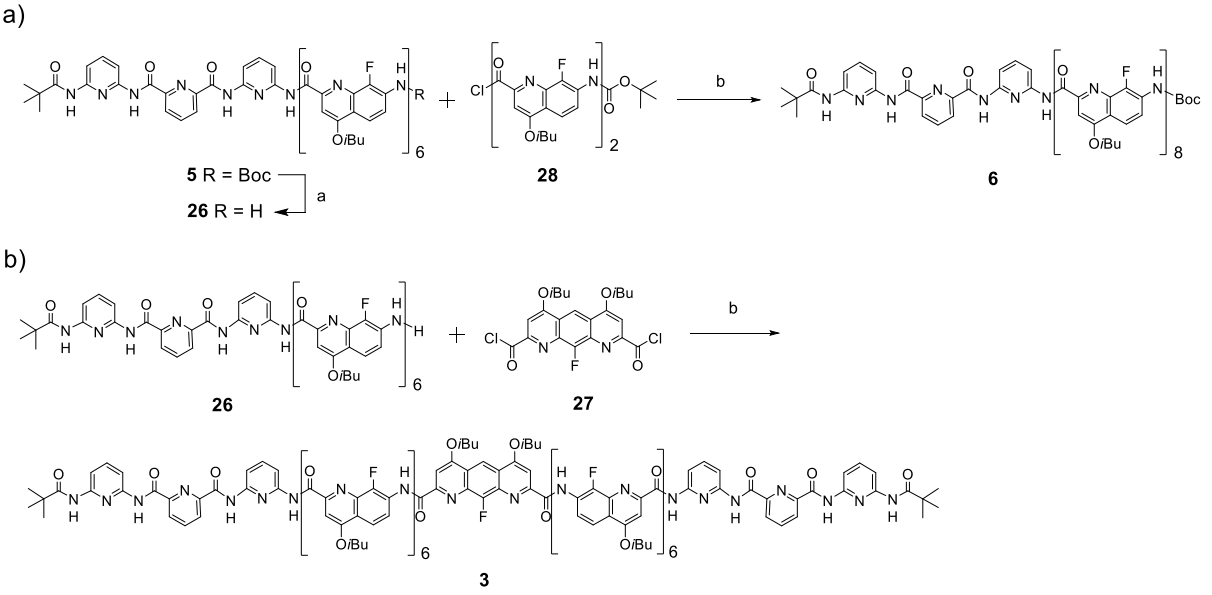

Scheme 1. Synthesis of foldamers **6** and **3**: a) TFA, CH_2Cl_2, room temperature, 6 h; b) DIEA, $CHCl_3$, room temperature, 12 h.

13. V. Berl, I. Huc, R. Khoury, J.-M. Lehn. Helical molecular programming. folding of oligopyridine -dicarboxamides into molecular single helices. *Chem. Eur. J.* **2001**, *7*, 2798–2809.
14. V. Berl, I. Huc, R. Khoury, J.-M. Lehn. Helical Molecular programming. Supramolecular double helices by dimerization of helical oligopyridine-dicarboxamide strands. *Chem. Eur. J.* **2001**, *7*, 2810–2820.
15. B. Baptiste, J. Zhu, D. Haldar, B. Kauffmann, J.-M. Léger, I. Huc. Hybridization of long pyridine -dicarboxamide oligomers into multi-turn double helices: slow strand association and dissociation, solvent dependence, and solid state structures. *Chem. Asian J.* **2010**, *5*, 1364–1375.
16. Q. Gan, C. Bao, B. Kauffmann, A. Grélard, J. Xiang, S. Liu, I. Huc, H. Jiang. Quadruple and double helices of 8-fluoroquinoline oligoamides. *Angew. Chem. Int. Ed.* **2008**, *47*, 1715–1718.
17. C. Bao, B. Kauffmann, Q. Gan, K. Srinivas, H. Jiang, I. Huc. Converting sequences of aromatic amino acid monomers into functional three-dimensional structures: second-generation helical capsules. *Angew. Chem. Int. Ed.* **2008**, *47*, 4153–4156.

2.2 Synthesis of guests

Following the same strategy for achiral rods[11,12], all couplings were done with *p*-nitrophenyl chloroformate as the coupling reagent. Single station rods **15**-(*R*,*R*) were obtained by directly activating (*R*)-1-phenylethanol with *p*-nitrophenyl chloroformate and subsequently coupling with 0.5 equivalent of diamine.

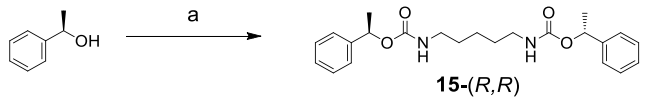

Scheme 2. Synthesis of chiral guests. a) 4-nitrophenyl chloroformate, Et_3N, CH_2Cl_2, room temperature, 0.5 h, then 1,5-diaminopentane (0.5 equiv.), room temperature, 12 h.

For the synthesis of multistation rods, commercially available chiral alcohol precursors (*R*)-(+)-1-phenylethanol and (*R*)-(+)-1-(1-naphthyl)ethanol were activated with *p*-nitrophenyl chloroformate, and subsequently reacted with excess corresponding diamines to afford the mono amine **29** and **31**. Then compound **29** was activated with *p*-nitrophenyl chloroformate, and the resulting intermediate was refluxed with excess ethylene glycol in chloroform to give **30** with an alcohol terminus. At last, **30** was activated with *p*-nitrophenyl chloroformate and coupled with **31** to afford the two station rod **25**-(*R*,*R*). The synthetic details of other rods are described in section 5.4.

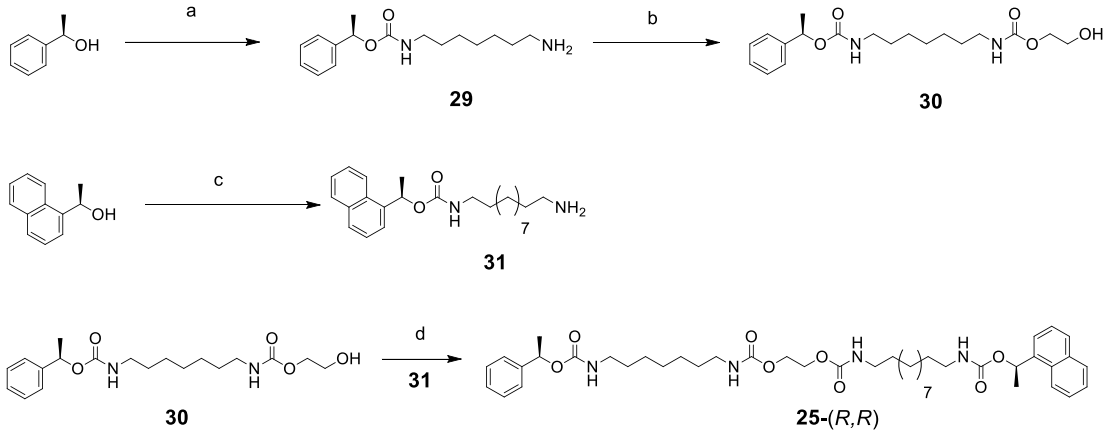

Scheme 3. Synthesis of chiral guests **25**-(*R*,*R*). ; a) 4-nitrophenyl chloroformate, Et_3N, CH_2Cl_2, room temperature, 0.5 h, then 1,7-diaminoheptane (5 equiv.), room temperature, 12 h; b) 4-nitrophenyl chloroformate, Et_3N, $CHCl_3$, room temperature, 3 h, then ethylene glycol (50 equiv.), refluxed, 24 h; c) 4-nitrophenyl chloroformate, Et_3N, CH_2Cl_2, room temperature, 24 h, then 1,11-diaminoundecane (5 equiv.), room temperature, 12 h; d) 4-nitrophenyl chloroformate, Et_3N, CH_2Cl_2, room temperature, 12 h, then **31**, room temperature, 12 h.

3. Results and discussion

3.1 Double helix formation of foldamers

Like shorter foldamers **1**, **2**, and **4**, [11,12] elongated sequences **3, 5,** and **6** also have the tendency to form double helix in solution. When oligomer **6** was dissolved in $C_2D_2Cl_4$**,** the dimerization finished before the first NMR can be done, resulting in broad peaks in amide region (Fig. 5a). However, upon rising temperature from 298K to 353K, a new set of peaks appeared at low field (Fig. 5b), which can be identified as signals of single helix having slow exchange with double helix. Whilst the dimerization kinetics of oligomer **6** is extremely fast, it took days for oligomer **3** to reach single/double helix equilibrium at 298K. Based on the signal intensity of single helix and double helix, the dimerization constants in $C_2D_2Cl_4$ at 353K can be calculated (7.5×10^3 L mol^{-1} for **3**, 1.0×10^4 L mol^{-1} for **5**, 1.8×10^4 L mol^{-1} for **6**, respectively). The increased dimerization constant from **4** to **6** can be explained by the fact that increasing the number of Q^F unit strengthens the π-π interaction in the double helix. But the tendency is reversed with foldamers **1**-**3**. This is probably due to the fact that the narrower termini of oligomer **1**-**3** hindered the interaction of central Q^F sequence. While the elongation of the foldamer can increase the π-π interaction between two helices, this increase is not large enough to compensate the π-π interaction lose caused by the extension of the helices to intercalate each other.

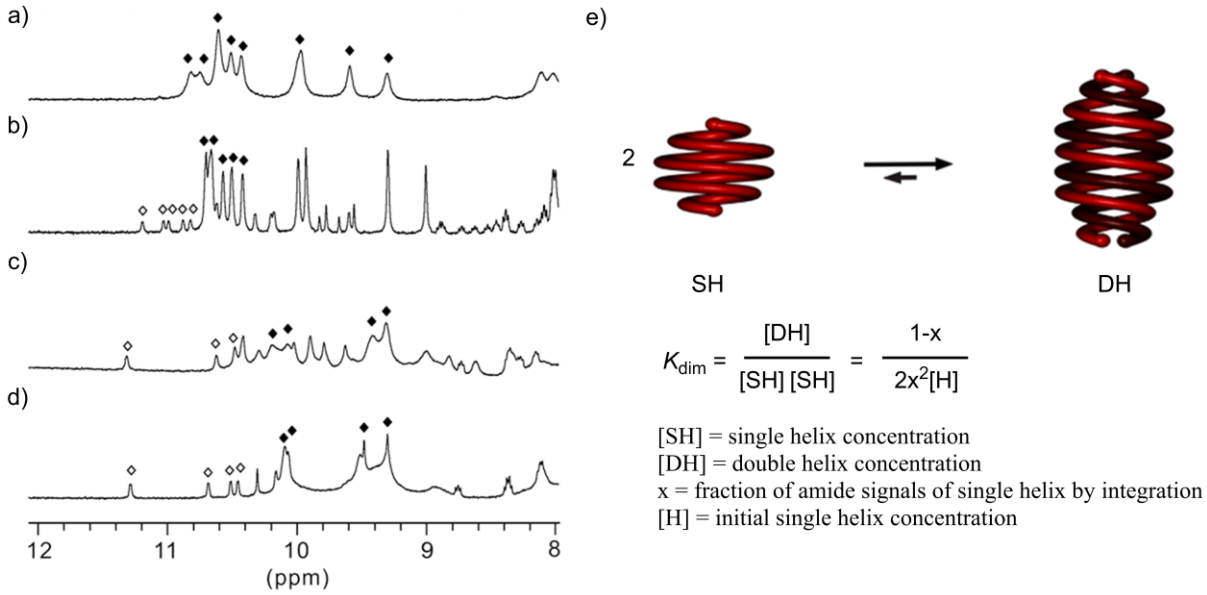

Figure 5. Excerpts of the ^{1}H NMR spectra in $C_2D_2Cl_4$ (400 MHz) of: a) **6** (2 mM) at 298K; b) **6** (2 mM) at 353K; c) **3** (2 mM) at 298K and d) **3** (2 mM) at 353K. Amide signals of the double helix are marked with black diamonds whereas those of the single helix which are in slow exchange on the NMR timescale are denoted with white diamonds. e) Scheme of calculation of the dimerization constant K_{dim}.

3.2 The thermodynamics of the foldamer-guest complex

Helix-rod complexes have been previously shown to form upon mixing dicarbamates derived from α,ω-diaminoalkanes and foldamers that may be either single[11] or double[12] helical once wound around the rod (Fig. 2). In addition to previously described oligomers **1**, **2**, and **4**, the stability of newly synthesized longer oligomers **3**, **5**, **6** towards single station rods **7**-**12** were investigated.

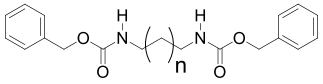

7: n = 3 **8**: n = 4 **9**: n = 5 **10**: n = 6
11: n = 7 **12**: n = 8 **13**: n = 9 **14**: n = 10

Figure 6. Formulas of single station rods **7**-**14**.

When guest **9** was added to the solution of single helix foldamer **3**, a new set of NMR signals appeared which can be attributed to the helix-rod complex in slow exchange with the free helix (Fig. 7a-d). The relative intensity of the signals of the free single helix and host-guest complex represents the molar ratio of the corresponding species in solution. Since the dimerization kinetics of **3** is extremely slow, thermodynamic equilibrium between foldamer **3** and guest **9** is reached prior to the formation of double helix. Thus, by applying equation 2 (Fig. 7e), the binding constants between **3** and **9** can be obtained as 3.87×10^5 L mol^{-1}.

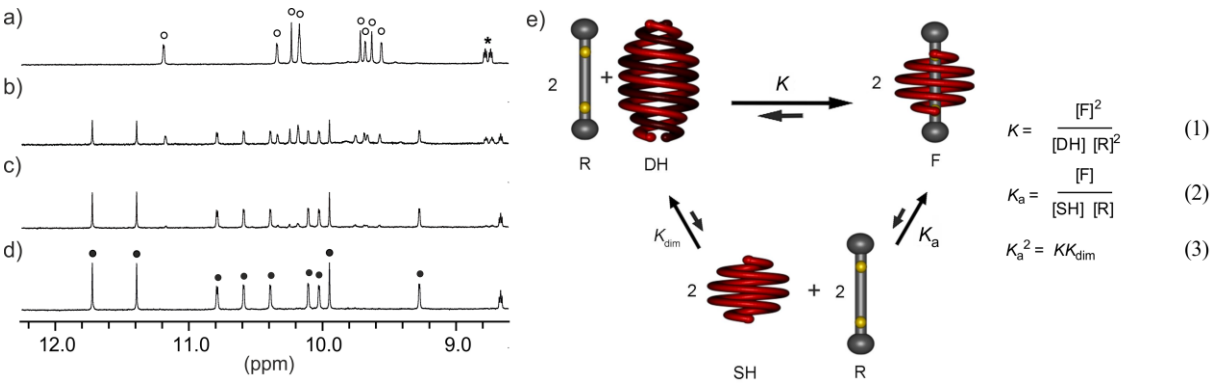

Figure 7. Part of the ^{1}H NMR spectrum of the amide region (700 MHz) at 298K of **3** (0.1 mM) in $CDCl_3$ in the presence of: a) 0 equiv.; b) 0.5 equiv.; c) 1 equiv.; d) 2 equiv. of rod **9**. Signals of the free **3** single helix and of complex **3**⊃**9** are marked with empty and black circles, respectively. Some aromatic resonances are denoted with stars. e) Schematic representation of the overall equilibrium between the single, double helix and the complex and the calculation of binding constant. [F] = foldaxane concentration; [R] = rod concentration; [SH] = single helix concentration; [DH] = double helix concentration; K = the equilibrium constant of host-guest complex between double helix and complex; K_a = the equilibrium constant of host-guest complex between single helix and complex; K_{dim} = the dimerization constant. $K_a = 3.87 \pm 0.04 \times 10^5$ L mol^{-1}.

Unlike the sharp peaks of free single helix **3**, free double helix (**6**)$_2$ gave broad peaks due to screwing motion within the double helix and antiparallel-parallel exchange. However, upon

addition of guest **13** to the double helix solution, a new set of sharp peaks appeared, indicating the formation of helix-rod complex (Fig. 8a-d). The sharp peaks suggest that the complex is rather stable and is in slow exchange with the free double helix. Using equation 4 (Fig. 8e), the binding constant can be drawn from the integration of signals of free double helix and complex.

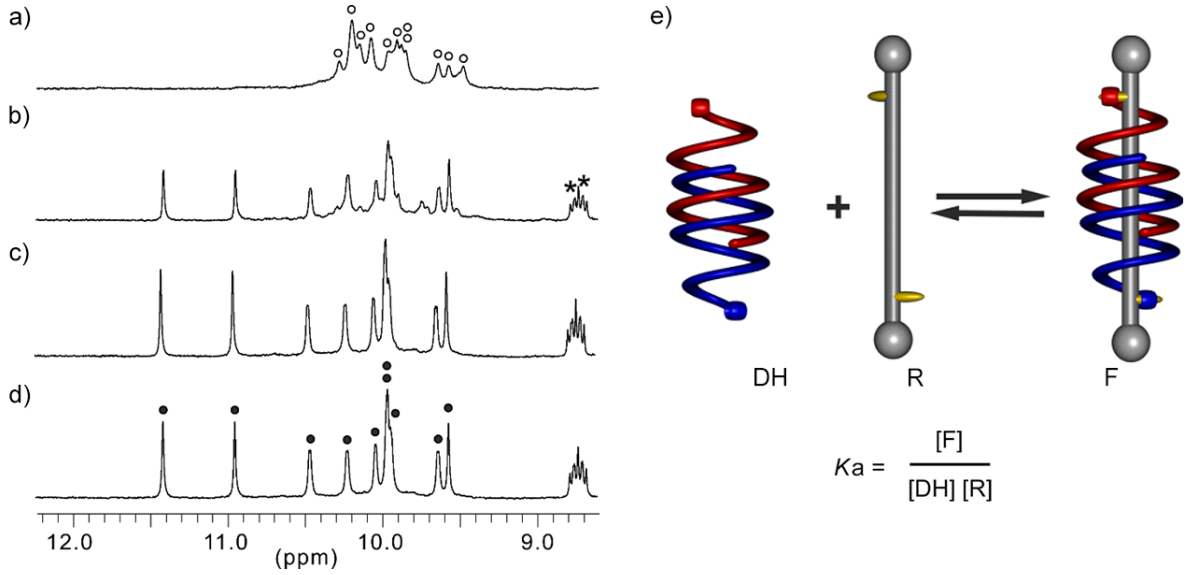

Figure 8. Part of the ^{1}H NMR spectrum (400 MHz) of the amide region at 298K of **6** (4 mM) in $CDCl_3$ in the presence of: a) 0 equiv.; b) 0.5 equiv.; c) 1 equiv. and d) 2 equiv. of rod **13**. Signals of the free parallel and antiparallel double helix $(\mathbf{6})_2$ and of complex $(\mathbf{6})_2\supset\mathbf{13}$ signals are marked with empty and black circles, respectively. An aromatic resonance is denoted with a star. e) Schematic representation of the overall equilibrium between the double helix and the complex and the calculation of binding constant. [F] = foldaxane concentration; [R] = rod concentration; [DH] = double helix concentration; K_a = the equilibrium constant of host-guest complex between double helix and complex. $K_a = 2.9 \times 10^4$ L mol^{-1}.

The binding constants of different foldamers towards rods with varied alkyl length were thus measured (Table 1). Since the driving force for complex formation is the anchoring of carbamate groups on the rod by peripheral 2,6-pyridinedicarboxamide units via hydrogen bond, the number of CH_2 unit between the terminal carbamate groups effects the stability of the complex. Whilst the rigidity of single helix implies that a single CH_2 unit change of the rod may result in a large or even complete loss of stability, the screw motion within the double helices allowed the tolerance of rods differing by 3 to 4 CH_2 units with comparable affinities.[11,12]

Table 1. Titration of oligomers by different dumbbell molecules monitored by ^{1}H NMR in $CDCl_3$. Dashes reflect no measurable affinity of the oligomers for the rods. All experimental errors < 5%. SH and DH stand for single and double helix, respectively.

	38 (*3 CH_2*)	**39** (*4 CH_2*)	**7** (*5 CH_2*)	**8** (6 CH_2)	**9** (7 CH_2)	**10** (8 CH_2)	**11** (9 CH_2)	**12** (10 CH_2)	**13** (11 CH_2)	**14** (12 CH_2)
1 (SH)	1×10^3 (± 40)	90 (± 3)	< 1	-	-	-	-	-	-	-
2 (SH)	-	45 (± 2)	3.1×10^4 (± 1000)	2.2×10^4 (± 300)	140 (± 5)	-	-	-	-	-
3 (SH)	-	-	< 1	1.4×10^4 (± 100)	3.87×10^5 (± 4000)	3.8×10^4 (± 1000)	4.2×10^4 (± 600)	840 (± 30)	< 1	-
4 (DH)	55	20	140	35	-	-	-	-	-	-
5 (DH)	-	-	65	2×10^3	550	2.8×10^3	160	< 1	-	-
6 (DH)	-	-	-	97	720	3.7×10^3	2.7×10^4	4.5×10^3	2.9×10^4	5×10^3

3.3 Chiral rod to helix handedness induction

A major unsolved problem was the control of helix handedness. In the absence of translation of chiral information from the rod into preferred handedness of the helix hosts, and in the absence of end-to-end helix-helix handedness communication between contiguous helices on the rod, the loading of numerous helices would only yield complex mixtures of diastereomeric helix arrangements.

First, we endeavored to control helix handedness using stereogenic centers on the rod. After 0.5 hour of addition of guest **15**-(*R,R*) to a solution of foldamer **2**, NMR suggests that the helix-rod complex is the dominant species. But, the existence of two distinct peaks in the pivaloyl region means that two kinds of helix-rod complex formed, namely the homochiral complex and heterochiral complex (Fig. 9a). When thermodynamic equilibrium was reached, the peak corresponding to heterochiral complex decreased dramatically (Fig. 9b), indicating that with two chiral phenethyl group the chiral induction is very effective. Based on the intensity of pivaloyl peaks, the diastereomeric excess (*d.e.* = ([*P* helix] - [*M* helix]) / ([*P* helix] + [*M* helix]) × 100. *i.h*. stands for induced handedness (*P* or *M*).) was calculated to be 93%.

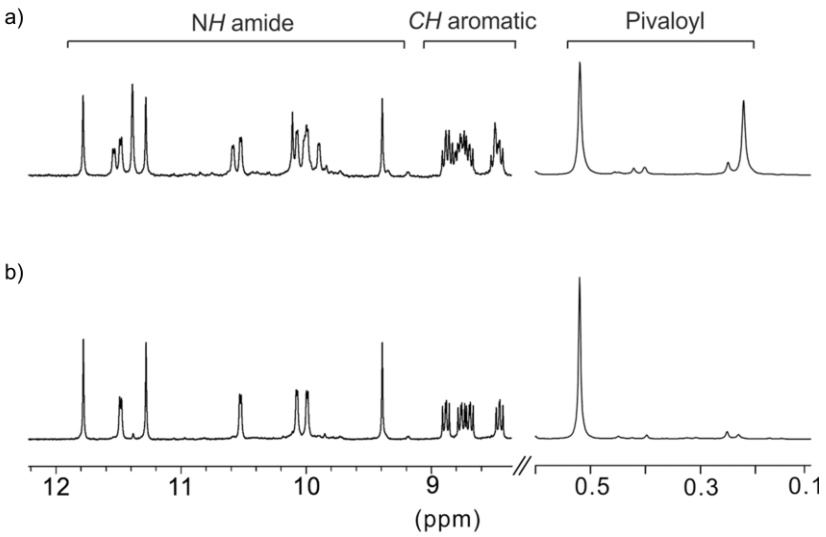

Figure 9. Representative 300 MHz NMR spectra of **2** (1 mM) with 2 equiv. of **15**-(*R,R*) (2 mM) in $CDCl_3$ after: a) 0.5 hours; b) 3 days (at equilibrium). The diastereoselectivity (*d.e.*) was calculated to be 93% based on the integration of the pivaloyl resonances.

The host-guest complexes of a series of rods having one helix binding station and bearing one or two terminal chiral group were investigated with corresponding single or double helical foldamer of matching length. Handedness induction efficiency was moderate when the rod possessed a single chiral group (**3**⊃**17**, *d.e.* = 35%, Fig. 10a). Handedness induction was also moderate when the host was a double helix (**5**⊃**16**, *d.e.* = 56%, Fig. 10c). Using a chiral terminal naphthylethyl group gave rise to similar handedness induction (**3**⊃**18**, *d.e.* = 38%, Fig. 10b and **6**⊃**19**, *d.e.* = 64%, Fig. 10d).

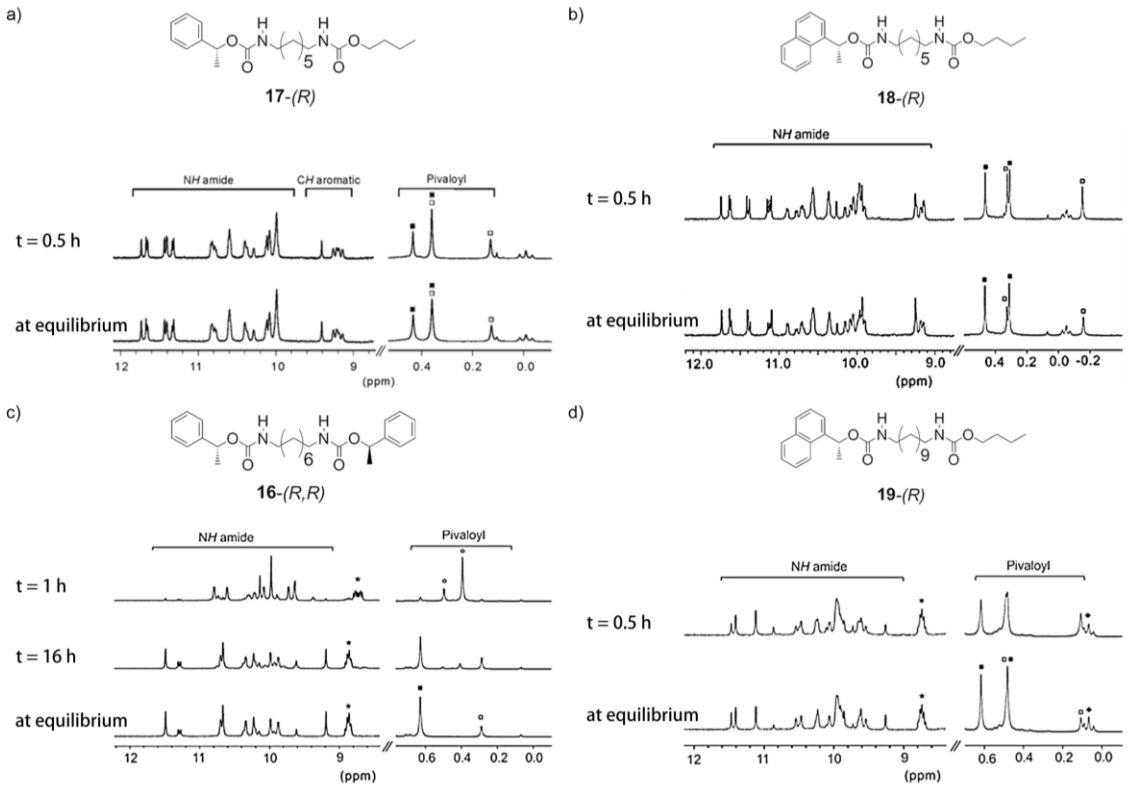

Figure 10. Representative 300 MHz NMR spectra of oligomers with corresponding chiral rods at 298K in $CDCl_3$. a) **3** (1 mM) with 2 equiv. of **17**-*R* (2 mM), *d.e.* = 35%; b) **3** (1 mM) with 2 equiv. of **18**-(*R)* (2 mM), *d.e.* = 38%; c) **5** (4 mM) with 2 equiv. of **16**-(*R,R*) (4 mM), *d.e.* = 56%; d) **6** (2 mM) with 2 equiv. of **19**-(*R*) (2 mM), *d.e.* =64%. Empty circles denote the pivaloyl protons of free single and double helix **5**; Pivaloyl signals of *M* conformation host-guest complexes are marked with black squares whereas whereas those of *P* conformation host-guest complexes are denoted with white squares. Stars (*) denote some aromatic resonances whereas the terminal methyl group of the bound guest is marked with a black diamond.

The induced handedness of foldamer **2** by **15**-(*R,R*) resulted in a strong negative circular dichroism (CD) band at 342 nm whilst the (*S,S*) enantiomer induced a positive band (Fig. 11).

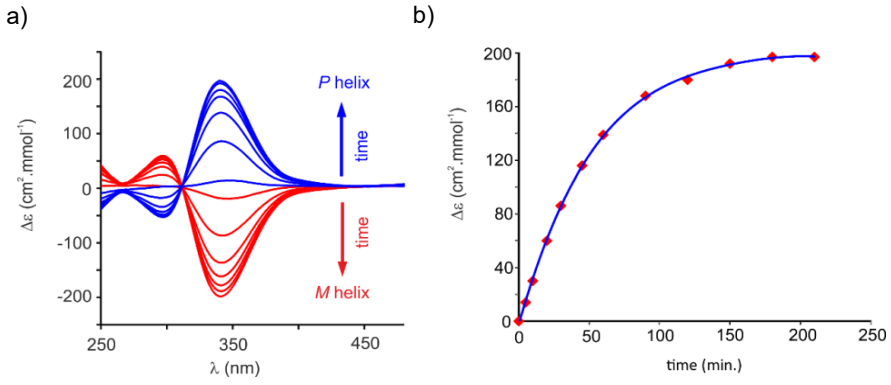

Figure 11. a) Circular dichroism spectra of **2** (20 μM) in $CDCl_3$ at 313K at different time intervals after the addition of 3 equiv. of **15**-(*S,S*) (blue) or **15**-(*R,R*) (red). b) Time trace of the CD intensity shown in function of the time (blue curve) monitored at 341 nm.

In all cases, *R* conformation on the rod gave a negative CD band (Fig. 12a), indicating the rise of same handedness for different oligomers. A crystal structure of the **2**⊃**15** complex (Fig. 12b) allowed to unambiguously assign *M* helicity as being favored by (*R*,*R*) chirality on the rod.

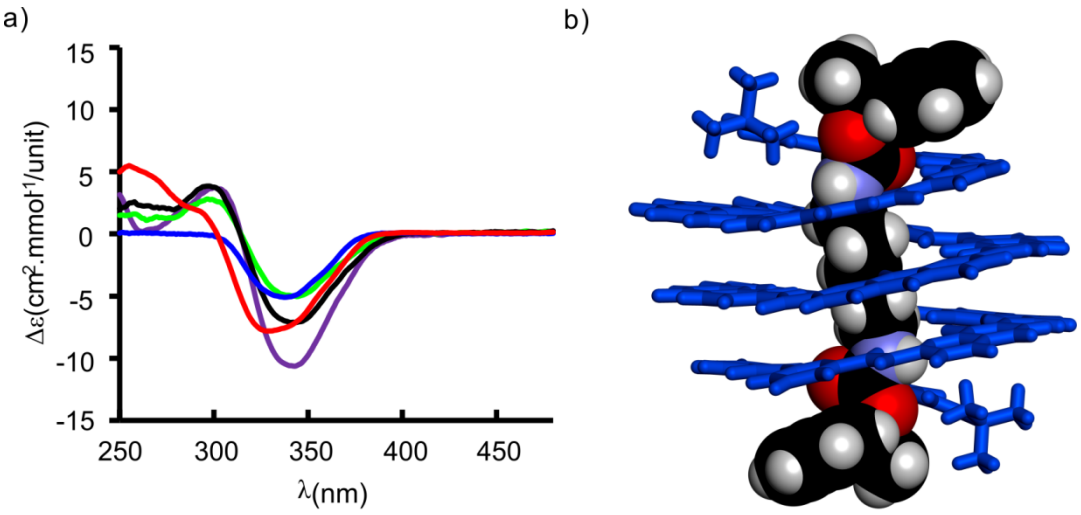

Figure 12. a) CD spectra in $CHCl_3$ (298K) at equilibrium of: 15mer **2** (20 μM) and of 2 equiv. of **15**-(*R,R*) (purple spectrum); 19mer **3** (20 μM) and of 2 equiv. of **17**-(*R*) (green spectrum);19mer **3** (20 μM) and of 2 equiv. of **18**-(*R*) (black spectrum); **5** (300 μM) and 8 equiv. of **16**-(*R,R*) (blue spectrum); **6** (40 μM) and 2 equiv. of **19**-(*R*) (red spectrum). b)Tube (helix) and CPK (rod) representation of the solid state crystal structure of *P*-**2**⊃**15**-(*S,S*). Side chains (O*iBu* groups) and included solvent molecules have been removed for clarity.

3.4 Handedness communication between homo multihelices

We assessed helix-helix end-to-end handedness communication when multiple helices were loaded on a multistation rod. Initial attempts using the double helix $(\mathbf{4})_2$ as a host showed that its affinity for guests of matching length was too low to achieve quantitative binding of several stations on a single rod at low mM concentration. Longer oligomer **5** was thus prepared and shown to bind as a double helix to single station rod **20** with high affinity (1700 M^{-1} in $CDCl_3$ at 298 K). The crystal structure unambiguously showed the formation of **20**⊃$(\mathbf{5})_2$ as displayed in Figure 13b.

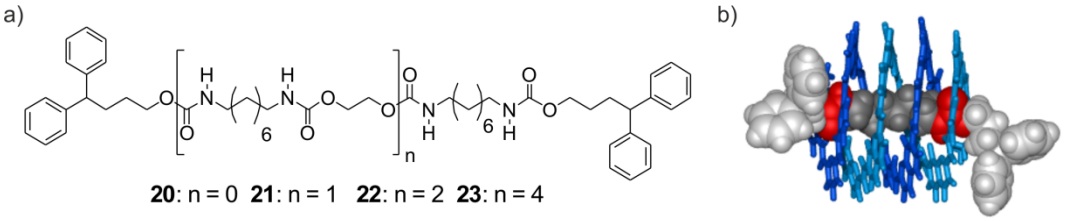

Figure 13. a) Formulas of oligocarbamate guest template sequences **20**, **21**, **22**, and **23**. b) crystal structure of **20**⊃$(\mathbf{5})_2$ (side view) in CPK and tube representations for the rod and the double helix, respectively. Side chains (O*iBu* groups) and included solvent molecules have been removed for clarity

Rods **21**-**23** possess 2, 3 and 5 binding stations each having a length identical to that of **20** and may in principle bind to 2, 3 or 5 duplexes $(\mathbf{5})_2$, respectively. The stations are separated by an ethylene glycol spacer which plays a critical role in the design. Too short a spacer would cause steric hindrance between duplexes $(\mathbf{5})_2$ bound to contiguous stations resulting in negative binding cooperativity and eventually in unoccupied stations. Too long a spacer and the absence of contacts between adjacent duplexes would result in the absence of helix handedness communication, giving rise to complex mixtures of diastereomeric aggregates.

Indeed, [5]foldaxane **21**⊃$(\mathbf{5})_4$ may exist as a pair of enantiomers *PP*/*MM* or as a *PM meso* species. Similarly, [7]foldaxane **22**⊃$(\mathbf{5})_6$ may exist as three distinct pairs of enantiomers and [11]foldaxane **23**⊃$(\mathbf{5})_{10}$ as ten pairs of enantiomers.

1. *PPPPP/MMMMM*	2. *PPPPM/PMMMM*
3. *PMPPP/MPMMM*	4. *PPMPP/MMPMM*
5. *PPPMM/PPMMM*	6. *PMMPP/MPPMM*
7. *PMPMP/MPMPM*	8. *MPPPM/ PMMMP*
9. *PPMPM/MMPMP*	10. *PMPPM/MPMMP*

Table 2. List of theoretical diastereoisomers which can form for $(\mathbf{5})_{10}$⊃**23**. The list consists of ten pairs of enantiomers, *PPPPP/MMMMM* proving to be the most stable.

However, upon mixing $(\mathbf{5})_2$ with **21**, **22** or **23**, ^{1}H NMR initially showed complex patterns which simplified over time, eventually resulting in the emergence of a major species. Integration of the rod and helix signals allowed to establish the expected stoichiometry corresponding to binding of helices to all stations on each rod (Fig. 14a-e).

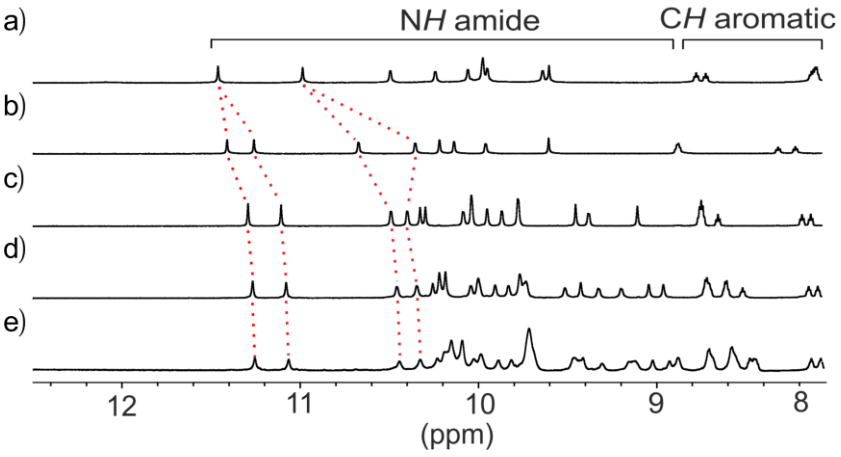

Figure 14. Part of the 700 MHz ^{1}H NMR in $CDCl_3$ (0.25 mM) showing the amide and some aromatic resonances of a) $(\mathbf{5})_2$; b) **20**⊃$(\mathbf{5})_2$; c) **21**⊃$(\mathbf{5})_4$; d) **22**⊃$(\mathbf{5})_6$; e) **23**⊃$(\mathbf{5})_{10}$. Red dashes illustrate the shielding of terminal aromatic amide protons.

In the case of **21** and **22**, the major species was unambiguously identified in the solid state by X-ray crystallography as being racemic homohelical **21**⊃(**5**)$_4$ and **22**⊃(**5**)$_6$, in which all helices on a given rod have the same handedness (Fig. 15b,d). Thus, contacts between helices having a "like" handedness are more favorable than contacts between helices having an "unlike" handedness, resulting in the translation of the sequence of stations on the rods into a well-defined arrangement of helical aromatic oligoamides. It was assumed that the same rule holds true for **23**⊃(**5**)$_{10}$ of which a molecular model was built showing a 9 nm long structure (Fig. 15f). Single crystals of this very large complex (21 kDa) could also be obtained, but diffraction intensity was too weak to resolve the structure.

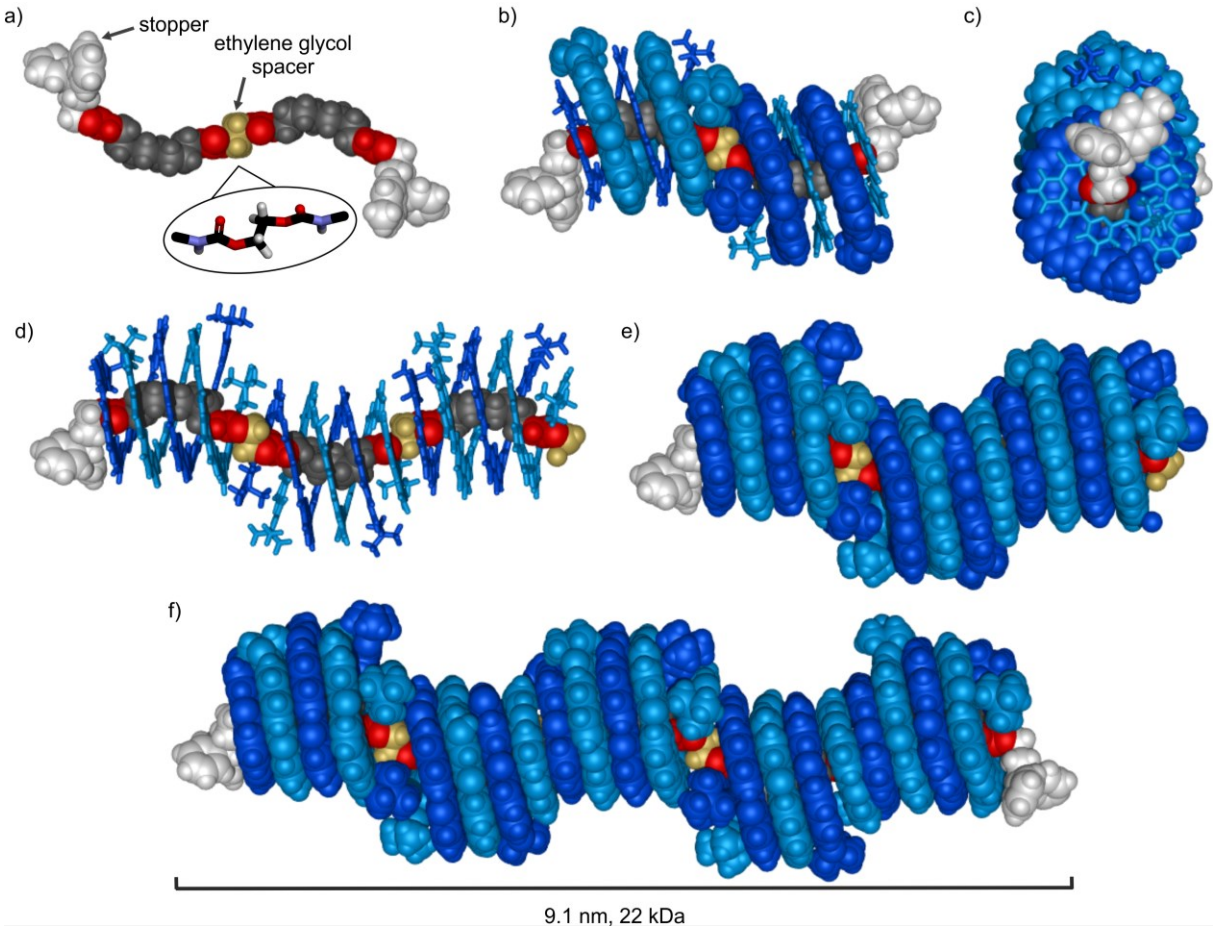

Figure 15. Structures in the solid state analyzed by single crystal X -ray crystallography of: a) rod **21**; b) **21**⊃(**5**)$_4$ (side view) in CPK and tube/CPK representations for the rod and the double helix, respectively; c) **21**⊃(**5**)$_4$ (top view); d) **22**⊃(**5**)$_6$ (side view) in CPK and tube representations for the rod and the double helix, respectively. e) **22**⊃(**5**)$_6$ in full CPK representation. f) Energy minimized molecular model using the Merck Molecular Force Field static (MMFFs) of the structure of **23**⊃(**5**)$_{10}$. In (b-f) isobutoxy side chains and included solvent molecules were omitted for clarity. The rods **20**, **21**, **22** and **23** are shown as CPK representations whereas the helices (**5**)$_2$ are shown as light blue/blue tube or CPK representations. Only the all *P* helical isomers are shown. The structures belong to centrosymmetrical space groups and thus also contain the all *M* isomers.

The crystal structures of **21**⊃(**5**)$_4$ and **22**⊃(**5**)$_6$ revealed direct face-to-face π-π contacts between the helices. At each station, the alkyl moiety of the rod is slightly bent which makes its two ends protrude from the helix at an angle. In contrast, the rods adopt a linear conformation at helix-helix junctions where a "like" handedness permits the same tilt angle of each helix with respect to the rod. This alternation of linear and bent segments of the rods gives rise to an undulated shape of the multi-helical aggregates.

The translation of sequences of stations on the rods into well-defined homohelical arrays of aromatic oligoamides is to be compared to other complexes between rods and multi-helical (or macrocyclic hosts) in which no communication between the hosts took place.[18,19,20,21] Efficient helix-helix end-to-end handedness communication induced by self-assembly onto a rod relates to the piling up of helices to form columnar aggregates in the solid state where the preferred contacts may be either of "like"[22,23,24] or "unlike"[25] handedness. It also relates to side-by-side helix-helix handedness communication.[26,27]

3.5 Handedness communication between hetero helices

With rod-helix and helix-helix chiral communication in hand, we took a further step to integrate all types of information that a rod may contain to be translated into an organized sequence of helices: chiral groups to control absolute helix handedness, multiple stations to bind to multiple helices, different stations to bind to different helices, *e.g.* a single and a double helix.

Rods **24** and **25** possess two distinct and long stations to ensure a high thermodynamic stability of their complexes with the matching helices, separated by an ethylene glycol spacer to induce helix-helix end-to-end handedness communication. A terminal phenethyl group is placed next to a station complementary to the single helix of **3**, and a terminal naphthylethyl group is placed next to a station complementary to the duplex (**6**)$_2$. Rods **24** and **25** differ from

18. A. Petitjean, L. A. Cuccia, M. Schmutz, J.-M. Lehn. Naphthyridine-based helical foldamers and macrocycles: synthesis, cation binding, and supramolecular assemblies. *J. Org. Chem.* **2008**, *73*, 2481–2495.
19. C.-F. Lee, D. A. Leigh, R. G. Pritchard, D. Schultz, S. J. Teat, G. A. Timco, R. E. P. Winpenny. Hybrid organic–inorganic rotaxanes and molecular shuttles. *Nature*, **2009**,*458*, 314–318.
20. C. Talotta, C. Gaeta, Z. Qi, C. A. Schalley, P. Neri. Pseudorotaxanes with self-sorted sequence and stereochemical orientation. *Angew. Chem. Int. Ed.* **2013**, *52*, 7437–7441.
21. S. Lee, C.-H. Chen, A. H. Flood. A pentagonal cyanostar macrocycle with cyanostilbene CH donors binds anions and forms dialkylphosphate[3]rotaxanes. *Nat. Chem.* **2013**, *5*, 704–710.
22. D. Sánchez-García, B. Kauffmann, T. Kawanami, H. Ihara, M. Takafuji, M.-H. Delville, I. Huc. Nanosized hybrid oligoamide foldamers: aromatic templates for the folding of multiple aliphatic units *J. Am. Chem. Soc.* **2009**, *131*, 8642–8648.
23. H. Zhao, W. Q. Ong, F. Zhou, X. Fang, X. Chen, S. F. Y. Li, H. Su, N.-J. Chob, H. Zeng. Chiral crystallization of aromatic helical foldamers via complementarities in shape and end functionalities. *Chem. Sci.* **2012**, *3*, 2042–2046.
24. K. Nakano, H. Oyama, Y. Nishimura, S. Nakasako, K. Nozaki. λ^5-phospha[7]helicenes: synthesis, properties, and columnar aggregation with one-way chirality. *Angew. Chem. Int. Ed.* **2012**, *51*, 695–699.
25. D. Haldar, H. Jiang, J.-M. Léger, I. Huc. Double versus single helical structures of oligopyridine-dicarboxamide strands. Part 2: the role of side-chains. *Tetrahedron* **2007**, *63*, 6322–6330.
26. N. Delsuc, S. Massip, J.-M. Léger, B. Kauffmann, I. Huc. Relative helix-helix conformations in branched aromatic oligoamide foldamers, *J. Am. Chem. Soc.* **2011**, *133*, 3165–3172.
27. K. Maeda, M. Ishikawa, E. Yashima. Macromolecular helicity induction in a cationic polyacetylene assisted by an anionic polyisocyanide with helicity memory in water: replication of macromolecular helicity *J. Am. Chem. Soc.* **2004**, *126*, 15161–15166.

the relative stereochemistry of their two stereogenic centers which may favor the binding of two hosts having opposite handedness in the case of **24** or the same handedness in the case of **25**, thus acting either antagonistically or synergistically with respect to helix-helix handedness communication.

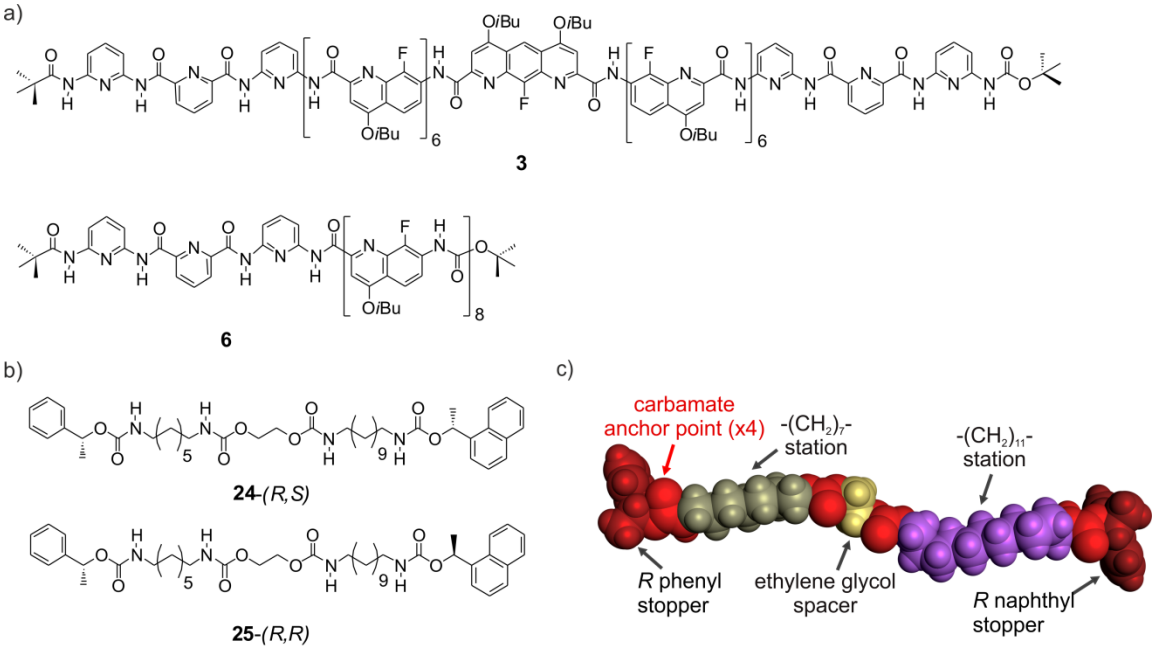

Figure 16. a) Formulas of aromatic oligoamides forming single helical **3** and double helical **6** host-guest helix-rod complexes. b) Formulas of oligocarbamate guest template sequences **24**-*(R,S)* and **25**-*(R,R)*. c) crystal structure of **25**-*(R,R)*.

Indeed, upon mixing **3** and (**6**)$_2$ with either **24**-(*R*,*S*) or **25**-(*R*,*R*), very different outcomes resulted. With **24**-(*R*,*S*), a complex NMR spectrum formed corresponding to a mixture of four possible *P*(*P*)$_2$, *M*(*M*)$_2$, *P*(*M*)$_2$ and *M*(*P*)$_2$ **24**⊃(**3**.(**6**)$_2$) complexes, none of which had a strong prevalence (Fig. 17c). In contrast, with **25**-(*R*,*R*), a sharp ^{1}H NMR spectrum indicated the presence of a dominant species (Fig. 17d).

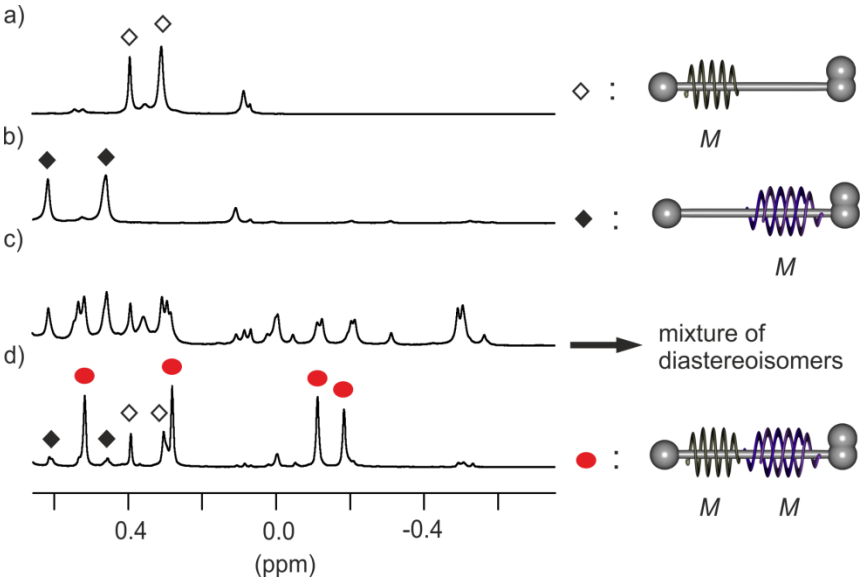

Figure 17. Part of the 400 MHz ^{1}H NMR spectra (resonances of the pivaloyl end groups of the helices) in $CDCl_3$ at 298K of: a) **3**⊃**25**-*(R,R)* (1 mM); b) (**6**)$_2$⊃**25**-*(R,R)* (1 mM); c) **3** (1 mM) and (**6**)$_2$ (1 mM) in the presence of rod **24**-*(R,S)* (1 equiv.); d) **3** (1 mM) and (**6**)$_2$ (1 mM) in the presence of rod **25**-*(R,R)* (1 equiv.). White diamonds denote *M*-**3**⊃**25**-*(R,R)* whereas *M*-(**6**)$_2$⊃**25**-*(R,R)* are marked with black diamonds. Red circles denote the homochiral complex (*M*-**3**.*M*-(**6**)$_2$)⊃**25**-*(R,R)*.

The structure of the resulting homochiral complex (*M*-**3**.*M*-(**6**)$_2$)⊃**25**-(*R,R*) was identified in the solid state as being the favored homohelical arrangement (Fig. 18a). The structure showed that the helix-helix end-to-end homohelical contact is similar for single helix-double helix communication to that found for double helix-double helix communication. Thus, the stereogenic centers at each end of the rod as well as the helix-helix contact, although all remote from each other,[28] all concur to the emergence of a complex multi-helical aggregate through the translation of information contained on a multistation guest.

28. J. Clayden, A. Lund, L. Vallverdú, M. Helliwell. Ultra-remote stereocontrol by conformational communication of information along a carbon chain. *Nature*, **2004**, *431*, 966–971.

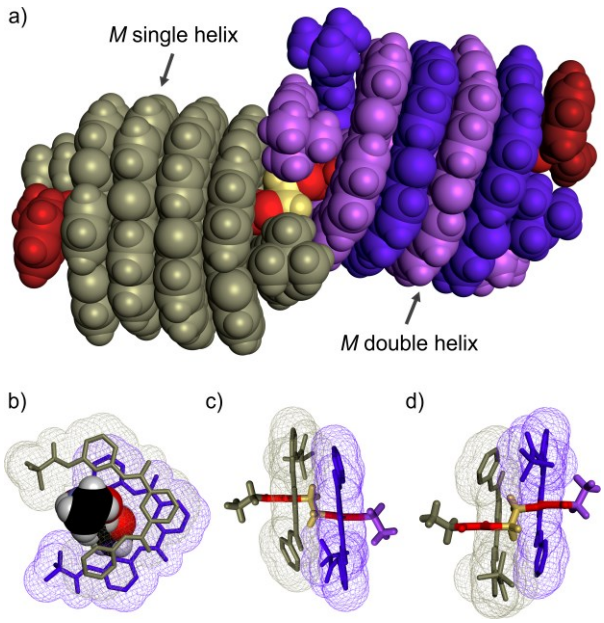

Figure 18. a) Side view of the crystal structure of (*M*-**3**.*M*-(**6**)$_2$)⊃**25**-*(R,R)*. **3** is shown in grey taupe and **(6)**$_2$ in purple and light purple. b) Top view of the two pyridine trimers from **3** (grey taupe tube) and (**6**)$_2$ (purple tube) which are shown to be in close contact and to hydrogen bond to the rod **25**-*(R,R)* in CPK representation. c) Side view from the same structure showing a kink (gold tube) in **25**-*(R,R)*. d) Side view from the same structure with a 180° rotation along the rod axis. The volumes of the pyridine trimers of the single helix and one strand of the double helix are shown as green and blue isosurfaces, respectively, in quad mesh representation. Side chains (O*i*Bu groups) and included solvent molecules have been removed for clarity.

4. Conclusion

In summary, we have established a robust and versatile scheme to produce well-defined homochiral arrangements of helical oligomers wound around multistation rod-like template guest sequences. Templates having up to ten urethane functions were translated to form the largest abiotic folded architectures known to date. As other helix-rod recognition patterns are being identified,[29] the scheme may be further expanded and allow the organization in space of various functional groups attached to each helical component of a given assembly. Another extension would consist in optimizing the covalent capture[30,31] of these non-covalent assemblies to convert the stack of helices into a single molecular polymeric chains.

29. Q. Gan, Y. Ferrand, N. Chandramouli, B. Kauffmann, C. Aube, D. Dubreuil, I. Huc. Identification of a foldaxane kinetic byproduct during guest-induced single to double helix conversion. *J. Am. Chem. Soc.* **2012**, *134*, 15656–15659.
30. T. D. Clark, M. R. Ghadiri. Supramolecular design by covalent capture. Design of a peptide cylinder via hydrogen-bond-promoted intermolecular olefin metathesis. *J. Am. Chem. Soc.* **1995**, *117*, 12364–12365.
31. J. Li, J. M. A. Carnall, M. C. A. Stuart, S. Otto. Hydrogel formation upon photoinduced covalent capture of macrocycle stacks from dynamic combinatorial libraries. *Angew. Chem. Int. Ed.* **2011**, *50*, 8384–8386.

5. Experimental part

5.1 Methods for NMR

NMR spectra were recorded on 3 different NMR spectrometers: (1) an Avance II NMR spectrometer (Bruker Biospin) with a vertical 7,05T narrow-bore/ultrashield magnet operating at 300 MHz for ^{1}H observation and 75 MHz for ^{13}C observation by means of a 5-mm direct BBO H/X probe with Z gradient capabilities; (2) an Avance 400 NMR spectrometer (Bruker Biospin) with a vertical 9.4T narrow-bore/ultrashield magnet operating at 400 MHz for ^{1}H observation by means of a 5-mm direct QNP $^{1}H/^{13}C/^{31}P/^{19}F$ probe with gradient capabilities; (3) an Avance III NMR spectrometer (Bruker Biospin) with a vertical 16.45T narrow-bore/ultrashield magnet operating at 700 MHz for ^{1}H observation by means of a 5-mm TXI $^{1}H/^{13}C/^{15}N$ probe with Z gradient capabilities. Chemical shifts are reported in parts per million (ppm, δ) relative to the ^{1}H residual signal of the deuterated solvent used. ^{1}H NMR splitting patterns with observed first-order coupling are designated as singlet (s), doublet (d), triplet (t), or quartet (q). Coupling constants (*J*) are reported in hertz. Data processing was performed with Topspin 2.0 software. Samples were not degassed. $CDCl_3$ from Eurisotop was used after filtration through an alumina pad followed by a distillation over calcium hydride.

5.1.1 ^{1}H NMR titration of foldamer 3 by different dumbbell molecules

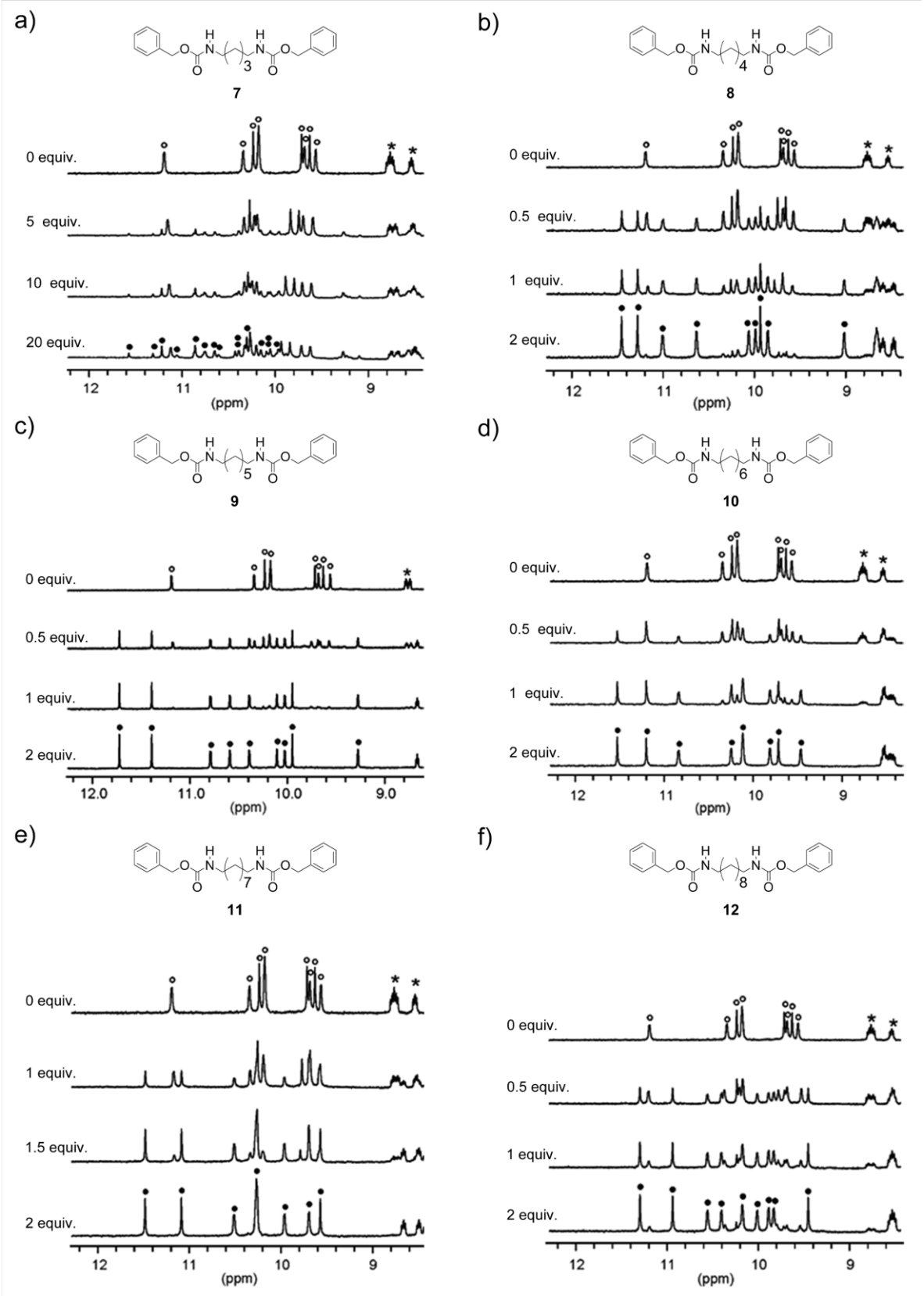

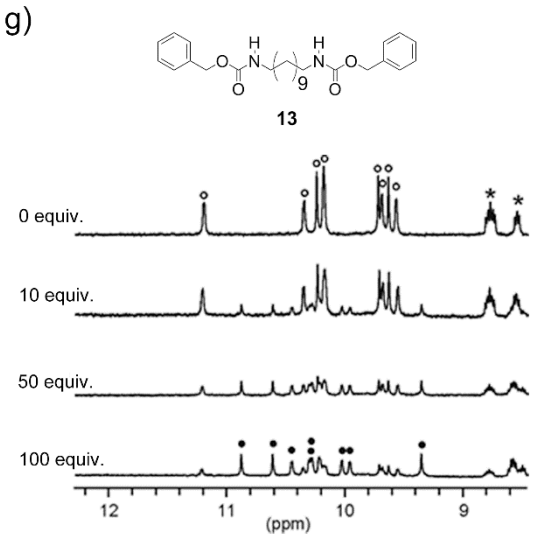

Figure 19. Representative ^{1}H NMR spectra of titration experiments of **3** in $CDCl_3$ at 298K with various guests. The experiments were carried out with the concentration of **3** at: a) 1 mM; b) 0.25 mM; c) 0.1 mM; d) 0.25 mM; e) 0.25 mM; f) 4 mM; g) 0.25 mM. Amide signals of the free single helix and foldaxane are marked with empty and black circles, respectively. Some aromatic resonances are denoted with stars.

5.1.2 ^{1}H NMR titration of foldamer 5 by different dumbbell molecules

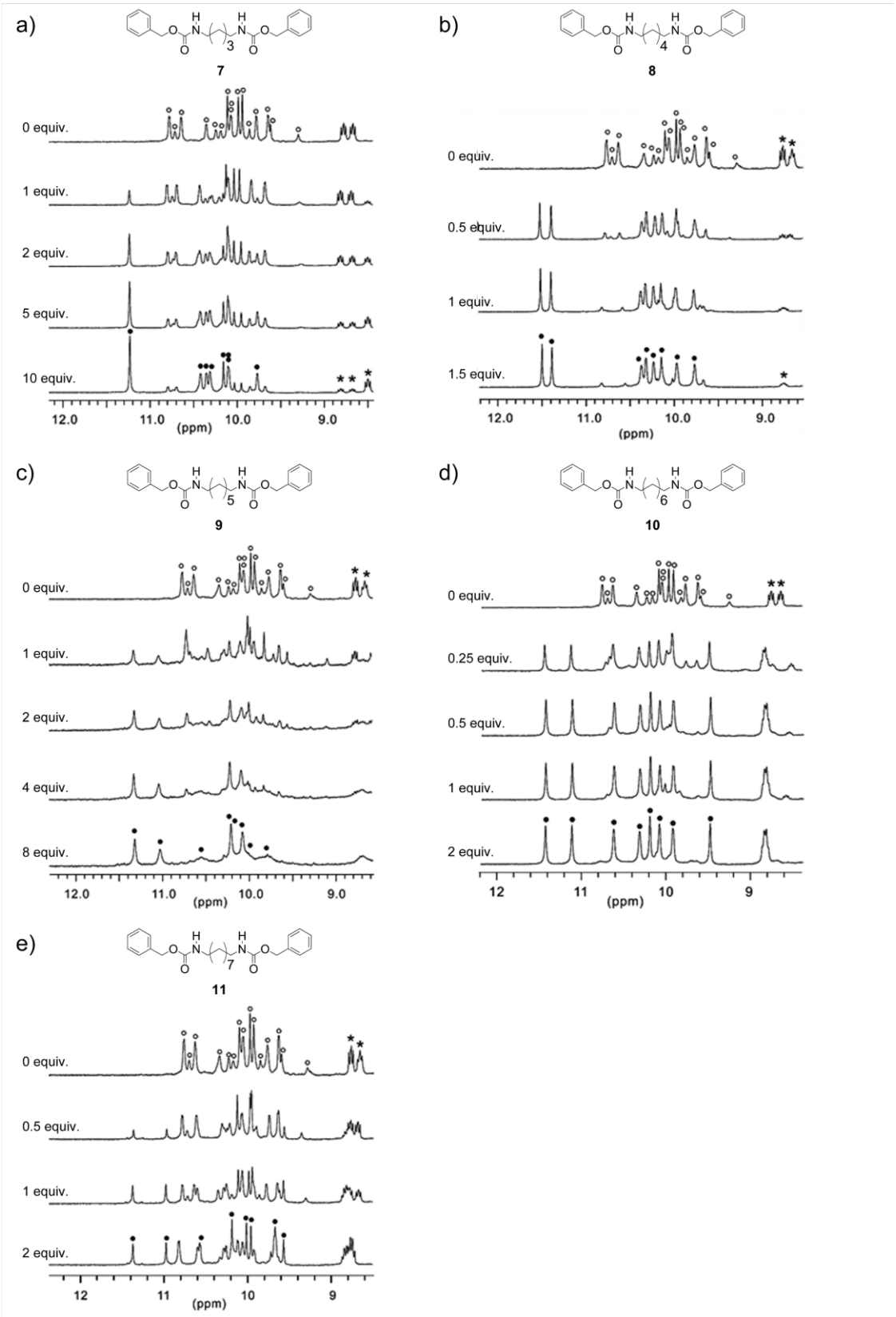

Figure 20. Representative ^{1}H NMR spectra of **5** (4 mM) in $CDCl_3$ at 298K titrated with various guests. Amide signals of the free parallel and antiparallel double helix $(\mathbf{5})_2$ and foldamer-guest complex are marked with empty and black circles, respectively. Some aromatic resonances are denoted with stars.

5.1.3 ^{1}H NMR titration of foldamer 6 by different dumbbell molecules

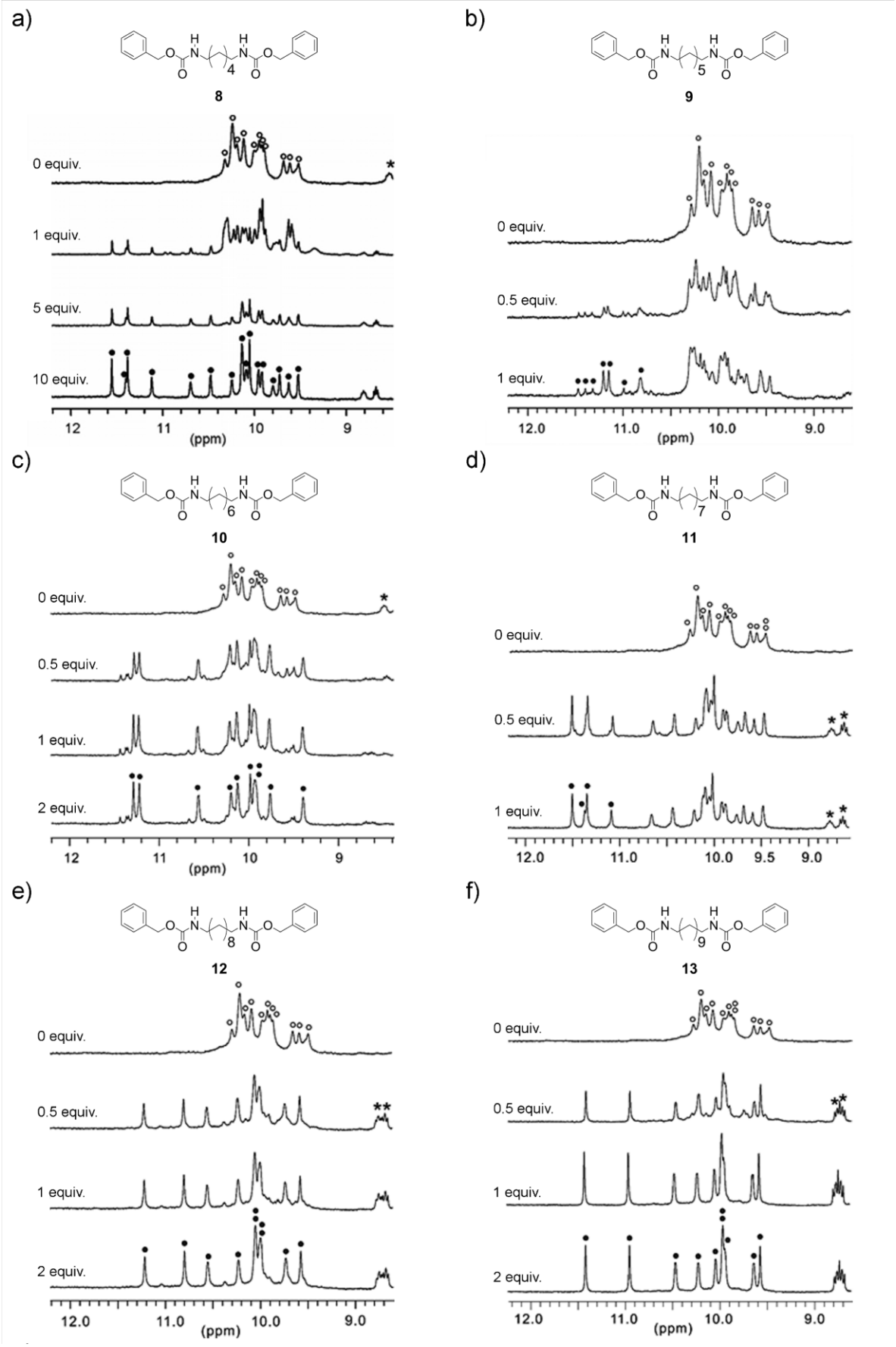

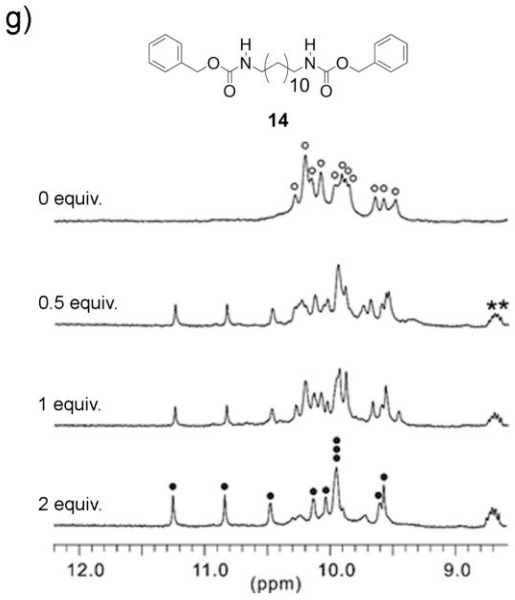

Figure 21. Representative ^{1}H NMR spectra of **6** (4 mM) in $CDCl_3$ at 298K titrated with various guests. Amide signals of the free parallel and antiparallel double helix $(\mathbf{6})_2$ and foldamer-guest complex are marked with empty and black circles, respectively. Some aromatic resonances are denoted with stars.

5.2 Methods for Circular Dichroism

Circular dichroism studies were carried out in distilled chloroform using 2 or 10 mm pathlength cell. Homogenization and sample equilibration were performed after each addition of guest and CD spectra were recorded on a Jasco J-815 spectropolarimeter at 298 K.

5.3 Methods for X-ray crystallography

Crystallographic data for host-guest complexes were collected at the IECB x-ray facility (UMS 3033 – UMS001) on a Rigaku MM007 rotating anode (0.8 kW). Data were collected at the copper kα wavelength with a partial chi goniometer. The X-ray source is equipped with high flux Osmic Varimax mirrors and a RAPID SPIDER image plate detector. Crystallographic data for host-guest complexes were collected at the BM30A (ESRF) beamline at respectively 0.8, 0.78 and 0.85 Å. Phi-scans were performed and data recorded with a large ADSC Q315r CCD detector. The Rigaku CrystalClear suite was used to index and integrate the home source data with a multiscan absorption correction. Data collected at the synchrotron were processed with the XDS package[32].

All structures were solved by charge-flipping with Superflip[33] and refined by full-matrix least-squares methods using WinGX[34] software, which utilizes the SHELXH 2013 module[35]. The SQUEEZE procedure[36] implemented in PLATON was used for all structures in order to treat the regions with highly disordered solvent molecules (mainly chloroform, water, methanol and *n*-hexane molecules).

In all cases, the positions of carbon-bound and nitrogen-bound hydrogen atoms from the capsule were calculated and refined as riding on the parent carbon atoms with UH=1.2 UC. For some isobutoxy side chains the terminal methyl groups were refined with two idealized positions (HFIX 123). SHELX SIMU and DELU restraints were used in the refinement strategy, as listed in the cif files, mostly for the main chain of the foldamers. These are restraints on Displacement Parameters that take into account that atoms, which are bound to one another, move similarly, both in direction and amount. EADP constraints were applied for some side chains. This constraint forces atoms to have identical Atomic Displacement Parameters.

32. W. Kabsch, XDS. *Acta Cryst* **2010**, *D66*, 125–132.
33. L. Palatinus, G. Chapuis, SUPERFLIP–a computer program for the solution of crystal structures by charge flipping in arbitrary dimensions. *Appl. Crystallogr.* **2007**, *40*, 786–790.
34. L. J. Farrugia, WinGX suite for single crystal small molecule crystallography. *J. Appl. Cryst.* **1999**, *32*, 837–838.
35. G. M. Sheldrick, A short history of SHELX. *Acta Cryst.* **2008**, *A64*, 112–122.
36. A. L. Spek, SQUEEZE. *J. Appl. Cryst.* **2003**, *36*, 7–13.

As a rule of thumb, every time where disorder could be modelled with partial occupation, it was so. However, more often than not, no simple models of the side chains and solvents can be obtained because multiple positions exist and because complexity is introduced by the swapping of side chains and solvent molecules at some positions, leading to unstable refinement. Introducing too many restraints on the side chains destabilizes the main chain and thus also has to be ruled out. Under such circumstances, an approach that many crystallographers would follow would be to squeeze out the disordered areas that cannot be modelled. However, we did not use this approach which amounts to removing information from our data and which does affect the main chain displacement parameters. Instead, the side chains are modelled using the EADP constraints (equal atomic displacement parameters) and in most cases refined with isotropic atomic displacement parameters. The outcome is a view of the side chains in an average position which, in our view represents real information contained in the data. Such modelling is efficient at avoiding negative displacement parameters and thus well takes into account the measured electron density.

5.4 Methods for chemical synthesis

All reactions were carried out under a dry nitrogen atmosphere. Commercial reagents were purchased from Sigma-Aldrich, Alfa-Aesar or TCI and were used without further purification unless otherwise specified. Tetrahydrofurane (THF) and dichloromethane (CH_2Cl_2) were dried over alumina columns; chloroform ($CHCl_3$), triethylamine (Et_3N) and diisopropylethylamine (DIEA) were distilled over calcium hydride (CaH_2) prior to use. Reactions were monitored by thin layer chromatography (TLC) on Merck silica gel 60-F254 plates and observed under UV light. Column chromatography purifications were carried out on Merck GEDURAN Si60 (40-63 µm). ESI mass spectra were obtained from the Mass Spectrometry Laboratory at the European Institute of Chemistry and Biology (UMS 3033 - IECB), Pessac, France.

5.4.1 Synthesis of oligomers

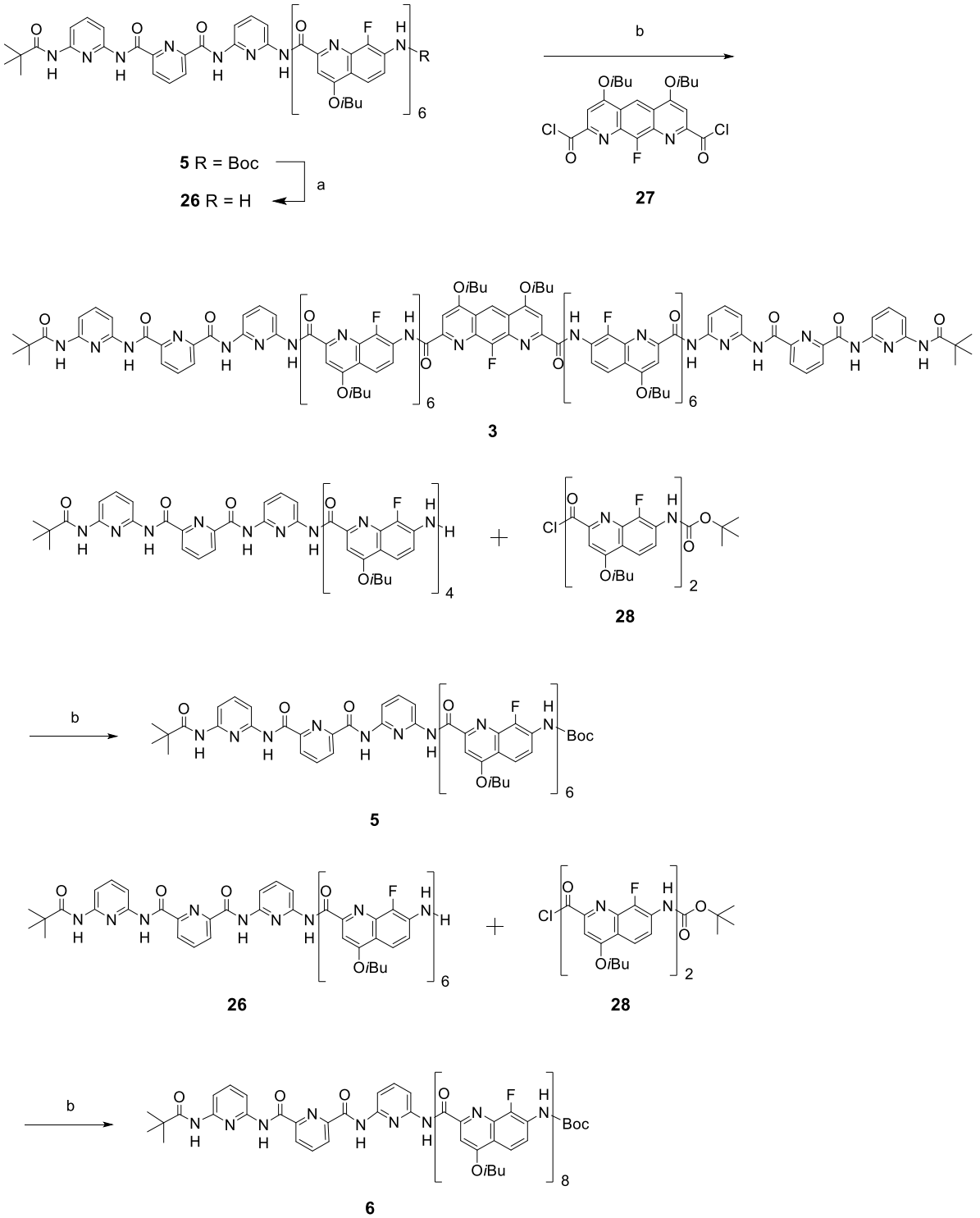

Scheme 4. Synthesis of oligomer **3**, **5**, and **6**. a) TFA, CH_2Cl_2, room temperature, 6 h; b) DIEA, $CHCl_3$, room temperature, 12 h.

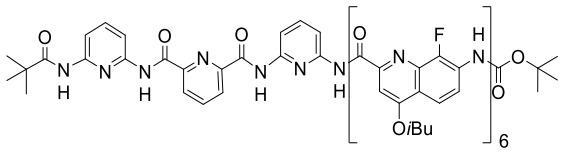

5

Oligomer 5. Heptamer $\mathbf{P_3Q^F_4}$ amine**17**[37] (147 mg, 0.1 mmol) and DIEA (0.03 mL, 0.4 mmol) were dissolved in dry CH_2Cl_2 (10 mL), the freshly prepared dimer acid chloride[16] (98 mg, 0.15 mmol) in CH_2Cl_2 (5 mL) was added dropwise at room temperature. After stirring overnight, solvents were evaporated and the product was purified by flash chromatography (SiO_2) eluting with cyclohexane/EtOAc (70:30 vol/vol) to obtain heptamer **5** as a white solid (0.17 g, 83%). ^{1}H NMR (d_6-DMSO, 400 MHz, 353 K): δ 11.44 (s, 1H), 10.97 (s, 1H), 10.53 (s, 1H), 10.41 (s, 1H), 10.12 (s, 2H), 9.85 (s, 1H), 9.80 (s, 1H), 8.46 (s, 1H), 8.30 (t, *J*(H, H) = 7.6, 1H), 8.09-7.87 (m, 3H), 7.68-7.21 (m, 15H), 7.03-6.61 (m, 8H), 4.31-3.92 (m, 12H), 2.45-2.26 (m, 6H), 1.42-1.18 (m, 36H), 1.05 (s, 9H), 0.46 (s, 9H). MS (ESI): *m/z* calcd for $C_{111}H_{110}F_6N_{19}O_{17}$ $[2M+2H]^{2+}$ 2094.8231; found 2094.8175.

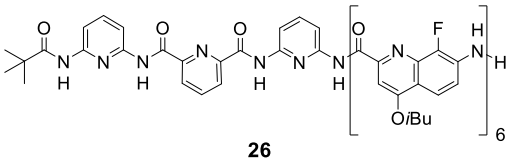

26

Oligomer amine 26. Oligomer **5** (0.21 g, 0.10 mmol) was dissolved in dichloromethane (4 mL), and excess trifluoroacetic acid (TFA) (1 mL) was added dropwise. The mixture was allowed to stir at room temperature for 6 h. The solvent was evaporated and the residue was dissolved in CH_2Cl_2 (20 mL), washed with saturated $NaHCO_3$ and brine, dried over Na_2SO_4, filtered and then concentrated to give amine **26** (0.19 g, 95% yield) as a yellow solid which was used without further purification. ^{1}H NMR (d_6-DMSO, 400 MHz, 298 K): δ 11.70 (s, 1H), 11.09 (s, 1H), 10.55 (s, 1H), 10.29 (s, 1H), 10.16 (s, 1H), 10.05 (s, 1H), 9.94 (s, 1H), 9.87 (s, 1H), 8.73 (s, 1H), 8.29 (s, 1H), 8.09 (t, *J*(H, H) = 8.0, 1H), 7.89-6.57 (m, 24H), 6.21 (t, *J*(H, H) = 8.0, 1H), 4.44-3.89 (m, 14H), 2.50-2.22 (m, 6H), 1.38-1.17 (m, 36H), 0.43 (s, 9H). MS (ESI): *m/z* calcd for $C_{212}H_{204}F_{12}N_{38}O_{30}$ $[2M+2H]^{2+}$ 1994.7707 found 1994.7686.

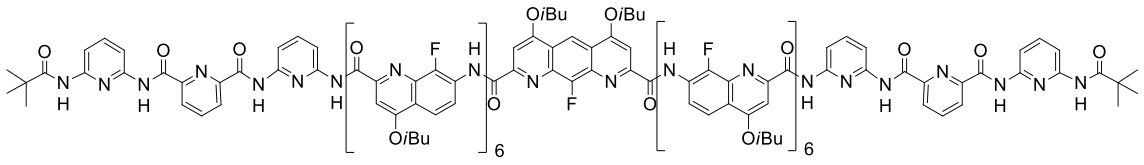

3

Oligomer 3. To a solution of nonamer amine **26** (200 mg, 0.1 mmol) and DIEA (0.07 mL, 0.4 mmol) in dry $CHCl_3$ (10 mL) was added dropwise a solution of the freshly prepared diacid chloride[17] **27** (32 mg, 0.07 mmol) in $CHCl_3$ (5 mL) via a syringe at 0 °C. The reaction was allowed to proceed at room temperature for 12 h. The solution was evaporated and the residue was purified by flash chromatography (SiO_2) eluting with EtOAc/CH_2Cl_2 (5:95 to 20:80 vol/vol) to obtain **3** as a yellowish solid (160 mg, 73% yield). ^{1}H NMR (d_6-DMSO, 400 MHz, 353 K): δ 11.45 (s, 2H), 11.14 (s, 2H), 10.79 (s, 2H), 10.48 (s, 2H), 10.29 (s, 2H), 10.04 (s, 2H), 9.83 (s, 2H), 9.52 (s, 2H), 9.13 (s, 2H), 8.82 (t, *J*(H, H) = 7.2, 2H), 8.66(s, 2H), 8.39 (t, *J*(H, H) = 7.2, 2H), 8.29 (t, *J*(H, H) = 7.2, 2H), 8.00-7.73 (m, 6H), 7.59-6.60 (m, 41H), 6.40 (s, 2H), 6.00 (s, 2H), 4.26-4.00 (m, 28H), 2.50-2.33 (m, 14H), 1.40-1.24 (m, 84H), 0.34 (s, 18H). MS (ESI): *m/z* calcd for $C_{234}H_{223}F_{13}N_{40}O_{34}$ $[M+2H]^{2+}$ 2191.8371 found 2191.8343, $C_{234}H_{221}F_{13}N_{40}O_{34}Na_2$ $[M+2Na]^{2+}$ 2213.8191 found 2213.8162.

37. C. Bao, Q. Gan, B. Kauffmann, H. Jiang, I. Huc, A self-assembled foldamer capsule: combining single and double helical segments in one aromatic amide sequence, *Chem. Eur. J.* **2009,** *15,* 11530.

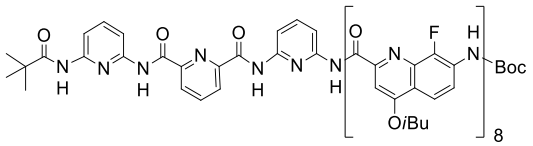

6

Oligomer 6. To a solution of nonamer amine **26** (200 mg, 0.1 mmol) and distilled DIEA (0.07 mL, 0.4 mmol) in dry dichloromethane (10 mL) was added dropwise a solution of the freshly prepared quinoline dimer acid chloride[16] **28** (98 mg, 0.15 mmol) in dichloromethane (10 mL) via a syringe at 0 °C. The reaction mixture was allowed to proceed at room temperature for 12 h. The solution was evaporated and the residue was purified by flash chromatography (SiO_2) eluting with cyclohexane/EtOAc (60:40 vol/vol) to obtain product **6** as a white solid (0.21 g, 81% yield). ^{1}H NMR (d_6-DMSO, 400 MHz, 298 K): δ 11.26 (s, 1H), 10.86 (s, 1H), 10.43 (s, 1H), 10.36 (s, 1H), 10.23 (s, 1H), 10.15 (s, 1H), 9.99 (s, 1H), 9.92 (s, 1H), 9.80 (s, 1H), 9.75 (s, 1H), 8.43 (s, 1H), 7.98 (s, 1H), 7.74 (d, *J*(H, H) = 7.2, 1H), 7.57-6.59 (m, 32H), 4.22-3.95 (m, 16H), 2.39-2.27 (m, 8H), 1.36-1.10 (m, 48H), 1.01 (s, 9H), 0.45 (s, 9H). MS (ESI): *m/z* calcd for $C_{278}H_{272}F_{16}N_{46}O_{42}$ $[2M+2H]^{2+}$ 2616.0216 found 2616.0138; $C_{278}H_{271}F_{16}N_{46}O_{42}Na$ $[2M+H+Na]^{2+}$ 2626.0063 found 2626.0018.

5.4.2 Synthesis of chiral rods

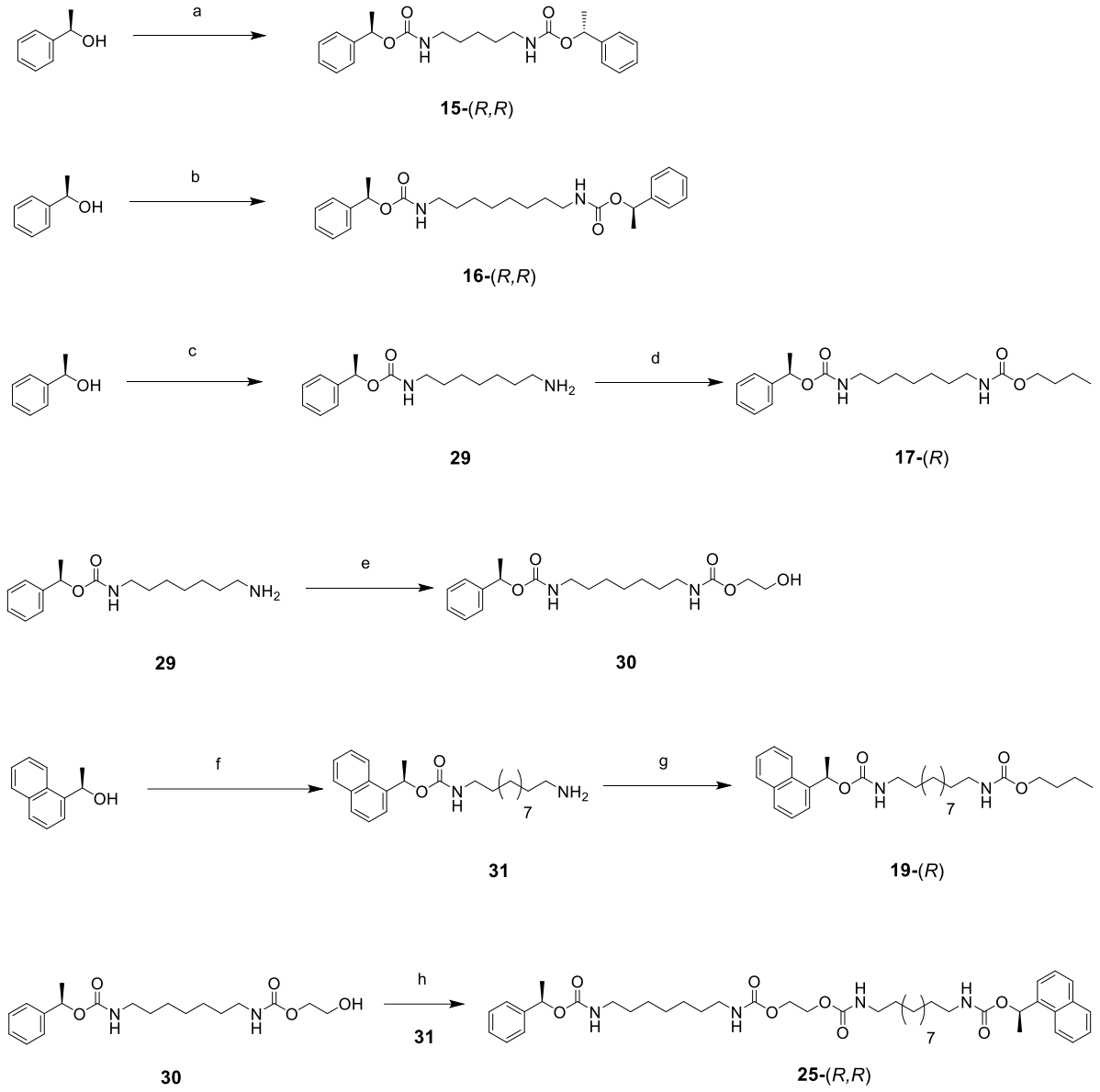

Scheme 5. Synthesis of chiral guests. a) 4-nitrophenyl chloroformate, Et_3N, CH_2Cl_2, room temperature, 0.5 h, then 1,5-diaminopentane (0.5 equiv.), room temperature, 12 h; b) 4-nitrophenyl chloroformate, Et_3N, CH_2Cl_2, room temperature, 0.5 h, then 1,8-diaminooctane (0.5 equiv.), room temperature, 12 h; c) 4-nitrophenyl chloroformate, Et_3N, CH_2Cl_2, room temperature, 0.5 h, then 1,7-diaminoheptane (5 equiv.), room temperature, 12 h; d) 4-nitrophenyl chloroformate, 1-butanol, Et_3N, CH_2Cl_2, room temperature, 0.5 h, then **29**, room temperature, 12 h; e) 4-nitrophenyl chloroformate, Et_3N, $CHCl_3$, room temperature, 3 h, then ethylene glycol (50 equiv.), refluxed, 24 h; f) 4-nitrophenyl chloroformate, Et_3N, CH_2Cl_2, room temperature, 24 h, then 1,11-diaminoundecane (5 equiv.), room temperature, 12 h; g) 4-nitrophenyl chloroformate, 1-butanol, Et_3N, CH_2Cl_2, room temperature, 0.5 h, then **31**, room temperature, 12 h; h) 4-nitrophenyl chloroformate, Et_3N, CH_2Cl_2, room temperature, 12 h, then **31**, room temperature, 12 h.

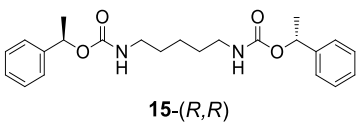

((*R*)-1-phenylethyl)pentane-1,5-dicarbamate 15-(*R,R*). To a solution of 4-nitrophenyl chloroformate (0.35 g, 1.7 mmol) in dry CH_2Cl_2 (20 mL) was added dropwise a mixture solution of (*R*)-(+)-1-phenylethanol (0.20 g, 1.6 mmol) and Et_3N (0.89 mL, 6.4 mmol) in CH_2Cl_2 (10 mL)

via a syringe at 0 °C. After 30 min stirring at room temperature, to the above reaction mixture was added a solution of 1,5-diaminopentane (82 mg, 0.8 mmol) in dry CH_2Cl_2 (10 mL) at 0 °C. Then the reaction mixture was allowed to proceed at room temperature for 12 h. The solution was washed with 1N NaOH and brine several times, dried over Na_2SO_4. After filtration and concentration, the residual oil was purified by flash chromatography (SiO_2) eluting with EtOAc/CH_2Cl_2 (20:80) to obtain product **15**-(*R,R*) as yellow oil (0.24 g, 77% yield). ^{1}H NMR ($CDCl_3$, 300 MHz): δ 7.35-7.27 (m, 10H), 5.82 (q, *J*(H, H) = 6.3, *J*(H, H) = 6.6, 2H), 4.71 (br, 2H), 3.18-3.10 (m, 4H), 1.54 (d, *J*(H, H) = 12.6, 6H), 1.49-1.44 (m, 4H), 1.35-1.26 (m, 2H). ^{13}C NMR ($CDCl_3$, 75 MHz): δ 156.1, 142.4, 128.6, 127.8, 126.1, 72.8, 40.8, 29.7, 23.9, 22.6. HRMS (ES$^+$): *m/z* calcd for $C_{23}H_{30}N_2O_4Na$ $[M+Na]^+$ 421.2103 found 421.2091.

The enantiomer 15-(*S,S*) was prepared using the same method.

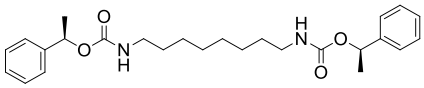

16-(*R,R*)

((*R*)-1-phenylethyl)octane-1,8-dicarbamate 16-(*R,R*) **was synthesized using simillar procedure as used for compound 15**-(*R,R*). ^{1}H NMR ($CDCl_3$, 300 MHz): δ 7.37-7.27 (m, 10H), 5.86-5.73 (q, *J*(H, H) = 5.8, *J*(H, H) = 5.8, 2H), 4.72-4.59 (br, 2H), 3.21-3.09 (q, *J*(H, H) = 3.1, *J*(H, H) = 3.1, 4H), 1.52-1.40 (m, 8H), 1.32-1.23 (m, 10H). ^{13}C NMR ($CDCl_3$, 75 MHz): δ 156.1, 142.4, 128.6, 127.8, 126.1, 72.6, 41.2, 30.0, 29.2, 26.7, 22.6. HRMS (ESI): *m/z* calcd for $C_{26}H_{37}N_2O_4$ $[M+H]^+$ 441.2748 found 441.2759.

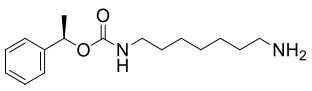

29-(*R*)

(*R*)-1-phenylethyl 7-aminoheptylcarbamate 29-(*R*). To a solution of 4-nitrophenyl chloroformate (1.1 g, 5.5 mmol) in dry CH_2Cl_2 (20 mL) was added dropwise a mixture solution of (*R*)-(+)-1-phenylethanol (0.61 g, 5.0 mmol) and Et_3N (2.8 mL, 20.0 mmol) in CH_2Cl_2 (10 mL) via a syringe at 0 °C. After 30 min stirring at room temperature, the above reaction mixture was added dropwise over a 1 h period to a solution of 1,7-diaminoheptane (3.25 g, 25.0 mmol) in dry CH_2Cl_2 (100 mL) at 0 °C. Then the reaction mixture was allowed to proceed at room temperature for 12 h. The solution was washed with 1N NaOH and brine several times, dried over Na_2SO_4. After filtration and concentration, the residual oil was purified by flash chromatography (SiO_2) eluting with MeOH/CH_2Cl_2/Et_3N (10:90:1 to 30:70:1) to obtain product **29**-(*R*) as yellow oil (1.11 g, 80% yield). ^{1}H NMR ($CDCl_3$, 300 MHz): δ 7.37-7.25 (m, 5H), 5.83 (q, *J*(H, H) = 6.6, *J*(H, H) = 6.6, 1H), 4.67 (s, 1H), 3.19 (q, *J*(H, H) = 6.6, *J*(H, H) = 6.6, 2H), 2.71 (t, *J*(H, H) = 6.9, 2H), 1.54 (d, *J*(H, H) = 6.6, 3H), 1.59-1.45 (m, 6H), 1.30 (br, 6H). ^{13}C NMR ($CDCl_3$, 75 MHz): δ 156.1, 142.4, 128.5, 127.8, 126.1, 72.6, 41.7, 41.0, 32.7, 30.0, 29.1, 26.8, 26.7, 22.5. HRMS (ESI): *m/z* calcd for $C_{16}H_{27}N_2O_2$ $[M+H]^+$ 279.2073 found 279.2068.

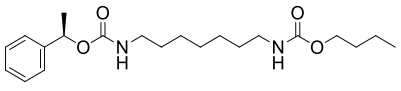

17-(*R*)

(*R*)-1-phenylethyl-*n*-butoxycarbonylaminoheptylcarbamate 17-(*R*). To a solution of 4-nitrophenyl chloroformate (0.23 g, 1.1 mmol) in dry CH_2Cl_2 (5 mL) was added dropwise a mixture solution of 1-butanol (80 μL, 0.87 mmol) and Et_3N (0.24 mL, 1.7 mmol) in CH_2Cl_2 (5 mL) via a syringe at 0 °C. After 30 min. stirring, a solution of (*R*)-1-phenylethyl 7-aminoheptylcarbamate **29**-(*R*) (0.24 g, 0.87 mmol) and Et_3N (0.24 mL, 1.7 mmol) in CH_2Cl_2 (10 mL) was added via a syringe. Then the reaction mixture was allowed to proceed at room temperature for 12 h. The solution was evaporated and the residue was purified by flash chromatography (SiO_2) eluting with EtOAc/CH_2Cl_2 (1:99 to 3:97 vol/vol) to obtain product **17**-(*R*) as a colorless oil (0.23 g, 70% yield). ^{1}H NMR ($CDCl_3$, 300 MHz): δ 7.37-7.26 (m, 5H), 5.79 (q, *J*(H, H) = 6.4, *J*(H, H) = 6.4, 1H), 4.68 (s, 1H), 4.61 (s, 1H), 4.22 (t, *J*(H, H) = 6.5, 2H), 3.14 (q, *J*(H, H) = 6.4, *J*(H, H) = 6.4, 4H), 1.64-1.55 (m, 2H), 1.52 (d, *J*(H, H) = 6.6, 3H), 1.50-1.42 (m, 4H), 1.42-1.32 (m, 2H), 1.32-1.23 (m, 6H), 0.92 (t, *J*(H, H) = 7.3, 3H). ^{13}C NMR ($CDCl_3$, 75 MHz): δ 156.9, 156.0, 142.3, 128.5, 127.7, 126.0, 64.6, 40.9, 31.2, 29.9, 28.9, 26.6, 22.5, 19.1, 13.8. HRMS (ESI): *m/z* calcd for $C_{19}H_{30}N_2O_5Na$ $[M+Na]^+$ 389.2052 found 389.2047.

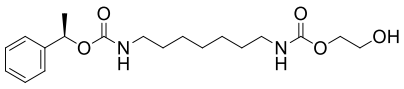

30-(*R*)

Compound 30-(*R*)**.** To a solution of 4-nitrophenyl chloroformate (0.734 g, 3.6 mmol) in dry $CHCl_3$ (20 mL) was added dropwise a mixture solution of (*R*)-1-phenylethyl 7-aminoheptylcarbamate **29**-(*R*) (0.92 g, 3.3 mmol) and Et_3N (1.83 mL, 13.2 mmol) in $CHCl_3$ (10 mL) via a syringe at 0 °C. After 3 h stirring at room temperature, the above reaction mixture was added dropwise over a 1 h period to a solution of ethylene glycol (9.2 mL, 160 mmol) in $CHCl_3$ (500 mL) at 0 °C. Then the reaction mixture was refluxed for 24 h. The solution was washed with 1N NaOH and brine several times, dried over Na_2SO_4. After filtration and concentration, the residual oil was purified by flash chromatography (SiO_2) eluting with EtOAc/CH_2Cl_2 (20:80 to 80:20) to obtain product **30**-(*R*) as colourless oil (0.85 g, 71% yield). ^{1}H NMR ($CDCl_3$, 300 MHz): δ 7.35-7.27 (m, 5H), 5.83 (q, *J*(H, H) = 6.6, *J*(H, H) = 6.6, 1H), 4.76 (s, 1H), 4.70 (s, 1H), 4.22 (t, *J*(H, H) = 4.5, 2H), 3.82 (t, *J*(H, H) = 4.5, 2H), 3.20-3.12 (m, 4H), 2.33 (br, 1H), 1.54 (d, *J*(H, H) = 6.6, 3H), 1.52-1.46 (m, 4H), 1.30 (br, 6H). ^{13}C NMR ($CDCl_3$, 75 MHz): δ 157.1, 156.1, 142.4, 128.5, 127.8, 126.1, 72.6, 41.7, 41.0, 32.7, 30.0, 29.1, 26.8, 26.7, 22.5. HRMS (ESI): *m/z* calcd for $C_{19}H_{30}N_2O_5Na$ $[M+Na]^+$ 389.2052 found 389.2047.

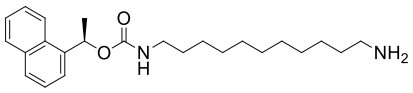

31-(*R*)

(*R*)-1-(1-napthyl)ethyl 11-aminoundecylcarbamate 31-(*R*). To a solution of 4-nitrophenyl chloroformate (0.7 g, 3.4 mmol) in dry CH_2Cl_2 (5 mL) was added a mixture solution of (*R*)-(+)-1-(1-naphthyl)ethanol (0.55 g, 3.2 mmol) and Et_3N (1.8 mL, 12.8 mmol) in CH_2Cl_2 (5 mL) at 0 °C. After 24 h stirring at room temperature, the above reaction mixture was added dropwise over a 1 h period to a solution of 1,11-diaminoundecane (2.9 g, 16.0 mmol) in dry CH_2Cl_2 (100 mL) at 0 °C. Then the reaction mixture was allowed to proceed at room temperature for 12 h. The solution was washed with 1N NaOH and brine several times, dried over Na_2SO_4. After filtration and concentration, the residual oil was purified by flash chromatography (SiO_2) eluting with MeOH/CH_2Cl_2/Et_3N (10:90:1 to 30:70:1) to obtain product **31**-(*R*) as yellow oil (0.77 g, 63% yield). ^{1}H NMR ($CDCl_3$, 300 MHz): δ 8.14 (d, *J*(H, H) = 8.1, 1H), 7.85 (d, *J*(H, H) = 7.2, 1H), 7.80 (d, *J*(H, H) = 8.1, 1H), 7.59-7.43 (m, 4H), 6.60 (q, *J*(H, H) = 6.6, *J*(H, H) = 6.6, 1H), 4.75 (s, 1H), 3.20 (q, *J*(H, H) = 6.0, *J*(H, H) = 6.9, 2H), 2.72 (t, *J*(H, H) = 6.9, 2H), 1.71 (d, *J*(H, H) = 6.6, 3H), 1.47 (br, 4H), 1.25 (br, 16H). ^{13}C NMR ($CDCl_3$, 75 MHz): δ 156.0, 138.0, 133.9, 130.4, 128.8, 128.3, 126.2, 125.6, 125.4, 123.4, 123.0, 63.6, 41.1, 40.9, 31.3, 30.0, 29.4, 29.3, 26.9, 26.8, 21.9. HRMS (ESI): *m/z* calcd for $C_{24}H_{37}N_2O_2$ $[M+H]^+$ 385.2855; found 385.2848.

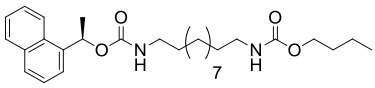

19-(R)

(*R*)-1-(1-napthyl)ethyl-*n*-butoxycarbonylaminoundecyl-carbamate 19-(*R*). To a solution of 4-nitrophenyl chloroformate (0.6 g, 3.0 mmol) in dry CH_2Cl_2 (10 mL) was added dropwise a mixture solution of 1-butanol (0.25 mL, 2.68 mmol) and Et_3N (0.74 mL, 5.3 mmol) in CH_2Cl_2 (10 mL) via a syringe at 0 °C. After 30 min. stirring, a solution of (*R*)-1-(1-napthyl)ethyl 11-aminoundecylcarbamate **31** (1.0 g, 2.68 mmol) and Et_3N (0.74 mL, 5.3 mmol) in CH_2Cl_2 (10 mL) was added via a syringe. Then the reaction mixture was allowed to proceed at room temperature for 12 h. The solution was evaporated and the residue was purified by flash chromatography (SiO_2) eluting with EtOAc/CH_2Cl_2 (10:90 to 30:70 vol/vol) to obtain product **19**-(*R*) as a white solid (1.0 g, 78% yield). ^{1}H NMR ($CDCl_3$, 300 MHz): δ 8.17 (d, *J*(H, H) = 8.1, 1H), 7.91 (d, *J*(H, H) = 7.2, 1H), 7.84 (d, *J*(H, H) = 8.1, 1H), 7.63-7.47 (m, 4H), 6.64 (q, *J*(H, H) = 6.6, *J*(H, H) = 6.6, 1H), 4.77 (s, 1H), 4.63 (s, 1H), 4.11 (7, *J*(H, H) = 6.6 2H), 3.24-3.15 (m, 4H), 1.75 (d, *J*(H, H) = 6.6, 3H), 1.64-1.37 (m, 8H), 1.30 (br, 14H), 0.99 (t, *J*(H, H) = 7.2, 3H). ^{13}C NMR ($CDCl_3$, 75 MHz): δ 156.9, 156.1, 138.1, 134.0, 130.5, 128.9, 128.4, 126.3, 125.7, 125.4, 123.5, 123.1, 69.7, 64.7, 41.2, 31.3, 30.1, 29.6, 29.4, 26.8, 22.0, 19.2, 13.9. HRMS (ESI): *m/z* calcd for $C_{29}H_{44}N_2O_4Na$ $[M+Na]^+$ 507.3199 found 507.3193.

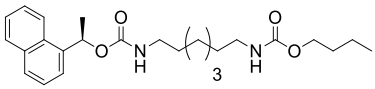

18-(*R*)

(*R*)-1-(1-napthyl)ethyl-*n*-butoxycarbonylaminoheptyl-carbamate 18-(*R*) **was synthesized using the same method as used for compound 19**-(*R*). ^{1}H NMR ($CDCl_3$, 300 MHz): δ 8.17 (d, *J*(H, H) = 8.1, 1H), 7.91 (d, *J*(H, H) = 7.2, 1H), 7.84 (d, *J*(H, H) = 8.1, 1H), 7.63-

7.47 (m, 4H), 6.64 (q, *J*(H, H) = 6.6, *J*(H, H) = 6.6, 1H), 4.78 (s, 1H), 4.62 (s, 1H), 4.11 (7, *J*(H, H) = 6.6 2H), 3.24-3.16 (m, 4H), 1.75 (d, *J*(H, H) = 6.6, 3H), 1.66-1.36 (m, 8H), 1.33 (br, 6H), 0.99 (t, *J*(H, H) = 7.2, 3H). ^{13}C NMR ($CDCl_3$, 75 MHz): δ 157.0, 156.1, 138.1, 134.0, 130.5, 128.9, 128.4, 126.3, 125.7, 125.4, 123.5, 123.1, 69.8, 64.7, 41.0, 31.2, 30.0, 28.9, 26.7, 21.9, 19.2, 13.9. HRMS (ESI): *m/z* calcd for $C_{25}H_{36}N_2O_4Na$ $[M+Na]^+$ 451.2573 found 451.2566.

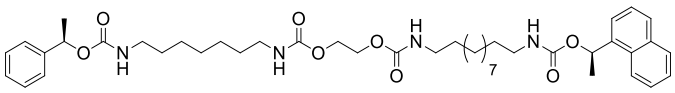

25-(*R,R*)

Compound 25-(*R,R*). To a solution of alcohol **30-**(*R*) (0.36 g, 1.0 mmol) and Et_3N (0.21 mL, 1.5 mmol) in dry CH_2Cl_2 (3 mL) was added dropwise a solution of 4-nitrophenyl chloroformate (0.22 g, 1.1 mmol) in CH_2Cl_2 (3 mL) via a syringe at 0 °C. The reaction mixture was stirred at room temperature for 12 h before adding (*R*)-1-(1-napthyl)ethyl 11-aminoundecylcarbamate **31**-(*R*) (0.38 g, 1.0 mmol) and Et_3N (0.21 mL, 1.5 mmol) in dry CH_2Cl_2 (3 mL). Then the resultant reaction mixture was allowed to proceed at room temperature for 12 h. The solution was washed several times with 1N NaOH and brine, dried over Na_2SO_4. After filtration and concentration, the residual oil was purified by flash chromatography (SiO_2) eluting with EtOAc/CH_2Cl_2 (20:80 to 50:50) to obtain product **25**-(*R,R*) as a white solid (0.55 g, 71% yield). ^{1}H NMR ($CDCl_3$, 300 MHz): δ 8.14 (d, *J*(H, H) = 8.1, 1H), 7.88 (d, *J*(H, H) = 7.2, 1H), 7.80 (d, *J*(H, H) = 8.1, 1H), 7.61-7.43 (m, 4H), 7.35-7.26 (m, 5H), 6.60 (q, *J*(H, H) = 6.6, *J*(H, H) = 6.6, 1H), 5.82 (q, *J*(H, H) = 6.6, *J*(H, H) = 6.6, 1H), 4.70 (br, 4H), 4.24 (s, 4H), 3.18-3.14 (m, 8H), 1.71 (d, *J*(H, H) = 6.6, 3H), 1.54 (d, *J*(H, H) = 6.6, 3H), 1.47 (br, 8H), 1.29-1.26 (m, 20H). ^{13}C NMR ($CDCl_3$, 75 MHz): δ 156.3, 156.1, 142.4, 138.1, 134.0, 130.5, 128.9, 128.6, 128.4, 127.8, 126.3, 126.1, 125.7, 125.4, 123.5, 123.1, 72.7, 69.7, 63.2, 41.2, 30.0, 29.6, 29.3, 28.9, 26.8, 26.7, 22.6, 22.0. HRMS (ESI): *m/z* calcd for $C_{44}H_{64}N_4O_8Na$ $[M+Na]^+$ 799.4622 found 799.4612.

The enantiomer 25-(*S,S*)**, diastereoisomers 24-**(*R,S*) **and 24-**(*S,R*) **were synthesized using the same method.**

Compound 24-(*S,R*): ^{1}H NMR ($CDCl_3$, 300 MHz): δ 8.14 (d, *J*(H, H) = 8.1, 1H), 7.88 (d, *J*(H, H) = 7.2, 1H), 7.80 (d, *J*(H, H) = 8.1, 1H), 7.61-7.43 (m, 4H), 7.35-7.26 (m, 5H), 6.60 (q, *J*(H, H) = 6.6, *J*(H, H) = 6.6, 1H), 5.82 (q, *J*(H, H) = 6.6, *J*(H, H) = 6.6, 1H), 4.70 (br, 4H), 4.24 (s, 4H), 3.18-3.14 (m, 8H), 1.71 (d, *J*(H, H) = 6.6, 3H), 1.54 (d, *J*(H, H) = 6.6, 3H), 1.47 (br, 8H), 1.29-1.26 (m, 20H). ^{13}C NMR ($CDCl_3$, 75 MHz): δ 156.3, 156.1, 142.4, 138.1, 134.0, 130.5, 128.9, 128.6, 128.4, 127.8, 126.3, 126.1, 125.7, 125.4, 123.5, 123.1, 72.7, 69.7, 63.2, 41.2, 41.1, 41.0, 30.1, 30.0, 29.9, 29.6, 29.3, 28.9, 26.8, 26.7, 22.6, 22.0

5.4.3 Synthesis of achiral rods

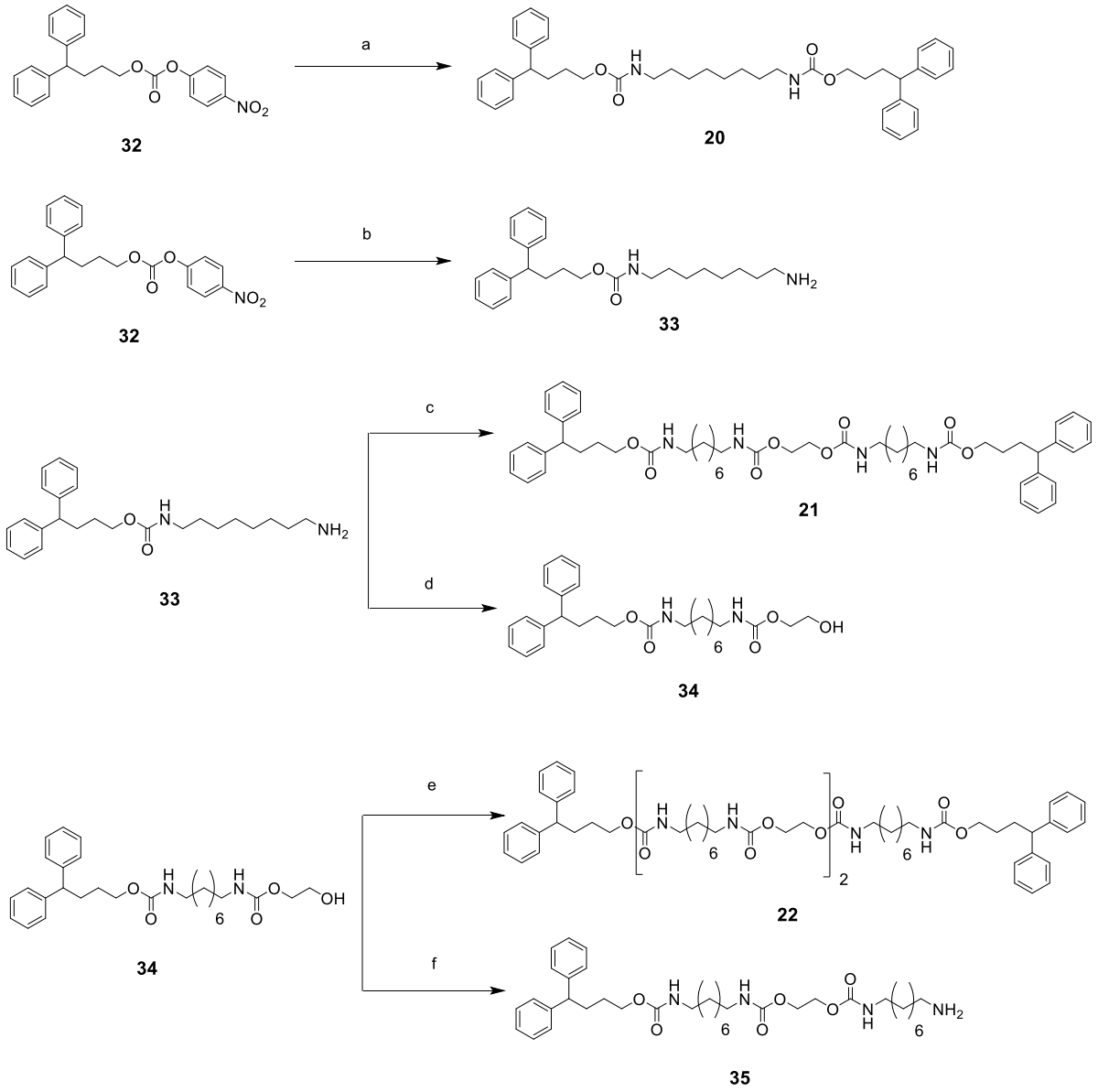

Scheme 6. Synthesis of achiral guests. a) 1,8-diaminooctane (0.5 equiv.), DIEA, CH_2Cl_2, room temperature, 12 h; b) 1,8-diaminooctane (5 equiv.), CH_2Cl_2, room temperature, 12 h; c) 4-nitrophenyl chloroformate, Et_3N, $CHCl_3$, room temperature, 0.5 h, then ethylene glycol (0.5 equiv.), reflux, 24 h; d) 4-nitrophenyl chloroformate, Et_3N, $CHCl_3$, room temperature, 0.5 h, then ethylene glycol (50 equiv.), reflux, 24 h; e) 4-nitrophenyl chloroformate, Et_3N, CH_2Cl_2, 40 °C, 24 h, then 1,8-diaminooctane (0.5 equiv.), CH_2Cl_2, room temperature, 12 h; f) 4-nitrophenyl chloroformate, Et_3N, CH_2Cl_2, 40 °C, 24 h, then 1,8-diaminooctane (5 equiv.), CH_2Cl_2, room temperature, 12 h;

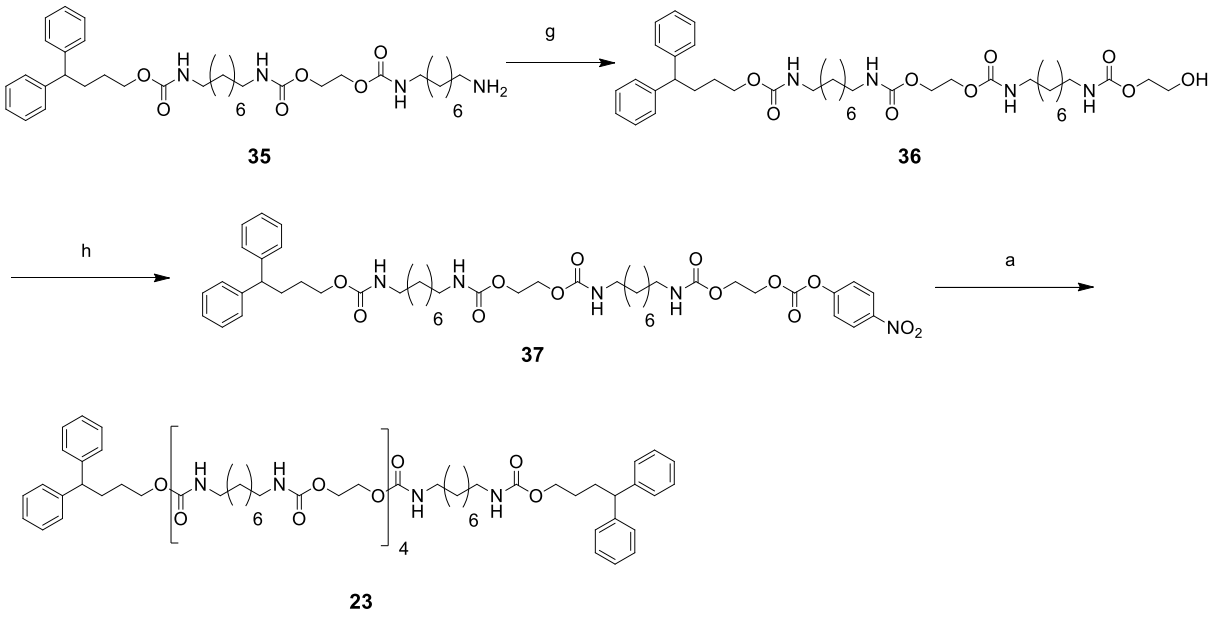

Scheme 7. Synthesis of achiral guests. g) 4-nitrophenyl chloroformate, Et_3N, $CHCl_3$, room temperature, 12 h, then ethylene glycol (50 equiv.), refluxed, 48 h; h) 4-nitrophenyl chloroformate, DIEA, CH_2Cl_2, 40 °C, 24 h.

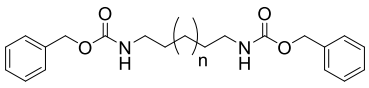

11 n = 5; **12** n = 6
13 n = 7; **14** n = 8

Benzylnonane-1,9-dicarbamate 11. To 1,9-diaminononane (0.32 g, 2.0 mmol) and DIEA (2.0 mL, 12.0 mol) in dichloromethane (10 mL) at 0 °C was added benzyl chloroformate (0.62 mL, 4.4 mmol) dropwise. Then the reaction mixture was allowed to come back at room temperature and was let to stir for 12 h. The solution was evaporated and the residue was purified by flash chromatography (SiO_2) eluting with EtOAc/CH_2Cl_2 (15:85) to obtain product **11** as a white solid (0.72 g, 85% yield). ^{1}H NMR ($CDCl_3$, 300 MHz): δ 7.37-7.30 (m, 10H), 5.10 (s, 4H), 4.71 (br, 2H), 3.21 (q, *J*(H, H) = 6.6, *J*(H, H) = 6.6, 4H), 1.51-1.46 (m, 4H), 1.28 (br, 10H).^{13}C NMR ($CDCl_3$, 75 MHz): δ 156.5, 136.8, 128.6, 128.3, 128.2, 66.7, 41.2, 30.1, 29.5, 29.2, 26.8. HRMS (ES^+): *m/z* calcd for $C_{25}H_{35}N_2O_4$ $[M+H]^+$ 427.2597 found 427.258.

Benzyldecane-1,10-dicarbamate 12. To 1,0-diaminodecane (0.344 g, 2.0 mmol) and DIEA (2.0 mL, 12.0 mol) in dichloromethane (10 mL) at 0 °C was added benzyl chloroformate (0.62 mL, 4.4 mmol) dropwise. Then the reaction mixture was allowed to come back at room temperature and was let to stir for 12 h. The solution was evaporated and the residue was purified by flash chromatography (SiO_2) eluting with EtOAc/CH_2Cl_2 (15:85) to obtain product **12** as a white solid (0.79 g, 90% yield). ^{1}H NMR ($CDCl_3$, 300 MHz): δ 7.37-7.31 (m, 10H), 5.10 (s, 4H), 4.71 (br, 2H), 3.21 (q, *J*(H, H) = 6.6, *J*(H, H) = 6.6, 4H), 1.51-1.46 (m, 4H), 1.27 (br, 12H). ^{13}C NMR ($CDCl_3$, 75 MHz): δ 156.5, 136.8, 128.6, 128.3, 128.2, 66.7, 41.2, 30.1, 29.5, 29.3, 26.8. HRMS (ES^+): *m/z* calcd for $C_{26}H_{37}N_2O_4$ $[M+H]^+$ 441.2753 found 441.274.

Benzylundecane-1,11-dicarbamate 13. To 1,11-diaminoundecane (0.37 g, 2.0 mmol) and DIEA (2.0 mL, 12.0 mol) in dichloromethane (10 mL) at 0 °C was added benzyl chloroformate (0.62 mL, 4.4 mmol) dropwise. Then the reaction mixture was allowed to come back at room temperature and was let to stir for 12 h. The solution was evaporated and the residue was purified by flash chromatography (SiO_2) eluting with EtOAc/CH_2Cl_2 (15:85) to obtain product **13** as a white solid (0.73 g, 80% yield). ^{1}H NMR

($CDCl_3$, 300 MHz): δ 7.37-7.31 (m, 10H), 5.10 (s, 4H), 4.71 (br, 2H), 3.22 (q, *J*(H, H) = 6.6, *J*(H, H) = 6.6, 4H), 1.51-1.47 (m, 4H), 1.26 (br, 14H). ^{13}C NMR ($CDCl_3$, 75 MHz): δ 156.5, 136.8, 128.7, 128.3, 66.7, 41.3, 30.1, 29.6, 29.4, 26.8. HRMS (ES^+): *m/z* calcd for $C_{27}H_{38}N_2O_4Na$ $[M+Na]^+$ 477.2729 found 477.272.

Benzyldodecane-1,12-dicarbamate 14. To 1,12-diaminododecane (0.40 g, 2.0 mmol) and DIEA (2.0 mL, 12.0 mol) in dichloromethane (10 mL) at 0 °C was added benzyl chloroformate (0.62 mL, 4.4 mmol) dropwise. Then the reaction mixture was allowed to come back at room temperature and was let to stir for 12 h. The solution was evaporated and the residue was purified by flash chromatography (SiO_2) eluting with EtOAc/CH_2Cl_2 (15:85) to obtain product **14** as a white solid (0.80 g, 85% yield). ^1H NMR ($CDCl_3$, 300 MHz): δ 7.37-7.31 (m, 10H), 5.10 (s, 4H), 4.71 (br, 2H), 3.22 (q, *J*(H, H) = 6.6, *J*(H, H) = 6.6, 4H), 1.51-1.46 (m, 4H), 1.27-1.25 (m, 16H). ^{13}C NMR ($CDCl_3$, 75 MHz): δ 156.5, 136.8, 128.7, 128.3, 128.2, 66.7, 41.3, 30.1, 29.6, 29.4, 26.9. HRMS (ES^+): *m/z* calcd for $C_{28}H_{41}N_2O_4$ $[M+H]^+$ 469.3066 found 469.305.

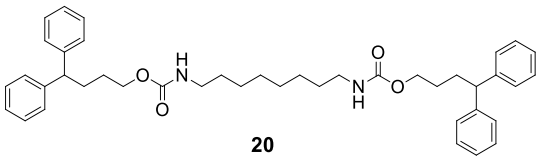

20

(4,4-diphenylbutyl)octane-1,8-dicarbamate 20. To a solution of 4,4-diphenylbutyl-(4-nitrophenyl) carbonate[11] **32** (0.18 g, 0.46 mmol) in dry CH_2Cl_2 (10 mL) was added dropwise a mixture solution of 1,8-diaminooctane (33 mg, 0.23 mmol) and DIEA (0.50 mL, 2.8 mmol) in CH_2Cl_2 (10 mL) by a syringe at 0 °C. Then the reaction mixture was allowed to proceed at room temperature for 12 h. The solution was evaporated and the residue was purified by flash chromatography (SiO_2) eluting with EtOAc/CH_2Cl_2 (30:70) to obtain product **20** as a white solid (0.125 g, 84% yield). ^1H NMR ($CDCl_3$, 300 MHz): δ 7.30-7.14 (m, 20H), 4.58 (s, 2H), 4.08 (t, *J*(H, H) = 6.6, 4H), 3.93 (t, *J*(H, H) = 7.8, 2H), 3.16 (q, *J*(H, H) = 6.6, *J*(H, H) = 6.6, 4H), 2.14 (q, *J*(H, H) = 7.8, *J*(H, H) = 7.8, 4H), 1.62-1.55 (m, 4H), 1.48-1.43 (m, 4H), 1.27 (br, 8H). ^{13}C NMR ($CDCl_3$, 75 MHz): δ 156.8, 144.9, 128.6, 127.9, 126.3, 64.7, 51.1, 41.1, 32.0, 30.1, 29.3, 27.8, 26.8. HRMS (ESI): *m/z* calcd for $C_{42}H_{53}N_2O_4$ $[M+H]^+$ 649.4005 found 649.3998.

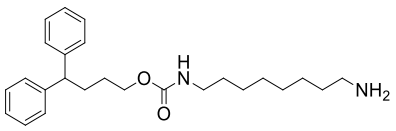

33

4,4-diphenylbutyl 8-aminooctylcarbamate 33. To a solution of 1,8-diaminooctane (3.3 g, 23 mmol) in dry CH_2Cl_2 (200 mL) was added dropwise a solution of 4,4-diphenylbutyl-(4-nitrophenyl) carbonate **32** (1.8 g, 4.6 mmol) in in dry CH_2Cl_2 (100 mL) by a syringe over 1 h period at 0 °C. Then the reaction mixture was allowed to proceed at room temperature for 12 h. The solution was washed with 1N NaOH and brine several times, dried over Na_2SO_4. After filtration and concentration, the residual oil was purified by flash chromatography (SiO_2) eluting with MeOH/CH_2Cl_2/Et_3N (10:90:1 to 30:70:1) to obtain product **33** as yellow gel (1.43 g, 78% yield). ^1H NMR ($CDCl_3$, 300 MHz): δ 7.30-7.15 (m, 10H), 4.56 (s, 1H), 4.08 (t, *J*(H, H) = 6.3, 2H), 3.93 (t, *J*(H, H) = 7.8, 1H), 3.17 (q, *J*(H, H) = 6.3, *J*(H, H) = 6.6, 2H), 2.70 (t, *J*(H, H) = 6.9, 2H), 2.14 (q, *J*(H, H) = 7.8, *J*(H, H) = 7.8, 2H), 1.60-1.45 (m, 8H) 1.29 (br, 8H). ^{13}C NMR ($CDCl_3$, 75 MHz): δ 156.8, 144.9, 128.6, 127.9, 126.3, 64.7, 51.1, 42.1, 41.1, 33.4, 32.0, 30.1, 29.4, 29.3, 27.7, 26.9, 26.8. HRMS (ESI): *m/z* calcd for $C_{25}H_{37}N_2O_2$ $[M+H]^+$ 397.2855 found 397.2839.

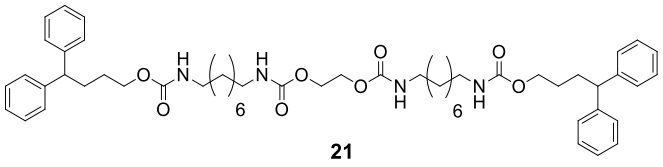

21

Compound 21. To a solution of 4-nitrophenyl chloroformate (0.336 g, 1.7 mmol) in dry $CHCl_3$ (20 mL) was added dropwise a mixture solution of 4,4-diphenylbutyl 8-aminooctylcarbamate **33** (0.63 g, 1.6 mmol) and Et_3N (1.33 mL, 9.6 mmol) in $CHCl_3$ (10 mL) via a syringe at 0 °C. After 30 min stirring at room temperature, a solution of ethylene glycol (0.044 mL, 0.8 mmol) was added to the above reaction mixture at room temperature. Then the reaction mixture was refluxed for 24 h. The solution was washed with 1N NaOH and brine several times, dried over Na_2SO_4. After filtration and

concentration, the residual oil was purified by flash chromatography (SiO2) eluting with EtOAc/CH_2Cl_2 (20:80 to 50:50) to obtain product **21** as a white solid (0.40 g, 56% yield). ^{1}H NMR ($CDCl_3$, 300 MHz): δ 7.30-7.14 (m, 20H), 4.76 (s, 2H), 4.64 (s, 2H), 4.24 (s, 4H), 4.08 (t, *J*(H, H) = 6.3, 4H), 3.93 (t, *J*(H, H) = 7.8, 2H), 3.18 (q, *J*(H, H) = 6.3, *J*(H, H) = 6.0, 8H), 2.14 (q, *J*(H, H) = 7.8, *J*(H, H) = 7.8, 4H), 1.62-1.55 (m, 4H), 1.52-1.46 (m, 8H), 1.28 (br, 16H). ^{13}C NMR ($CDCl_3$, 75 MHz): δ 156.8, 156.3, 144.9, 128.6, 127.9, 126.3, 64.7, 63.2, 51.1, 41.2, 41.1, 32.0, 30.1, 30.0, 29.2, 27.8, 26.7. HRMS (ESI): *m/z* calcd for $C_{54}H_{75}N_4O_8$ $[M+H]^+$ 907.5585 found 907.5582.

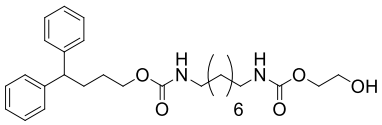

34

Compound 34. To a solution of 4-nitrophenyl chloroformate (0.61 g, 3.0 mmol) in dry $CHCl_3$ (20 mL) was added dropwise a mixture solution of 4,4-diphenylbutyl 8-aminooctylcarbamate **33** (1.0 g, 2.5 mmol) and Et_3N (0.42 mL, 3.0 mmol) in $CHCl_3$ (10 mL) via a syringe at 0 °C. After 30 min stirring at room temperature, a solution of ethylene glycol (7.0 mL, 125 mmol) and Et_3N (1.4 mL, 10.0 mmol) in $CHCl_3$ (50 mL) was added to the above reaction mixture at room temperature. Then the reaction mixture was refluxed for 24 h. The solution was washed with 1N NaOH and brine several times, dried over Na_2SO_4. After filtration and concentration, the residual oil was purified by flash chromatography (SiO_2) eluting with EtOAc/CH_2Cl_2 (20:80 to 100:1) to obtain product **34** as a white solid (0.92 g, 76% yield). ^{1}H NMR ($CDCl_3$, 300 MHz): δ 7.30-7.14 (m, 10H), 4.88 (s, 1H), 4.69 (t, *J*(H, H) = 5.4, 1H), 4.21 (t, *J*(H, H) = 4.2, 2H), 4.07 (t, *J*(H, H) = 6.3, 2H), 3.93 (t, *J*(H, H) = 7.8, 1H), 3.80 (t, *J*(H, H) = 4.2, 2H), 3.19-3.10 (m, 4H), 2.66 (br, 1H), 2.14 (q, *J*(H, H) = 7.8, *J*(H, H) = 7.8, 2H), 1.62-1.46 (m, 6H) 1.29 (br, 8H). ^{13}C NMR ($CDCl_3$, 75 MHz): δ 157.1, 156.8, 144.9, 128.6, 127.9, 126.3, 66.8, 64.7, 62.1, 51.1, 41.2, 41.0, 32.0, 30.1, 29.9, 29.2, 27.7, 26.7. HRMS (ESI): *m/z* calcd for $C_{28}H_{40}N_2O_5Na$ $[M+Na]^+$ 507.2835 found 507.2824.

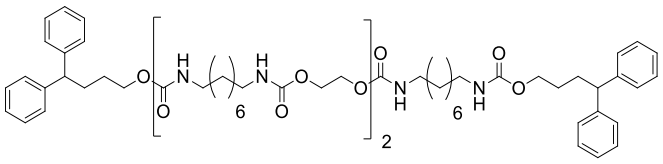

22

Compound 22. To a solution of 4-nitrophenyl chloroformate (87 mg, 0.4 mmol) in dry CH_2Cl_2 (5 mL) was added dropwise a mixture solution of compound **34** (0.2 g, 0.4 mmol) and Et_3N (0.12 mL, 0.8 mmol) in CH_2Cl_2 (5 mL) via a syringe at 0 °C. Then the reaction mixture was allowed to proceed at 40 °C for 24 h. A solution of 1,8-diaminooctane (0.03 g, 0.2 mmol) and Et_3N (0.12 mL, 0.08 mmol) in CH_2Cl_2 (10 mL) was added to the reaction mixture at 0 °C. Then the reaction mixture was allowed to proceed at room temperature for 12 h. The solution was washed with 1N NaOH and brine several times, dried over Na_2SO_4. After filtration and concentration, the residual oil was purified by flash chromatography (SiO_2) eluting with EtOAc/CH_2Cl_2 (20:80 to 90:10) to obtain product **22** as a white solid (0.11 g, 48% yield). 7.30-7.14 (m, 20H), 4.78 (s, 4H), 4.65 (s, 2H), 4.23 (s, 8H), 4.07 (t, *J*(H, H) = 6.3, 4H), 3.92 (t, *J*(H, H) = 7.8, 2H), 3.18 (q, *J*(H, H) = 6.3, *J*(H, H) = 6.3, 12H), 2.14 (q, *J*(H, H) = 7.8, *J*(H, H) = 7.8, 4H), 1.60-1.42 (m, 16H), 1.28 (br, 24H). ^{13}C NMR ($CDCl_3$, 75 MHz): δ 156.8, 156.3, 144.9, 128.6, 127.9, 126.3, 64.7, 63.2, 51.1, 41.2, 32.0, 30.1, 30.0, 29.3, 29.2, 27.8, 26.8, 26.7. HRMS (ESI): *m/z* calcd for $C_{66}H_{96}N_6O_{12}Na$ $[M+Na]^+$ 1187.6984 found 1187.6958.

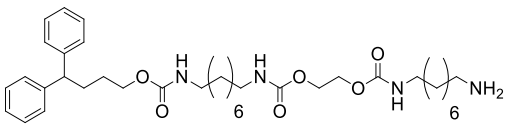

35

Compound 35. To a solution of 4-nitrophenyl chloroformate (0.357 g, 1.77 mmol) in dry CH_2Cl_2 (10 mL) was added dropwise a mixture solution of compound **34** (0.78 g, 1.6 mmol) and Et_3N (0.46 mL, 3.2 mmol) in CH_2Cl_2 (10 mL) via a syringe at 0 °C. Then the reaction mixture was allowed to proceed at 40 °C for 24 h. To a solution of 1,8-diaminooctane (1.15 g, 8 mmol) and Et_3N (0.46 mL, 3.2 mmol) in CH_2Cl_2 (100 mL) was added the above reaction solution dropwise at 0 °C. Then the reaction mixture was allowed to proceed at room temperature for 12 h. The solution was washed with 1N NaOH and brine several times, dried over Na_2SO_4. After filtration and concentration, the residual oil was purified by flash chromatography (SiO_2) eluting with MeOH/CH_2Cl_2/Et_3N (10:90:1 to 50:50:1) to obtain product **35** as a yellow solid (0.71

g, 68% yield). ^{1}H NMR ($CDCl_3$, 300 MHz): δ 7.30-7.14 (m, 10H), 4.82 (s, 2H), 4.65 (s, 1H), 4.23 (s, 4H), 4.07 (t, *J*(H, H) = 6.3, 2H), 3.92 (t, *J*(H, H) = 7.8, 1H), 3.18 (q, *J*(H, H) = 6.0, *J*(H, H) = 6.6, 6H), 2.86 (br, 2H), 2.76 (t, *J*(H, H) = 6.9, 2H), 2.14 (q, *J*(H, H) = 7.8, *J*(H, H) = 7.8, 2H), 1.60-1.48 (m, 10H) 1.30 (br, 16H). ^{13}C NMR ($CDCl_3$, 75 MHz): δ 156.8, 156.3, 144.9, 128.6, 127.9, 126.3, 64.7, 63.2, 51.1, 41.6, 41.1, 41.1, 32.1, 32.0, 30.1, 30.0, 29.2, 27.7, 26.7. HRMS (ESI): *m/z* calcd for $C_{37}H_{59}N_4O_6$ $[M+H]^+$ 655.4435 found 655.4414.

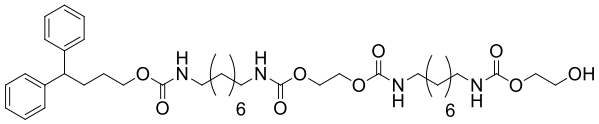

36

Compound 36. To a solution of 4-nitrophenyl chloroformate (0.22 g, 1.1 mmol) in dry $CHCl_3$ (5 mL) was added dropwise a mixture solution of compound **35** (0.654 g, 1.0 mmol) and Et_3N (0.28 mL, 2.0 mmol) in $CHCl_3$ (10 mL) via a syringe at 0 °C. After 12 h stirring at room temperature, a solution of ethylene glycol (2.78 mL, 50 mmol) and Et_3N (0.56 mL, 4.0 mmol) in $CHCl_3$ (10 mL) was added to the above reaction mixture at room temperature. Then the reaction mixture was refluxed for 48 h. The solution was washed with 1N NaOH and brine several times, dried over Na_2SO_4. After filtration and concentration, the residual oil was purified by flash chromatography (SiO_2) eluting with MeOH/CH_2Cl_2 (5:95 to 20:80) to obtain product **36** as a white solid (0.46 g, 62% yield). ^{1}H NMR ($CDCl_3$, 300 MHz): δ 7.30-7.14 (m, 10H), 4.76 (s, 3H), 4.62 (s, 1H), 4.24-4.19 (m, 6H), 4.07 (t, *J*(H, H) = 6.3, 2H), 3.93 (t, *J*(H, H) = 7.8, 1H), 3.82 (t, *J*(H, H) = 4.2, 2H), 3.21-3.12 (m, 8H), 2.86 (br, 1H), 2.14 (q, *J*(H, H) = 7.8, *J*(H, H) = 7.8, 2H), 1.60-1.48 (m, 10H) 1.30 (br, 16H). ^{13}C NMR ($CDCl_3$, 75 MHz): δ 157.1, 156.8, 156.3, 144.9, 128.6, 127.9, 126.3, 66.8, 64.7, 63.2, 62.1, 51.1, 41.2, 32.0, 30.1, 30.0, 29.2, 29.1, 27.8, 26.7, 26.6. HRMS (ESI): *m/z* calcd for $C_{40}H_{62}N_4O_9Na$ $[M+Na]^+$ 765.4414 found 765.4403.

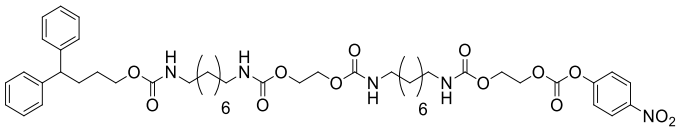

37

Compound 37. To a solution of 4-nitrophenyl chloroformate (74 mg, 0.37 mmol) in dry CH_2Cl_2 (10 mL) was added dropwise a mixture solution of compound **36** (0.25 g, 0.34 mmol) and DIEA (0.18 mL, 1.0 mmol) in CH_2Cl_2 (10 mL) via a syringe at 0 °C. Then the reaction mixture was allowed to proceed at 40 °C for 24 h. The solvent was evaporated, and the residual oil was purified by flash chromatography (SiO_2) eluting with EtOAc/CH_2Cl_2 (10:90 to 40:60) to obtain product **37** as a yellow solid (0.23 g, 75% yield). ^{1}H NMR ($CDCl_3$, 300 MHz): δ 8.30 (d, *J*(H, H) = 7.2, 2H), 7.41 (d, *J*(H, H) = 7.2, 2H), 7.30-7.14 (m, 10H), 4.82 (s, 1H), 4.74 (s, 2H), 4.62 (s, 1H), 4.48-4.45 (m, 2H), 4.39-4.36 (m, 2H), 4.24 (s, 4H), 4.07 (t, *J*(H, H) = 6.3, 2H), 3.92 (t, *J*(H, H) = 7.8, 1H), 3.19-3.12 (m, 8H), 2.11 (q, *J*(H, H) = 7.8, *J*(H, H) = 7.8, 2H), 1.62-1.47 (m, 10H) 1.28 (br, 16H). ^{13}C NMR ($CDCl_3$, 75 MHz): δ 156.8, 156.3, 156.0, 155.5, 152.5, 145.6, 144.9, 128.6, 127.9, 126.3, 125.5, 121.9, 67.7, 64.7, 63.2, 62.0, 51.1, 41.2, 41.1, 32.0, 30.1, 30.0, 29.2, 27.7, 26.7. HRMS (ESI): *m/z* calcd for $C_{47}H_{65}N_5O_{13}Na$ $[M+Na]^+$ 930.4477 found 930.4463.

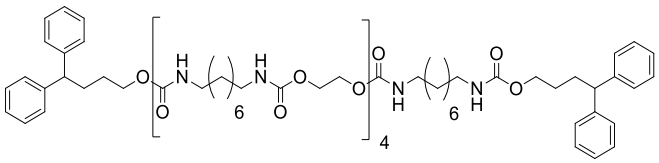

23

Compound 23. To a mixture solution of compound **37** (91 mg, 0.1 mmol) and DIEA (0.07 mL, 0.4 mmol) in dry CH_2Cl_2 (5 mL) was added a solution of 1,8-diaminooctane (7.2 mg, 0.05 mmol) in dry CH_2Cl_2 (5 mL) at 0 °C, then the resulting mixture was stirred at room temperature for 12 h. The solution was washed with 1N NaOH and brine several times, dried over Na_2SO_4. After filtration and concentration, the residual oil was purified by flash chromatography (SiO_2) eluting with MeOH/CH_2Cl_2 (1:99 to 15:85) to obtain product **23** as a white solid (40 mg, 48% yield). ^{1}H NMR (d_6-DMSO, 400 MHz): 7.30-6.80 (m, 30H), 4.07 (br, 16H), 3.94-3.91 (m, 6H), 2.96-2.91 (m, 20H), 2.07 (q, *J*(H, H) = 7.6, *J*(H, H) = 7.6, 4H), 1.44-1.35 (m, 24H), 1.21 (br, 40H). ^{13}C NMR (d_6-DMSO, 100 MHz): δ 156.2, 155.9, 145.0, 128.4, 127.5, 126.0, 63.2, 62.3, 50.1, 31.1, 29.4, 28.7, 27.4, 26.2. HRMS (ESI): *m/z* calcd for $C_{90}H_{140}N_{10}O_{20}Na$ $[M+Na]^+$ 1704.0143 found 1704.0103.

Chapter 3

Orchestrating directional molecular motions: kinetically controlled supramolecular pathways of a helical foldamer host on linear oligourethane rod-like guests

1. Introduction

Controlling the kinetics of self-assembly processes is crucial to create complex artificial machinery at the molecular level. In nature, motion occurs independently from the length scale, ranging from the molecular to the cellular level. Advanced functionality is achieved through the self-assembly of complex folded or unfolded oligomers or polymers (*e.g.* proteins or nucleic acids) working far from equilibrium. Biological machinery has evolved existence systems to synthesize proteins (*e.g.* ribosome), to disassemble nucleic acid double helices (*e.g.* helicase), to transport cargo in the cell (*e.g.* kinesin), or even to power some small organisms (*e.g.* spermatozoid flagellum).

Inspired by the biomachinery organic chemists have developed a wide range of artificial molecular machines[1,2] among which some are able to move directionally along tracks. For example, the elucidation of the kinesin I motion mechanism[3] paved the way to the development of artificial molecular walkers.[4-17] Specifically, walkers are designed to generate a directional motion on a single molecular track through repetitive operations powered by an external source of fuel. Another representative example of a biological molecular machine is DNA polymerase, a biotic pseudorotaxane-like protein assembly which can bind and move along a nucleic acid polymer while elongating it. The latter can be related to some artificial architecture in which a directional motion is generated via the threading of a macromolecule on a rod possessing a

1. A. Credi, S. Silvi, M. Venturi, Eds. Molecular machines and motors: recent advances and perspectives. Springer International Publishing: Switzerland, **2014**.
2. S. Erbas-Cakmak, D. A. Leigh, C. T. McTernan, A. L. Nussbaumer. Artificial molecular machines. *Chem. Rev.* **2015**, *115*, 10081–10206.
3. R. D. Vale, T. S. Reese, M. P. Sheetz. Identification of a novel force-generating protein, kinesin, involved in microtubule-based motility. *Cell* **1985**, *42*, 39−50.
4. M. von Delius, D. A. Leigh. Walking molecules. *Chem Soc. Rev.* **2011**, *40*, 3656–3676.
5. J. Pan, F. Li, T. G. Cha, H. Chen, J. H. Choi, Recent progress on DNA based walkers. *Curr. Opin. Biotechnol.* **2015**, *34*, 56-64.
6. W. B. Sherman, N. C. Seeman. A precisely controlled DNA biped walking device. *Nano Letters*, **2004**, *4*, 1203–1207.
7. K.-Y. Kwon, K. L. Wong, G. Pawin, L. Bartels, S. Stolbov, T. S. Rahman. Unidirectional adsorbate motion on a high-symmetry surface: "walking" molecules can stay the course. *Phys. Rev. Lett.* **2005**, *95*, 166101–116104.
8. M. von Delius, E. M. Geertsema, D. A. Leigh, D. T. D. Tang. Design, synthesis, and operation of small molecules that walk along tracks. *J. Am. Chem. Soc.* **2010**, *132*, 16134−16145.
9. M. von Delius, E. M. Geertsema, D. A. Leigh. A synthetic small molecule that can walk down a track. *Nat. Chem.* **2010**, *2*, 96−101.
10. M. J. Barrell, A. G. Campana, M. von Delius, E. M. Geertsema, D. A. Leigh. Light-driven transport of a molecular walker in either direction along a molecular track. *Angew. Chem. Int. Ed.* **2011**, *50*, 285−290.
11. A. Perl, A. Gomez-Casado, D. Thompson, H. H. Dam, P. Jonkheijm, D. N. Reinhoudt, J. Huskens. Gradient-driven motion of multivalent ligand molecules along a surface functionalized with multiple receptors. *Nat. Chem.* **2011**, *3*, 317−322.
12. P. Kovaricek, J.-M. Lehn. Merging constitutional and motional covalent dynamics in reversible imine formation and exchange processes. *J. Am. Chem. Soc.* **2012**, *134*, 9446−9455.
13. A. G. Campana, A. Carlone, K. Chen, D. T. F. Dryden, D. A. Leigh, U. Lewandowska, K. M. Mullen. A small molecule that walks on-directionally along a track without external intervention. *Angew. chem. Int. Ed.* **2012**, *51*, 5480−5483.
14. A. G. Campana, D. A. Leigh, U. Lewandowska. One dimensional random walk of a synthetic small molecule toward a thermodynamic sink. *J. Am. Chem. Soc.* **2013**, *135*, 8639−8645.
15. J. E. Beves, V. Blanco, B. A. Blight, R. Carrillo, D. M. D'Souza, D. Howgego, D. A. Leigh, A. M. Z. Slawin, M. D. Symes. Toward metal complexes that can directionally walk along tracks: controlled stepping of a molecular biped with a palladium(II) foot. *J. Am. Chem. Soc.* **2014**, *136*, 2094−2100.
16. G. S. Pulcu, E. Mikhailova, L. S. Choi, H. Bayley. Continuous observation of the stochastic motion of an individual small-molecule walker. *Nat. Nanotechnol.* **2014**, *10*,76−83
17. P. Kovaricek, J.-M. Lehn, Directional dynamic covalent motion of a carbonyl walker on a polyamine track. *Chem. - Eur. J.* **2015**, *21*, 9380−9384.

single stopper at only one extremity. Pseudorotaxanes based on cyclodextrin [18, 19] or macrocyclic[20-25] architectures have been extensively used for the design of threading oligomers or polymers. Some of these designs have even been shown to perform processive catalysis along the polymer track.[26-30]

As observed in nature, artificial molecular motions can be obtained via the dynamic self-assembly of abiotic oligomers. Recently, our group has shown that multi-turn helical aromatic oligoamide foldamers can wind around dumbbell shape molecule and form stable pseudo-rotaxane complexes termed foldaxane.[31-35] These helical molecular tapes can slowly wrap around oligocarbamate dumbbell rods then slide rapidly along them (Fig. 1). Segregating motion kinetics rather than banning some of them allowed to construct self-assembled molecular pistons.[31,32]

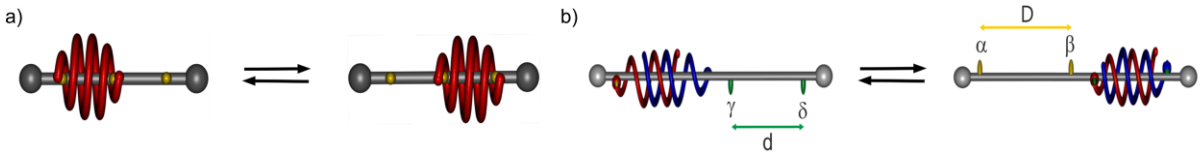

Figure 1. a) Schematic representation of shuttling motion of a single helix foldamer on two identical stations of a rod guest without dissociation. b) Schematic representation of screwing motion of a double helix whilst shuttling between two degenerated stations of a rod guest without dissociation.

18. A. Harada, J. Li, M. Kamachi. The molecular necklace: a rotaxane containing many threaded α-cyclodextrins. *Nature* **1992**, *356*, 325–327.
19. W. Herrmann. B. Keller, G. Wenz. Kinetics and thermodynamics of the inclusion of ionene-6, 10 in α-cyclodextrin in an aqueous solution. *Macromolecules* **1997**, *30*, 4966–4972.
20. R. G. E. Coumans, J. A. A. W. Elemans, R. J. M. Nolte, A. E. Rowan. Processive enzyme mimic: kinetics and thermodynamics of the threading and sliding process. *Proc. Natl. Acad. Sci. U.S.A.* **2006**, *103*, 19647–19651.
21. A. B. C. Deutman, C. Monnereau, J. A. A. W. Elemans, G. Ercolani, R. J. M. Nolte, A. E. Rowan. Mechanism of threading a polymer through a macrocyclic ring. *Science*, **2008**, *322*, 1668–1671.
22. A. B. C. Deutman, S. Cantekin, J. A. A. W. Elemans, A. E. Rowan, R. J. M. Nolte. Designing processive catalytic systems. threading polymers through a flexible macrocycle ring. *J. Am. Chem. Soc.* **2014**, *136*, 9165-9172.
23. S. Cantekin, A. J. Markvoort, J. A. A. W. Elemans, A. E. Rowan, R. J. M. Nolte. Allosterically controlled threading of polymers through macrocyclic dimers. *J. Am. Chem. Soc.* **2015**, *137*, 3915–3923.
24. E. M. Peck, W. Liu, G. T. Spence, S. K. Shaw, A. P. Davis, H. Destecroix, B. D. Smith. Rapid macrocycle threading by a fluorescent dye-polymer conjugate in water with nanomolar affinity. *J. Am. Chem. Soc.* **2015**, *137*, 8668–8671.
25. W. Liu, E. M. Peck, K. D. Hendzel, B. D. Smith. Sensitive structural control of macrocycle threading by a fluorescent squaraine dye flanked by polymer chains. *Org. Lett.* **2015**, *17*, 5268–5271.
26. P. Thordarson, E. J. A. Bijsterveld, A. E. Rowan, R. J. M. Nolte. Epoxidation of polybutadiene by a topologically linked catalyst. *Nature* **2003**, *424*, 915–918.
27. Y. Takashima, M. Osaki, Y. Ishimaru, H. Yamaguchi, A. Harada. Artificial molecular clamp: a novel device for synthetic polymerases. *Angew. Chem. Int. Ed.* **2011**, *50*, 7524–7528.
28. B. Lewandowski, G. De Bo, J. W. Ward, M. Papmeyer, S. Kuschel, M. J. Aldegunde, P. M. E. Gramlich, D. Heckmann, S. M. Goldup, D. M. D'Souza, A. E. Fernandes, D. A. Leigh. Sequence-specific peptide synthesis by an artificial small-molecule machine. *Science*, **2013**, *339*, 189–193.
29. G. De Bo, S. Kuschel, D. A. Leigh, B. Lewandowski, M. Papmeyer, J. W. Ward. Efficient assembly of threaded molecular machines for sequence-specific synthesis. *J. Am. Chem. Soc.* **2014**, *136*, 5811−5814.
30. S. F. M. van Dongen, J. Clerx, K. Nørgaard, T. G. Bloemberg, J. J. L. Cornelissen, M. A. Trakselis, S. W. Nelson, S. J. Benkovic, A. E. Rowan, R. J. M. Nolte. A clamp-like biohybrid catalyst for DNA oxidation. *Nat. Chem.* **2013**, *5*, 945–951.
31. Q. Gan, Y. Ferrand, C. Bao, B. Kauffmann, A. Grélard, H. Jiang, I. Huc. Helix-rod host-guest complexes with shuttling rates much faster than disassembly. *Science* **2011**, *331*, 1172–1175.
32. Y. Ferrand, Q. Gan, B. Kauffmann, H. Jiang, I. Huc. Template-induced screw motions within an aromatic amide foldamer double helix. *Angew. Chem. Int. Ed.* **2011**, *50*, 7572–7575.
33. Q. Gan, Y. Ferrand, N. Chandramouli, B. Kauffmann, C. Aube, D. Dubreuil, I. Huc. Identification of a foldaxane kinetic byproduct during guest-induced single to double helix conversion. *J. Am. Chem. Soc.* **2012**, *134*, 15656–15659.
34. S. A. Denisov, Q. Gan, X.Wang, L. Scarpantonio, Y. Ferrand, B. Kauffmann, G. Jonusauskas, I. Huc, N. D. McClenaghan. Electronic energy transfer modulation in a dynamic foldaxane: proof-of-principle of a lifetime-based conformation probe. *Angew. Chem. Int. Ed.* **2016**, *55*, 1328–1333.
35. Q. Gan, X. Wang, B. Kauffmann, Y. Ferrand, I. Huc. see Chapter 2 in this thesis.

To extend its scope and to validate this strategy we decided to apply it to a newly designed architecture. Specifically, the shuttle consists of an aromatic oligoamide double helix which can bind reversibly to a rod possessing several binding stations of varying affinities and presenting both a non-bulky termination and a bulky stopper at the other end (Fig. 2a). Linear urethane guests are composed of two (or three) successive stations, the initial binding site showing a low affinity (weak-binder, α-station) whereas the terminal station was designed with a high affinity (strong binder, ω-station) for the cavity of the double helix; the two stations are separated by a spacer of varying length and bulkiness. In our earlier design, the complexation process required a slow helix unfolding-refolding process imposed by the bulky stoppers at each extremity of the guest, meanwhile our new construct favors a fast threading mechanism to reach the first station. Once threaded on the rod, the shuttle can follow two distinct molecular pathways depending of the rod structure. In the case of non-hindered spacer (*i.e.* can fit in the helix cavity), the shuttle can slide from the weak binder station towards the strong binder station until reaching the thermodynamic equilibrium (Fig. 1b). If the spacer proved too large to be accommodated in the helix hollow, thereby creating a high kinetic barrier, the helix can quickly unthread from the rod and form the thermodynamically favored complex via a slow helix unfolding-refolding process (Fig. 1c).

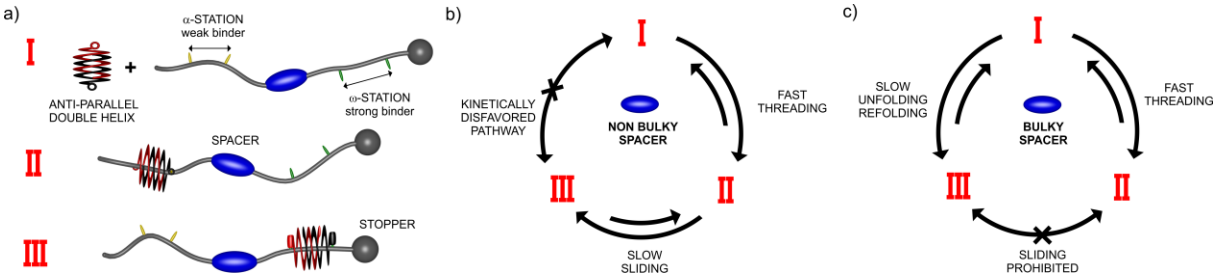

Figure 2. a) Cartoon representation of the host-guest components and assembly. The host exist as an anti-parallel double helix whereas the rod-like guests possess carbonyl hydrogen bond acceptors (yellow or green spheroids) defining two stations of varying length having either a weak (station α) or a strong affinity (station ω) for the host. In addition of the two stations, each rod is composed of a non-bulky terminus on which the host can be threaded, a bulky stopper at the other extremity of the rod and a spacer (blue spheroid) of varying size connecting the two stations. I, II and III stand for the three long lived supramolecular states of the host. b) Cycle showing the supramolecular pathway (sliding) taken by the host in the case of a non-bulky spacer. c) Cycle showing the supramolecular pathway (unfolding-refolding) used by the host in the case of a bulky spacer.

2. Synthesis

2.1 Design and synthesis of foldamer

In the recent years, our group proposed that single and double helix of aromatic oligoamide foldamers can bind to organic rods bearing carbamate groups separated by linear segment of α,ω-alkanes.[31,32,34,35] Specifically, sequence **1**[35] self-assembles as an anti-parallel duplex presenting two pyridine trimers at each extremity of the construct acting as hydrogen bond donors able to complex two carbonyl functions at a time (Fig. 3). The sixteen 8-fluoroquinoline monomers define a cylindrical 1 nm long channel able to accommodate linear alkyl segments of varying length. A strict match between the host and the guest is necessary, yet $(\mathbf{1})_2$ being a dynamic structure capable of screwing-unscrewing motions a two methylene tolerance for guest length is accepted.[35]

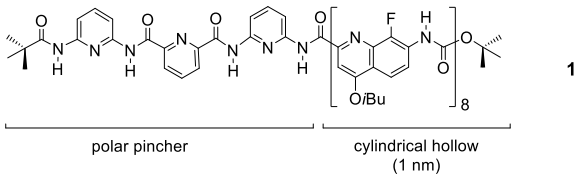

1

Figure 3. Formula of aromatic oligoamide foldamer **1**.

The synthesis of foldamer **1** is illustrated in Chapter 2. In brief, the convergent synthesis of **1** involved the coupling of a $\mathbf{P}_3$ amine segment with the acid chloride of $\mathbf{Q}^{\mathbf{F}}{}_2$-Boc dimer. After Boc cleavage in acidic medium three successive deprotection-coupling steps with the same dimer were repeated to give $\mathbf{P}_3\mathbf{Q}^{\mathbf{F}}{}_8$ in 50% overall yield over 7 steps on 300 mg scale.[35]

2.2 Design and synthesis of rods

It follows that foldaxanes with different thermodynamic stability can be constructed and assembled via the concatenation of binding stations of varying length that should lead to multi-site rod-guest molecules. To induce the directional movement of the helix from one extremity of a rod to its other end, the design is as following: (i) the entrance of the guest is made of a thin linear alkyl segment on which the helix hollow can be threaded without a substantial deformation of the foldamer; (ii) the affinity of the first station is sufficient to bind quickly to the helix but significantly lower enough to avoid host trapping; (iii) spacers placed in between the binding station can orchestrate the supramolecular pathways used by the shuttle. A non-bulky spacer will induce a kinetically favored sliding mechanism whereas a bulky spacer will force the helix to unfold and refold to reach its thermodynamically favored state; (iv) the successive stations have to show a progressive increase of their affinity towards the terminal

station to drive a directional movement; (v) the rod is terminated by a bulky aryl group stopping the shuttle and preventing a reverse slipping mechanism by the back of the rod.

To elucidate the helix motion along polyurethane rods, various molecular threads were prepared. A series of rod-like guests having up to three binding stations separated by spacers varying either by their length, their polarity or their bulkiness were synthesized. For example, oligourethane rod **4** were synthesized via the activation of amine **16** with 4-nitrophenyl chloroformate. The activated carbamate was subsequently reacted with 1,12-dodecanediol in boiling chloroform to generate the desired carbamate **21**, which possesses an alcohol end. This alcohol end of **21** was subsequently activated with 4-nitrophenyl chloroformate and coupled with amine **18** to afford rod **4**. Detailed synthesis of other rods is described in section 5.4.

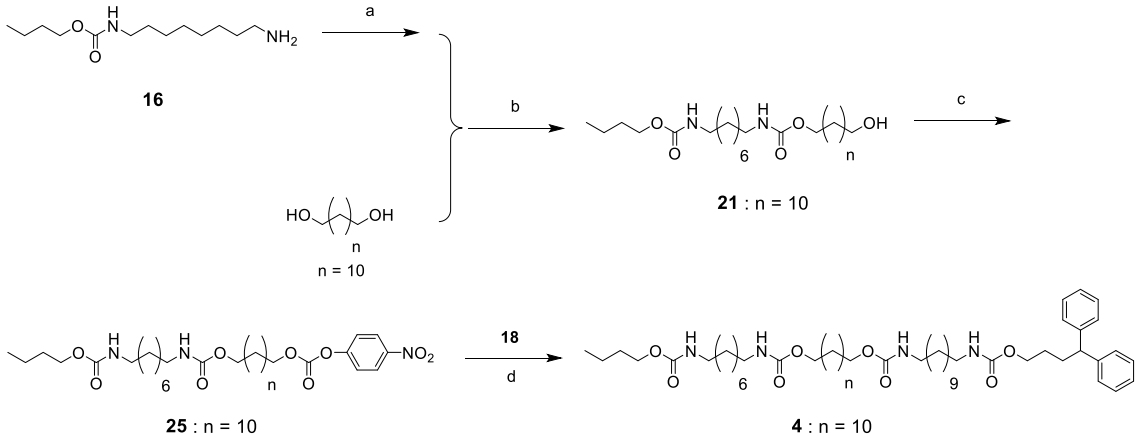

Scheme 1. Synthesis of two station rods with alkyl spacer: a) 4-nitrophenyl chloroformate, Et_3N, $CHCl_3$, 0 °C, 0.5 h, then room temperature, overnight; b) reflux, 10 d, 38%; c) 4-nitrophenyl chloroformate, Et_3N, $CHCl_3$, 40 °C, overnight, 78%; d) **18**, Et_3N, $CHCl_3$, room temperature, overnight, 95%.

Based on this synthetic strategy two types of multi-stations rod architectures **2**-**11** were prepared (Fig. 4). Binding stations were introduced according to their affinity which was established previously for their single station analogues (see Chatpter 2, section 3.2). Rods with linear non hindered spacers were synthesized to evaluate the kinetic of sliding motions. We chose first to evaluate the influence of the track polarity by comparing unbranched alkyl (**2**, **3**, **4** and **5**) and polyethylene glycol (**2**, **6** and **7**) spacers. For the two types of rods length could vary from 2 to 18 atoms. Two additional rods bearing three binding stations were also prepared (**8**, **9**). In parallel, to assess motion modes, rods bearing bulky spacers able to ban sliding motions were synthesized. Xylene (**10**) and anthracene (**11**) were selected as bulky obstacles of varying size able to block the shuttle and to force an unfolding-refolding mechanism.

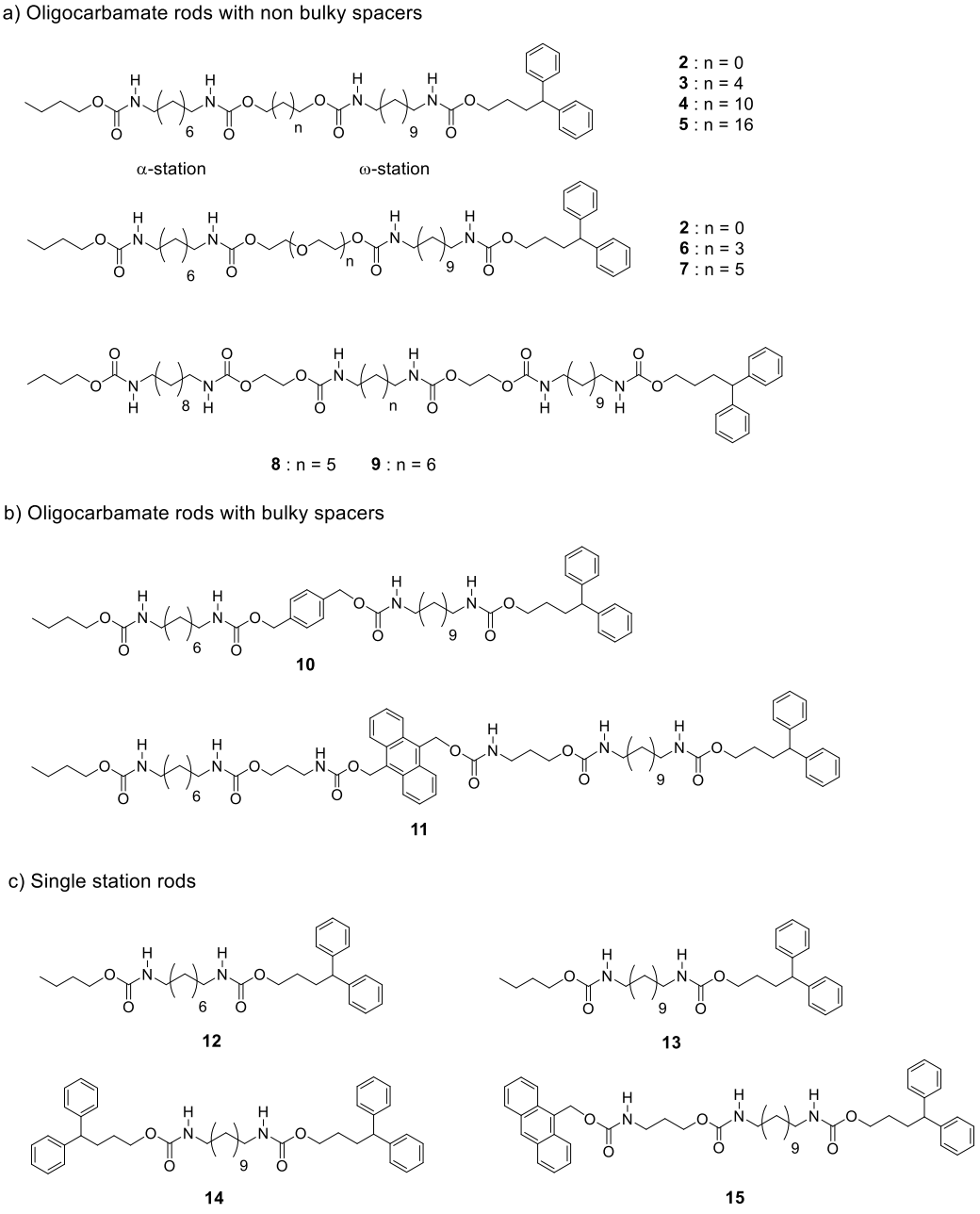

Figure 4. Formulas of the various rod-like guests used in this study.

3. Results and discussion

3.1 Exchange between antiparallel-parallel double helix

The anti-parallel nature of $(\mathbf{1})_2$ was assessed both in solution and in the solid state. As shown by ^{1}H NMR, duplex $(\mathbf{1})_2$ proved to exist as a mixture of parallel and antiparallel assemblies after purification on silica gel chromatography (Fig. 5a). Fortunately, the precipitation of the double helix in methanol provides $(\mathbf{1})_2$ as a single anti-parallel configuration.

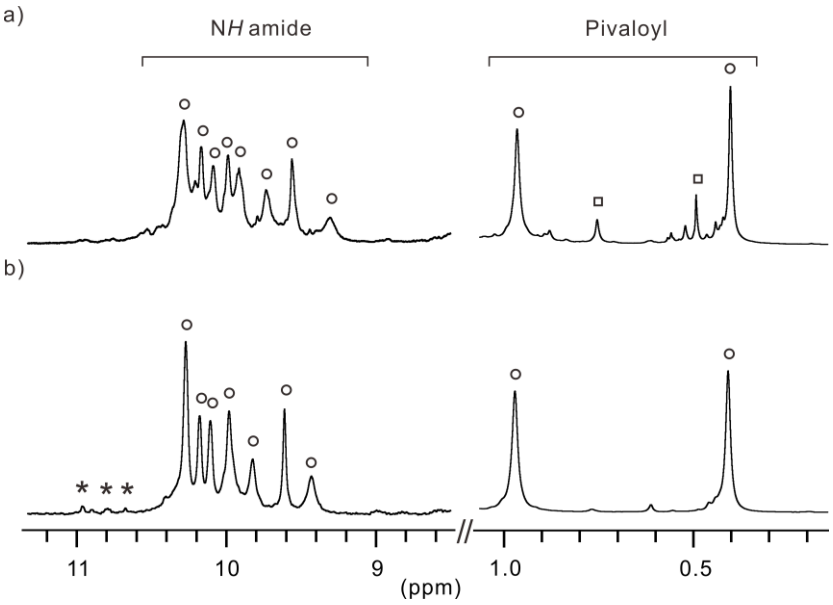

Figure 5. Representative 400 MHz NMR spectrum of **1** (2 mM) a) after column purification; b) after precipitation from MeOH. Resonances of the anti-parallel double helix and parallel double helix are marked with empty circles and empty squares, respectively. Stars denote to single helix.

X-ray quality crystals of $(\mathbf{1})_2$ were also obtained from the slow diffusion of *n*-hexane in a chloroform solution containing the foldamer. The solid-state structure was resolved and confirmed the anti-parallel arrangement of $(\mathbf{1})_2$ as well as the existence of a perfectly defined channel of 1 nm long (Fig. 6).

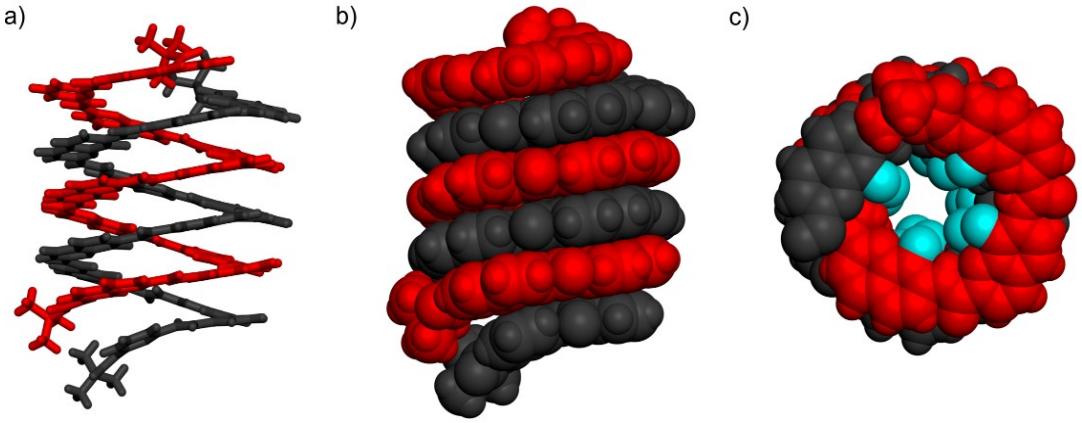

Figure 6. Structures in the solid state analyzed by single crystal x-ray crystallography of the antiparallel double helix of $(\mathbf{1})_2$: a) side view in tube and b) in CPK representations; c) top view in CPK representation. In c), P_3 trimers have been deleted to highlight the hollow of the helix; fluorine atoms are shown in light blue color. Isobutoxy side chains and solvent molecules have been omitted for clarity.

^{1}H NMR monitoring of the antiparallel $(\mathbf{1})_2$ in $CDCl_3$ at 17°C showed that the parallel/antiparallel equilibrium was slowly reached after 10 hours (Fig. 7, ratio anti/para = 63/37). Thus, the antiparallel $(\mathbf{1})_2$ can be considered as a long lived configuration (*i.e.* kinetically stable) which can be trapped quantitatively upon complexing a rod-like guest molecule.

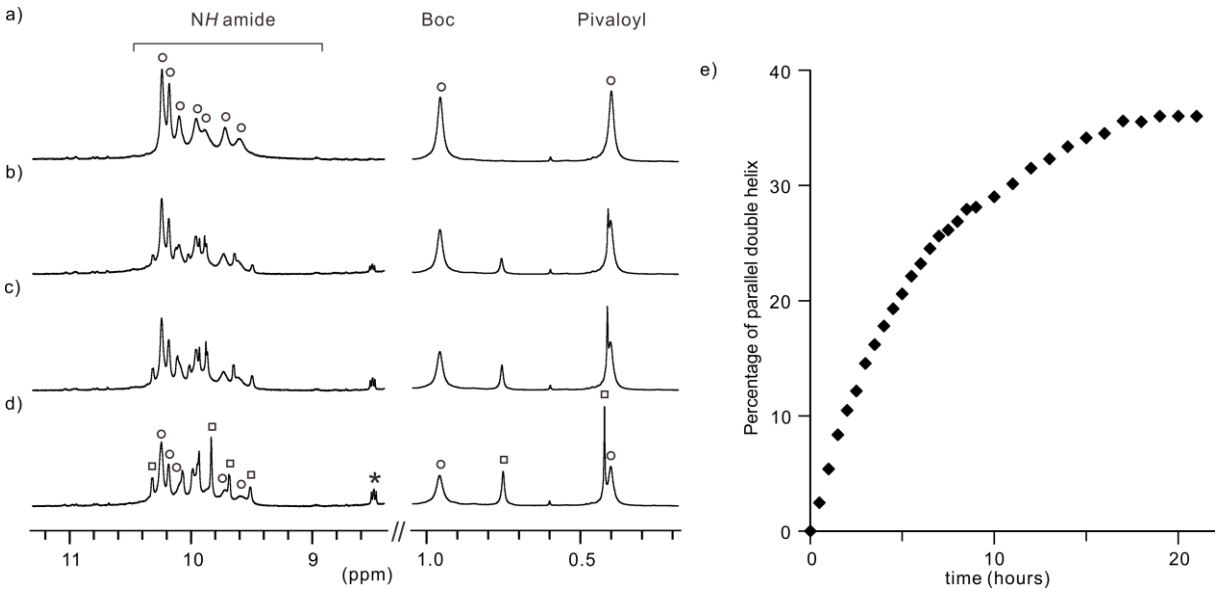

Figure 7. Representative 400 MHz NMR spectrum showing the conversion of **1** (4 mM) from antiparallel double helix to parallel double helix at 290K in $CDCl_3$. a) after 10 min.; b) after 3 hours; c) after 6 hours; d) at equilibrium. The ratio between antiparallel double helix and parallel double helix is calculated as 63:37, based on the integration of the pivaloyl resonance of the two species. Amide signals of the anti-parallel double helix and parallel double helix are marked with empty circles and empty squares, respectively. e) Time traces of percentage of parallel double helix $(\mathbf{1})_2$. Aromatic proton resonances are marked with stars. Concentration of the antiparallel and parallel double helix was obtained using ^{1}H NMR through the integration of the Boc and pivaloyl peaks of each species.

3.2 Structural and thermodynamic study of guest threading

As mentioned above, duplex $(\mathbf{1})_2$ can be obtained as its pure antiparallel form which corresponds to the matching configuration to bind linear dicarbamate rods. To compare with the affinities of $(\mathbf{1})_2$ for dumbbell shape guest measured in a recent study,[35] titrations with rods **12** and **13** were monitored. The two rods differ by the number of atoms in between the two carbamate functions: 8 and 11 atoms, respectively.

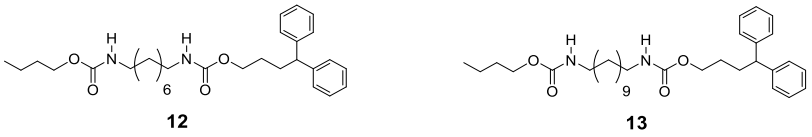

Figure 8. Formulas of single station rods **12** and **13**.

As anticipated, foldaxane complexes between the antiparallel double helix $(\mathbf{1})_2$ and guest **12** and **13** guests form readily at 17°C preventing the isomerization of free $(\mathbf{1})_2$. Upon adding guests **12** and **13** to a $CDCl_3$ solution containing $(\mathbf{1})_2$, a single set of well-resolved NMR signals was observed for the formation of $(\mathbf{1})_2\supset\mathbf{12}$ and $(\mathbf{1})_2\supset\mathbf{13}$ (Fig. 9a and 9b). It should be noted that despite the absence of stoppers on the rod, exchange was found to be slow on the NMR time scale. The binding constants for $(\mathbf{1})_2\supset\mathbf{12}$ and $(\mathbf{1})_2\supset\mathbf{13}$ were measured accurately through the integral ratios of the free and bound host amide resonances to be $K_a = 6.4\times10^3$ and 4.8×10^4 L mol^{-1}, respectively, at 17°C in $CDCl_3$.

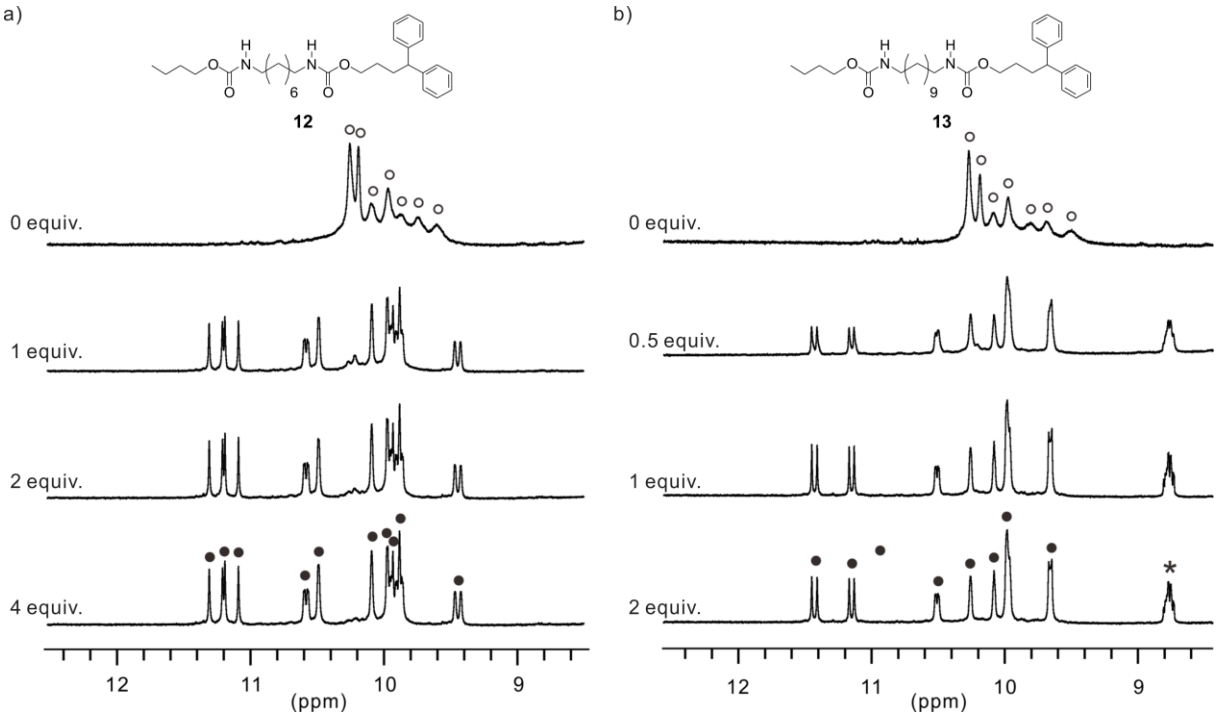

Figure 9. Representative ^{1}H NMR spectra of **1** in $CDCl_3$ at 298K titrated with various guests. a) 2 mM of **1** with rod **12**; b) 1 mM of **1** with rod **13**. Signals of the free anti-parallel $(\mathbf{1})_2$ double helix and of

complex are marked with empty and black circles, respectively. Aromatic proton resonances are marked with stars. Concentration of the antiparallel double helix $(\mathbf{1})_2$ and of complex was obtained using ^{1}H NMR through the integration of the amide peaks of the complex and the overall amide peaks.

To confirm the guest selectivity, the differing affinity were exploited in a competition experiment which confirmed the duplex preference for **13** (Fig. 10). As expected from the individual K_a calculations, the addition to foldaxane $(\mathbf{1})_2\supset\mathbf{12}$ of rod **13** caused the dissociation of $(\mathbf{1})_2$ and its quick threading on **13** to form $(\mathbf{1})_2\supset\mathbf{13}$ ($[(\mathbf{1})_2\supset\mathbf{13}]/[(\mathbf{1})_2\supset\mathbf{12}] = 79/21$). Overall, the one order of magnitude difference between the two affinities was estimated sufficient to create a gradient of affinity on multistation rod molecules.

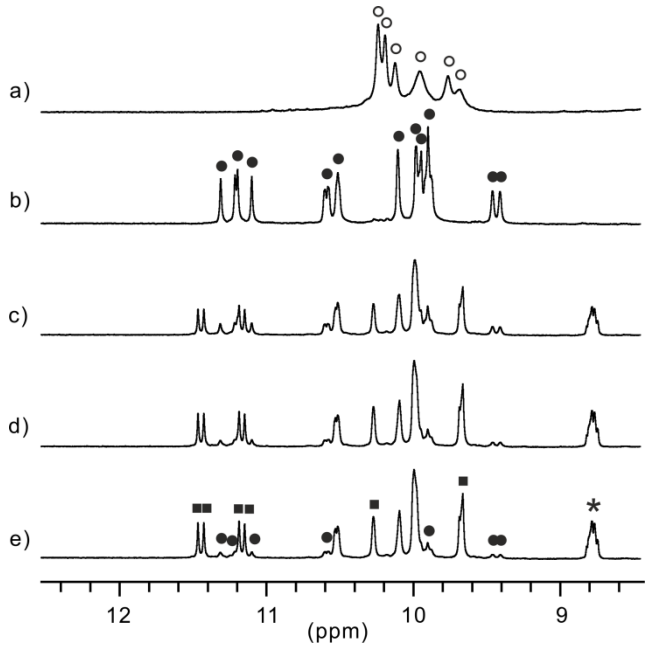

Figure 10. Part of the 400 MHz NMR spectrum of the amide region at 290K of **1** (4 mM) in $CDCl_3$: a) without guest; b) in the presence of 5 equiv. of **12**; c-e) after addition of 5 equiv. of **13** at c) t = 10 min.; d) t = 30 min, and e) t = 40 min, at thermodynamic equilibrium. Amide signals of the free double helix $(\mathbf{1})_2$, foldaxane $(\mathbf{1})_2\supset\mathbf{12}$, and foldaxane $(\mathbf{1})_2\supset\mathbf{13}$ are marked with empty circles, black circles, and black squares, respectively. Aromatic proton resonances are marked with stars.

In parallel, structural insights were also gathered in the solid state. Crystals of $(\mathbf{1})_2\supset\mathbf{12}$ and $(\mathbf{1})_2\supset\mathbf{13}$ were obtained from the slow diffusion of *n*-hexane in a chloroform solution of each complex. A close-up look at both crystal structures confirmed the relative screw-motion of the helix[31,32,34,35] necessary to adjust the positioning of the pyridine trimer pinchers toward the carbonyl groups of the rod (Fig. 11a,b). One should notice that in $(\mathbf{1})_2\supset\mathbf{12}$ the terminal diamino pyridine unit of one of the strand is flipped out, most probably to allow for the tight screwing of the duplex.

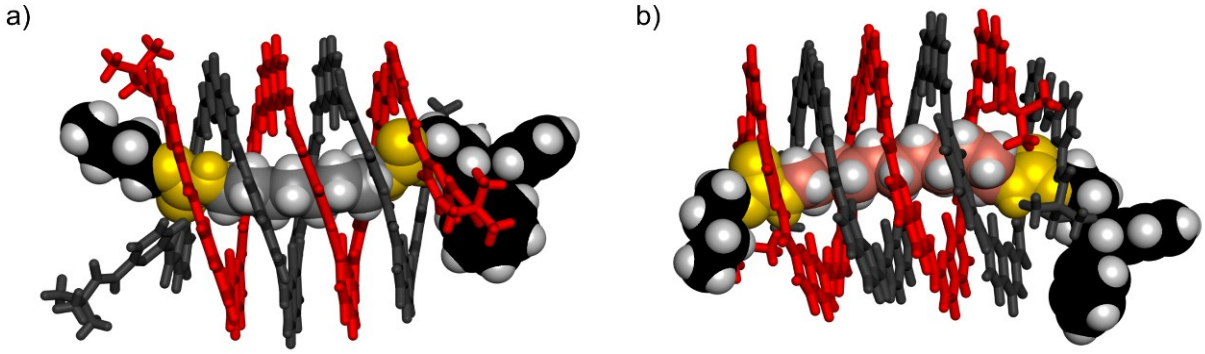

Figure 11. Side views of the two [3]foldaxanes a) $(\mathbf{1})_2\supset\mathbf{12}$ and b) $(\mathbf{1})_2\supset\mathbf{13}$, in tube (double helix) and CPK (rod) representations. Only the *P* helical enantiomers are shown. The structures belong to centrosymmetrical space groups and thus also contain the *M* enantiomers. Isobutoxy side chains and solvent molecules have been omitted for clarity.

3.3 Directional sliding motion

Following the results obtained with rods **12** and **13**, various rods (Fig. 12, rods **2**-**7**) bearing both a weak binder station (α–station, 8 atoms) and a strong binder station (ω–station , 11 atoms) were prepared. In this series of guests, the length and the polarity of the linear spacer placed in between the two binding stations were varied.

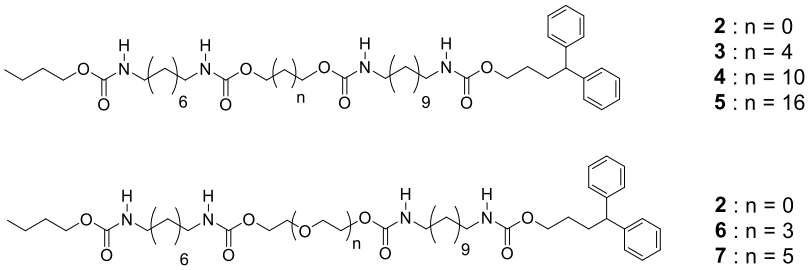

Figure 12. Formulas of single station rods **2**-**7**.

To test our design strategy, guest **2** was first equipped with a short ethylene glycol spacer (2 atoms) separating the two binding stations. Upon adding an excess (5 equiv.) of rod **2** to a $CDCl_3$ solution containing $(\mathbf{1})_2$ in its antiparallel configuration one can observe the concomitant disappearance of free $(\mathbf{1})_2$ associated with the emergence of a single set of resonances corresponding to the fast and quantitative threading of $(\mathbf{1})_2$ on **2** (Fig. 13b). Strong NOE contacts observed between the bound rod and the double helix clearly indicate that the new species can be assigned to the threading of the duplex on the α–station (Fig. 14). This [3]foldaxane was named $(\mathbf{1})_2\supset\mathbf{2}\alpha$ in reference to the weak binder station and represent the kinetically favored state. Upon standing at 17°C, $(\mathbf{1})_2\supset\mathbf{2}\alpha$ progressively disappeared over the course of days and was replaced by another foldaxane species (Fig. 13c-e) reflecting that $(\mathbf{1})_2\supset\mathbf{2}\alpha$ was not the thermodynamic complex. The new species was assigned to be the double helix $(\mathbf{1})_2$ positioned

on the strong binder station (11 atoms) and was named $(\mathbf{1})_2\supset\mathbf{2}\omega$. The ^{1}H NMR resonances of $(\mathbf{1})_2\supset\mathbf{2}\omega$ appears downfield shifted which is consistent with an unscrewing motion inducing a global decrease of the ring current effect in the duplex. Moreover, no measurable amount of the higher aggregate, [5]foldaxane, in which two double helices are bound to the rod, was observed. The equilibrium was reached after almost 3 days and the final ratio ω/α was found to be 75/25 (Table 1, page 88). Thus, the [3]foldaxane $(\mathbf{1})_2\supset\mathbf{2}\omega$ can be viewed as the thermodynamically favored state.

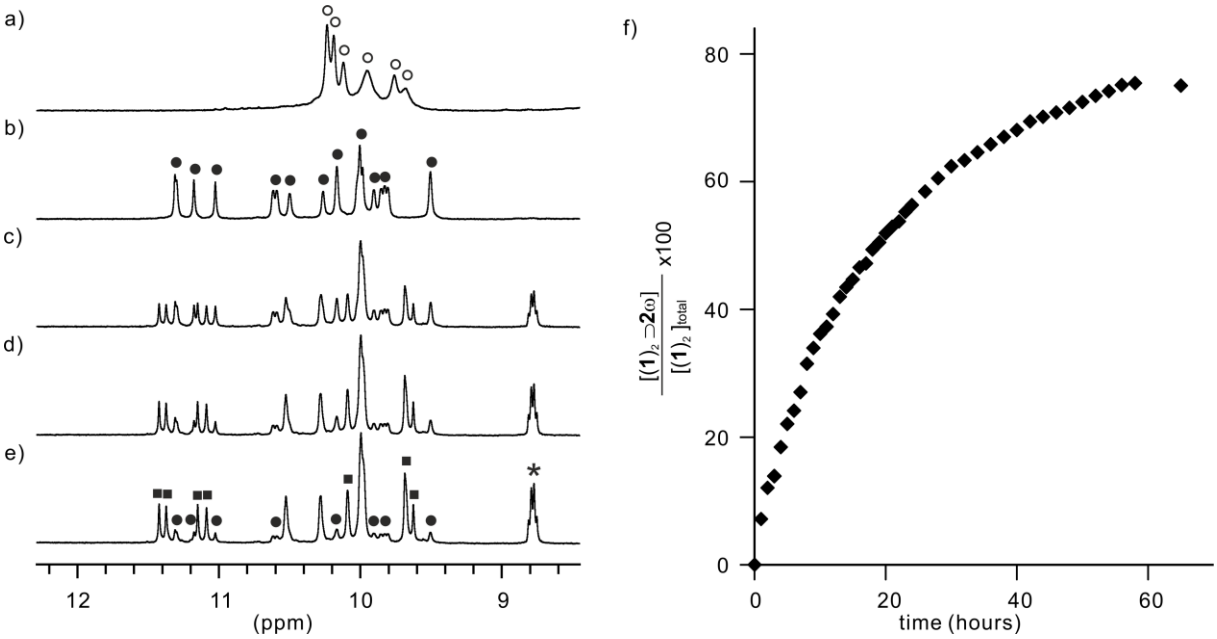

Figure 13. Part of the 400 MHz NMR spectrum of the amide region at 290K of **1** (4 mM) in $CDCl_3$: a) without guest; b-e) after addition of 5 equiv. of **2** at b) t = 15 min.; c) t = 20 h; d) t = 40 h; e) t = 56 h, at thermodynamic equilibrium. Resonances denoted with empty circles stand for the free double helix $(\mathbf{1})_2$ whereas black circles and black squares stand for $(\mathbf{1})_2\supset\mathbf{2}\alpha$ and $(\mathbf{1})_2\supset\mathbf{2}\omega$, respectively. Aromatic proton resonances are marked with stars. f) Time traces of threading and sliding motion of $(\mathbf{1})_2$ on rods **2**. Concentration of host on each station was obtained using ^{1}H NMR through the integration of the amide resonances of the double helix.

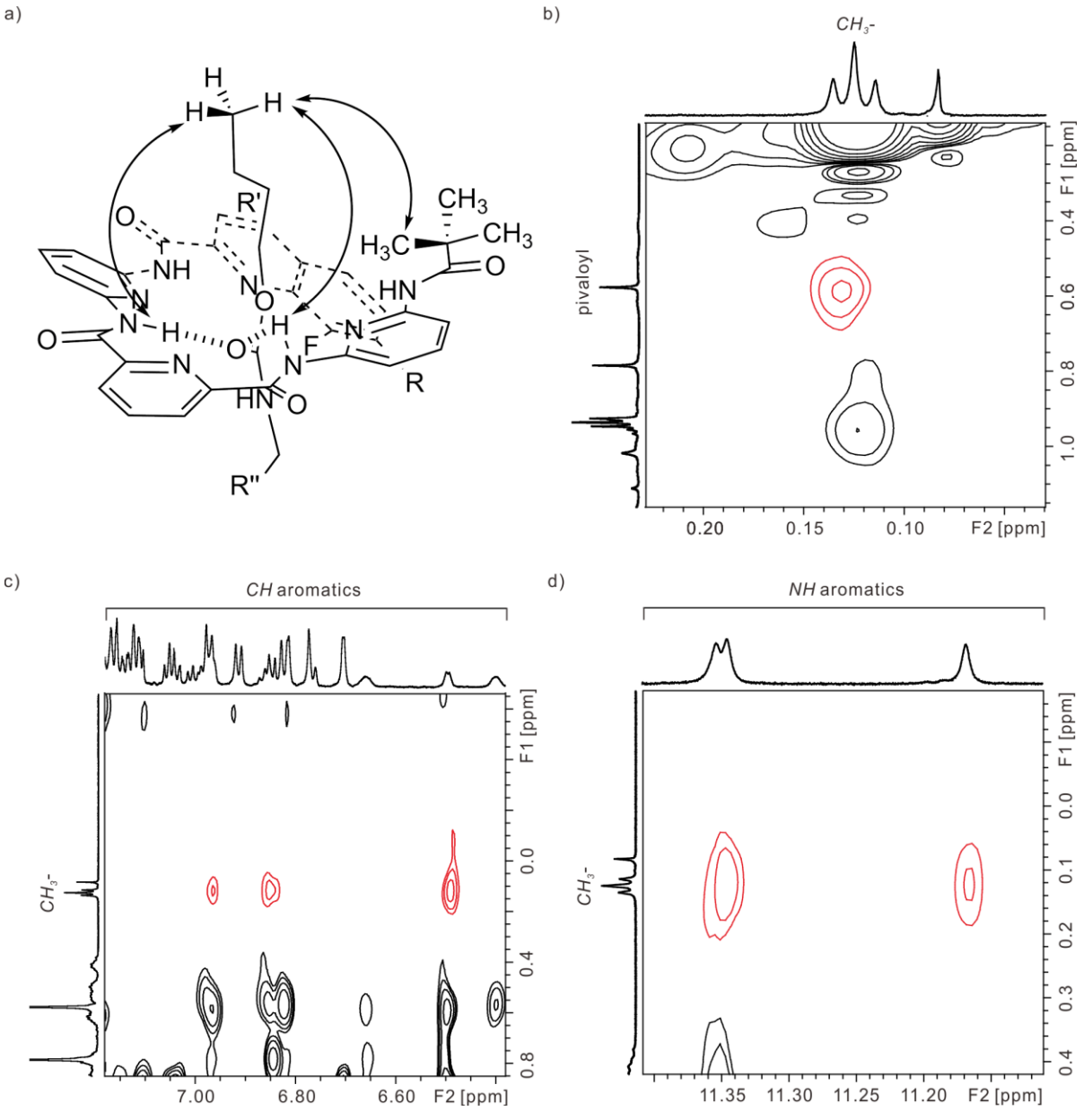

Figure 14. Excerpt of the 2D NOESY spectrum in $CDCl_3$ at -15 °C (700 MHz) of $(\mathbf{1})_2\supset\mathbf{2}\alpha$ recorded with 300 ms mixing time showing the NOE correlations between the methyl group of the nButyl entrance and a) the pivaloyl group of the pyridine adjacent to the entrance; b) the *CH* aromatics and c) the *NH* aromatics.

X-ray-quality single crystals were obtained by slow diffusion of *n*-hexane into a $CDCl_3$ solution of $(\mathbf{1})_2$ and **2** beforehand let to reach thermodynamic equilibrium. Surprisingly, despite the use of an excess of guest **2** to favor the crystallization of the [3]foldaxane $(\mathbf{1})_2\supset\mathbf{2}\omega$, the resolution of the solid-state structure revealed a five component assembly made of two double helices threaded on rod **2** (Fig. 15). Due to the flexibility of its pending α–station, $(\mathbf{1})_2\supset\mathbf{2}\omega$ is most probably less prone to crystallize than the highly folded and compact [5]foldaxane $(\mathbf{1})_4\supset\mathbf{2}$.

Yet, the structure confirmed that **2** can complex both stations and can undergo a relative screw-motion to adjust its structure to the rod.

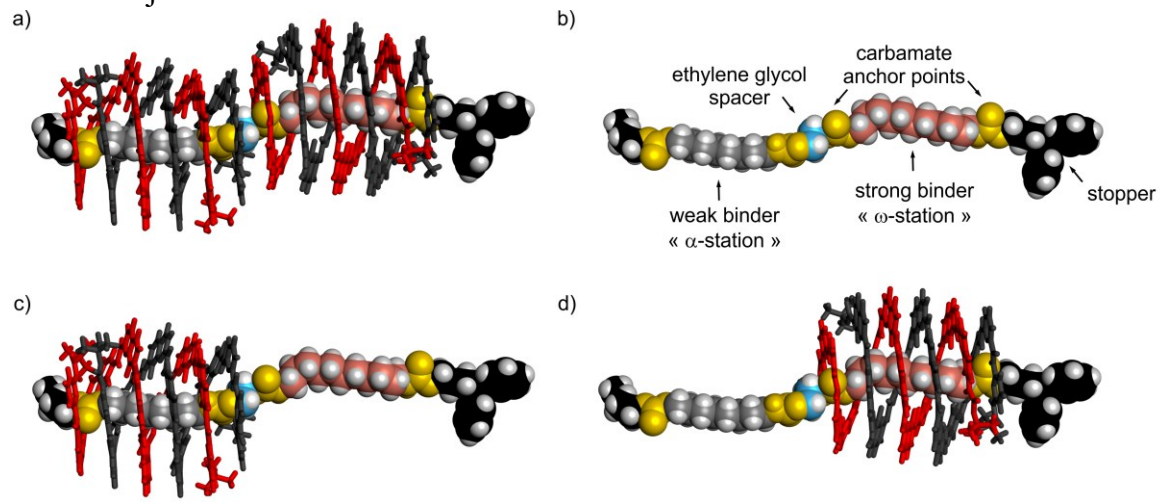

Figure 15. Structures in the solid state analyzed by single crystal X-ray crystallography: a) Side views of the X-ray structure of $(\mathbf{1})_4\supset\mathbf{2}$, the guest and the helices appear in CPK and tube representations, respectively. b) Isolated representation of the crystalline structure of the rod-like guest **2** as it exists in [5]foldaxane $(\mathbf{1})_4\supset\mathbf{2}$. c, d) tube (host) and CPK (guest) representations of [3]foldaxane $(\mathbf{1})_2\supset\mathbf{2}\alpha$ and $(\mathbf{1})_2\supset\mathbf{2}\omega$, respectively. In c) and d) a double helix has been omitted on the strong binder or the weak binder stations, respectively. Only the *P* helical enantiomers are shown. The structures belong to centrosymmetrical space groups and thus also contain the *M* enantiomers. Isobutoxy side chains and solvent molecules have been omitted for clarity.

At this stage of the study the helix motion mode cannot be established with certainty. However, the absence of parallel duplex trace during the experiment let us think that the motion could only proceed via a sliding mechanism. Indeed, an unfolding-refolding mechanism would only occur through the dissociation of $(\mathbf{1})_2$ implying its reassembly into both anti-parallel and parallel double helix, the latter being not able to bind $(\mathbf{1})_2\supset\mathbf{2}$. Based on this assumption, the monitoring of the process as a function of time by ^{1}H NMR gives us an estimate of the rate of sliding of the double helix. Assuming that a first order kinetic is valid during this initial phase of the sliding motion (reverse reaction negligible), a first order kinetic constant can be calculated to be $k = 1.2 \times 10^{-5}$ s^{-1} (Fig. 16 and Table 1).

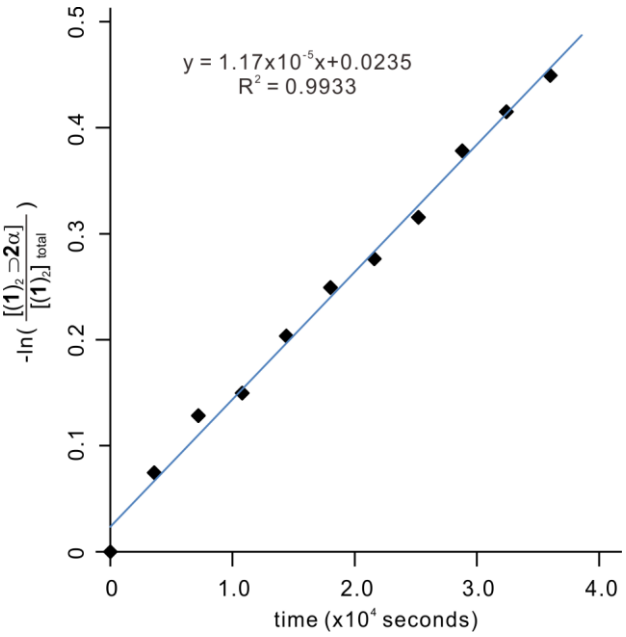

Figure 16. Plot of $-\ln([(\mathbf{1})_2\supset\mathbf{2}\alpha]/[(\mathbf{1})_2]_{total})$ against t, where $([(\mathbf{1})_2\supset\mathbf{2}\alpha]/[(\mathbf{1})_2]_{total})$ denotes the ratio of $(\mathbf{1})_2\supset\mathbf{2}\alpha$, and t is time. The linear relationship indicated a first order kinetics, and the rate constant *k* was obtained from the slope as 1.2×10^{-5} s^{-1}.

Then, we examined the sliding rates of $(\mathbf{1})_2$ on rods equipped with linear aliphatic spacers ranging in length from 6 to 18 atoms. As in the experiment described above for **2** sliding rate were calculated for rods **3**, **4** and **5**. In each of this three rods the spacer length was elongated to reach 6, 12 and 18 methylenes, respectively. To our great surprise, the shuttle proved to slide 30 times faster on rod **3** than on rod **2** despite being 4 atoms longer ($k = 37.3 \times 10^5$ s^{-1}). Similarly, the motion of $(\mathbf{1})_2$ on the longer rods **4** and **5** were shown to be almost 10 times faster than on **2**. An explanation would be that antiparallel duplex $(\mathbf{1})_2$ has weak interaction with the carbamate group adjacent to the α-station, slowing down the sliding process. Unexpectedly, the effect of the spacer elongation on the sliding rate follows an unexpected non-monotonous trend. However, this first set of data on linear alkyl spacers clearly indicates that the rates of sliding are clearly influenced by the spacer length and thus imply that the double helix uses a sliding mechanism to transit from the α– to the ω–station.

Then, we decided to investigate the influence of the spacer polarity against the sliding rate of the double helix. Rods **6** and **7** were prepared and equipped with tetraethylene- and hexaethyleneglycol spacers (11 and 17 atoms), respectively. In addition of these two new molecular tracks **2** was also considered in this series as its spacer can be viewed indifferently either as a two methylene long alkane or a monoethylene glycol spacer. As observed for the alkane series, $(\mathbf{1})_2$ threaded quickly on the α–station then it was shown to slide progressively on the ω–station. For both rods **6** and **7**, the rates of sliding were found to be significantly faster than for rods **4** and **5** equipped with alkane spacers of similar length. The shuttle was found to

travel at a rate of 36 × 10^5 s^{-1} and 23 × 10^5 s^{-1} on rods **6** and **7** (Table 1), respectively, which proved to be 2 and 3 times faster than on **4** and **5**. Again when compared to the short ethylene glycol spacer, the apparent sliding rates on tetraethylene glycol and hexaethylene glycol were found to be higher by 30 and 20 fold, respectively.

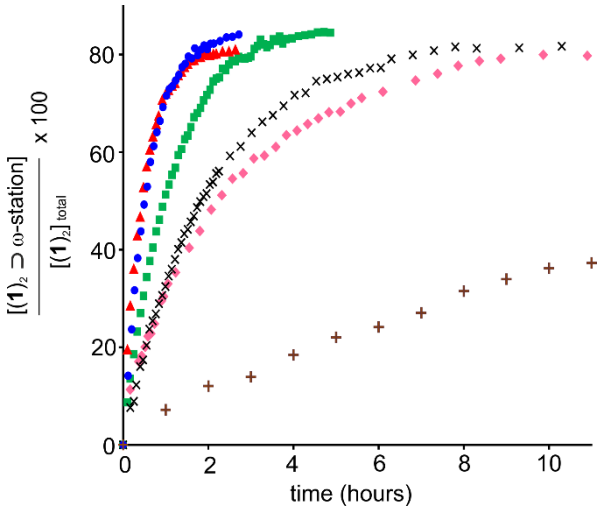

Figure 17. Time traces of threading and sliding motion of $(\mathbf{1})_2$ on rods **2** (+), **3** (▲), **4** (×), **5** (◆), **6** (●) and **7** (■). Concentration of host on each station was obtained using ^{1}H NMR through the integration of the amide resonances of the double helix.

Table 1. Kinetic data for the sliding of the investigated complexes determined by ^{1}H NMR.

[3]foldaxane	**1⊃2**	**1⊃3**	**1⊃4**	**1⊃5**	**1⊃6**	**1⊃7**	**1⊃ 8**	**1⊃9**
k (10^{-5} s^{-1})[a]	1.2	37.3	11.3	9.7	36.3	23.0	n. d.	n. d.
time to reach equilibrium (hours)	55	1.9	7.8	11.4	2.4	3.5	216	216
% of $(\mathbf{1})_2$ on ω-station	75	81	82	81	83	85	80	64
spacer length in atoms	2	6	12	18	11	17	18	19

[a] the first order kinetic constant k was calculated based on the integration of the ^{1}H NMR amide resonances corresponding to each complex $(\mathbf{1})_2\supset\mathbf{2}\alpha$ and $(\mathbf{1})_2\supset\mathbf{2}\omega$. The slope extracted from the plot of $-\ln([(\mathbf{1})_2\supset\mathbf{2}\alpha]/[(\mathbf{1})_2]_{total})$ as function of time corresponds to the kinetic constant of the sliding process. Calculation was performed during the initial phase of the helix motion for which the back sliding can be considered negligible.

Following this result, the rod design was taken one step further by placing an additional binding station, in between the α– and ω–stations. First, rod **8** was prepared with an extra binding station coding for a weak affinity for the antiparallel $(\mathbf{1})_2$ (K_a = 1100 L mol^{-1}). A second

molecular thread, rod **9**, was synthesized with two successive α–stations separated by an ethylene glycol spacer and a ω–station to terminate the track (Fig. 18).

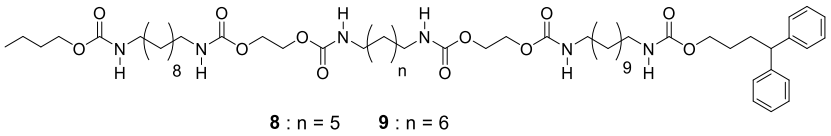

8 : n = 5 **9** : n = 6

Figure 18. Formulas of three station rods **8** and **9** with non-bulky spacer.

The threading experiments with rod **8** and **9** were further analyzed by ^{1}H NMR. However, the apparent sliding rate constant determination did not prove as straightforward as for the previous rods due to intermediate binding sites and reverse sliding. Instead, to compare with the others molecular threads we monitored the time needed to reach the thermodynamic equilibrium (Table 1). When compared to rods **3**-**7**, sliding kinetic of (**1**)$_2$ to reach equilibrium (Table 1) was found to be at least 20 times slower. Both rods **8** and **9** showed a similar sliding time (216 hours) to join the terminal ω–station. As expected, the final percentage of double helix on the terminal ω–station of **9** was found to be lowered by the competition binding between the ω– and the two α–stations. In the case of rod **8**, at thermodynamic equilibrium, the final ratio was found to be only slightly altered due to weak competition of the intermediate binding site with the ω-station.

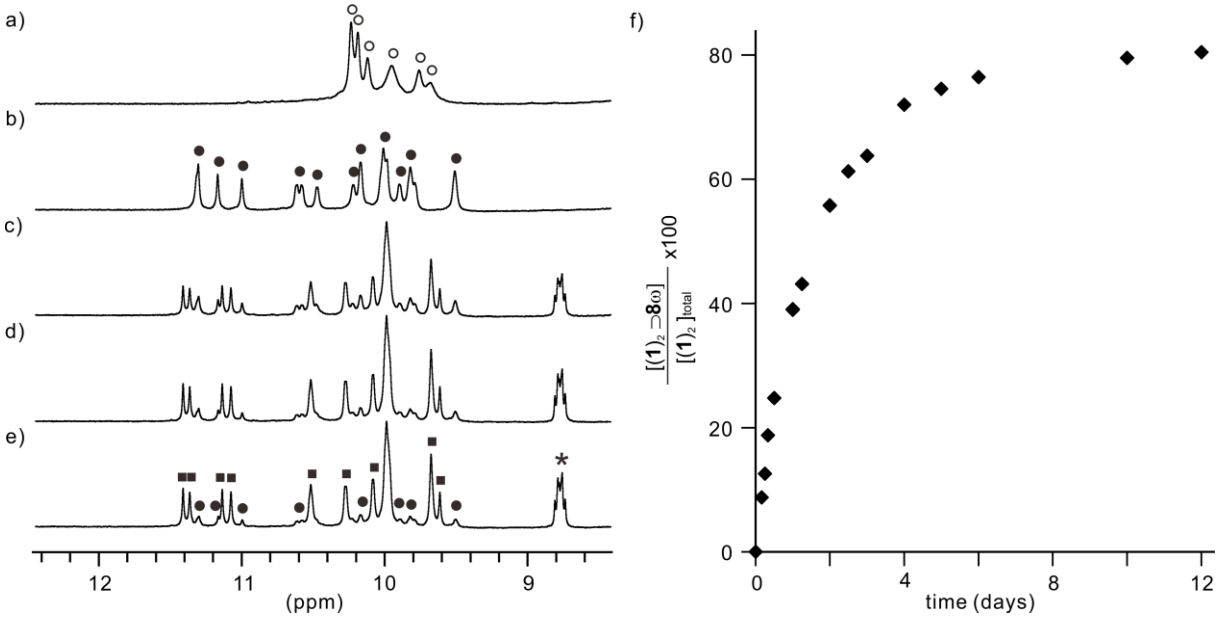

Figure 19. Part of the 300 MHz ^{1}H NMR spectrum of the amide region at 290K of **1** (4 mM) in $CDCl_3$: a) without guest; b-e) after addition of 5 equiv. of **8** at b) t = 6 min.; c) t = 3 days; d) t = 6 days; e) t = 12 days, at thermodynamic equilibrium. Resonances denoted with empty circles stand for the free double helix (**1**)$_2$ whereas black circles and black squares stand for (**1**)$_2$⊃**8**α and (**1**)$_2$⊃**8**ω, respectively. Aromatic proton resonances are marked with stars. f) Time traces of threading and sliding motion of (**1**)$_2$ on rods

8. Concentration of host on each station was obtained using ^{1}H NMR through the integration of the amide resonances of the double helix.

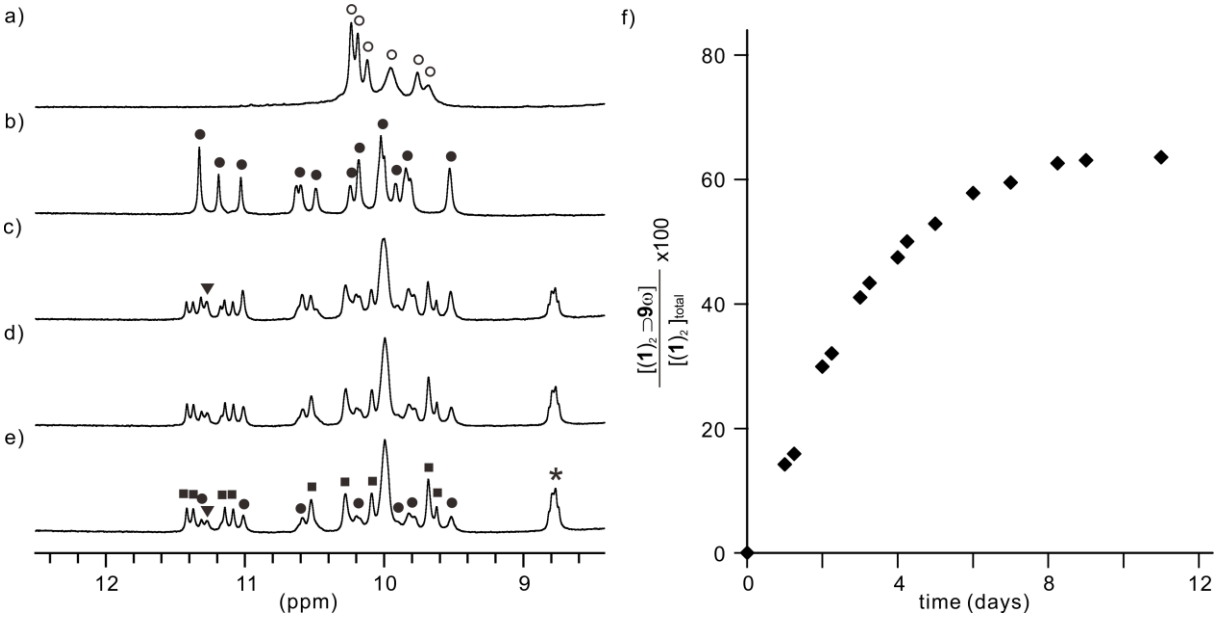

Figure 20. Part of the 300 MHz NMR spectrum of the amide region at 290K of **1** (4 mM) in $CDCl_3$: a) without guest; b-e) after addition of 5 equiv. of **9** at b) t = 6 min.; c) t = 3 days; d) t = 6 days; e) t = 12 days, at thermodynamic equilibrium. Resonances denoted with empty circles stand for the free double helix $(\mathbf{1})_2$ whereas black circles, black triangles, and black squares stand for $(\mathbf{1})_2\supset\mathbf{9}$ with $(\mathbf{1})_2$ on the first α-station, $(\mathbf{1})_2\supset\mathbf{9}$ with $(\mathbf{1})_2$ on the second α-station, and $(\mathbf{1})_2\supset\mathbf{9}$ with $(\mathbf{1})_2$ on the ω-station, respectively. Aromatic proton resonances are marked with stars. f) Time traces of threading and sliding motion of $(\mathbf{1})_2$ on rods **9**. Concentration of host on each station was obtained using ^{1}H NMR through the integration of the amide resonances of the double helix.

In conclusion, the study of this first series of rod allows to demonstrate that non-hindered alkyl rods induce the quick sequestration of a kinetically favored intermediate followed by its fast sliding along the molecular track. Moreover, the increase thread polarity was found to enhance dramatically the sliding rate of the shuttle.

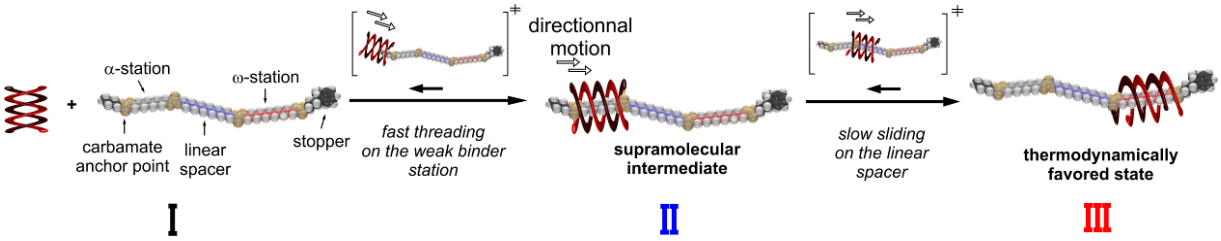

Figure 21. Schematic representation of the relative unidirectional translations of the double helix along an oligourethane rod having no obstacle.

3.4 Threading-sliding *vs.* unfolding-refolding mechanism

To validate the sliding mechanism described above and to generate an alternative motion mode for the helix, we decided to introduce a new design of rods made of two binding stations

(α and ω) separated by a bulky spacer. In contrast with the behaviour of the architecture reported above, the sliding motion of the helical shuttle is expected to be prohibited as the spacer should in theory not be able to fit in the hollow of the cavity. Thus, to reach its thermodynamic state, $(\mathbf{1})_2$, which is initially kinetically trapped on the α–station, has to unthread quickly from the rod then slowly unfold and refold on the ω–station. Based on this assumption, the self-assembly processes of $(\mathbf{1})_2$ with rods **10** and **11** equipping with spacers of varying bulkiness were investigated.

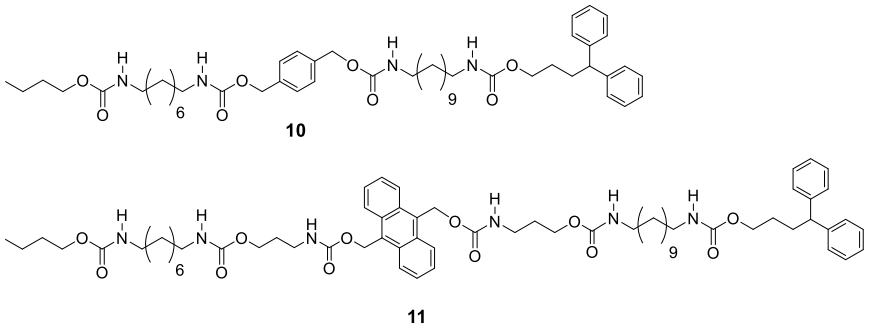

Figure 22. Formulas of two station rods **10** and **11** with bulky stopper.

The kinetics of the self-assembly processes were monitored in the same experimental conditions as for other threads. As expected, upon mixing **10** with $(\mathbf{1})_2$ one can observe the quick formation of the kinetically favored species $(\mathbf{1})_2\supset\mathbf{10}\alpha$ (Fig. 23a,b). However, the monitoring of the complex by ^{1}H NMR revealed the slow emergence of a new set of resonances corresponding $(\mathbf{1})_2\supset\mathbf{10}\alpha$. After 2 days at 17°C, around 50% of the supramolecular intermediate was replaced by the thermodynamically favored foldaxane $(\mathbf{1})_2\supset\mathbf{10}\omega$ (Fig. 23c). The equilibrium was reached after around 14 days, a value which is 6 times slower than the slowest linear foldaxane analog $(\mathbf{1})_2\supset\mathbf{2}$. The difference of motion rate is even more important when compared to $(\mathbf{1})_2\supset\mathbf{3}$, the closest linear foldaxane analog in length, against which a 175 fold rate decrease was observed. Similar monitoring with $(\mathbf{1})_2\supset\mathbf{11}$ gave an identical equilibration rate, indicating a similar motion mechanism.

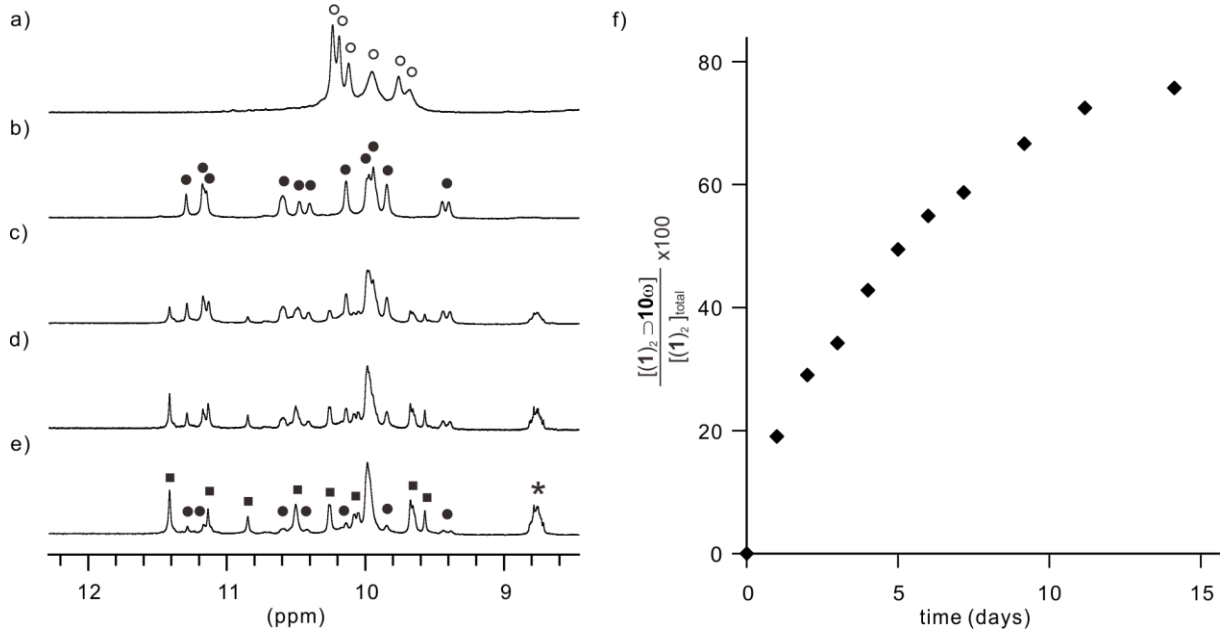

Figure 23. Part of the 300 MHz NMR spectrum of the amide region at 290K of **1** (4 mM) in $CDCl_3$: a) without guest; b-e) after addition of 5 equiv. of **10** at b) t = 10 min.; c) t = 2 days; d) t = 5 days; e) t = 15 days, at thermodynamic equilibrium. Resonances denoted with empty circles stand for the free double helix $(\mathbf{1})_2$ whereas black circles and black squares stand for $(\mathbf{1})_2\supset\mathbf{10}\alpha$ and $(\mathbf{1})_2\supset\mathbf{10}\omega$, respectively. Aromatic proton resonances are marked with stars. f) Time traces of unfolding-refolding of $(\mathbf{1})_2$ from the weak binder to the strong binder station on rods **10**. Concentration of host on each station was obtained using ^{1}H NMR through the integration of the amide resonances of the double helix.

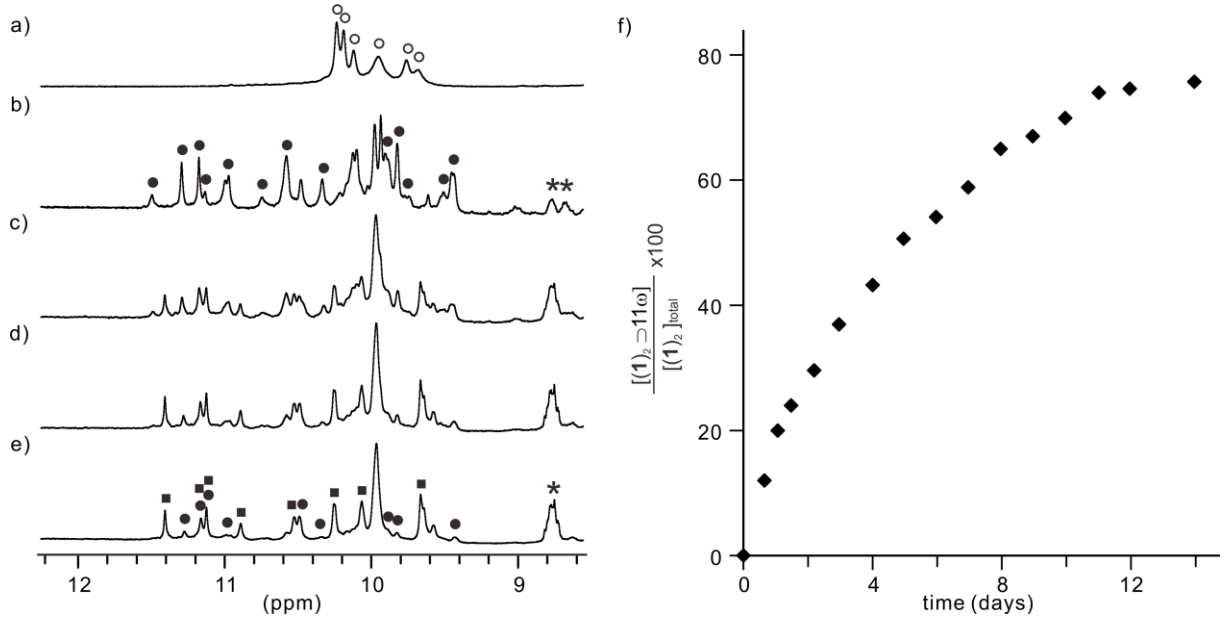

Figure 24. Part of the 300 MHz NMR spectrum of the amide region at 290K of **1** (4 mM) in $CDCl_3$: a) without guest; b-e) after addition of 5 equiv. of **11** at b) t = 6 min.; c) t = 4 days; d) t = 8 days; e) t = 14 days, at thermodynamic equilibrium. Resonances denoted with empty circles stand for the free double helix $(\mathbf{1})_2$ whereas black circles and black squares stand for $(\mathbf{1})_2\supset\mathbf{11}\alpha$ and $(\mathbf{1})_2\supset\mathbf{11}\omega$, respectively. Aromatic proton resonances are marked with stars. f) Time traces of unfolding-refolding of $(\mathbf{1})_2$ from the weak binder to the strong binder station on rods **11**. Concentration of host on each station was obtained using ^{1}H NMR through the integration of the amide resonances of the double helix.

To discard a sliding mechanism between the two stations, an additional experiment was performed in which (**1**)$_2$⊃**12** was directly mixed with rod **15** which can act as the dumbbell rod model of ω-station of **11**.

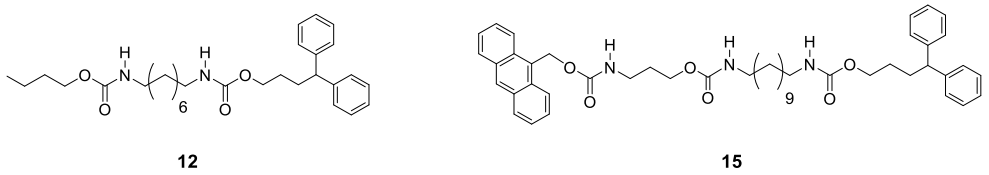

12 **15**

Figure 25. Formulas of two station rods **10** and **11** with bulky stopper.

As observed in previous studies, the formation of (**1**)$_2$⊃**15** can only occur via an unfolding-refolding mechanism.[32] Again a ^{1}H NMR monitoring of the mixture of (**1**)$_2$⊃**12** and **15** (Fig. 26) allowed us to estimate the rate of formation of (**1**)$_2$⊃**15**. We found that the equilibrium was reached after 12 days, a value which is very close to the one obtained for (**1**)$_2$⊃**10**ω and (**1**)$_2$⊃**11**ω, indicating that for these latter the helix had to unfold and refold to move from the α–station to the ω–station.

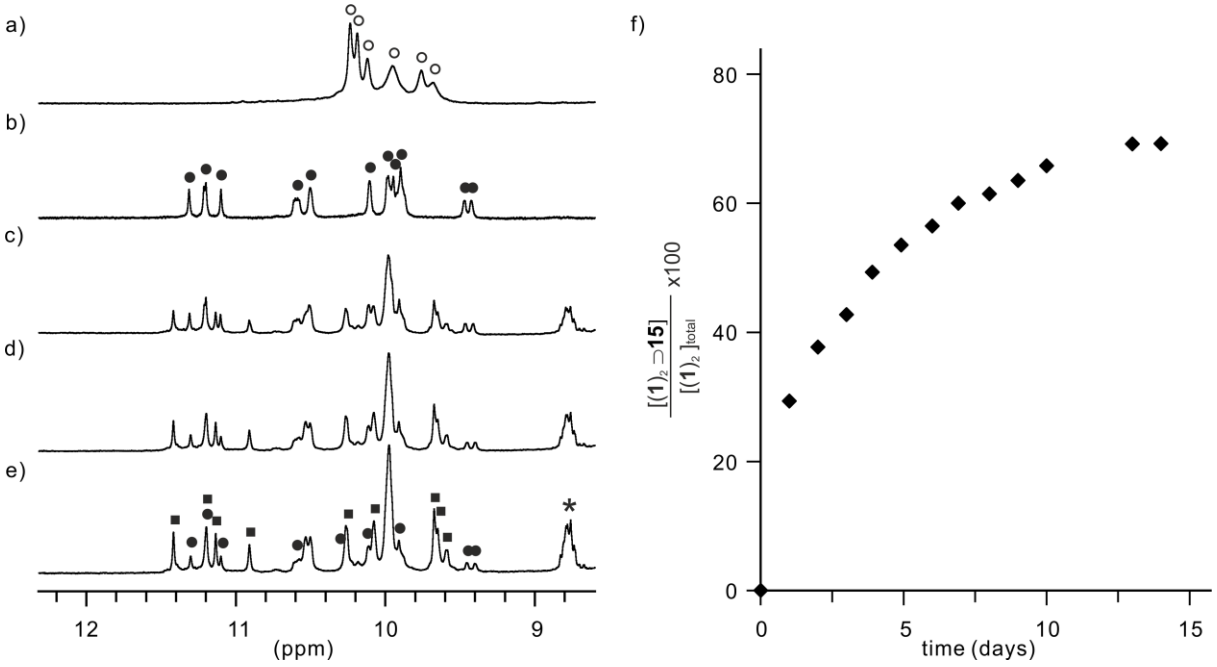

Figure 26. Part of the 300 MHz NMR spectrum of the amide region at 290K of **1** (4 mM) in $CDCl_3$: a) without guest; b) in the presence of 5 equiv. of **12**; c-e) after addition of 5 equiv. of **15** at c) t = 5 days; d) t = 10 days; e) t = 14 days, at thermodynamic equilibrium. Amide signals of the free double helix (**1**)$_2$, (**1**)$_2$⊃**12** and (**1**)$_2$⊃**15** are marked with empty circles, black circles, and black squares, respectively. Aromatic proton resonances are marked with stars. f) Time traces of unfolding-refolding of (**1**)$_2$ from rod **12** to rods **15**. Concentration of host on each station was obtained using ^{1}H NMR through the integration of the amide resonances of the double helix.

The study of this series of rod verified that by installation of a bulky spacer between the α and ω stations, the fast sliding motion is prohibited. Foldamer $(\mathbf{1})_2$ have to unthread from the α-station, following an unfolding-refolding process to associate to the thermodynamically favored ω-station.

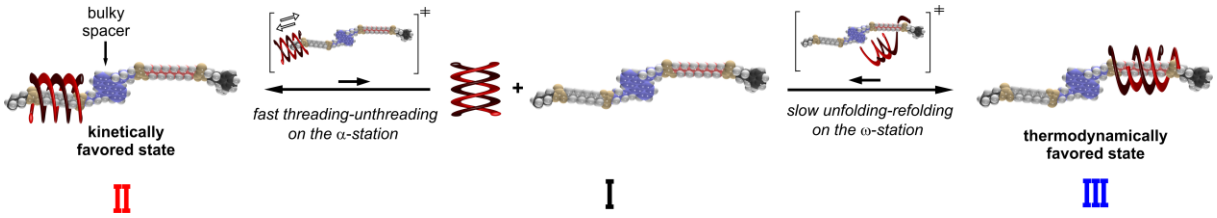

Figure 27. Schematic representation of the crossing of a bulky obstacle by a double helix through unfolding-refolding mechanism from the α-station which correspond to the kinetically favored state to the thermodynamically favored ω-station.

4. Conclusion

We showed that an antiparallel double helix can move directionally from a weak binding station to a strong binding station through distinct supramolecular pathways. When the linear track is unhindered, the double helix can quickly slide along the track to reach the thermodynamically favored station. Installation of a bulky spacer blocks the sliding process, forcing the motion process to follow kinetically less favored unfolding-refolding process. It can be envisaged that the kinetically favored sliding process allows the construction of molecular devices by functionalization of the foldamer and the track. Such molecular device can perform repeated work thanks to the unfolding-refolding of the foldamer between tracks.

5. Experimental part

5.1 Methods for NMR

NMR spectra were recorded on 3 different NMR spectrometers: (1) an Avance II NMR spectrometer (Bruker Biospin) with a vertical 7,05T narrow-bore/ultrashield magnet operating at 300 MHz for ^{1}H observation and 75 MHz for ^{13}C observation by means of a 5-mm direct BBO H/X probe with Z gradient capabilities; (2) an Avance 400 NMR spectrometer (Bruker Biospin) with a vertical 9.4T narrow-bore/ultrashield magnet operating at 400 MHz for ^{1}H observation by means of a 5-mm direct QNP $^{1}H/^{13}C/^{31}P/^{19}F$ probe with gradient capabilities; (3) an Avance III NMR spectrometer (Bruker Biospin) with a vertical 16.45T narrow-bore/ultrashield magnet operating at 700 MHz for ^{1}H observation by means of a 5-mm TXI $^{1}H/^{13}C/^{15}N$ probe with Z gradient capabilities. Chemical shifts are reported in parts per million (ppm, δ) relative to the ^{1}H residual signal of the deuterated solvent used. ^{1}H NMR splitting patterns with observed first-order coupling are designated as singlet (s), doublet (d), triplet (t), or quartet (q). Coupling constants (*J*) are reported in hertz. Data processing was performed with Topspin 2.0 software. Samples were not degassed. $CDCl_3$ from Eurisotop was used after filtration through an alumina pad followed by a distillation over calcium hydride.

NOESY. Nuclear Overhauser Effect SpectroscopY (NOESY) experiments were recorded at 700 MHz and were used to distinguish dipolar interactions and exchange between free and bound double helices with the following acquisition parameters: the acquisition was performed with 2048(t_2) x 256 (t_1) data points, in States-TPPI mode with Z gradients selection and with CW-spinlock for mixing, relaxation delay of 1.5 s, and 110 scans per increment; sweep width of 11200 Hz in both dimensions; mixing time of 300 ms. Processing was done after a sine-bell multiplication in both dimensions and Fourier transformation in 1*K* x 1*K* real points.

5.2 Kinetic studies of the sliding motion on different rods

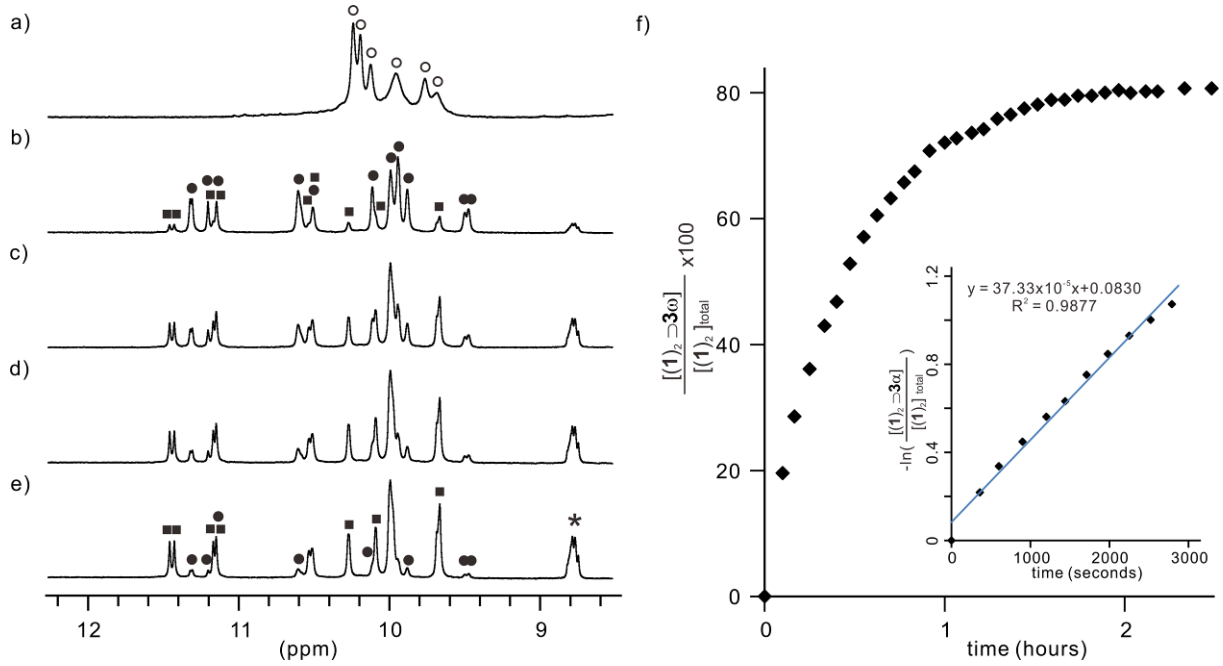

Figure 28. Part of the 400 MHz NMR spectrum of the amide region at 290K of **1** (4 mM) in $CDCl_3$: a) without guest; b-e) after addition of 5 equiv. of **3** at b) t = 6 min.; c) t = 0.5 hours; d) t = 1 hours; e) t = 1.8 hours, at thermodynamic equilibrium. Resonances denoted with empty circles stand for the free double helix $(\mathbf{1})_2$ whereas black circles and black squares stand for $(\mathbf{1})_2\supset\mathbf{3}\alpha$ and $(\mathbf{1})_2\supset\mathbf{3}\omega$, respectively. Aromatic proton resonances are marked with stars. f) Time traces of threading and sliding motion of $(\mathbf{1})_2$ on rods **3**. Concentration of host on each station was obtained using ^{1}H NMR through the integration of the amide resonances of the double helix. Inset: Plot of -ln([**1**] on first station/[**1**] total) against t, where ([**1**] on first station/[**1**] total)) denotes the ratio of $(\mathbf{1})_2\supset\mathbf{3}\alpha$, and t is time. The linear relationship indicated a first order kinetics, and the rate constant *k* was obtained from the slope as 37.33×10^{-5} s^{-1}.

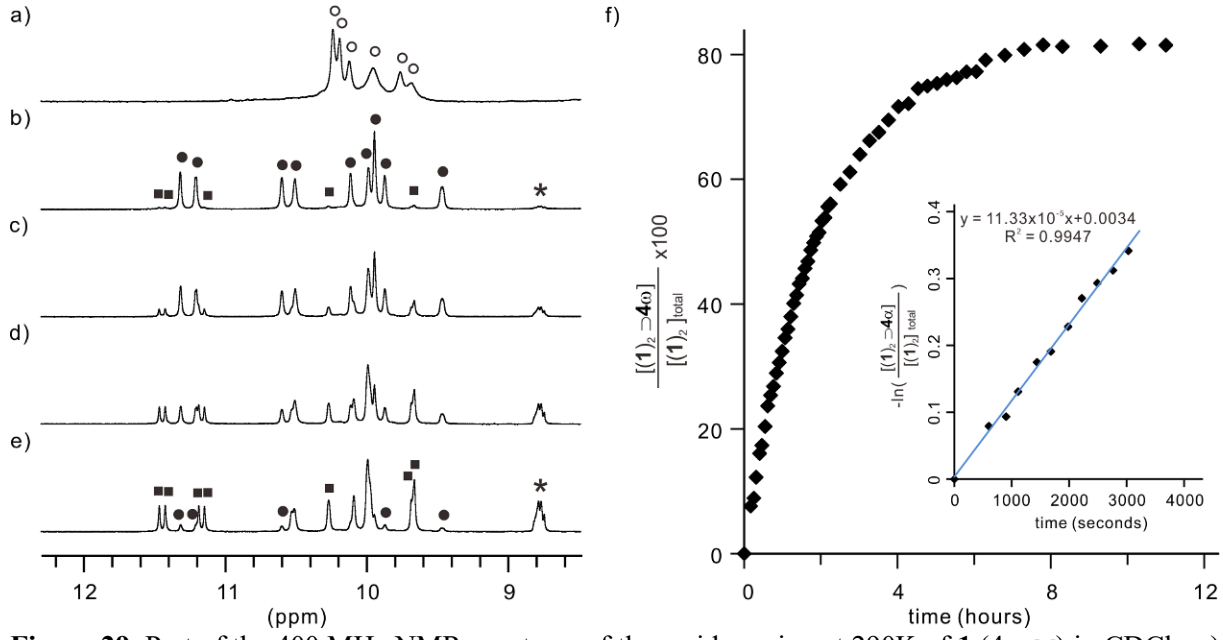

Figure 29. Part of the 400 MHz NMR spectrum of the amide region at 290K of **1** (4 mM) in $CDCl_3$: a) without guest; b-e) after addition of 5 equiv. of **4** at b) t = 10 min.; c) t = 0.75 hours.; d) t = 2.25 hours; e) t = 11 hours, at thermodynamic equilibrium. Resonances denoted with empty circles stand for the free double helix $(\mathbf{1})_2$ whereas black circles and black squares stand for $(\mathbf{1})_2\supset\mathbf{4}\alpha$ and $(\mathbf{1})_2\supset\mathbf{4}\omega$, respectively.

Aromatic proton resonances are marked with stars. f) Time traces of threading and sliding motion of $(\mathbf{1})_2$ on rods **4**. Concentration of host on each station was obtained using ^{1}H NMR through the integration of the amide resonances of the double helix. Inset: Plot of -ln([**1**] on first station/[**1**] total) against t, where ([**1**] on first station/[**1**] total)) denotes the ratio of $(\mathbf{1})_2\supset\mathbf{4}\alpha$, and t is time. The linear relationship indicated a first order kinetics, and the rate constant *k* was obtained from the slope as 11.33×10^{-5} s^{-1}.

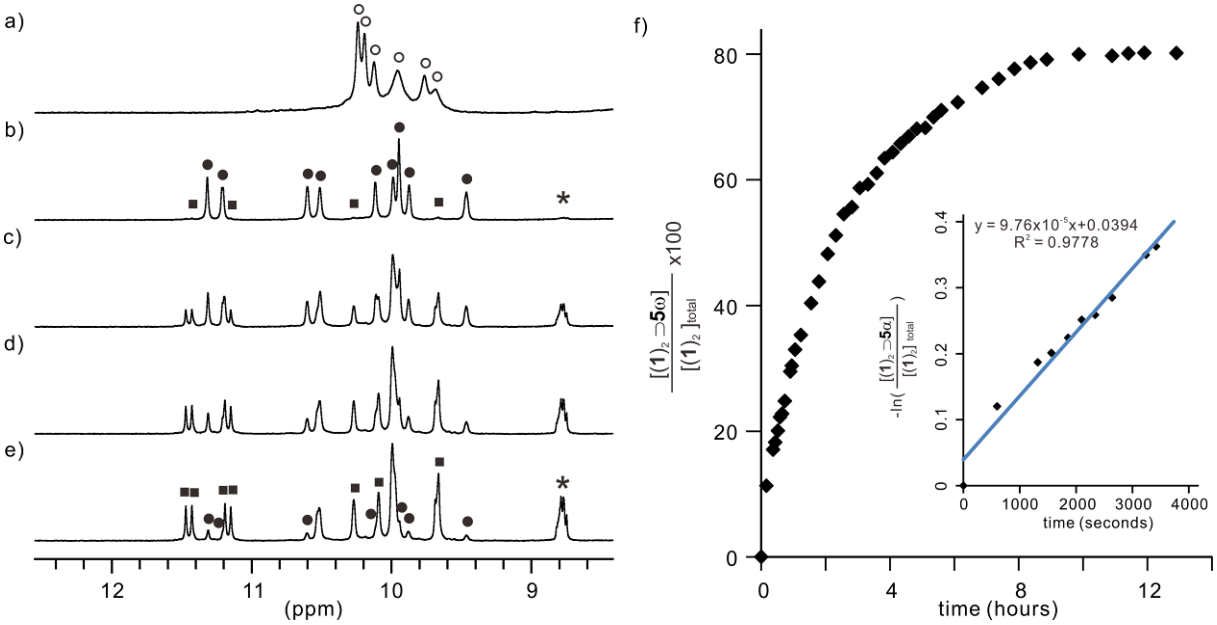

Figure 30. Part of the 400 MHz NMR spectrum of the amide region at 290K of **1** (4 mM) in $CDCl_3$: a) without guest; b-e) after addition of 5 equiv. of **5** at b) t = 10 min.; c) t = 2 hours; d) t = 4 hours; e) t = 13 hours, at thermodynamic equilibrium. Resonances denoted with empty circles stand for the free double helix $(\mathbf{1})_2$ whereas black circles and black squares stand for $(\mathbf{1})_2\supset\mathbf{5}\alpha$ and $(\mathbf{1})_2\supset\mathbf{5}\omega$, respectively. Aromatic proton resonances are marked with stars. f) Time traces of threading and sliding motion of $(\mathbf{1})_2$ on rods **5**. Concentration of host on each station was obtained using ^{1}H NMR through the integration of the amide resonances of the double helix. Inset: Plot of -ln([**1**] on first station/[**1**] total) against t, where ([**1**] on first station/[**1**] total)) denotes the ratio of $(\mathbf{1})_2\supset\mathbf{5}\alpha$, and t is time. The linear relationship indicated a first order kinetics, and the rate constant *k* was obtained from the slope as 9.67×10^{-5} s^{-1}.

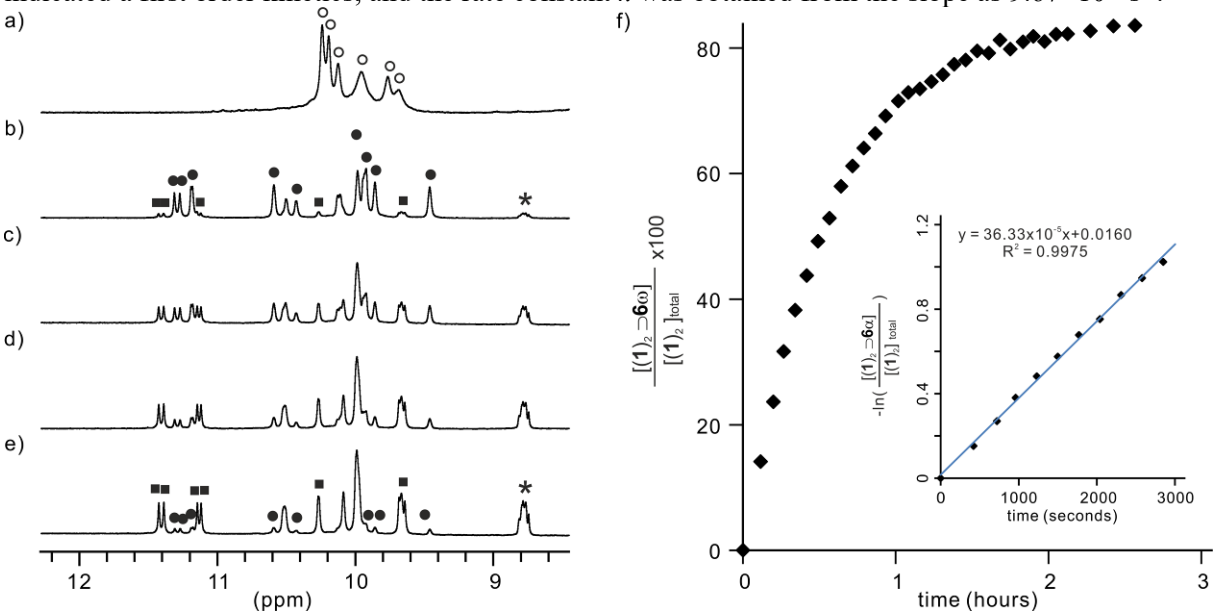

Figure 31. Part of the 400 MHz NMR spectrum of the amide region at 290K of **1** (4 mM) in $CDCl_3$: a) without guest; b-e) after addition of 5 equiv. of **6** at b) t = 7 min.; c) t = 30 min.; d) t = 60 min.; e) t = 145 min., at thermodynamic equilibrium. Resonances denoted with empty circles stand for the free

double helix $(\mathbf{1})_2$ whereas black circles and black squares stand for $(\mathbf{1})_2\supset\mathbf{6}\alpha$ and $(\mathbf{1})_2\supset\mathbf{6}\omega$, respectively. Aromatic proton resonances are marked with stars. f) Time traces of threading and sliding motion of $(\mathbf{1})_2$ on rods **6**. Concentration of host on each station was obtained using ^{1}H NMR through the integration of the amide resonances of the double helix. Inset: Plot of -ln([**1**] on first station/[**1**] total) against t, where ([**1**] on first station/[**1**] total)) denotes the ratio of $(\mathbf{1})_2\supset\mathbf{6}\alpha$, and t is time. The linear relationship indicated a first order kinetics, and the rate constant *k* was obtained from the slope as 36.33×10^{-5} s^{-1}.

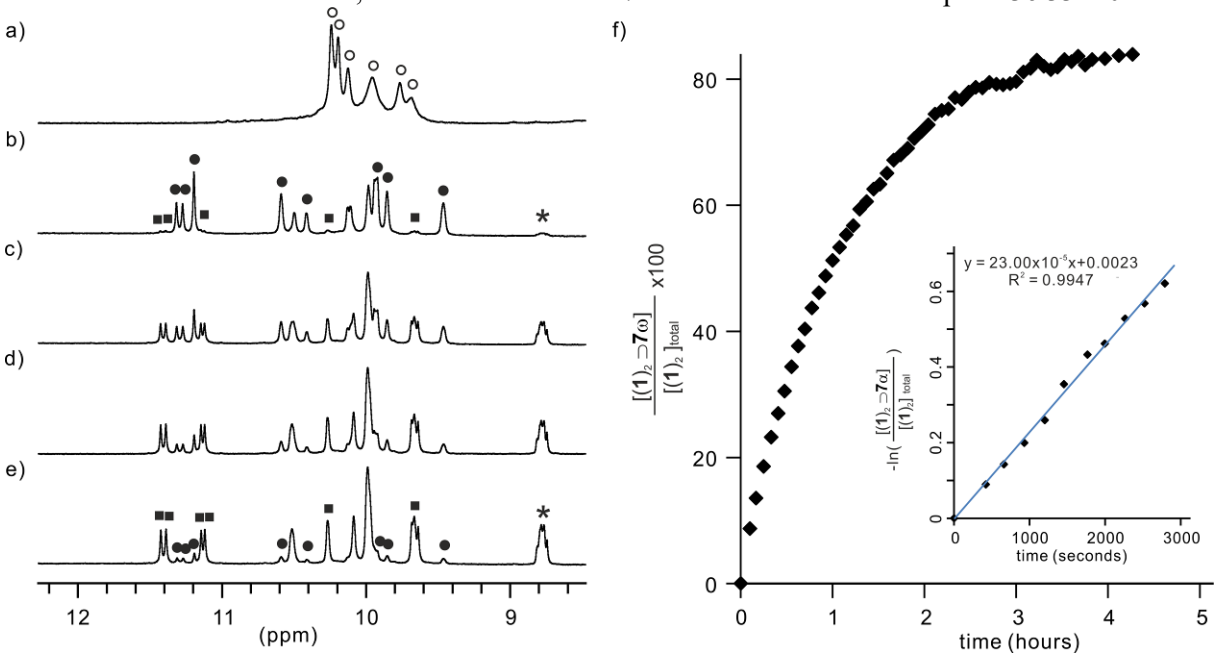

Figure 32. Part of the 400 MHz NMR spectrum of the amide region at 290K of **1** (4 mM) in $CDCl_3$: a) without guest; b-e) after addition of 5 equiv. of **7** at b) t = 6 min.; c) t = 60 min.; d) t = 120 min.; e) t = 190 min., at thermodynamic equilibrium. Resonances denoted with empty circles stand for the free double helix $(\mathbf{1})_2$ whereas black circles and black squares stand for $(\mathbf{1})_2\supset\mathbf{7}\alpha$ and $(\mathbf{1})_2\supset\mathbf{7}\omega$, respectively. Aromatic proton resonances are marked with stars. f) Time traces of threading and sliding motion of $(\mathbf{1})_2$ on rods **7**. Concentration of host on each station was obtained using ^{1}H NMR through the integration of the amide resonances of the double helix. Inset: Plot of -ln([**1**] on first station/[**1**] total) against t, where ([**1**] on first station/[**1**] total)) denotes the ratio of $(\mathbf{1})_2\supset\mathbf{7}\alpha$, and t is time. The linear relationship indicated a first order kinetics, and the rate constant *k* was obtained from the slope as 23.00×10^{-5} s^{-1}.

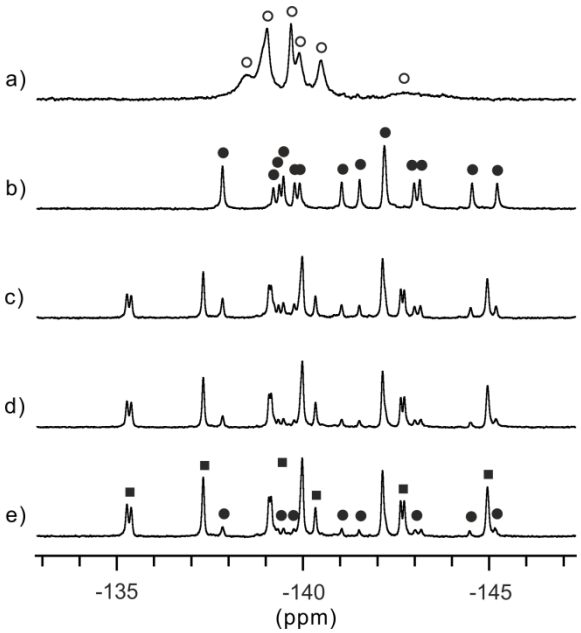

Figure 33. 282 MHz ^{19}F NMR spectrum at 290K of **1** (4 mM) in $CDCl_3$: a) without guest; b-e) after

addition of 5 equiv. of **8** at b) t = 6 min.; c) t = 3 days; d) t = 6 days; e) t = 12 days, at thermodynamic equilibrium. Resonances denoted with empty circles stand for the free double helix (**1**)$_2$ whereas black circles and black squares stand for (**1**)$_2$⊃**8**α and (**1**)$_2$⊃**8**ω, respectively.

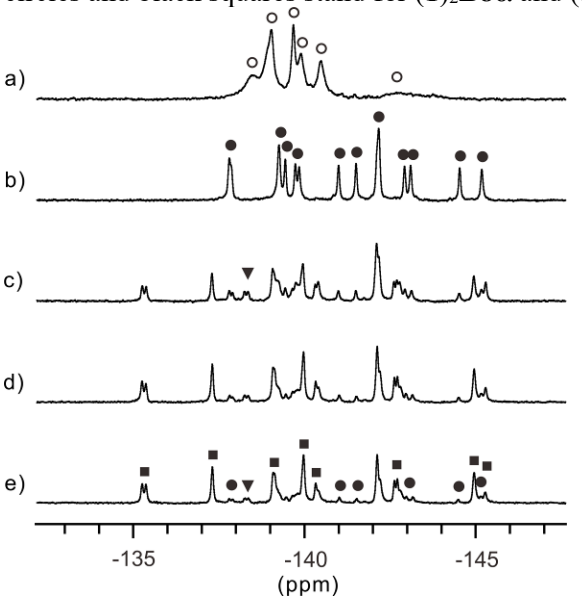

Figure 34. 282 MHz ^{19}F NMR spectrum at 290K of **1** (4 mM) in $CDCl_3$: a) without guest; b-e) after addition of 5 equiv. of **9** at b) t = 6 min.; c) t = 3 days with 41% on C11; d) t = 6 days with 58% on C11; e) t = 12 days, at thermodynamic equilibrium. Resonances denoted with empty circles stand for the free double helix (**1**)$_2$ whereas black circles, black triangles, and black squares stand for (**1**)$_2$⊃**8**α with (**1**)$_2$ on the first α station, (**1**)$_2$⊃**8**α with (**1**)$_2$ on the second α station, and (**1**)$_2$⊃**8**ω, respectively.

5.3 Methods for X-ray crystallography

X-Ray diffraction studies for (**1**)$_2$, (**1**)$_2$⊃**12**, and (**1**)$_2$⊃**13** have been performed at the IECB X-ray facility (UMS 3033 – UMS001) on a Rigaku FRX rotating anode (2.9 kW). Data were collected at the copper kα wavelength with a partial chi goniometer. The X-ray source is equipped with high flux Osmic Varimax mirrors and a Dectris Pilatus 200K detector. Reflection intensities for (**1**)$_4$⊃**2** were measured at BL13-XALOC (ALBA) beamline using 0.85 Å wavelength. Phi-scans were performed and data recorded with a large Dectris Pilatus 6M detector. The Rigaku CrystalClear suite[36] was used to index and integrate the home source data with a multi-scan absorption correction. Data collected at the synchrotron were processed with the XDS package.[37] The (**1**)$_2$⊃**12** was solved with Shelxd[38] and (**1**)$_2$⊃**13** were solved with and Shelxt.[38] Charge-flipping algorithm implemented in Superflip[39] program was used for solving the (**1**)$_2$ and (**1**)$_4$⊃**2** structures. All structures were refined by full-matrix least-squares method on F^2 with Shelxl-2014.[38] In the case of the (**1**)$_2$ and (**1**)$_4$⊃**2**, SQUEEZE[40] procedure was

36. CrystalClear-SM Expert 2.1 (Rigaku, Jun 7th 2013) Software, Version 5.6.2.0, Tokyo, Japan.
37. W. Kabsch, XDS. *Acta Cryst* **2010**, *D66*, 125–132.
38. G. M. Sheldrick, A short history of SHELX. *Acta Cryst.* **2008**, *A64*, 112–122.
39. L. Palatinus, G. Chapuis, SUPERFLIP–a computer program for the solution of crystal structures by charge flipping in arbitrary dimensions. *Appl. Crystallogr.* **2007**, *40*, 786–790.
40. A. L. Spek, SQUEEZE. *J. Appl. Cryst.* **2003**, *36*, 7–13.

employed for removing disordered solvent molecules that could not be reliably modeled. Big size of the structures, large volume fractions of disordered solvent molecules and side chains, small size of the crystals are main reason for rather moderate quality of the diffraction data and refinement statistics.

5.3 Summary of X-Ray crystallographic data

Name	$(\mathbf{1})_2$	$(\mathbf{1})_2\supset\mathbf{12}$	$(\mathbf{1})_2\supset\mathbf{13}$	$(\mathbf{1})_4\supset\mathbf{2}$
Formula	$2(C_{139}H_{135}F_8N_{23}O_{21})\cdot 1.35(CHCl_3)\cdot 5.12(H_2O)$	$2(C_{139}H_{135}F_8N_{23}O_{21})\cdot C_{30}H_{44}N_2O_4\cdot 5.52(C_6H_5Cl)\cdot C_6H_{14}\cdot 2(H_2O)$	$2(C_{139}H_{135}F_8N_{23}O_{21})\cdot C_{33}H_{50}N_2O_4\cdot 4.51(CHCl_3)\cdot 0.39(C_6H_{14})\cdot 0.97(H_2O)$	$4(139H_{135}F_8N_{23}O_{21})\cdot C_{45}H_{72}N_4O_8\cdot 12(CHCl_3)\cdot 4.33(H_2O)$
M	5484.71 g/mol	6471.72 g/mol	6359.85 g/mol	12770.25 g/mol
Crystal system	Triclinic	Triclinic	Triclinic	Monoclinic
Space group	*P*-1	*P*-1	*P*-1	*P*c
a/Å	23.185(5)	20.680(1)	22.289(2)	36.365(7)
b/Å	38.283(8)	23.925(2)	22.954(2)	49.686(10)
c/Å	59.517(12)	36.653(3)	33.748(2)	46.097(9)
α/o	74.38(3)	91.789(2)	81.019(2)	90
β/o	79.15(3)	98.467(2)	80.632(2)	105.91(3)
γ/o	76.21(3)	108.197(2)	73.048(2)	90
U/Å^3	48973 (20)	16983(2)	16187(2)	80098 (30)
T /*K*	150 (2)	150 (2)	150	100
Z	6, (Z'=3)	2, (Z'=1)	2, (Z'=1)	4, (Z'=2)
ρ/g cm^{-3}	1.116	1.266	1.304	1.053
size (mm)	0.10 × 0.06 × 0.05	0.10 × 0.05 × 0.05	0.10 × 0.05 × 0.04	0.10 × 0.05 × 0.04
λ/ Å	1.54178	1.54178	1.54178	0.850
μ/mm^{-1}	0.99	1.14	1.78	0.31
Absorption correction	Multi-scan	Multi-scan	Multi-scan	none
unique data	163699	40503	33239	157077
parameters/restraints	9185/342	3596/73	3590/486	10284/1332
*R*1, *wR*2	0.2170, 0.4999	0.1915, 0.3913	0.1868, 0.3848	0.2018, 0.4325
goodness of fit	1.53	1.30	2.21	1.63

5.4 Methods for chemical synthesis

All reactions were carried out under a dry nitrogen atmosphere. Commercial reagents were purchased from Sigma-Aldrich, Alfa-Aesar or TCI and were used without further purification unless otherwise specified. Tetrahydrofurane (THF) and dichloromethane (CH_2Cl_2) were dried over alumina columns; chloroform ($CHCl_3$), triethylamine (Et_3N) and diisopropylethylamine (DIEA) were distilled over calcium hydride (CaH_2) prior to use. Reactions were monitored by thin layer chromatography (TLC) on Merck silica gel 60-F254 plates and observed under UV light. Column chromatography purifications were carried out on Merck GEDURAN Si60 (40-63 µm). ESI mass spectra were obtained from the Mass Spectrometry Laboratory at the European Institute of Chemistry and Biology (UMS 3033 - IECB), Pessac, France.

5.4.1 Synthesis of rods with non-bulky spacers

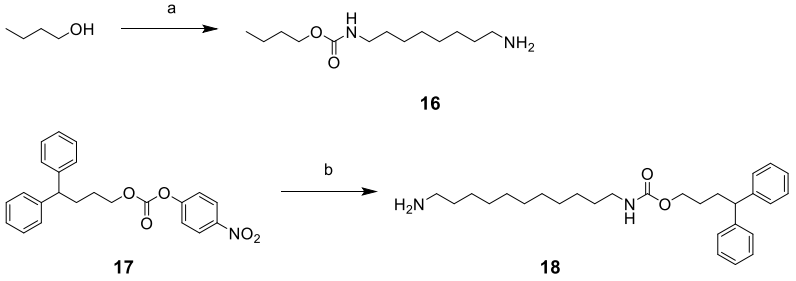

Scheme 2. Synthesis of mono amino intermediates: a) 4-nitrophenyl chloroformate, Et_3N, CH_2Cl_2, room temperature, overnight, then 1,8-diaminooctane (5 equiv), 0 °C, 1 h, then room temperature, 20 h; b) 1,11-diaminoundecane, 0 °C, 1 h, then room temperature, overnight.

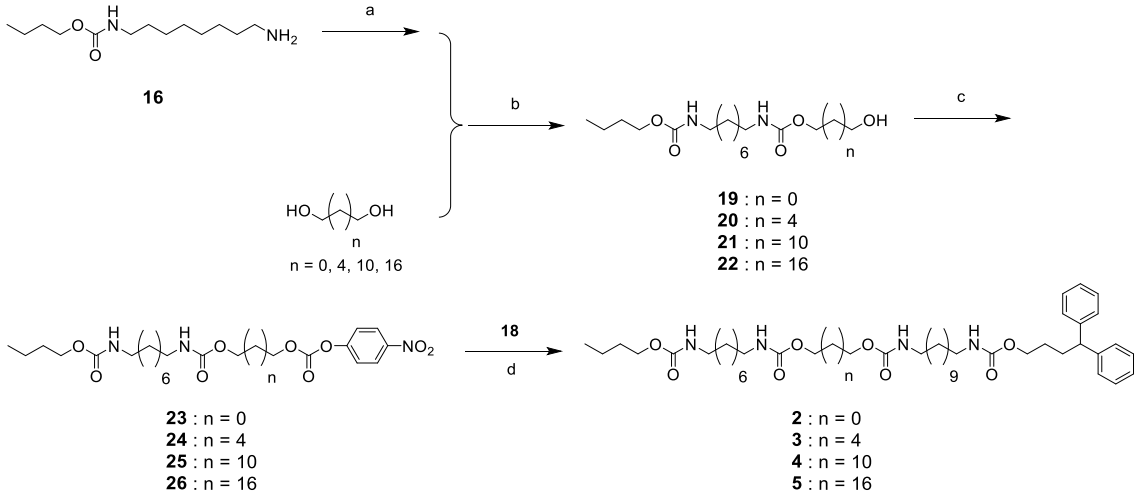

Scheme 3. Synthesis of two station rods with alkyl spacer: a) 4-nitrophenyl chloroformate, Et_3N, $CHCl_3$, 0 °C, 0.5 h, then room temperature, overnight; b) reflux, 10 d; c) 4-nitrophenyl chloroformate, Et_3N, $CHCl_3$, 40 °C, overnight; d) **18**, Et_3N, $CHCl_3$, room temperature, overnight.

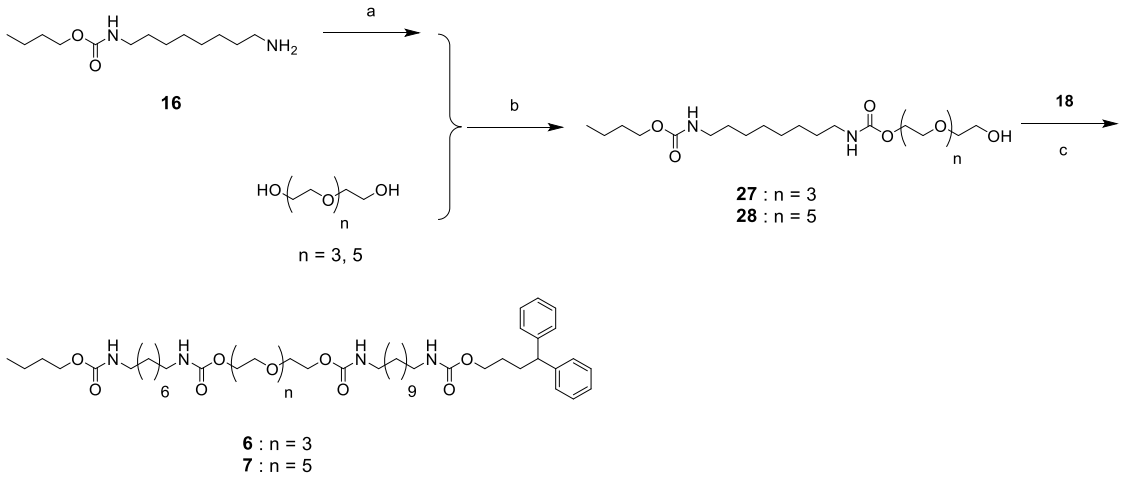

Scheme 4. Synthesis of two station rods with oligoethylene glycol spacer: a) 4-nitrophenyl chloroformate, Et_3N, $CHCl_3$, 0 °C, 0.5 h, then room temperature, overnight; b) reflux, 10 d; c) 4-nitrophenyl chloroformate, Et_3N, $CHCl_3$, 40 °C, overnight, then **18**, Et_3N, $CHCl_3$, room temperature, 20 h.

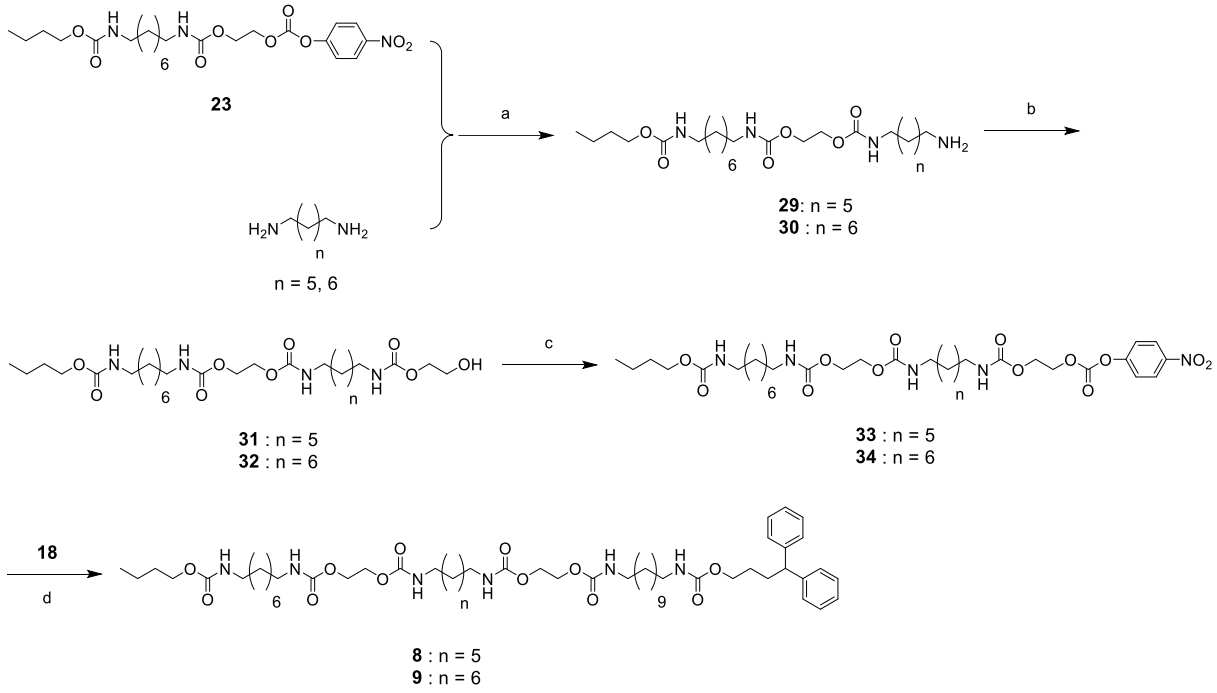

Scheme 5. Synthesis of three station rods: a) 0 °C, 0.5 h, then room temperature, overnight; b) 4-nitrophenyl chloroformate, Et_3N, $CHCl_3$, 0 °C, 0.5 h, then room temperature, overnight, then ethylene glycol (50 equiv.), reflux, 2 d; c) 4-nitrophenyl chloroformate, Et_3N, CH_2Cl_2, room temperature, 2 d; d) **18**, Et_3N, $CHCl_3$, room temperature, overnight.

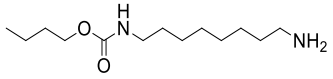

16

Compound 16. A solution of n-butanol (0.46 mL, 5 mmol) and Et_3N (1.39 mL, 10 mmol) in dry CH_2Cl_2 (25 mL) was added dropwise to a solution of 4-nitrophenyl chloroformate (1.2 g, 6 mmol) in dry CH_2Cl_2 (25 mL) at 0 °C. After stirring overnight at room temperature, the solution was added dropwise to a

solution of 1,8-diaminooctane (3.6 g, 25 mmol) and Et_3N (1.39 mL, 10 mmol) in dry CH_2Cl_2 (50 mL) at 0 °C over 1 hour. The stirring was continued for 20 hours at room temperature. The solution was washed with 1M NaOH solution (3×20 mL), dried over $MgSO_4$, and concentrated to dryness. The residue was purified by silica column chromatography eluting with MeOH/DCM/Et_3N (99:1:1 to 90:10:1) to get the product as a colorless oil (1.0 g, 82% yield). ^{1}H NMR ($CDCl_3$, 300 MHz): δ 4.64 (br, 1H), 4.04 (t, *J*(H, H) = 6.5, 2H), 3.14 (q, *J*(H, H) = 6.5, *J*(H, H) = 6.5, 2H), 2.67 (t, *J*(H, H) = 6.9, 2H), 1.64-1.51 (m, 2H), 1.51-1.41 (m, 6H), 1.41-1.33 (m, 2H), 1.29 (br, 8H), 0.92 (t, *J*(H, H) = 7.3, 3H). ^{13}C NMR ($CDCl_3$, 75 MHz): δ 156.50, 63.63, 41.47, 40.29, 33.01, 30.64, 29.45, 28.84, 28.73, 26.27, 26.18, 18.53, 13.17. HRMS (ESI): *m/z* calcd for $C_{13}H_{29}N_2O_2$ $[M+H]^+$ 245.2224 found 245.2230.

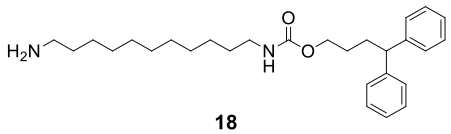

18

Compound 18. A solution of compound **17**[31] (1.0 g, 2.5 mmol) in dry CH_2Cl_2 (40 mL) was added dropwise to a solution of 1,11-diaminoundecane (1.40 g, 7.6 mmol) and Et_3N (0.70 mL, 5 mmol) in dry CH_2Cl_2 (40 mL) at 0 °C over 0.5 hour. The stirring was continued overnight at room temperature. The solution was washed with 1M NaOH solution (3×20 mL), dried over $MgSO_4$, and concentrated to dryness. The residue was purified by silica column chromatography eluting with MeOH/DCM/Et_3N (99:1:1 to 90:10:1) to get the product as a colorless oil (0.84 g, 75% yield). ^{1}H NMR ($CDCl_3$, 300 MHz): δ 7.31-7.26 (m, 2H), 7.26-7.13 (m, 8H), 4.61 (br, 1H), 4.05 (t, *J*(H, H) = 6.5, 2H), 3.90 (t, *J*(H, H) = 7.9, 1H), 3.13 (q, *J*(H, H) = 6.6, *J*(H, H) = 6.6, 2H), 2.68 (t, *J*(H, H) = 7.0, 2H), 2.10 (q, *J*(H, H) = 7.8, *J*(H, H) = 7.8, 2H) 1.64-1.53 (m, 2H), 1.53-1.49 (m, 2H), 1.49-1.36 (m, 4H), 1.36-1.17 (br, 14H). ^{13}C NMR ($CDCl_3$, 75 MHz): δ 156.80, 144.89, 128.60, 127.95, 126.33, 64.68, 51.09, 42.40, 41.14, 33.96, 32.05, 30.15, 29.72, 29.65, 29.62, 29.41, 27.78, 27.03, 26.88. HRMS (ESI): *m/z* calcd for $C_{28}H_{43}N_2O_2$ $[M+H]^+$ 439.3319 found 439.3317.

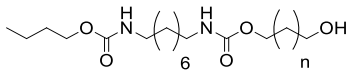

Compound 19 (n = 0). A solution of compound **16** (244 mg, 1 mmol) and Et_3N (0.28 mL, 2 mmol) in dry $CHCl_3$ (30 mL) was added dropwise to a solution of 4-nitrophenyl chloroformate (302 mg, 1.5 mmol) in dry $CHCl_3$ (30 mL) at 0 °C over 0.5 hour. After stirring overnight at room temperature, the resulting solution was added to a solution of ethylene glycol (620 mg, 10 eq) and Et_3N (0.28 mL, 2 mmol) in dry $CHCl_3$ (40 mL). The reaction was refluxed at 70 °C for 10 days. After cooling down to room temperature, the solution was washed with 1M NaOH solution (3×20 mL), dried over $MgSO_4$, and concentrated to dryness. The residue was purified by silica column chromatography eluting with EtOAc/CH_2Cl_2 (10:90 to 50:50 vol/vol) to get the product as a white solid (230 mg, 70% yield). ^{1}H NMR ($CDCl_3$, 300 MHz): δ 4.78 (br, 1H), 4.63 (br, 1H), 4.21 (t, *J*(H, H) = 4.4, 2H), 4.05 (t, *J*(H, H) = 6.6, 2H), 3.80 (m, 2H), 3.16 (m, 4H), 2.41 (br, 1H), 1.64-1.42 (m, 4H), 1.42-1.33(m, 2H), 1.33-1.24 (m, 8H), 0.93 (t, *J*(H, H) = 7.3, 3H). ^{13}C NMR ($CDCl_3$, 75 MHz): δ 157.12, 156.99, 66.75, 64.69, 61.90, 41.14, 41.01, 31.20, 30.04, 29.91, 29.16, 29.15, 26.65, 19.17, 13.83. HRMS (ESI): *m/z* calcd for $C_{16}H_{33}N_2O_5$ $[M+H]^+$ 333.2384 found 333.2390.

Compound 20, 21, and 22 were synthesized following similiar procedure.

Compound 20 (n = 4). Synthesized from 1,6-hexanediol. White solid, 54% yield. ^{1}H NMR ($CDCl_3$, 300 MHz): δ 4.62 (br, 2H), 4.05 (t, *J*(H, H) = 6.4, 4H), 3.74-3.58 (m, 2H), 3.15 (q, *J*(H, H) = 6.7, *J*(H, H) = 6.7, 4H), 1.67-1.57 (m, 4H), 1.52-1.43 (m, 4H), 1.43-1.35 (m, 6H), 1.34-1.23 (m, 10H), 0.93 (t, *J*(H, H) = 7.3, 3H). ^{13}C NMR ($CDCl_3$, 75 MHz): δ 156.95, 64.79, 62.91, 41.08, 32.75, 31.26, 30.12, 29.26, 29.18, 26.75, 25.79, 25.51, 19.23, 13.89. HRMS (ESI): *m/z* calcd for $C_{20}H_{41}N_2O_5$ $[M+H]^+$ 389.3010 found 389.3013.

Compound 21 (n = 10). Synthesized from 1,12-dodecanediol. White solid, 38% yield. ^{1}H NMR ($CDCl_3$, 300 MHz): δ 4.60 (br, 2H), 4.13-3.97 (m, 4H), 3.64 (q, *J*(H, H) = 5.4, *J*(H, H) = 5.4, 2H), 3.15 (q, *J*(H,

H) = 6.4, *J*(H, H) = 6.4, 4H), 1.65-1.55 (m, 4H), 1.52-1.43 (m, 4H), 1.43-1.33 (m, 4H), 1.33-1.24 (m, 24H), 0.93 (t, *J*(H, H) = 7.3, 3H). ^{13}C NMR ($CDCl_3$, 75 MHz): δ 156.97, 65.04, 64.75, 63.22, 41.09, 32.95, 31.27, 30.14, 29.84, 29.70, 29.65, 29.55, 29.40, 29.29, 29.21, 26.78, 26.01, 25.87, 19.24, 13.90. HRMS (ESI): *m/z* calcd for $C_{26}H_{53}N_2O_5$ $[M+H]^+$ 473.3949 found 473.3949.

Compound 22 (n = 16). Synthesized from 1,18-octadecanediol[41]. White solid, 46% yield. ^{1}H NMR ($CDCl_3$, 300 MHz): δ 4.60 (br, 2H), 4.12-3.95 (m, 4H), 3.64 (m, 2H), 3.23-3.04 (m, 4H), 1.65-1.56 (m, 4H), 1.53-1.43 (m, 4H), 1.43-1.20 (m, 40H), 0.93 (t, *J*(H, H) = 7.3, 3H). ^{13}C NMR ($CDCl_3$/CD_3OD, 75 MHz): δ 13.45, 18.89, 25.62, 25.70, 26.48, 28.87, 28.99, 29.14, 29.33, 29.39, 29.42, 29.51, 29.66, 30.91, 32.37, 32.42, 40.61, 40.74, 62.22, 62.36, 64.55, 64.88, 157.42. HRMS (ESI): *m/z* calcd for $C_{32}H_{65}N_2O_5$ $[M+H]^+$ 557.4888 found 557.4894.

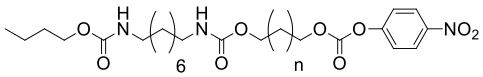

Compound 23 (n = 0). A solution of compound **19** (330 mg, 1 mmol) and Et_3N (0.84 mL, 6 mmol) in dry $CHCl_3$ (5 mL) was added dropwise to a solution of 4-nitrophenyl chloroformate (600 mg, 3 mmol) in dry $CHCl_3$ (5 mL). After stirring overnight at 40 ºC, solvent was removed under reduced pressure, and the residue was purified by silica column chromatography eluting with EtOAc/CH_2Cl_2 (1:99 to 20:80 vol/vol) to get the product as a white solid (430 mg, 86% yield). ^{1}H NMR ($CDCl_3$, 300 MHz): δ 8.29 (d, *J*(H, H) = 9.2, 2H), 7.40 (d, *J*(H, H) = 9.2, 2H), 4.76 (br, 1H), 4.60 (br, 1H), 4.48 (m, 2H), 4.38 (m, 2H), 4.05 (t, *J*(H, H) = 6.5, 2H), 3.16 (m, 4H), 1.64-1.55 (m, 2H), 1.53-1.44 (m, 4H), 1.43-1.34 (m, 2H), 1.33-1.25 (m, 8H), 0.93 (t, *J*(H, H) = 7.3, 3H). ^{13}C NMR ($CDCl_3$, 75 MHz): δ 156.86, 155.96, 155.42, 152.33, 145.39, 125.26, 121.76, 67.54, 64.51, 61.85, 41.05, 40.87, 31.08, 29.92, 29.79, 29.08, 26.57, 19.03, 13.70. HRMS (ESI): *m/z* calcd for $C_{23}H_{36}N_3O_9$ $[M+H]^+$ 498.2446 found 498.2449.

Compound 24, 25, and 26 were synthesized following similiar procedure.

Compound 24 (n = 4). Synthesized from compound **20**. White solid, 89% yield. ^{1}H NMR ($CDCl_3$, 300 MHz): δ 8.34-8.22 (m, 2H), 7.43-7.33 (m, 2H), 4.61 (br, 2H), 4.29 (t, *J*(H, H) = 6.9, 2H), 4.13-3.98 (m, 4H), 3.15 (q, *J*(H, H) = 6.6, *J*(H, H) = 6.6, 4H), 1.85-1.71 (m, 2H), 1.71-1.55 (m, 4H), 1.53-1.42 (m, 8H), 1.42-1.34 (m, 2H), 1.34-1.23 (m, 10H), 0.93 (t, *J*(H, H) = 7.3, 3H). ^{13}C NMR ($CDCl_3$, 75 MHz): δ 156.94, 156.83, 155.71, 152.67, 145.49, 125.42, 121.92, 69.56, 64.72, 64.64, 41.08, 31.25, 30.11, 29.26, 29.02, 28.53, 26.76, 25.60, 25.46, 19.21, 13.88. HRMS (ESI): *m/z* calcd for $C_{27}H_{43}N_3NaO_9$ $[M+Na]^+$ 576.2892 found 576.2893.

Compound 25 (n = 10). Synthesized from compound **21**. White solid, 78% yield. ^{1}H NMR ($CDCl_3$, 300 MHz): δ 8.33-8.23 (m, 2H), 7.43-7.34 (m, 2H), 4.60 (br 2H), 4.29 (t, *J*(H, H) = 6.7, 2H), 4.12-3.98 (m, 4H), 3.15 (q, *J*(H, H) = 6.6, *J*(H, H) = 6.6, 4H), 1.82-1.70 (m, 2H), 1.67-1.55 (m, 4H), 1.52-1.44 (m, 4H), 1.44-1.34 (m, 6H), 1.33-1.22 (m, 22H), 0.93 (t, *J*(H, H) = 7.3, 3H). ^{13}C NMR ($CDCl_3$, 75 MHz): δ 156.93, 155.74, 152.68, 145.47, 125.41, 121.92, 69.82, 65.01, 64.72, 41.08, 31.26, 30.12, 29.64, 29.62, 29.57, 29.41, 29.28, 29.26, 29.20, 28.63, 26.76, 25.99, 25.76, 19.22, 13.88. HRMS (ESI): *m/z* calcd for $C_{33}H_{56}N_3O_9$ $[M+H]^+$ 638.4011 found 638.4020.

Compound 26 (n = 16). Synthesized from compound **22**. White solid, 80% yield. ^{1}H NMR ($CDCl_3$, 300 MHz): δ 8.28 (d, *J*(H, H) = 9.2, 2H), 7.38 (d, *J*(H, H) = 9.2, 2H), 4.60 (br, 2H), 4.29 (t, *J*(H, H) = 6.7, 2H), 4.40 (q, *J*(H, H) = 4.9, *J*(H, H) = 4.9, 4H), 3.15 (q, *J*(H, H) = 6.5, *J*(H, H) = 6.5, 4H), 1.76 (m, 2H), 1.66-1.54 (m, 4H), 1.52-1.43 (m, 4H), 1.43-1.33 (m, 6H), 1.33-1.22 (m, 34H0, 0.93 (t, *J*(H, H) = 7.3, 3H). ^{13}C NMR ($CDCl_3$, 75 MHz): δ 156.95, 155.75, 152.69, 145.47, 125.42, 121.92, 69.84, 65.05, 64.74, 41.07, 31.26, 30.13, 29.82, 29.80, 29.76, 29.73, 29.69, 29.60, 29.44, 29.30, 29.27, 29.21, 28.64, 26.76, 26.01, 25.77, 19.22, 13.89. HRMS (ESI): *m/z* calcd for $C_{39}H_{68}N_3O_9$ $[M+H]^+$ 722.4950 found 722.4949.

41. J. Z. Vlahakis, S.Mitu, G.Roman, E. P. Rodriguez, I. E. Crandall, W. A. Szarek. The anti-malarial activity of bivalent imidazolium salts. *Bioorg. Med. Chem.* **2011**, *19*, 6525–6542.

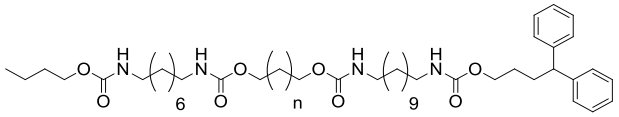

Compound 2. To a solution of compound **23** (125 mg, 0.25 mmol) and compound **18** (110mg, 0.25 mmol) in dry $CHCl_3$ (5 mL) was added Et_3N (0.07 mL, 0.5 mmol). After stirring overnight at room temperature, the solution was washed 3 times with 1M NaOH solution (10 mL), dried over $MgSO_4$, and concentrated to dryness. The residue was purified by silica column chromatography eluting with EtOAc/CH_2Cl_2 (1:99 to 40:60 vol/vol) to get the product as a white solid (192 mg, 96% yield). ^{1}H NMR ($CDCl_3$, 300 MHz): δ 7.31-7.27 (m, 2H), 7.25-7.13 (m, 8H), 4.70 (br, 2H), 4.60 (br, 2H), 4.24 (s, 4H), 4.06 (m, 4H), 3.90 (t, *J*(H, H) = 7.9, 1H), 3.15 (m, 8H), 2.10 (q, *J*(H, H) = 7.8, *J*(H, H) = 7.8, 2H), 1.64-1.54 (m, 4H), 1.52-1.42 (m, 8H), 1.42-1.33 (m, 2H), 1.33-1.21 (m, 22H), 0.93 (t, *J*(H, H) = 7.3, 3H). ^{13}C NMR ($CDCl_3$, 75 MHz): δ 156.97, 156.81, 156.29, 144.85, 128.58, 127.91, 126.31, 64.66, 63.21, 51.05, 41.14, 32.01, 31.24, 30.10, 30.02, 29.59, 29.36, 29.23, 27.74, 26.83, 26.72, 19.21, 13.89. HRMS (ESI): *m/z* calcd for $C_{45}H_{73}N_4O_8$ $[M+H]^+$ 797.5423 found 797.5423.

Compound 3, 4, and 5 were synthesized following similiar procedure.

Compound 3 (n = 4). Synthesized from compound **24**. White solid, 93% yield. ^{1}H NMR ($CDCl_3$, 300 MHz): δ 7.31-7.27 (m, 2H), 7.26-7.13 (m, 8H), 4.63 (br, 4H), 4.14-3.98 (m, 8H), 3.90 (t, *J*(H, H) = 7.8, 1H), 3.96-3.85 (m, 8H), 3.22-3.04 (m, 8H), 2.17-2.04 (m, 2H), 1.67-1.54 (m, 8H), 1.53-1.42 (m, 8H), 1.42-1.34 (m, 6H), 1.33-1.23 (m, 22H), 0.93 (t, *J*(H, H) = 7.3, 3H). ^{13}C NMR ($CDCl_3$, 75 MHz): δ 156.90, 156.81, 144.88, 128.60, 127.94, 126.33, 64.79, 51.09, 41.14, 32.04, 31.27, 30.14, 29.61, 29.39, 29.28, 29.05, 27.77, 26.87, 26.77, 25.68, 19.23, 13.90. HRMS (ESI): *m/z* calcd for $C_{49}H_{81}N_4O_8$ $[M+H]^+$ 853.6049 found 853.6048.

Compound 4 (n = 10). Synthesized from compound **25**. White solid, 95% yield. ^{1}H NMR ($CDCl_3$, 300 MHz): δ 7.31-7.26 (m, 2H), 7.25-7.13 (m, 8H), 4.61 (br, 4H), 4.69-4.53 (m, 8H), 4.12-3.98 (m, 8H), 3.90 (t, *J*(H, H) = 7.8, 1H), 3.22-3.05 (m, 8H), 2.16-2.05 (m, 2H), 1.66-1.54 (m, 8H), 1.52-1.42 (m, 8H), 1.42-1.31 (m, 6H), 1.31-1.23 (m, 36H), 0.93 (t, *J*(H, H) = 7.3, 3H). ^{13}C NMR ($CDCl_3$, 75 MHz): δ 156.93, 156.79, 144.84, 128.55, 127.90, 126.28, 64.97, 64.67, 51.05, 41.08, 32.00, 31.23, 30.09, 29.62, 29.58, 29.38, 29.35, 29.24, 29.17, 27.73, 26.83, 26.73, 25.97, 19.19, 13.86. HRMS (ESI): *m/z* calcd for $C_{55}H_{93}N_4O_8$ $[M+H]^+$ 937.6988 found 937.6990.

Compound 5 (n = 16). Synthesized from compound **26.** White solid, 84% yield. ^{1}H NMR ($CDCl_3$, 300 MHz): δ 7.30-7.27 (m, 2H), 7.26-7.12 (m, 8H), 4.60 (br, 4H), 4.15-3.97 (m, 8H), 3.90 (t, *J*(H, H) = 7.8, 1H), 3.22-3.06 (m, 8H), 2.17-2.20 (m, 2H), 1.66-1.54 (m, 8H), 1.52-1.42 (m, 8H), 1.42-1.33 (m, 6H), 1.32-1.23 (m, 46H), 0.93 (t, *J*(H, H) = 7.3, 3H). ^{13}C NMR ($CDCl_3$, 75 MHz): δ 156.94, 156.79, 144.87, 128.59, 127.94, 126.32, 65.04, 64.72, 51.08, 41.10, 32.04, 31.27, 30.13, 29.81, 29.79, 29.73, 29.69, 29.61, 29.44, 29.38, 29.27, 29.22, 27.77, 26.86, 26.77, 26.02, 19.23, 13.89. HRMS (ESI): *m/z* calcd for $C_{61}H_{105}N_4O_8$ $[M+H]^+$ 1021.7927 found 1021.7920.

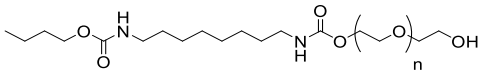

Compound 27 and 28 was synthesized following similiar procedure as Compound 19.

Compound 27 (n = 3). White solid, 37% yield. ^{1}H NMR ($CDCl_3$, 300 MHz): δ 4.99 (br, 1H), 4.26-4.17 (m, 2H), 4.05 (t, *J*(H, H) = 6.5, 2H), 3.77-3.57 (m, 14H), 3.15 (q, *J*(H, H) = 6.4, *J*(H, H) = 6.4, 4H), 2.64 (t, *J*(H, H) = 6.0, 1H), 1.65-1.52 (m, 2H), 1.52-1.43 (m, 4H), 1.43-1.33 (m, 2H), 1.33-1.24 (m, 8H), 0.93 (t, *J*(H, H) = 7.3, 3H). ^{13}C NMR ($CDCl_3$, 75 MHz): δ 156.95, 156.55, 72.67, 70.68, 70.57, 70.51, 70.37, 69.74, 64.67, 63.78, 61.78, 41.05, 31.21, 30.06, 29.95, 29.21, 26.71, 19.17, 13.84. HRMS (ESI): *m/z* calcd for $C_{22}H_{45}N_2O_8$ $[M+H]^+$ 465.3170 found 465.3170.

Compound 28 (n = 5). White solid, 36% yield. ^{1}H NMR ($CDCl_3$, 300 MHz): δ 4.85 (br, 1H), 4.63 (br, 1H), 4.27-4.15 (m, 2H), 4.04 (t, *J*(H, H) = 6.5, 2H), 3.76-3.56 (m, 22H), 3.15 (q, *J*(H, H) = 6.5, *J*(H, H) = 6.5, 4H), 2.57 (t, *J*(H, H) = 5.9, 1H), 1.66-1.53 (m, 2H), 1.53-1.42 (m, 4H), 1.42-1.33 (m, 2H), 1.33-1.23 (m, 8H), 0.93 (t, *J*(H, H) = 7.3, 3H). ^{13}C NMR ($CDCl_3$, 75 MHz): δ 156.94, 156.55, 72.60, 70.73,

70.70, 70.63, 70.48, 69.81, 64.70, 63.95, 61.85, 41.10, 31.24, 30.10, 30.02, 29.26, 26.75, 19.21, 13.89. HRMS (ESI): *m/z* calcd for $C_{26}H_{52}N_2NaO_{10}$ $[M+Na]^+$ 575.3514 found 575.3520.

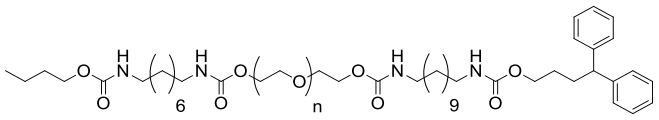

Compound 6 (n = 3). A solution of compound **27** (100 mg, 0.22 mmol) and Et_3N (0.12 mL, 0.88 mmol) in dry $CHCl_3$ (5 mL) was added dropwise to a solution of 4-nitrophenyl chloroformate (65 mg, 1.5eq) in dry $CHCl_3$ (5 mL). After stirring overnight at room temperature, the resulting solution was added to a solution of compound **18** (193 mg, 2 equiv) in dry $CHCl_3$ (5 mL). The reaction was proceeded at room temperature for 20 hours, then the solution was washed 3 times with 1M NaOH solution (10 mL), dried over $MgSO_4$, and concentrated to dryness. The residue was purified by silica column chromatography eluting with MeOH/CH_2Cl_2 (1:99 to 7:93 vol/vol) to get the product as a white solid (120 mg, 59% yield). ^{1}H NMR ($CDCl_3$, 300 MHz): δ 7.31-7.26 (m, 2H), 7.25-7.13 (m, 8H), 4.85 (br, 2H), 4.62 (br, 2H), 4.27-4.16 (m, 4H), 4.12-3.98 (m, 4H), 3.90 (t, *J*(H, H) = 7.8, 1H), 3.73-3.61 (m, 12H), 3.22-3.04 (m, 8H), 2.17-2.03 (m, 2H), 1.60-1.53 (m, 4H), 1.53-1.41 (m, 8H), 1.41-1.32 (m, 2H), 1.32-1.20 (m, 22H), 0.93 (t, *J*(H, H) = 7.3, 3H). ^{13}C NMR ($CDCl_3$, 75 MHz): δ 156.95, 156.80, 156.55, 144.86, 128.58, 127.92, 126.30, 70.73, 70.61, 69.82, 64.70, 63.93, 51.06, 41.11, 32.02, 31.24, 30.11, 30.04, 29.59, 29.36, 29.26, 27.75, 26.85, 26.75, 19.20, 13.88. HRMS (ESI): *m/z* calcd for $C_{51}H_{85}N_4O_{11}$ $[M+H]^+$ 929.6209 found 929.6221.

Compound 7 was synthesized following similiar procedure.

Compound 7 (n = 5). White solid, 70% yield. ^{1}H NMR ($CDCl_3$, 300 MHz): δ 7.30-7.26 (m, 2H), 7.25-7.13 (m, 8H), 4.83 (br, 2H), 4.61 (br, 2H),4.26-4.15 (m, 4H), 4.12-3.99 (m, 4H), 3.90 (t, *J*(H, H) = 7.8, 1H), 3.72-3.61 (m, 20H), 3.21-3.06 (m, 8H), 2.16-2.05 (m, 2H), 1.65-1.56 (m, 4H), 1.53-1.42 (m, 8H), 1.42-1.33 (m, 2H), 1.33-1.21 (m, 22H), 0.93 (t, *J*(H, H) = 7.3, 3H). ^{13}C NMR ($CDCl_3$, 75 MHz): δ 156.95, 156.80, 156.55, 144.87, 128.59, 127.93, 126.31, 70.75, 70.72, 70.68, 70.65, 69.82, 64.70, 63.94, 51.07, 41.12, 32.03, 31.26, 30.12, 30.07, 29.60, 29.38, 29.27, 27.76, 26.86, 26.76, 19.22, 13.88. HRMS (ESI): *m/z* calcd for $C_{55}H_{93}N_4O_{13}$ $[M+H]^+$ 1017.6734 found 1017.6735.

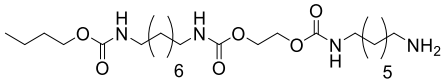

29

Compound 29. A solution of compound **23** (430 mg, 0.86 mmol) in dry CH_2Cl_2 (10 mL) was added dropwise to a solution of 1,7-diaminoheptane (560 mg, 4.3 mmol) and Et_3N (0.24 mL, 1.72 mmol) in dry CH_2Cl_2 (10 mL) at 0 °C over 0.5 hour. The stirring was continued overnight at room temperature. The solution was washed 3 times with 1M NaOH solution (10 mL), dried over $MgSO_4$, and concentrated to dryness. The residue was purified by silica column chromatography eluting with MeOH/DCM/Et_3N (99:1:1 to 90:10:1) to get the product as a white solid (310 mg, 73% yield). ^{1}H NMR ($CDCl_3$, 300 MHz): δ 4.73 (br, 2H), 4.65 (br, 1H), 4.24 (s, 4H), 4.05 (t, *J*(H, H) = 6.6, 2H), 3.23-3.06 (m, 6H), 2.68 (t, *J*(H, H) = 6.9, 2H), 1.65-1.53 (m, 2H), 1.53-1.44 (m, 6H), 1.44-1.35 (m, 4H), 1.34-1.23 (m, 14H), 0.93 (t, *J*(H, H) = 7.3, 3H). ^{13}C NMR ($CDCl_3$, 75 MHz): δ 156.95, 156.29, 64.65, 63.15, 42.25, 41.11, 33.76, 31.22, 30.06, 29.95, 29.20, 26.84, 26.70, 19.17, 13.84. HRMS (ESI): *m/z* calcd for $C_{24}H_{49}N_4O_6$ $[M+H]^+$ 489.3647 found 489.3650.

Compound 30 was synthesized following similiar procedure.

Compound 30. White solid,70% yield. ^{1}H NMR ($CDCl_3$, 300 MHz): δ 4.74 (br, 2H), 4.65 (br, 1H), 4.24 (s, 4H), 4.05 (t, *J*(H, H) = 6.6, 2H), 3.24-3.07 (m, 6H), 2.68 (t, *J*(H, H) = 6.9, 2H), 1.64-1.53 (m, 2H), 1.53-1.44 (m, 6H), 1.44-1.35 (m, 4H), 1.34-1.24 (m, 16H), 0.93 (t, *J*(H, H) = 7.3, 3H). ^{13}C NMR ($CDCl_3$, 75 MHz): δ 156.95, 156.29, 64.66, 63.18, 42.32, 41.13, 41.03, 33.89, 31.23, 30.08, 29.98, 29.45, 29.30, 29.22, 26.88, 26.74, 26.71, 19.18, 13.85. HRMS (ESI): *m/z* calcd for $C_{25}H_{51}N_4O_6$ $[M+H]^+$ 503.3803 found 503.3810.

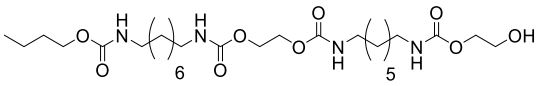

31

Compound 31. A solution of compound **29** (310 mg, 0.63 mmol) and Et_3N (0.18 mL, 1.26 mmol) in dry $CHCl_3$ (20 mL) was added dropwise to a solution of 4-nitrophenyl chloroformate (190 mg, 0.95 mmol) in dry $CHCl_3$ (20 mL) at 0 °C over 0.5 h. After stirring overnight at room temperature, the solution was added to a solution of ethylene glycol (1.75 mL, 32 mmol) and Et_3N (0.18 mL, 1.26 mmol) in dry $CHCl_3$ (60 mL). The reaction was refluxed at 70 °C for 2 days. The solution was washed 3 times with 1M NaOH solution (10 mL), dried over $MgSO_4$, and concentrated to dryness. The residue was purified by silica column chromatography eluting with MeOH/CH_2Cl_2 (1:99 to 20:80 vol/vol) to get the product as a white solid (340 mg, 93% yield). ^{1}H NMR (DMSO-*d*6, 300 MHz): δ 7.16 (t, *J*(H, H) = 5.5, 2H), 7.07 (t, *J*(H, H) = 5.7, 1H), 7.01 (t, *J*(H, H) = 5.5, 1H), 4.68 (t, *J*(H, H) = 5.4, 1H), 4.13-4.03 (m, 4H), 3.99-3.86 (m, 4H), 3.52 (q, *J*(H, H) = 5.3, *J*(H, H) = 5.3, 2H), 3.00-2.86 (m, 8H), 1.59-1.44 (m, 2H), 1.44-1.33 (m, 8H), 1.33-1.27 (m, 2H), 1.27-1.17 (m, 14H), 0.88 (t, *J*(H, H) = 7.3, 3H). ^{13}C NMR (DMSO-*d*6, 100 MHz): δ 156.30, 155.94, 65.37, 63.17, 62.32, 59.48, 30.80, 30.70, 29.40, 28.68, 28.43, 26.22, 26.19, 18.61, 13.62. HRMS (ESI): *m/z* calcd for $C_{27}H_{53}N_4O_9$ $[M+H]^+$ 577.3807 found 577.3808.

Compound 32 was synthesized following similiar procedure.

Compound 32. White solid, 34% yield. ^{1}H NMR (DMSO-*d*6, 300 MHz): δ 7.15 (t, *J*(H, H) = 5.4, 2H), 7.06 (t, *J*(H, H) = 5.4, 1H), 7.00 (t, *J*(H, H) = 5.4, 1H), 4.68 (t, *J*(H, H) = 5.3, 1H), 4.14-4.03 (m, 4H), 3.92 (q, *J*(H, H) = 5.9, 4H), 3.52 (q, *J*(H, H) = 5.3, *J*(H, H) = 5.3, 2H), 3.00-2.87 (m, 8H), 1.57-1.44 (m, 2H), 1.44-1.33 (m, 8H), 1.33-1.26 (m, 2H), 1.26-1.15 (m, 16H), 0.88 (t, *J*(H, H) = 7.4, 3H). ^{13}C NMR (DMSO-*d*6, 75 MHz): δ 156.33, 155.94, 65.37, 63.17, 62.32, 59.49, 30.80, 29.41, 29.35, 28.68, 26.19, 18.60, 13.60. HRMS (ESI): *m/z* calcd for $C_{28}H_{55}N_4O_9$ $[M+H]^+$ 591.3964 found 591.3968.

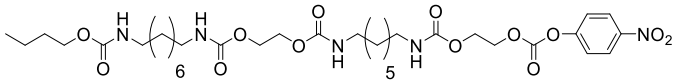

33

Compound 33. A solution of compound **31** (340 mg, 0.59 mmol) and Et_3N (0.84 mL, 6 mmol) in dry $CHCl_3$ (5 mL) was added dropwise to a solution of 4-nitrophenyl chloroformate (600 mg, 3.0 mmol) in dry $CHCl_3$ (5 mL). After stirring for 2 days at room temperature, the solution was concentrated to dryness. The residue was purified by silica column chromatography eluting with EtOAc/CH_2Cl_2 (10:90 to 50:50 vol/vol) to get the product as a white solid (240 mg, 54% yield). ^{1}H NMR ($CDCl_3$, 300 MHz): δ 8.29 (d, *J*(H, H) = 9.1, 2H), 9.40 (d, *J*(H, H) = 9.1, 2H), 4.82 (br, 1H), 4.74 (br, 2H), 4.63 (br, 1H), 4.53-4.43 (m, 2H), 4.42-4.33 (m, 2H), 4.24 (s, 4H), 4.04 (t, *J*(H, H) = 6.6, 2H), 3.25-3.07 (m, 8H), 1.63-1.56 (m, 2H), 1.54-1.43 (m, 8H), 1.43-1.35 (m, 2H), 1.35-1.27 (m, 14H), 0.93 (t, *J*(H, H) = 7.3, 3H). ^{13}C NMR ($CDCl_3$, 75 MHz): δ 156.97, 156.31, 156.05, 155.56, 152.50, 145.60, 125.45, 121.90, 67.67, 64.72, 63.22, 62.04, 41.15, 41.05, 31.24, 30.10, 29.98, 29.92, 29.23, 28.87, 26.72, 26.64, 19.20, 13.87. HRMS (ESI): *m/z* calcd for $C_{34}H_{56}N_5O_{13}$ $[M+H]^+$ 742.3869 found 742.3872.

Compound 34 was synthesized following similiar procedure.

Compound 34. White solid, 62% yield. ^{1}H NMR ($CDCl_3$, 300 MHz): δ 8.33-8.23 (m, 2H), 7.45-7.36 (m, 2H), 4.80 (br,1H), 4.72 (br, 2H), 4.63 (br, 1H), 4.52-4.43 (m, 2H), 4.42-4.33 (m, 2H), 4.24 (s, 4H), 4.05 (t, *J*(H, H) = 6.3, 2H), 3.24-3.06 (m, 8H), 1.65-1.55 (m, 2H), 1.55-1.44 (m, 8H), 1.43-1.34 (m, 2H), 1.34-1.27 (m, 16H), 0.93 (t, *J*(H, H) = 7.3, 3H). ^{13}C NMR ($CDCl_3$, 75 MHz): δ 156.97, 156.30, 156.05, 155.57, 152.52, 145.61, 125.47, 121.91, 67.69, 64.76, 63.24, 62.05, 41.24, 41.17, 31.26, 30.12, 30.00, 29.82, 29.24, 29.22, 26.71, 19.22, 13.89. HRMS (ESI): *m/z* calcd for $C_{35}H_{58}N_5O_{13}$ $[M+H]^+$ 756.4026 found 756.4027.

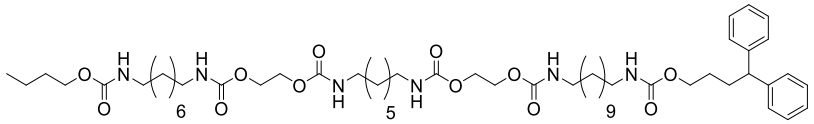

8

Compound 8. To a solution of compound **33** (200 mg, 0.27 mmol) and compound **18** (118 mg, 0.27 mmol) in dry $CHCl_3$ (5 mL) was added Et_3N (0.08 mL, 0.54 mmol). After stirring overnight at room temperature, the solution was washed 3 times with 1M NaOH solution (10 mL), dried over $MgSO_4$, and concentrated to dryness. The residue was purified by silica column chromatography eluting with $MeOH/CH_2Cl_2$ (1:99 to 20:80 vol/vol) to get the product as a white solid (190 mg, 84% yield). ^1H NMR ($CDCl_3$, 300 MHz): δ 7.31-7.27 (m, 2H), 7.25-7.12 (m, 8H), 4.79 (br, 4H), 4.63 (br, 2H), 4.24 (s, 8H), 4.13-3.98 (m, 4H), 3.90 (t, *J*(H, H) = 7.9, 1H), 3.25-3.05 (m, 12H), 2.15-2.04 (m, 2H), 1.63-1.54 (m, 4H), 1.54-1.42 (m, 12H), 1.42-1.34 (m, 2H), 1.34-1.21 (m, 28H), 0.92 (t, *J*(H, H) = 7.3, 3H). ^{13}C NMR ($CDCl_3$, 75 MHz): δ 156.95, 156.79, 156.32, 144.83, 128.55, 127.88, 126.28, 64.66, 63.18, 51.03, 41.12, 41.01, 31.98, 31.22, 30.07, 29.99, 29.95, 29.86, 29.56, 29.33, 29.21, 28.79, 27.72, 26.81, 26.70, 26.59, 19.17, 13.85. HRMS (ESI): *m/z* calcd for $C_{56}H_{96}N_7O_{12}$ $[M+NH_4]^+$ 1058.7111 found 1058.7109.

Compound 9 was synthesized following similiar procedure.

Compound 9. White solid, 95% yield. ^1H NMR ($CDCl_3$, 300 MHz): δ 7.31-7.26 (m, 2H), 7.26-7.13 (m, 8H), 4.75 (br, 4H), 4.62 (br, 2H), 4.24 (s, 8H), 4.14-4.00 (m, 4H), 3.90 (t, *J*(H, H) = 7.8, 1H), 3.24-3.04 (m, 12H), 2.18-2.04 (m, 2H), 1.65-1.54 (m, 4H), 1.54-1.42 (m, 12H), 1.41-1.35 (m, 2H), 1.34-1.22 (m, 30H), 0.93 (t, *J*(H, H) = 7.3, 3H). ^{13}C NMR ($CDCl_3$, 75 MHz): δ 156.97, 156.82, 156.31, 144.88, 128.60, 127.94, 126.33, 64.69, 63.24, 51.09, 41.16, 32.04, 31.27, 30.13, 30.00, 29.83, 29.61, 29.38, 29.25, 29.20, 27.77, 26.86, 26.75, 26.70, 19.23, 13.90. HRMS (ESI): *m/z* calcd for $C_{57}H_{95}N_6O1_2$ $[M+H]^+$ 1055.7002 found 1055.7003.

5.4.2 Synthesis of rods with bulky spacers

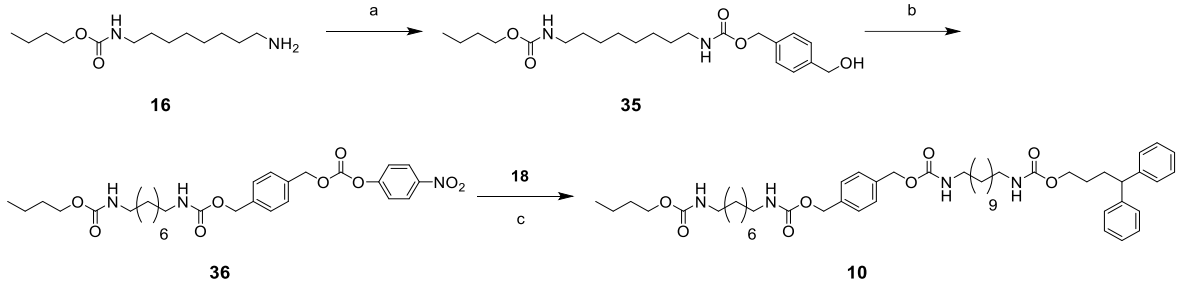

Scheme 6. Synthesis of two station rods with xylene spacer: a) 4-nitrophenyl chloroformate, Et_3N, $CHCl_3$, 0 °C, 0.5 h, then room temperature, overnight, then 1,4-phenylenedimethanol (10 equiv.), reflux, 2d; b) 4-nitrophenyl chloroformate, Et_3N, $CHCl_3$, 50 °C, 24 h; c) **18**, Et_3N, $CHCl_3$, room temperature, overnight.

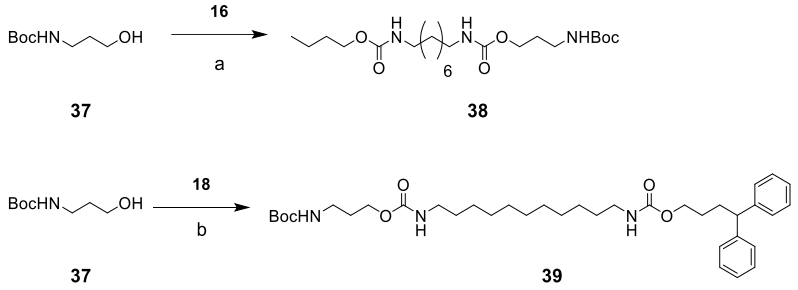

Scheme 7. Synthesis of propyl appended single station intermediates: a) 4-nitrophenyl chloroformate, Et_3N, CH_2Cl_2, room temperature, overnight, then **16**, room temperature, 20 h; b) 4-nitrophenyl chloroformate, Et_3N, CH_2Cl_2, room temperature, overnight, then **18**, room temperature, 20 h.

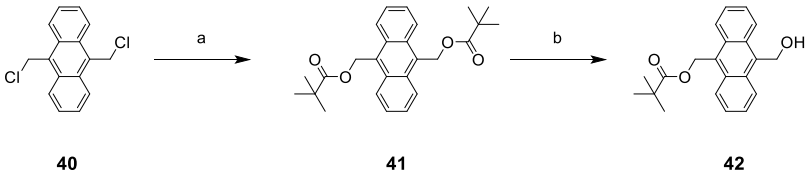

Scheme 8. Synthesis of the anthracene mono alcohol: a) pivalic acid, Cs_2CO_3, DMF, 35 °C, 20 h; b) NaOH, THF/MeOH, 2h.

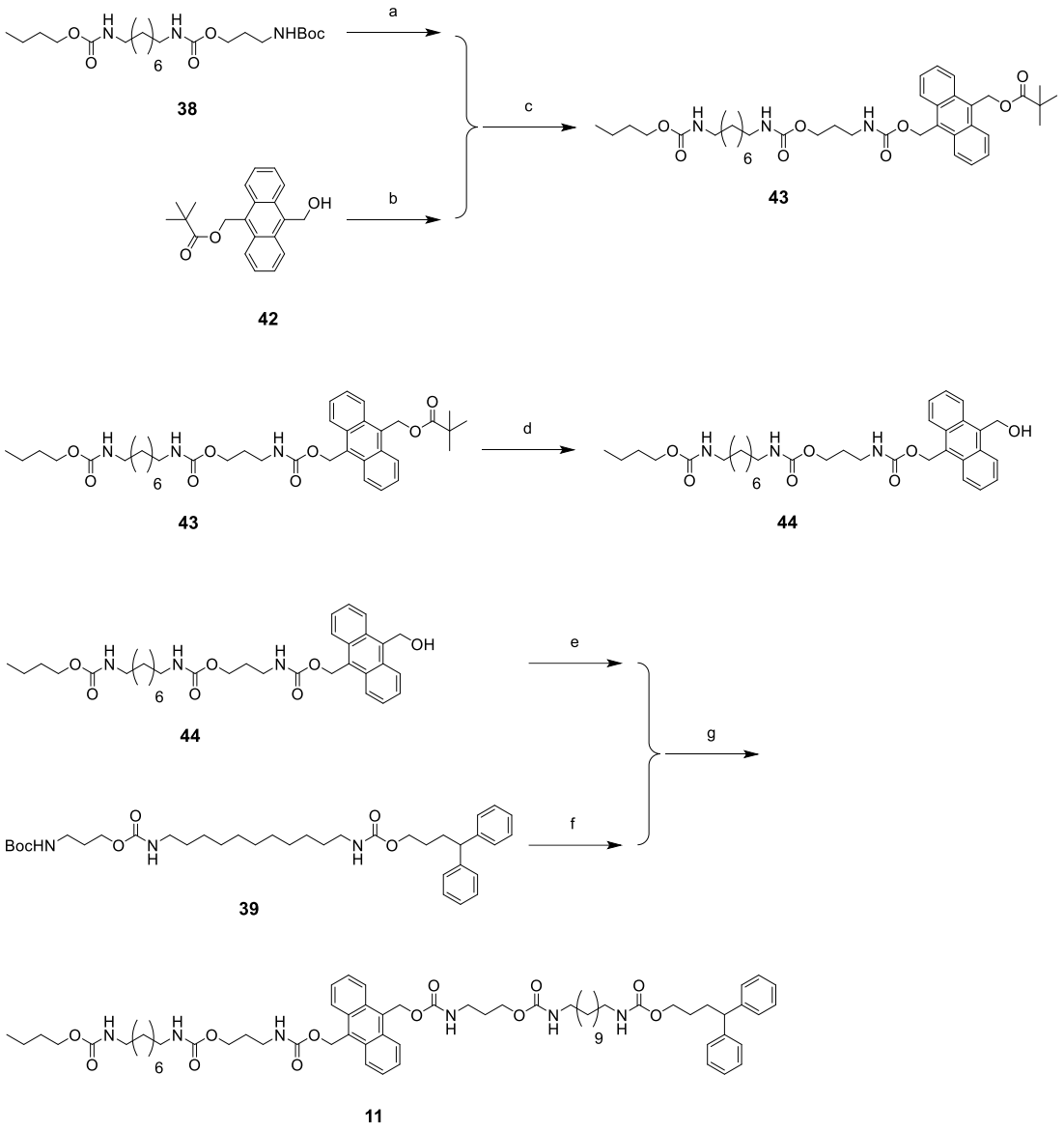

Scheme 9. Synthesis of two station rod with anthracene spacer: a) TFA, CH_2Cl_2, room temperature, 6 h; b) 4-nitrophenyl chloroformate, pyridine, THF, overnight; c) $CHCl_3$, Et_3N, 20 h; d) NaOH, THF/MeOH, 4 h; e) 4-nitrophenyl chloroformate, pyridine, THF, overnight; f) TFA, CH_2Cl_2, room temperature, 6 h; g) $CHCl_3$, Et_3N, 20 h.

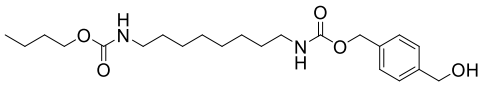

35

Compound 35. A solution of compound **16** (244 mg, 1 mmol) and Et_3N (0.28 mL, 2 mmol) in dry $CHCl_3$ (40 mL) was added dropwise to a solution of 4-nitrophenyl chloroformate (302 mg, 1.5 mmol) in dry $CHCl_3$ (40 mL) at 0 °C over 0.5 hour. After stirring overnight at room temperature, the solution was added to a solution of 1,4-phenylenedimethanol (1.38 g, 10 mmol) and Et_3N (0.28 mL, 2 mmol) in dry $CHCl_3$ (120 mL). The reaction was refluxed at 70 °C for 2 days. After cooling down to room temperature, the insoluble 1,4-phenylenedimethanol was filtered off. The solution was washed 3 times with 1M NaOH solution (20 mL), dried over $MgSO_4$, and concentrated to dryness. The residue was purified by silica column chromatography eluting with EtOAc/CH_2Cl_2 (10:90 to 30:70 vol/vol) to get the product

as a white solid (150 mg, 37% yield). ^{1}H NMR ($CDCl_3$, 300 MHz): δ 7.36 (s, 4H), 5.09 (s, 2H), 4.70 (m, 3H), 4.60 (br, 1H), 4.05 (t, *J*(H, H) = 6.6, 2H), 1.69 (t, *J*(H, H) = 6.0, 1H), 1.65-1.55 (m, 2H), 1.52-1.43 (m, 4H), 1.43-1.33 (m, 2H), 1.33-1.24 (m, 8H), 0.93 (t, *J*(H, H) = 7.3, 3H). ^{13}C NMR ($CDCl_3$, 75 MHz): δ 156.99, 156.52, 141.09, 136.10, 128.39, 127.15, 66.39, 64.99, 64.73, 45.02, 41.15, 41.04, 31.22, 30.07, 30.01, 29.21, 26.70, 21.56, 19.19, 13.86. HRMS (ESI): *m/z* calcd for $C_{22}H_{37}N_2O_5$ $[M+H]^+$ 409.2697 found 409.2702.

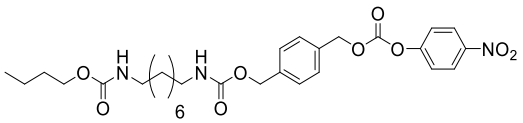

36

Compound 36. A solution of compound **35** (150 mg, 0.37 mmol) and Et_3N (0.52 mL, 3.7 mmol) in dry $CHCl_3$ (5 mL) was added dropwise to a solution of 4-nitrophenyl chloroformate (370 mg, 1.85 mmol) in dry $CHCl_3$ (5 mL). After stirring at 50 ºC for 2 days, the solution was concentrated to dryness. The residue was purified by silica column chromatography eluting with EtOAc/CH_2Cl_2 (1:99 to 5:95 vol/vol) to get the product as a white solid (180 mg, 85% yield). ^{1}H NMR ($CDCl_3$, 300 MHz): δ 8.27 (d, *J*(H, H) = 9.2, 2H), 7.42 (d, *J*(H, H) =4.0, 4H), 5.29 (s, 2H), 5.12 (s, 2H), 4.72 (br, 1H), 4.58 (br, 1H), 4.05 (t, *J*(H, H) = 6.5, 2H), 3.16 (m, 4H), 1.64-1.55 (m, 2H), 1.52-1.44 (m, 4H), 1.44-1.33 (m, 2H), 1.33-1.26 (m, 8H), 0.93 (t, *J*(H, H) = 7.3, 3H). ^{13}C NMR ($CDCl_3$, 75 MHz): δ 156.92, 156.35, 155.58, 152.50, 145.49, 137.88, 134.04, 128.92, 128.42, 125.37, 121.85, 70.69, 66.05, 64.66, 41.18, 41.01, 31.21, 30.06, 29.98, 29.20, 26.69, 19.16, 13.84. HRMS (ESI): *m/z* calcd for $C_{29}H_{40}N_3O_9$ $[M+H]^+$ 574.2759 found 574.2765.

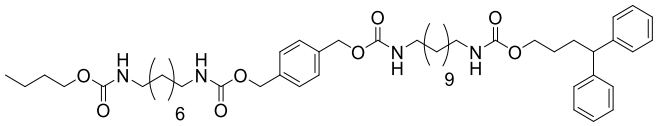

10

Compound 10. To a solution of compound **36** (180 mg, 0.31 mmol) and compound **18** (137 mg, 0.31 mmol) in dry $CHCl_3$ (5 mL) was added Et_3N (0.09 mL, 0.62 mmol). After stirring overnight at room temperature, the solution was washed 3 times with 1M NaOH solution (10 mL), dried over $MgSO_4$, and concentrated to dryness. The residue was purified by silica column chromatography eluting with EtOAc/CH_2Cl_2 (1:99 to 30:70 vol/vol) to get the product as a white solid (257 mg, 95% yield). ^{1}H NMR ($CDCl_3$, 300 MHz): δ 7.34 (s, 4H), 7.30-7.26 (m, 2H), 7.26-7.13 (m, 8H), 5.08 (s, 4H), 4.71 (br, 2H), 4.60 (br, 2H), 4.06 (m, 4H), 3.90 (t, *J*(H, H) = 7.8, 1H), 3.16 (m, 8H), 2.10 (q, *J*(H, H) = 7.8, *J*(H, H) = 7.8, 2H), 1.64-1.54 (m, 4H), 1.52-1.41 (m, 8H), 1.41-1.33 (m, 2H), 1.33-1.20 (m, 20H), 0.93 (t, *J*(H, H) = 7.3, 3H). ^{13}C NMR ($CDCl_3$, 75 MHz): δ 156.98, 156.82, 156.46, 144.87, 136.72, 128.59, 128.35, 127.93, 126.32, 66.32, 64.72, 51.07, 41.19, 32.02, 31.25, 30.10, 29.58, 29.36, 29.34, 29.24, 27.76, 26.84, 26.73, 19.21, 13.88. HRMS (ESI): *m/z* calcd for $C_{51}H_{77}N_4O_8$ $[M+H]^+$ 873.5736 found 873.5745.

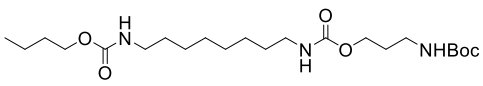

38

Compound 38. A solution of N-(t-butoxycarbonyl)-3-aminopropanol[42] **37** (357 mg, 2.04 mmol) and Et_3N (1.13 mL, 8.16 mmol) in dry CH_2Cl_2 (10 mL) was added dropwise to a solution of 4-nitrophenyl chloroformate (411 mg, 2.04 mmol) in dry CH_2Cl_2 (10 mL) at 0 °C. After stirring overnight at room

42. E. Delfourne, R. Kiss, L. Le Corre, F. Dujols, J. Bastide, F. Collignon, B. Lesur, A. Frydman, F. Darro. Synthesis and in vitro antitumor activity of phenanthrolin-7-one derivatives, analogues of the marine pyridoacridine alkaloids ascididemin and meridine: structure−activity relationship. *J. Med. Chem.* **2003**, *46*, 3536–3545.

temperature, the solution was added to a solution of compound **16** (500 mg, 2.04 mmol) in dry CH_2Cl_2 (10 mL). The stirring was continued for 20 hours at room temperature. The solution was washed 3 times with 1M NaOH solution (30 mL), dried over $MgSO_4$, and concentrated to dryness. The residue was purified by silica column chromatography eluting with EtOAc/CH_2Cl_2 (1:99 to 30:70 vol/vol) to get the product as a colorless oil (736 mg, 82% yield). ^{1}H NMR ($CDCl_3$, 300 MHz): δ4.80 (br, 1H), 4.67 (br, 2H), 4.11 (t, *J*(H, H) = 6.0, 2H), 4.04 (t, *J*(H, H) = 6.6, 2H), 3.17 (m, 6H), 1.78 (m, 2H), 1.68-1.54 (m, 2H), 1.41-1.32 (m, 13H), 1.32-1.23 (m, 8H), 0.93 (t, *J*(H, H) = 7.3, 3H). ^{13}C NMR ($CDCl_3$, 75 MHz): δ 156.86, 156.75, 155.97, 78.94, 64.41, 61.87, 40.89, 37.14, 31.06, 29.89, 29.84, 29.54, 29.08, 28.34, 26.57, 19.00, 13.69. HRMS (ESI): *m/z* calcd for $C_{22}H_{44}N_3O_6$ $[M+H]^+$ 446.3225 found 446.3221.

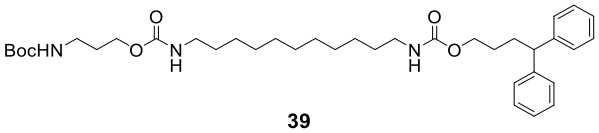

39

Compound 39. A solution of compound **37** (105 mg, 0.6 mmol) and Et_3N (0.17 mL, 1.2 mmol) in dry CH_2Cl_2 (10 mL) was added dropwise to a solution of 4-nitrophenyl chloroformate (145 mg, 0.72 mmol) in dry CH_2Cl_2 (10 mL) at 0 °C. After stirring overnight at room temperature, the solution was added to a solution of compound **18** (219 mg, 0.5 mmol) and Et_3N (0.17 mL, 1.2 mmol) in dry CH_2Cl_2 (10 mL). The stirring was continued for 20 hours at room temperature. The solution was washed 3 times with 1M NaOH solution (30 mL), dried over $MgSO_4$, and concentrated to dryness. The residue was purified by silica column chromatography eluting with EtOAc/CH_2Cl_2 (1:99 to 30:70 vol/vol) to get the product as a colorless oil (300 mg, 94% yield). ^{1}H NMR ($CDCl_3$, 300 MHz): δ 7.30-7.26 (m, 2H), 7.26-7.25 (m, 8H), 4.78 (br, 1H), 4.65 (br, 1H), 4.29 (br, 1H), 4.11 (t, *J*(H, H) = 6.0, 2H), 4.06 (m, 2H), 3.90 (t, *J*(H, H) = 7.8, 1H), 3.14 (m, 6H), 2.10 (q, *J*(H, H) = 7.8, *J*(H, H) = 7.8, 2H), 1.78 (m, 2H), 1.65-1.55 (m, 2H), 1.52-1.37 (m, 13H), 1.36-1.18 (m, 14H). ^{13}C NMR ($CDCl_3$, 75 MHz): δ 156.86, 156.75, 155.97, 78.94, 64.41, 61.87, 40.89, 37.14, 31.06, 29.89, 29.84, 29.54, 29.08, 28.34, 26.57, 19.00, 13.69. HRMS (ESI): *m/z* calcd for $C_{37}H_{58}N_3O_6$ $[M+H]^+$ 640.4320 found 640.4322.

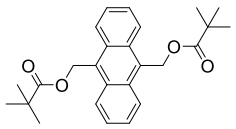

41

Compound 41. Under N_2 atmosphere, 9,10-bis(chloromethyl)anthracene **40**[43] (5.0 g, 18 mmol), pivalic acid (4.6g, 45 mmol) and Cs_2CO_3 (14.8 g, 45 mmol) in dry DMF (60 mL) was stirred at 35 °C for 20 h. The mixture was poured in to water, the precipitate was collected by filtration, washed with water, and dried to get the product as a yellow solid (7.6 g, 98% yield). ^{1}H NMR ($CDCl_3$, 300 MHz): δ 8.38 (dd, *J* (H, H) = 6.9, *J* (H, H) = 3.2, 4H), 7.59 (dd, *J* (H, H) = 6.9, *J* (H, H) = 3.2, 4H), 6.13 (s, 4H), 1.18 (s, 18H). ^{13}C NMR ($CDCl_3$, 75 MHz): δ 178.84, 130.91, 129.06, 126.28, 124.84, 59.24, 39.19, 27.32. HRMS (ESI): *m/z* calcd for $C_{21}H_{21}O_2$ $[M-t\text{BuC(O)O}^-]^+$ 305.1536 found 305.1539.

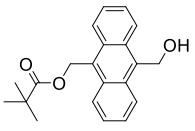

42

Compound 42. To a solution of compound **41** (458 mg, 0.12 mmol) in THF (15 mL) was added quickly a solution of NaOH (45 mg, 0.12 mmol) in MeOH (4 mL). After stirring for 2 h at room temperature,

43. M. J. Cloninger, H. W. Whitlock, A synthetic receptor which uses multiple edge-face interactions to bind aromatic guests. *J. Org. Chem.* **1998**, *63*, 6153–6159.

200 mL CH_2Cl_2 was added. The organic phase was washed 3 times with 5% citric acid aqueous solution (10 mL), dried over $MgSO_4$, and concentrated to dryness. The residue was purified by silica column chromatography eluting with EtOAc/CH_2Cl_2 (1:99 to 10:90 vol/vol) to get the product as a yellow solid (180 mg, 45% yield). ^{1}H NMR ($CDCl_3$, 300 MHz): δ 8.55-8.45 (m, 2H), 8.43-8.33 (m, 2H), 7.65-7.55 (m, 4H), 6.13 (s, 2H), 5.70 (d, *J* (H, H) = 5.6, 2H), 1.76 (t, *J* (H, H) = 5.6, 1H), 1.16 (s, 9H). ^{13}C NMR ($CDCl_3$, 75 MHz): δ 178.85, 133.27, 131.02, 130.10, 128.48, 126.30, 126.25, 124.90, 124.71, 59.17, 57.65, 39.18, 27.29. HRMS (ESI): *m/z* calcd for $C_{21}H_{21}O_2$ [M-OH^-]$^+$ 305.1542 found 305.1538; *m/z* calcd for $C_{16}H_{13}O$ [M-*t*BuC(O)O^-]$^+$ 221.0966 found 221.0959.

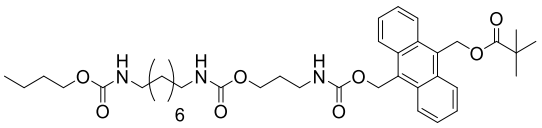

43

Compound 43. TFA (12 mL) was added slowly to a solution of compound **38** (668 mg, 1.5 mmol) in dry CH_2Cl_2 (24 mL) under N_2 atmosphere. After stirring for 6 h, the solution was concentrated under reduced pressure. The residue was dissolved in 200 mL CH_2Cl_2, washed 3 times with 1M NaOH solution. The organic phase was dried over $MgSO_4$, and concentrated to get the resulting amine, which was used directly without further purification.

A solution of compound **42** (322 mg, 1.0 mmol) in dry THF (8mL) was added slowly to a mixture of 4-nitrophenyl chloroformate (221 mg, 1.1 mmol) and pyridine (0.16 mL, 2 mmol) in dry THF (8 mL). After stirring overnight at room temperature, Et_3N (0.28 mL, 2.0 mmol) and a solution of the above amine in dry $CHCl_3$ (30 mL) was added successively. The reaction was allowed to proceed at room temperature for 20 hours. Then the solution was diluted into 200 mL CH_2Cl_2, washed 3 times with 1M NaOH solution (10 mL), dried over $MgSO_4$, and concentrated to dryness. The residue was purified by silica column chromatography eluting with EtOAc/CH_2Cl_2 (1:99 to 30:70 vol/vol) to get the product as a yellow solid (564 mg, 81% yield). ^{1}H NMR ($CDCl_3$, 300 MHz): δ 8.50-8.41 (m, 2H), 8.41-8.32 (m, 2H), 7.65-7.52 (m, 2H), 6.16 (s, 2H), 6.13 (s, 2H), 5.01 (br, 1H), 4.60 (br, 2H), 4.11 (m, 2H), 4.04 (t, *J*(H, H) = 6.6, 2H), 3.30 (q, *J*(H, H) = 6.3, *J*(H, H) = 6.3, 2H), 3.10 (m, 4H), 1.81 (m, 2H), 1.68-1.56 (m, 2H), 1.51-1.31 (m, 6H), 1.31-1.19 (m, 8H), 1.19-1.09 (m, 8H), 0.92 (t, *J*(H, H) = 7.3, 3H). ^{13}C NMR ($CDCl_3$, 75 MHz): δ 178.84, 156.68, 130.80, 129.05, 129.01, 126.33, 126.25, 124.89, 124.73, 64.69, 62.04, 59.25, 59.10, 41.04, 39.14, 38.04, 31.21, 30.06, 29.96, 29.58, 29.20, 27.26, 26.69, 19.19, 13.89. HRMS (ESI): *m/z* calcd for $C_{34}H_{46}N_3O_6$ [M-*t*BuC(O)O^-]$^+$ 592.3881 found 592.3887.

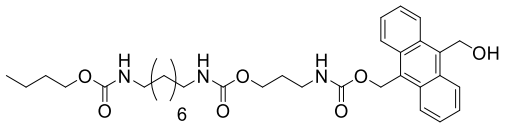

44

Compound 44. NaOH (480 mg, 12 mmol) in MeOH (10 mL) was added slowly to a solution compound **43** (416 mg, 0.6 mmol) in 5 mL THF. The mixture was stirred for 6 hours at room temperature. To the crude was added 200 mL CH_2Cl_2, and the organic phase was washed with brine, dried over $MgSO_4$. The solvent was removed to get the product as a yellow solid (338 mg, 92% yield). ^{1}H NMR (DMSO-d6, 300 MHz): δ 8.57-8.48 (m, 2H), 8.48-8.38 (m, 2H), 7.68-7.53 (m, 4H), 7.17 (t, *J*(H, H) = 5.5, 1H), 7.10-6.93 (m, 2H), 6.07 (s, 2H), 5.47 (d, *J*(H, H) = 4.7, 2H), 5.37 (t, *J*(H, H) = 4.9, 1H), 3.91 (t, *J*(H, H) = 6.5, 4H), 3.06 (q, *J*(H, H) = 6.0, *J*(H, H) = 6.0, 2H), 2.93 (q, *J*(H, H) = 6.3, *J*(H, H) = 6.3, 4H), 1.72-1.58 (m, 2H), 1.58-1.41 (m, 2H), 1.41-1.25 (m, 6H), 1.25-1.12 (m, 8H), 0.87 (t, *J*(H, H) = 7.3, 3H). ^{13}C NMR (DMSO-d6, 75 MHz): δ 156.28, 134.93, 130.28, 129.48, 127.88, 126.05, 125.46, 125.43, 124.63, 63.16, 61.34, 57.96, 55.45, 37.37, 30.79, 29.39, 29.16, 28.66, 26.17, 18.59, 13.60. HRMS (ESI): *m/z* calcd for $C_{34}H_{48}N_3O_7$ [M+H]$^+$ 610.3487 found 610.3499.

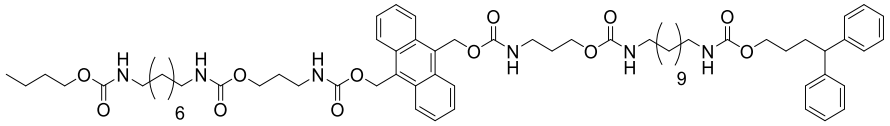

11

Compound 11. TFA (4 mL) was added slowly to a solution of compound **38** (300 mg, 0.47 mmol) in dry CH_2Cl_2 (8 mL) under N_2 atmosphere. After stirring for 6 h, the solution was concentrated under reduced pressure. The residue was dissolved in 200 mL CH_2Cl_2, washed 3 times with 1M NaOH solution, dried over $MgSO_4$, and concentrated to get the resulting amine, which was used directly without further purification.

A solution of compound **44** (286 mg, 0.47 mmol) in dry THF (4mL) was added slowly to a mixture of 4-nitrophenyl chloroformate (113 mg, 0.47 mmol) and pyridine (0.08 mL, 2 eq) in dry THF (4 mL). After stirring overnight at room temperature, Et_3N (0.13 mL, 2 eq) and a solution of the above amine in dry $CHCl_3$ (8 mL) was added successively. The reaction was proceeded at room temperature for 20 hours. The crude solution was diluted into 200 mL CH_2Cl_2, washed 3 times with 1M NaOH solution (10 mL), dried over $MgSO_4$, and concentrated to dryness. The residue was purified by silica column chromatography eluting with EtOAc/CH_2Cl_2 (1:99 to 50:50 vol/vol)to get the product as a yellow solid (180 mg, 32% yield). ^{1}H NMR ($CDCl_3$, 300 MHz): δ 8.41 (q, *J*(H, H) = 3.0, 4H), 7.57 (q, *J*(H, H) = 3.0, 4H), 7.30-7.26 (m, 2H), 7.26-7.12 (m, 8H), 6.12 (s, 4H), 5.06 (br, 2H), 4.62 (br, 4H), 4.22-3.95 (m, 8H), 3.89 (t, *J*(H, H) = 7.8, 1H), 3.37-3.20 (m, 4H), 3.18-2.99 (m, 8H), 2.09 (m, 2H), 1.88-1.72 (m, 4H), 1.64-1.50 (m, 4H), 1.50-1.40 (m, 6H), 1.40-1.30 (m, 4H), 1.30-1.18 (m, 22H), 0.92 (t, *J*(H, H) = 7.3, 3H). ^{13}C NMR ($CDCl_3$, 75 MHz): δ 156.96, 156.76, 144.85, 130.69, 128.95, 128.57, 127.91, 126.30, 126.21, 124.75, 64.69, 62.12, 59.17, 51.06, 41.06, 38.11, 32.00, 31.23, 30.43, 30.07, 30.02, 29.98, 29.81, 29.56, 29.34, 29.32, 29.21, 27.74, 26.82, 26.70, 19.20, 13.87. HRMS (ESI): *m/z* calcd for $C_{67}H_{98}N_7O_{12}$ $[M+NH_4]^+$ 1192.7268 found 1192.7254.

5.4.3 Synthesis of single station rods

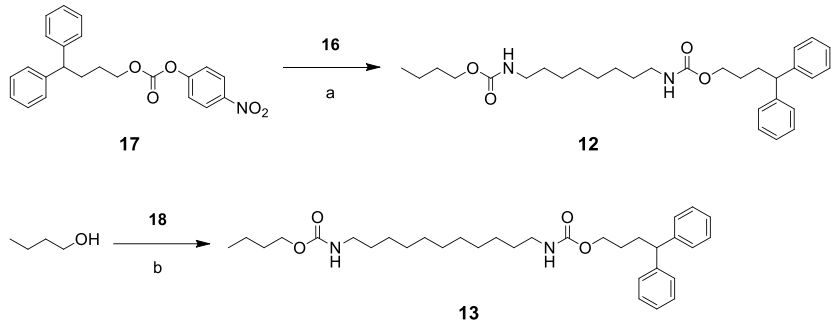

Scheme 10. Synthesis of single station rods with one stopper: a) **16**, Et_3N, CH_2Cl_2, room temperature, overnight; b) 4-nitrophenyl chloroformate, Et_3N, CH_2Cl_2, room temperature, overnight, then **18**, room temperature, 20 h.

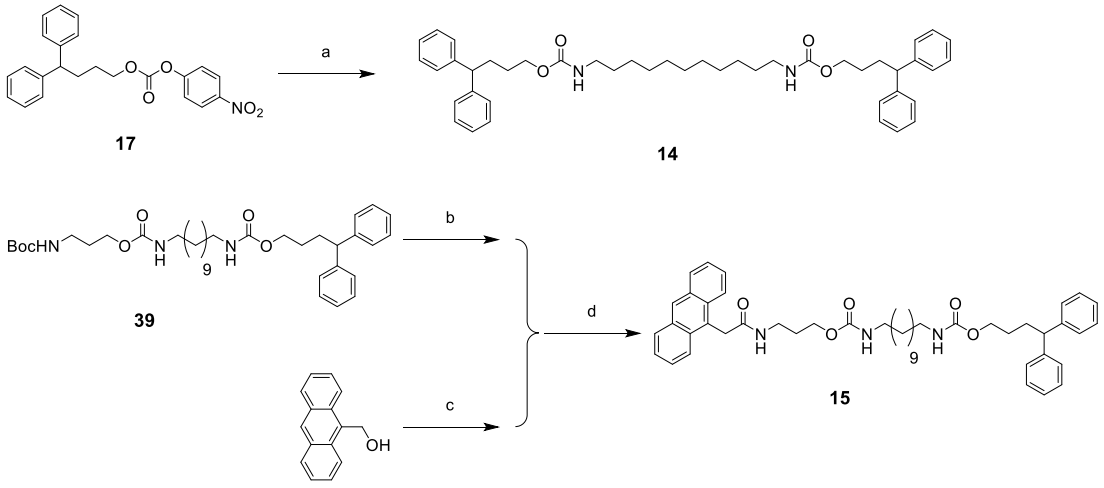

Scheme 11. Synthesis of dumbbell like single station rods: a) 1,11-diaminoundecane, Et_3N, CH_2Cl_2, room temperature, overnight; b) TFA, CH_2Cl_2, 6 h; c) 4-nitrophenyl chloroformate, pyridine, THF, overnight; d) $CHCl_3$, Et_3N, 20 h.

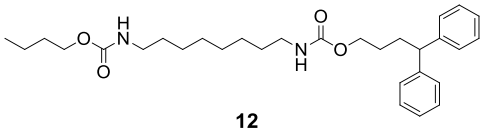

Compound 12. A solution of Compound **17** (173mg, 0.44 mmol) in dry CH_2Cl_2 (5 mL) was added slowly to a solution of Compound **16** (90 mg, 0.37 mmol) and Et_3N (0.12 mL, 0.88 mmol) in dry CH_2Cl_2 (5 mL). After stirring overnight at room temperature, the solution was diluted into 50 mL CH_2Cl_2, washed 3 times with 1M NaOH solution (10 mL), dried over $MgSO_4$, and concentrated to dryness. The residue was purified by silica column chromatography eluting with EtOAc/CH_2Cl_2 (1:99 to 20:80 vol/vol) to get the product as a white solid (137 mg, 74% yield). ^{1}H NMR ($CDCl_3$, 300 MHz): δ 7.32-7.26 (m, 2H), 7.26-7.13 (m, 8H), 4.59 (br, 2H), 4.06 (m, 4H), 3.90 (t, *J*(H, H) = 7.9, 1H), 3.14 (m, 4H), 2.10 (q, *J*(H, H) = 7.8, *J*(H, H) = 7.8, 2H), 1.66-1.52 (m, 4H), 1.52-1.42 (m, 4H), 1.42-1.32 (br, 8H), 0.93 (t, *J*(H, H) = 7.3, 3H). ^{13}C NMR ($CDCl_3$, 75 MHz): δ 156.95, 156.81, 144.88, 128.60, 127.94, 126.33, 64.73, 51.09, 41.08, 32.04, 31.27, 30.12, 29.26, 27.77, 26.76, 19.23, 13.89. HRMS (ESI): *m/z* calcd for $C_{30}H_{45}N_2O_4$ $[M+H]^+$ 497.3374 found 497.3375.

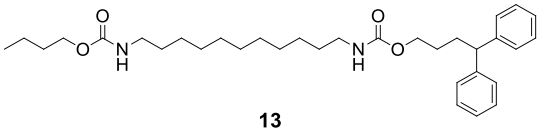

13

Compound 13. A solution of n-butanol (0.07 mL, 0.8 mmol) and Et_3N (0.22 mL, 1.6 mmol) in dry CH_2Cl_2 (10 mL) was added dropwise to a solution of 4-nitrophenyl chloroformate (193 mg, 0.96 mmol) in dry CH_2Cl_2 (10 mL) at 0 °C. After stirring overnight at room temperature, the solution was added to a solution of compound **18** (350 mg, 0.8 mmol) and Et_3N (0.22 mL, 1.6 mmol) in dry CH_2Cl_2 (10 mL). The stirring was continued at room temperature for 20 hours. The solution was washed 3 times with 1M NaOH solution (10 mL), dried over $MgSO_4$, and concentrated to dryness. The residue was purified by silica column chromatography eluting with EtOAc/CH_2Cl_2 (1:99 to 10:90 vol/vol) to get the product as a white solid (344 mg, 80% yield). ^{1}H NMR ($CDCl_3$, 300 MHz): δ 7.31-7.26 (m, 2H), 7.26-7.13(m, 8H), 4.58 (br, 1H), 4.06 (m, 4H), 3.90 (t, *J*(H, H) = 7.9, 1H), 3.13 (m, 4H), 2.10 (q, *J*(H, H) = 7.8, *J*(H, H) = 7.8, 2H) 1.67-1.53 (m, 4H), 1.53-1.43 (m, 4H), 1.43-1.33 (m, 2H), 1.32-1.21 (br, 14H), 0.93 (t, *J*(H, H) = 7.3, 3H). ^{13}C NMR ($CDCl_3$, 75 MHz): δ 156.95, 156.80, 144.88, 128.60, 127.94, 126.33, 64.71, 51.09, 41.13, 32.04, 31.27, 30.15, 29.60, 29.38, 27.77, 26.86, 19.23, 13.89. HRMS (ESI): *m/z* calcd for $C_{33}H_{51}N_2O_4$ $[M+H]^+$ 539.3843 found 539.3843.

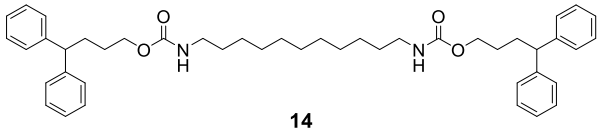

14

Compound 14. To a solution of compound **17** (400 mg, 1 mmol) and 1,11-diaminoundecane (93 mg, 0.5 mmol) in dry CH_2Cl_2 (10 mL) was added Et_3N (0.27 mL, 2 mmol). After stirring overnight at room temperature, the solution was diluted into 200 mL CH_2Cl_2, washed 3 times with 1M NaOH solution (10 mL), dried over $MgSO_4$, and concentrated to dryness. The residue was purified by silica column chromatography eluting with EtOAc/CH_2Cl_2 (1:99 to 10:90 vol/vol) to get the product as a white solid (320 mg, 94% yield). ^{1}H NMR ($CDCl_3$, 300 MHz): δ .31-7.27 (m, 4H), 7.25-7.13 (m, 16H), 4.57 (br, 2H), 4.05 (t, *J*(H, H) = 6.4, 4H), 3.90 (t, *J*(H, H) = 7.8, 2H), 3.13 (q, *J*(H, H) = 6.5, *J*(H, H) = 6.5, 4H), 2.18-2.02 (m, 4H) 1.67-1.55 (m, 4H), 1.52-1.37 (m, 4H), 1.34-1.20 (m, 14H). ^{13}C NMR ($CDCl_3$, 75 MHz): δ 156.81, 144.89, 128.61, 127.95, 126.34, 64.69, 51.10, 41.15, 32.05, 30.15, 29.61, 29.38, 27.78, 26.87. HRMS (ESI): *m/z* calcd for $C_{33}H_{51}N_2O_4$ $[M+H]^+$ 691.4469 found 691.4475.

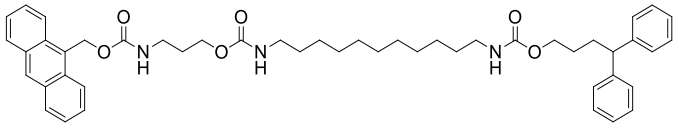

15

Compound 15. TFA (1.4 mL) was added slowly to a solution of compound **38** (110 mg, 0.17 mmol) in dry CH_2Cl_2 (2.8 mL) under N_2 atmosphere. After stirring for 6 h, the solution was concentrated under reduced pressure. The residue was dissolved in 300 mL CH_2Cl_2 and washed 3 times with 1M NaOH solution, dried over $MgSO_4$, and concentrated to get the resulting amine, which was used directly without further purification.

A solution of 9-anthracenemethanol (71 mg, 0.34 mmol) in dry THF (3mL) was added slowly to a mixture of 4-nitrophenyl chloroformate (82 mg, 0.37 mmol) and pyridine (0.06 mL, 0.68 mmol) in dry THF (3 mL). After stirring overnight at room temperature, Et_3N (0.10 mL, 0.68 mmol) and a solution of the above amine dry $CHCl_3$ (3 mL) was added successively. The reaction was proceeded at room temperature for 20 hours. Then the solution was diluted into 50 mL CH_2Cl_2, washed 3 times with 1M NaOH solution (10 mL), dried over $MgSO_4$, and concentrated to dryness. The residue was purified by silica column chromatography eluting with EtOAc/CH_2Cl_2 (1:99 to 30:70 vol/vol) to get the product as a yellow solid (80 mg, 81% yield). ^{1}H NMR ($CDCl_3$, 300 MHz): δ 8.50 (s, 1H), 8.40 (d, *J*(H, H) = 9.0,

2H), 8.03 (d, *J*(H, H) = 8.4, 2H), 7.62-7.45 (m, 4H), 7.30-7.26 (m, 2H), 7.26-7.12 (m, 8H), 6.15 (s, 2H), 4.97 (br, 2H), 4.58 (br, 2H), 4.20-3.99 (m, 4H), 3.89 (t, *J*(H, H) = 7.9, 1H), 3.29 (t, *J*(H, H) = 6.3, *J*(H, H) = 6.3, 2H), 3.18-2.96 (m, 4H), 2.18-2.02 (m, 2H), 1.91-1.72 (m, 2H), 1.67-1.51 (m, 2H), 1.51-1.35 (m, 4H), 1.33-1.16 (m, 14H). ^{13}C NMR ($CDCl_3$, 75 MHz): δ 156.78, 144.86, 131.51, 131.15, 129.15, 129.11, 128.58, 127.92, 126.92, 126.68, 126.31, 125.21, 124.25, 64.66, 62.12, 59.24, 51.06, 41.11, 38.11, 32.01, 30.10, 30.01, 29.81, 29.55, 29.34, 29.30, 27.74, 26.82, 26.78. HRMS (ESI): *m/z* calcd for $C_{48}H_{60}N_3O_6$ $[M+H]^+$ 774.4477 found 774.4481.

Chapter 4

Controlling the threading orientation and the sliding kinetics of an asymmetrical single helical foldamer along rod-like guests

1. Introduction

Over the last three decades, rotaxanes and pseudorotaxanes have been extensively investigated as prototypes for the construction of artificial molecular machines.[1-5] A typical [2]rotaxane consists of a macrocycle threading onto an axle with two bulky stoppers at the terminus of the axle. Removing a single bulky stopper yields a pseudo[2]rotaxane, in which the macrocycle can thread or unthread freely. When an asymmetrical macrocycle is threaded onto a nonsymmetrical axle, different orientations of the macrocycle give rise to two isomeric [2]rotaxanes. Control of such threading orientations will allow the emergence of sophisticated processive molecular machines.

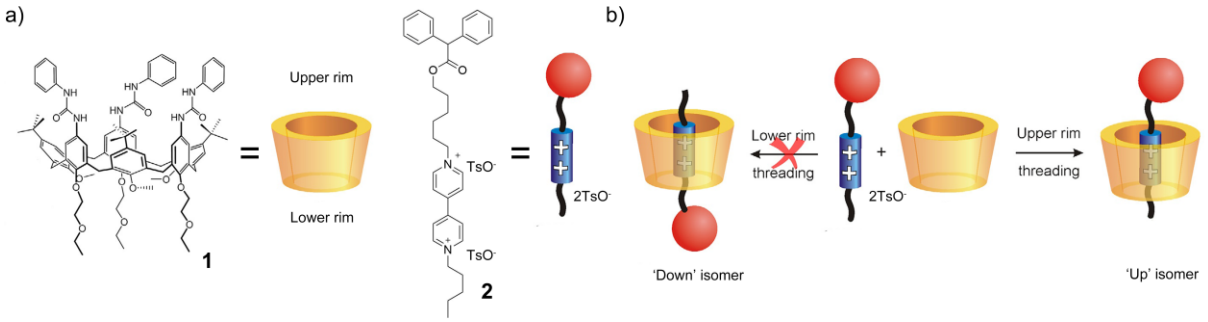

Figure 1. a) Formula and schematic representation of triphenylureidocalix[6]arene **1** and nonsymmetrical rod **2** with only one stopper. b) Schematic representation of the two possible pseudorotaxane isomers derived from **1** and **2**. Only upper rim threading is feasible in apolar solvent.

The threading orientation of cone-shaped macrocycles, such as cyclodextrins and calixarenes, have been shown to be controlled kinetically[6-11] or thermodynamically.[12-14] Credi

1. A. Credi, S. Silvi, M. Venturi (Eds.). Molecular machines and motors: recent advances and perspectives. *Top. Curr. Chem.* Springer, Berlin, **2014**.
2. S. Erbas-Cakmak, D. A. Leigh, C. T. McTernan, A. L. Nussbaumer. Artificial molecular machines. *Chem. Rev.* **2015**, *115*, 10081–10206.
3. B. Lewandowski, G. De Bo, J. W. Ward, M. Papmeyer, S.Kuschel, M. J. Aldegunde, P. M. E. Gramlich, D. Heckmann, S. M. Goldup, D. M. D'Souza, A. E. Fernandes, D. A. Leigh. Sequence-specific peptide synthesis by an artificial small-molecule machine. *Science* **2013**, *339*, 189–193.
4. Ragazzon, G.; Baroncini, M.; Silvi, S.; Venturi, M.; Credi, A. Light-powered autonomous and directional molecular motion of a dissipative self-assembling system. *Nat. Nanotechnol.* **2014**, *10*, 70–75.
5. C. Cheng, P. R. McGonigal, S. T. Schneebeli, H. Li, N. A. Vermeulen, C. Ke, J. F. Stoddart. An artificial molecular pump. *Nat. Nanotechnol.***2015**, *10*, 547–553.
6. T. Oshikiri, Y. Takashima, H. Yamaguchi, A. Harada. Kinetic control of threading of cyclodextrins onto axle molecules. *J. Am. Chem. Soc.* **2005**, *127*, 12186–12187.
7. Arduini, A.; Calzavacca, F.; Pochini, A.; Secchi, A. Unidirectional threading of triphenylureidocalix[6]arene-based wheels: oriented pseudorotaxane synthesis. *Chem. Eur. J.* **2003**, *9*, 793–799.
8. Arduini, A.; Ciesa, F.; Fragassi, M.; Pochini, A.; Secchi, A. Selective synthesis of two constitutionally isomeric oriented calix[6]arene-based rotaxanes. *Angew. Chem. Int. Ed.* **2005**, *44*, 278–281.
9. Arduini, A.; Bussolati, R.; Credi, A.; Faimani, G.; Garaudée, S.; Pochini, A.; Secchi, A.; Semeraro, M.; Silvi, S.; Venturi, M. Towards controlling the threading direction of a calix[6]arene wheel by using nonsymmetric axles. *Chem. Eur. J.* **2009**, *15* (13), 3230–3242.
10. A. Arduini, R. Bussolati, A. Credi, S. Monaco, A. Secchi, S. Silvi, M. Venturi. Solvent- and light-controlled unidirectional transit of a nonsymmetric molecular axle through a nonsymmetric molecular wheel. *Chem. Eur. J.* **2012**, *18*, 16203–16213.
11. A. Arduini, R. Bussolati, A. Credi, A. Secchi, S. Silvi, M. Semeraro; M. Venturi. Toward directionally controlled molecular motions and kinetic intra- and intermolecular self-sorting: threading processes of nonsymmetric wheel and axle components. *J. Am. Chem. Soc.* **2013**, *135*, 9924–9930.
12. Q.-C. Wang, X. Ma, D.-H. Qu, H. Tian. Unidirectional threading synthesis of isomer-free [2]rotaxanes. *Chem. Eur. J.* **2006**, *12*, 1088–1096.
13. C. Talotta, C. Gaeta, Z. Qi, C. A. Schalley, P. Neri. Pseudorotaxanes with self-sorted sequence and stereochemical orientation. *Angew. Chem. Int. Ed.* **2013**, *52*, 7437–7441.
14. H.-X. Wang, Z. Meng, J.-F. Xiang, Y.-X. Xia, Y. Sun, S.-Z. Hu, H. Chen, J. Yao, C.-F. Chen. Guest-dependent directional complexation based on triptycene derived oxacalixarene: formation of oriented rotaxanes. *Chem. Sci.* **2016**, *7*, 469–474.

et al. and Arduini et al. reported the unidirectional threading of triphenylureidocalix[6]arene derivative **1**.[7-11] In apolar solvents, the viologen of axle **2** forms strong ion pair with the tosylate counter ion. Hydrogen bonding between the tosylate groups and the three ureido groups facilitates the threading of the axle from the upper rim. The methoxy group of the lower rim faces inside the cavity, reducing the size of the rim and disfavoring the penetration of the axle.

As depicted in Chapter 1, polarized motion can also be achieved by molecular walkers. These molecular walkers possess two feet binding to adjacent footholds. These two feet can be released alternatively from their corresponding footholds and take a step forward or backward. By employing chemically orthogonal feet and kinetic trap, the motion can be controlled to move toward one direction.

In the previous chapter, it is shown that symmetrical single helix can wind around dumbbell-like rod guests to form foldaxanes. However, since the single helix is symmetrical, the threading orientation of one extremity is identical to the other (Fig. 2a). We envisage that a foldamer with two different extremities can bind an asymmetrical guest. Although two constitutionally isomeric foldaxanes can form, high selectivity of each extremity for the corresponding binding site will result in one favored thermodynamically stable foldaxane (Fig. 2b). Additionally, this foldamer can thread on to a rod-like guest without bulky stopper. By tuning the interactions of the foldamer with such guest molecule, it can be expected that the threading orientation of the asymmetrical foldamer can be polarized.

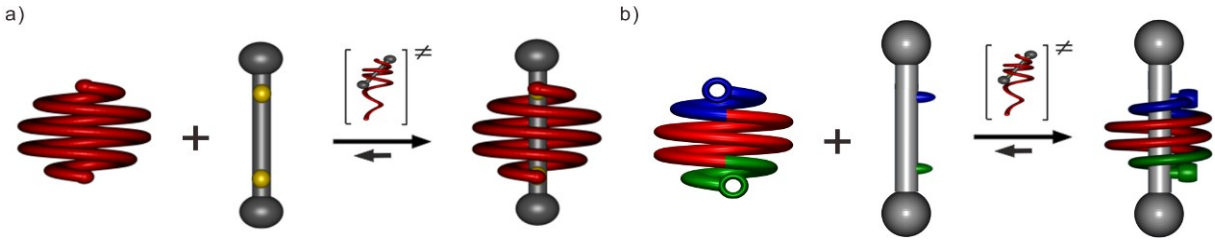

Figure 2. Schematic representation of a) the foldaxane formation of symmetrical single helix with symmetrical rod through unfolding/refolding mechanism. b) the foldaxane formation of asymmetrical single helix with asymmetrical rod through unfolding/refolding mechanism.

2. Synthesis

2.1 Design principle and synthesis of non-symmetrical foldamer

As described in Chapter 2, symmetrical foldamer **3** can bind to dicarbamate rod like guests to form stable host-guest complexes. ^{1}H NMR studies and X-ray crystallography data showed that hydrogen bonding between terminal pyridine trimers (**P$_3$**) and the carbamate groups of the rod-like guest pivoted the complex formation.[15,16] Based on this knowledge, we envisage that, by replacing the terminal 2,6-pyridinediamine unit with 2-amino-5-isobutoxy-1,8-naphthyridine-7-carboxylic acid (**N**) unit,[17] the new segment **NP$_2$** will have less affinity toward a carbamate group, thanks to the electrostatic repulsion between the nitrogen atom at eight position of **N** and the oxygen of the carbamate group. Instead, this new segment has the potential to bind an amide group. Therefore, the asymmetrical foldamer **4** with both **P$_3$** and **NP$_2$** can bind to a rod with both a carbamate and an amide group at each extremity, and selectivity can be expected.

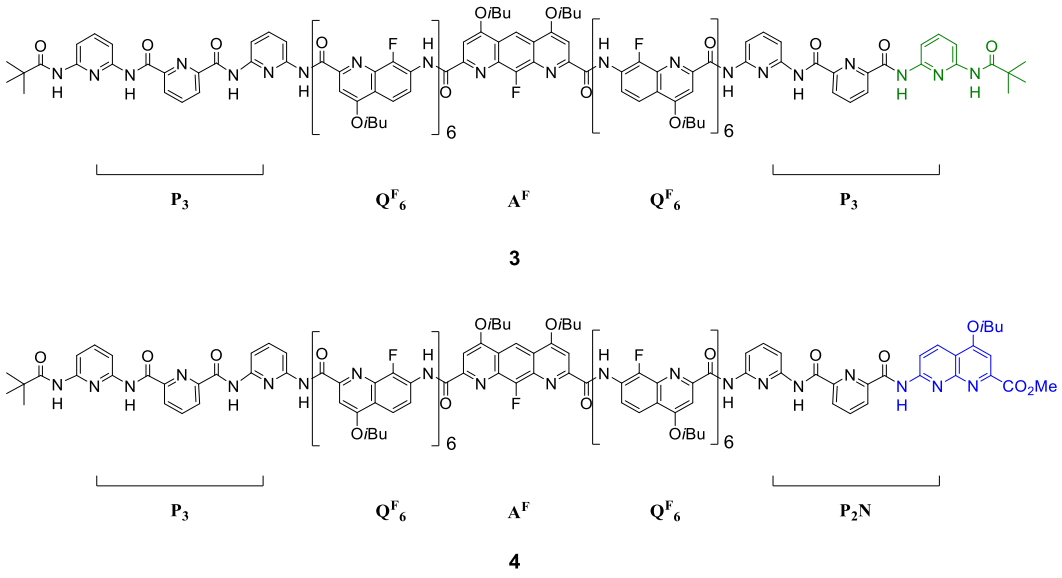

Figure 3. Formulas of aromatic oligoamides **3** and **4**.

Desymmetrization of the central **A^F** unit is crucial for the synthesis of foldamer **4** (Scheme 1). However, the low solubility of diester **15** precluded the possibility of saponifying a single

15. Q. Gan, Y. Ferrand, C. Bao, B. Kauffmann, A. Grélard, H. Jiang, I. Huc. Helix-rod host-guest complexes with shuttling rates much faster than disassembly. *Science*, **2011**, *331*, 1172–1175.
16. Y. Ferrand, Q. Gan, B. Kauffmann, H. Jiang, I. Huc. Template-induced screw motions within an aromatic amide foldamer double helix. *Angew. Chem. Int. Ed.* **2011**, *50*, 7572–7575.
17. Y. Ferrand, A. M. Kendhale, J. Garric, B. Kauffmann, I. Huc. Parallel and antiparallel triple Helices of naphthyridine oligoamides. *Angew. Chem. Int. Ed.* **2010**, *49*, 1778–1781.

methyl ester via the conventional method validated for other 1,8-diazaanthracene derivatives.[18] Fortunately, it was found that the reaction could be done in a large volume of 1:2 mixture of H_2O/THF at 0 ºC with a yield of 59%.

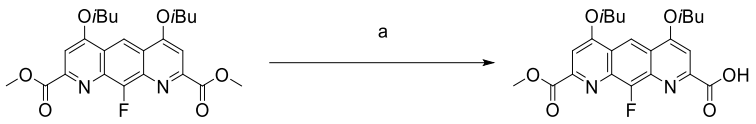

Scheme 1. Synthesis of mono acid **16**: a) NaOH, H_2O/THF, 0 ºC, 3h, 59%.

To synthesize decamer **19**, acid **16** was converted into its acid chloride using oxalyl chloride, and subsequently coupled with amine **18**. Then, the decamer **19** was saponified to afford the acid **20**.

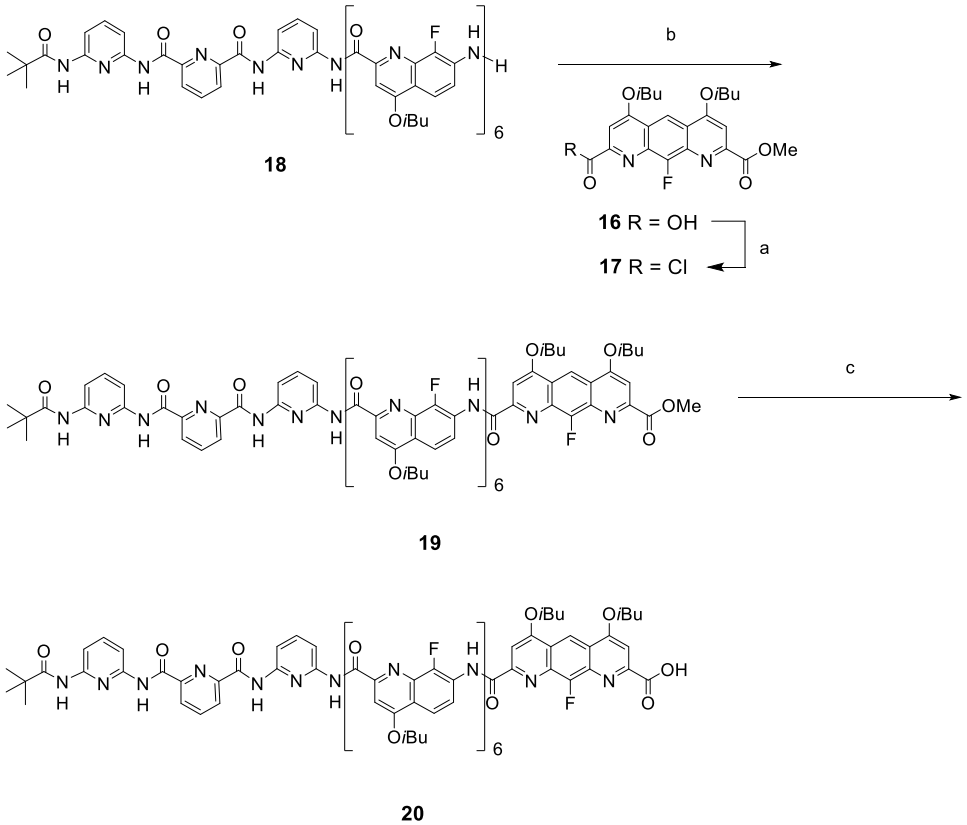

Scheme 2. Synthesis of oligomer **20**. a) oxalyl chloride, CH_2Cl_2, 3 h; b) DIEA, $CHCl_3$, room temperature, overnight, 95%; c) NaOH, H_2O/THF, 3 h, quantitative.

The amine **32** was synthesized following a similar procedure as for sequence **18**. As shown in Scheme 3, the starting trimer **24**, which can be synthesized from the PyBOP assisted coupling of pyridine dimer **22** with the acid of **N**, was treated with 50% TFA in dichloromethane to afford

18. M. L. Singleton, N. Castellucci, S. Massip, B. Kauffmann, Y. Ferrand, I. Huc, Synthesis of 1,8-diazaanthracenes as building blocks for internally functionalized aromatic oligoamide foldamers. *J. Org. Chem.* **2014**, *79*, 2115–2122.

the corresponding amine **25**. This amine was then coupled with a $\mathbf{Q^F}$ dimer acid chloride **26**[19] to give the pentamer **27**. Successive Boc deprotection of **27** and coupling with **26** yield the heptamer **29**, which was again deprotected with 50% TFA in CH_2Cl_2 and coupled with **26** to give the nonamer **31**. The nonamer **31** was treated with 50% TFA in CH_2Cl_2 to remove the Boc group to obtain amine **32**.

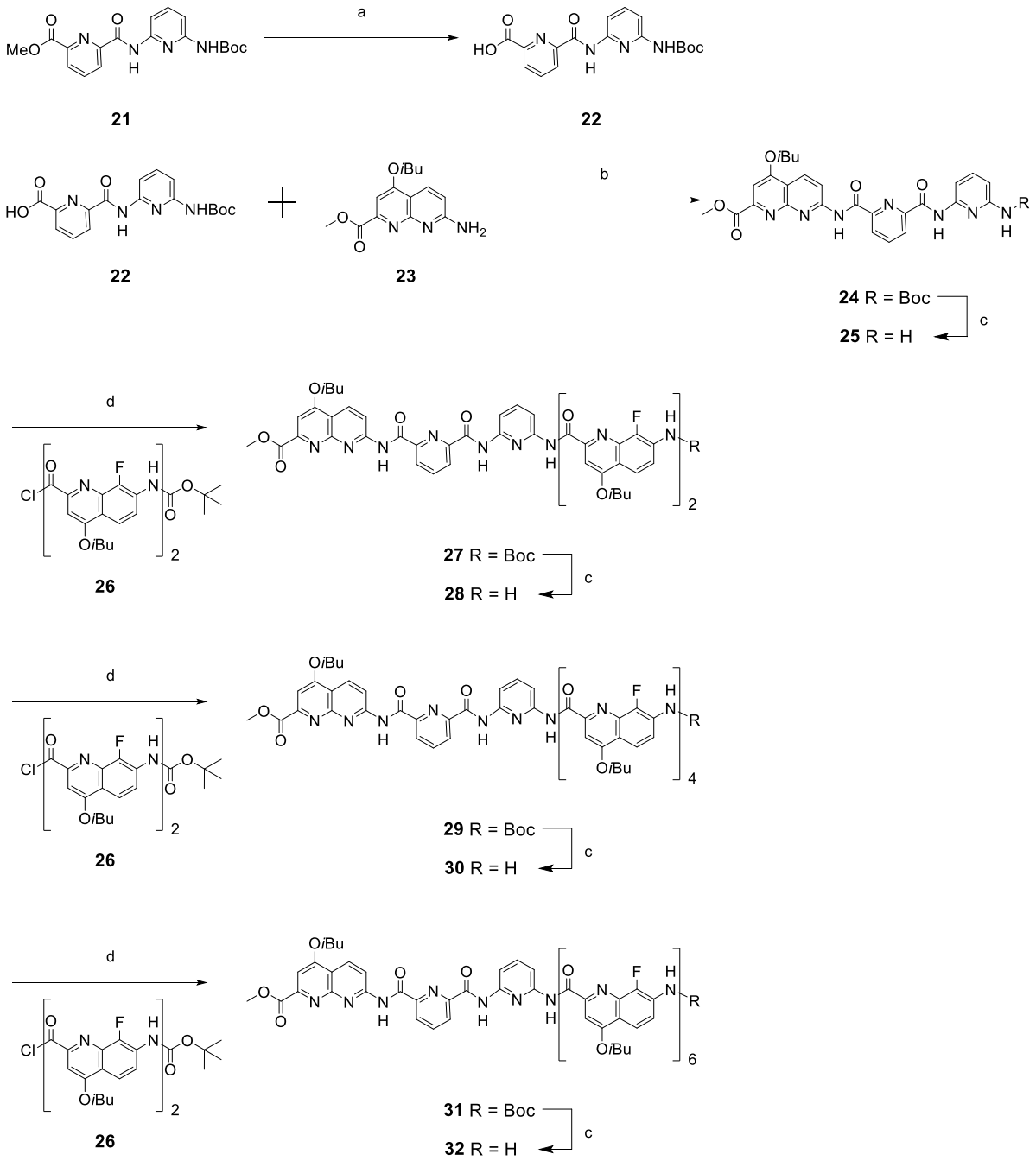

Scheme 3. Synthesis of oligomer **32**. a) NaOH, THF/H_2O, 3h, 97%; b) PyBOP, DIEA, $CHCl_3$, 45 ºC, overnight, 92%; c) TFA, CH_2Cl_2, room temperature, 6 h; d) DIEA, CH_2Cl_2, room temperature, overnight.

19. Q. Gan, C. Bao, B. Kauffmann, A. Grélard, J. Xiang, S. Liu, I. Huc, H. Jiang. Quadruple and double helices of 8-fluoroquinoline oligoamides. *Angew. Chem. Int. Ed.* **2008**, *47*, 1715–1718.

Finally, the acid **20**, despite its low solubility, was converted into an acid chloride using oxalyl chloride, A solution of amine **32** and DIEA in dry $CHCl_3$ was then injected into the acid chloride. After stirring the mixture overnight at room temperature, the crude was checked by ^1H NMR, which showed the full consumption of the amine.

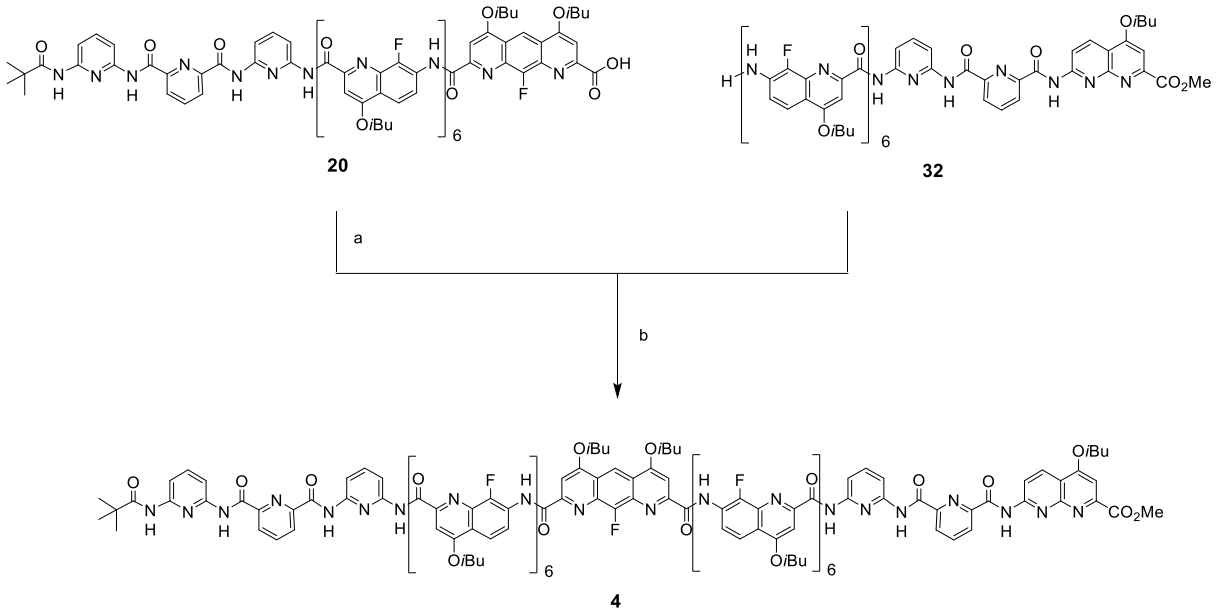

Scheme 4. Synthesis of oligomer **4**: a) Oxalyl chloride, CH_2Cl_2, 3 h; b) DIEA, $CHCl_3$, room temperature, overnight, 70%.

2.2 Pull-down purification of the foldamer with guest grafted resin beads

Thanks to the large polarity difference of carboxylic acid **30** and foldamer **4**, silica gel chromatography can be performed to obtain pure foldamer **4** with ease. However, the precious carboxylic acid **20** decomposed on the silica gel and could not be recycled. So an alternative purification method based on the slow dissociation kinetics of foldamer **4** from its complexation with dumbbell-like guest molecules was envisaged. Resin beads were functionalized with guest molecules which exhibits high and affinity specificity with foldamer **4** (Scheme 5).

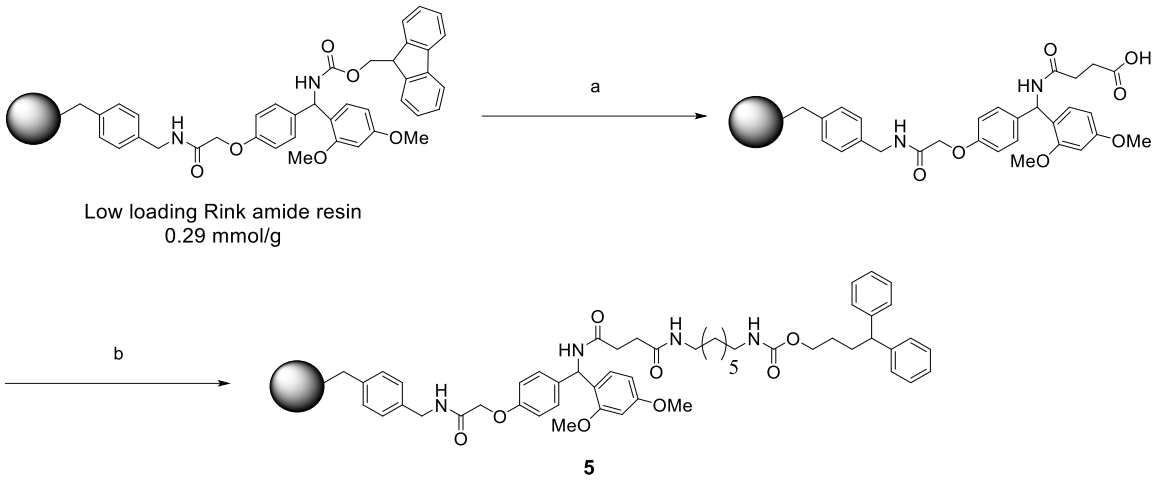

Scheme 5. Synthesis of resin beads **5**: a) 1. Piperidine, DMF, 2. succinic anhydride, DIEA; b) HBTU, HOBt, DIEA and **36**.

Low loading (0.29 mmol/g) Rink amide resin (1 g) was treated with 20% v/v piperidine in DMF at 25 ºC to remove the Fmoc group. After briefly washing with anhydrous DMF, the resin was suspended in 5 mL anhydrous DMF, to which was added succinic anhydride (290 mg, 10 equiv.) in 5 mL anhydrous DMF and DIEA (1.0 mL, 20 equiv.). The mixture was shaken for 30 minutes at 25 ºC. The resin was washed briefly with anhydrous DMF, and the process was repeated once. The resin was suspended in 5 mL anhydrous DMF, to which was added HBTU (110 mg, 1 equiv), HOBt (45 mg, 1 equiv.) in 5 mL anhydrous DMF, and anhydrous DIEA (0.3 mL, 6 equiv.). After shaking briefly for 10 minutes, **36** (330 mg, 2 equiv.) in anhydrous DMF was added. The mixture was shaken for 30 minutes. The resin was washed briefly with anhydrous DMF, and the process was repeated once. The resin was washed thoroughly with DMF, CH_2Cl_2, and CH_2Cl_2/MeOH (1:1), dried and desiccated. ^{1}H NMR of cleaved crude from the resin (TFA/CH_2Cl_2, 1:1, 1 h, 25 ºC) proved the success grafting of rod guest onto the resin beads.

The binding of foldamer **4** on resin **5** was tested. The resin was incubated with a solution of foldamer **4** in chloroform at 50 °C overnight, then the solution phase was filtered off. The resin was washed briefly with chloroform and dried. The colour change of the resin beads from white to yellow indicated the complexation of foldamer **4** to the resin. The resulting resin beads were subjected to solid NMR study. As shown in Figure 4, characteristic amide resonances at 13-9 ppm corresponding to foldaxane formation appeared, confirming the binding of **4** on the resin. A loading rate of 20% was calculated based on the mass gain of the resin.

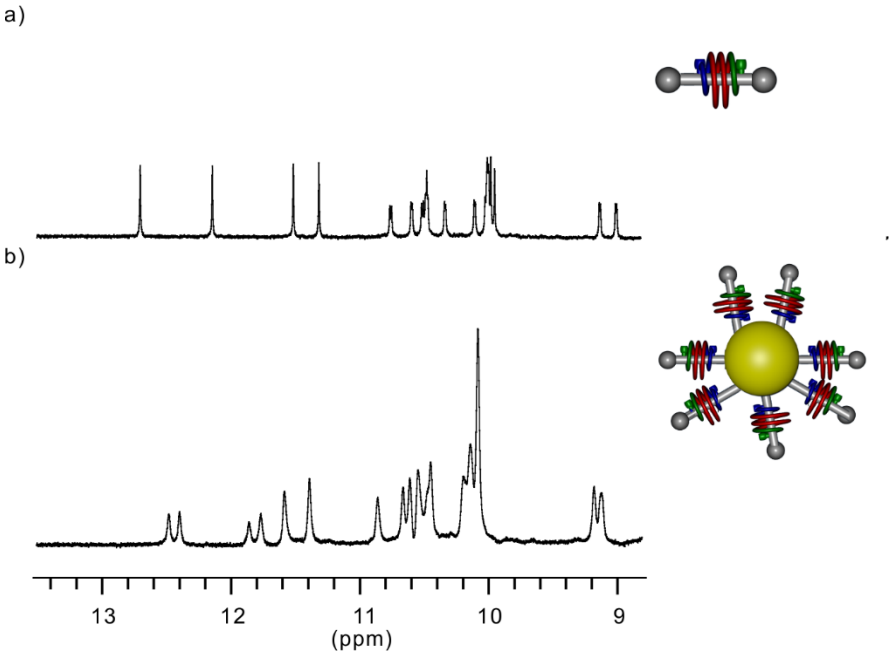

Figure 4. a) Part of the ^{1}H NMR spectrum of the amide region (400 MHz) at 298K of complex **4**⊃**7** in $CDCl_3$; b) Part of the ^{1}H HR-MAS NMR spectrum of the amide region (500 MHz) at 298K of complex of **4** with resin beads: recorded in 256 scans with a recycle delay of 4 s at 7 kHz magic angle spinning.

To purify foldamer **4** from its crude reaction, the crude was incubated overnight in 10 mL chloroform with 1 g of resin in $CHCl_3$ with a gentle stirring at 50 ºC. The solvent, which contained acid **20** and unbound **4**, was filtrated off. The resulting resin was washed thoroughly with $CHCl_3$, and subsequently suspended in a mixture of 40 mL $CHCl_3$ and 4 mL MeOH at 50 ºC for 4 hours to fully dissociate the complex. The mixture was filtrated and the resin was washed with $CHCl_3$ and recycled. The filtrate was combined and the solvents were removed to afford pure foldamer **4**. This procedure was repeated until no significant trace amount of foldamer **4** in solution could be detected. Acid **20** was collected through precipitation from the remaining residue with MeOH.

2.3 Synthesis of dumbbell-like asymmetrical guests

Treating an activated alcohol with 5 equivalents of the corresponding diamine afforded the monoamine, which was subsequently coupled with acid **41** using EDC as coupling reagent to give the single station rod.

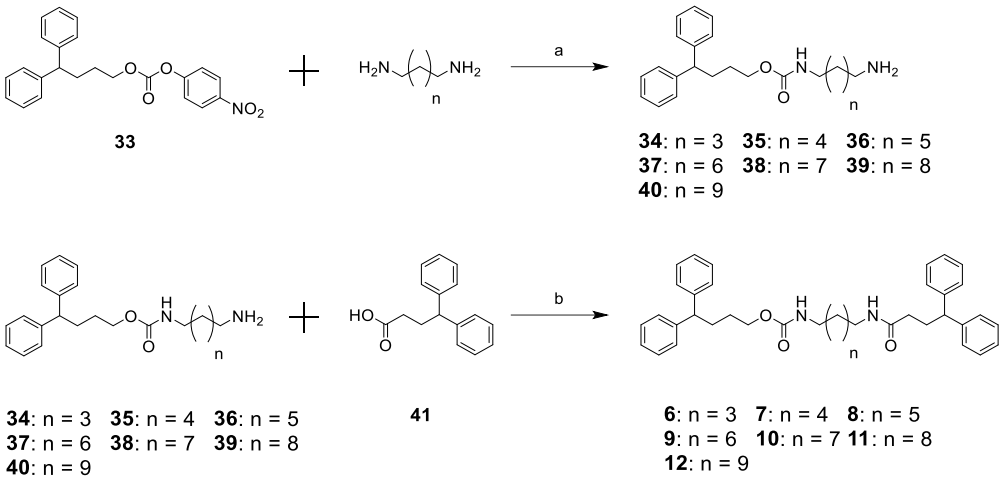

Scheme 6. Synthesis of dumbbell-like asymmetrical guests: a) 1. Et_3N, CH_2Cl_2, 0 °C, 1 h, 2. room temperature, overnight; b) HOBt, EDC, DIEA, CH_2Cl_2, room temperature, overnight.

2.4 Synthesis of polyethylene glycol appended guests

Boc protected mono amine **42**[20] was coupled with the acid **41** to get the mono-amide precursor. Boc group was subsequently removed to afford the amine, which was coupled directly with *p*-nitrophenyl chloroformate activated polyethylene glycol (PEG, Mw = 750 g/mol) to get rod **13** with 48% yield.

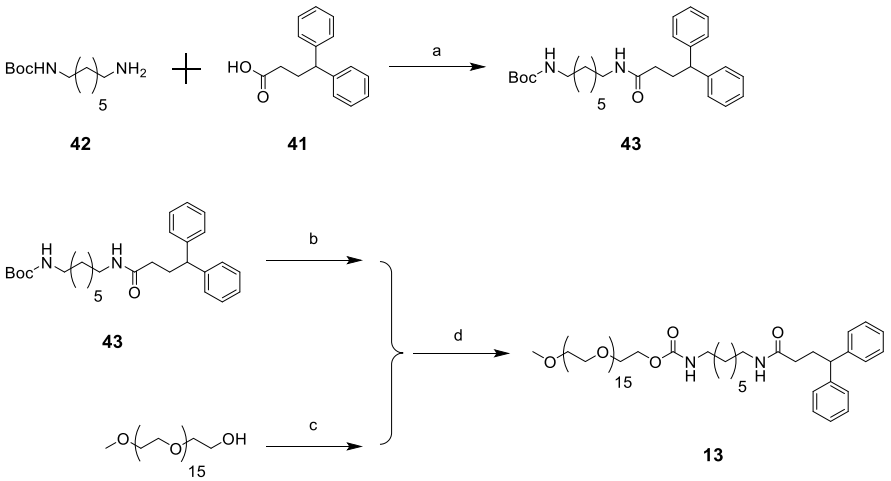

Scheme 7. Synthesis of PEG appended asymmetrical guest **13**: a) HOBt, EDC, DIEA, CH_2Cl_2, room temperature, overnight, 81%; b) TFA, CH_2Cl_2; c) p-nitrophenyl chloroformate, Et_3N, CH_2Cl_2, overnight; d) Et_3N, CH_2Cl_2, overnight, 48%.

Considering a rod with an amide group adjacent to the PEG chain, it was found that the foldamer **4** have reduced selectivity toward rod **44**, forming two isomeric complexes. This is

20. C. Dardonville, C. Fernandez-Fernandez, S.-L. Gibbons, G. J. Ryan, N. Jagerovic, A. M. Gabilondo, J. J. Meana, L. F. Callado. Synthesis and pharmacological studies of new hybrid derivatives of fentanyl active at the μ-opioid receptor and I 2–imidazoline binding sites. *Bioorg. Med. Chem.* **2006**, *14*, 6570-6580.

probably because that the insertion of *a* single methylene cannot fully prohibit the interaction of the terminal oxygen atom of the PEG chain with both ends of foldamer **4**. Thus propionyl group is used as a spacer, which gave good selectivity.

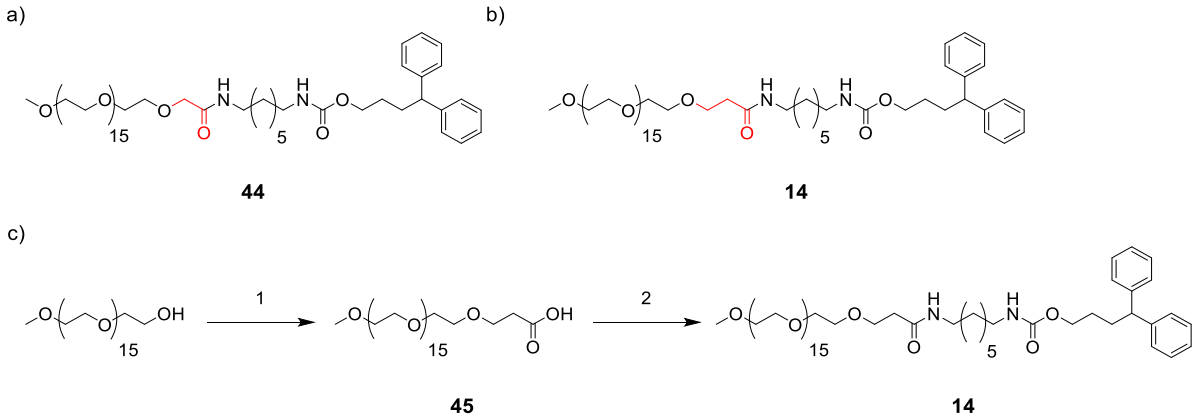

Scheme 8. Formulas of rod-like guests a) **44** and b) **14**. The two rods differ in the number of methylene group (coloured red) between the PEG chain and the amide group. c) Synthesis of PEG appended asymmetrical guest **14**. a) Et_3N, CH_2Cl_2, overnight, 48%; 1) i. catalytic NaH, methyl acrylate, ii. NaOH, THF/H_2O, 5 h, 43%; 2) HOBt, EDC, DIEA, CH_2Cl_2, room temperature, overnight, 83%.

Michael addition of PEG monomethyl ether with methyl acrylate in the presence of catalytic amount of NaH, followed by saponification and purification, afforded acid **45**. Subsequently, the acid was coupled with the mono amine **36** to give rod **14** in 83% yield.

3. Results and discussion

3.1 Double helix formation of foldamer

As for its symmetrical counterpart foldamer **3**, pure single helical foldamer **4** can be obtained by precipitation from methanol. In $CDCl_3$, the dimerization of foldamer **4** is very slow. Equilibrium was reached after 30 days at room temperature or 4 days at 50 °C. However, signal overlapping between the antiparallel and parallel double helices impeded the identification of both species. By applying the method described in Chapter 2, the dimerization constant in $CDCl_3$ at 323K can be calculated as 1.5×10^3 L mol^{-1}.

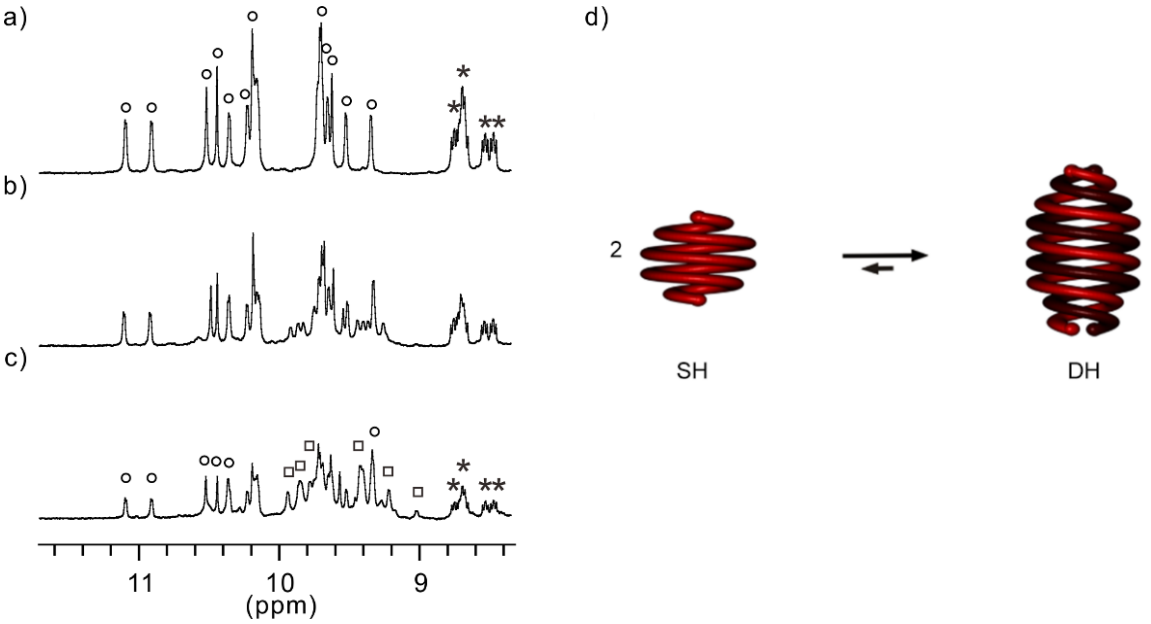

Figure 5. Excerpts of the ^{1}H NMR spectra in $CDCl_3$ (400 MHz) of **4** (1 mM) at 323K after a) t= 10 min; b) t = 1 day and c) at thermodynamic equilibrium. Amide signals of the double helix are marked with empty squares whereas those of the single helix which are in slow exchange on the NMR timescale are denoted with empty cycles. d) Schematic representation of the equilibrium between single helix and double helix.

3.2 The thermodynamics of foldamer-guest complexes

The binding affinities of foldamer **3** toward dicarbamate guests changed accordingly with different length of the α,ω-diaminoalkanes spacers. Similarly, to assess their association constants, a series of rod **6-12** bearing carbamate and amide groups at each extremity was synthesized.

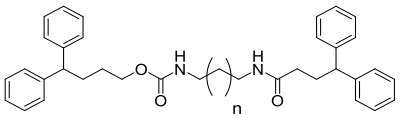

6: n = 3 **7**: n = 4 **8**: n = 5 **9**: n = 6
10: n = 7 **11**: n = 8 **12**: n = 9

Figure 6. Formulas of dumbbell-like asymmetrical guests.

Since both foldamer **4** and rod **8** are nonsymmetrical, two isomeric host-guest complexes can be expected, with foldamer **4** adopting reversed orientation in respect to rod **8**. However, upon addition of **8** into the solution of single helix foldamer **4**, a single new set of peaks in slow exchange with the free helix appeared, (Fig. 7a-d). This new set of peaks can be assigned to one of the two isomers of complex **4**⊃**8**, which possess a much higher thermodynamic stability than its counterpart. Based on the same equation as shown in Chapter 2, the binding constants between **4** and **8** can be calculated to be 28 200 L mol^{-1}.

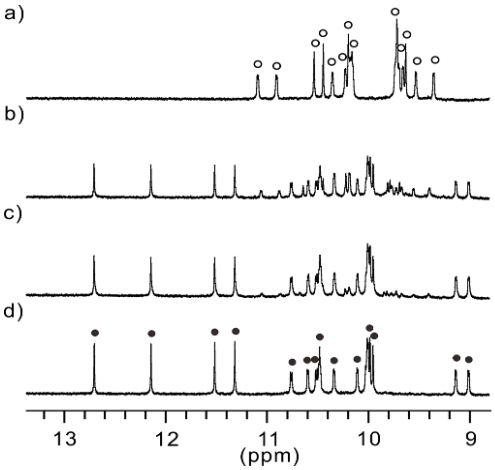

Figure 7. Part of the ^{1}H NMR spectrum of the amide region (400 MHz) at 323K of **4** (0.5 mM) in $CDCl_3$ in the presence of: a) 0 equiv.; b) 1 equiv.; c) 2 equiv.; d) 4 equiv. of rod **8**. Signals of the free **3** single helix and of complex **4**⊃**8** signals are marked with empty and black circles, respectively. K_a = 28 200 (± 200) L mol^{-1}.

The binding constants of foldamer **4** towards rods with varied alkyl length were thus measured (Fig. 6), and the binding constants are listed in Table **1**. Comparison with the binding constants of foldamer **3** towards dicarbamate guests suggested that, for rods with the same diamine, replacement of a pyridine with a naphthyridine decreased the binding affinity. Meanwhile, the binding affinity also changed dramatically when the length of the alkyl chains varied. This indicated that foldamer **4** embody a similar conformation and rigidity as foldamer **3**.

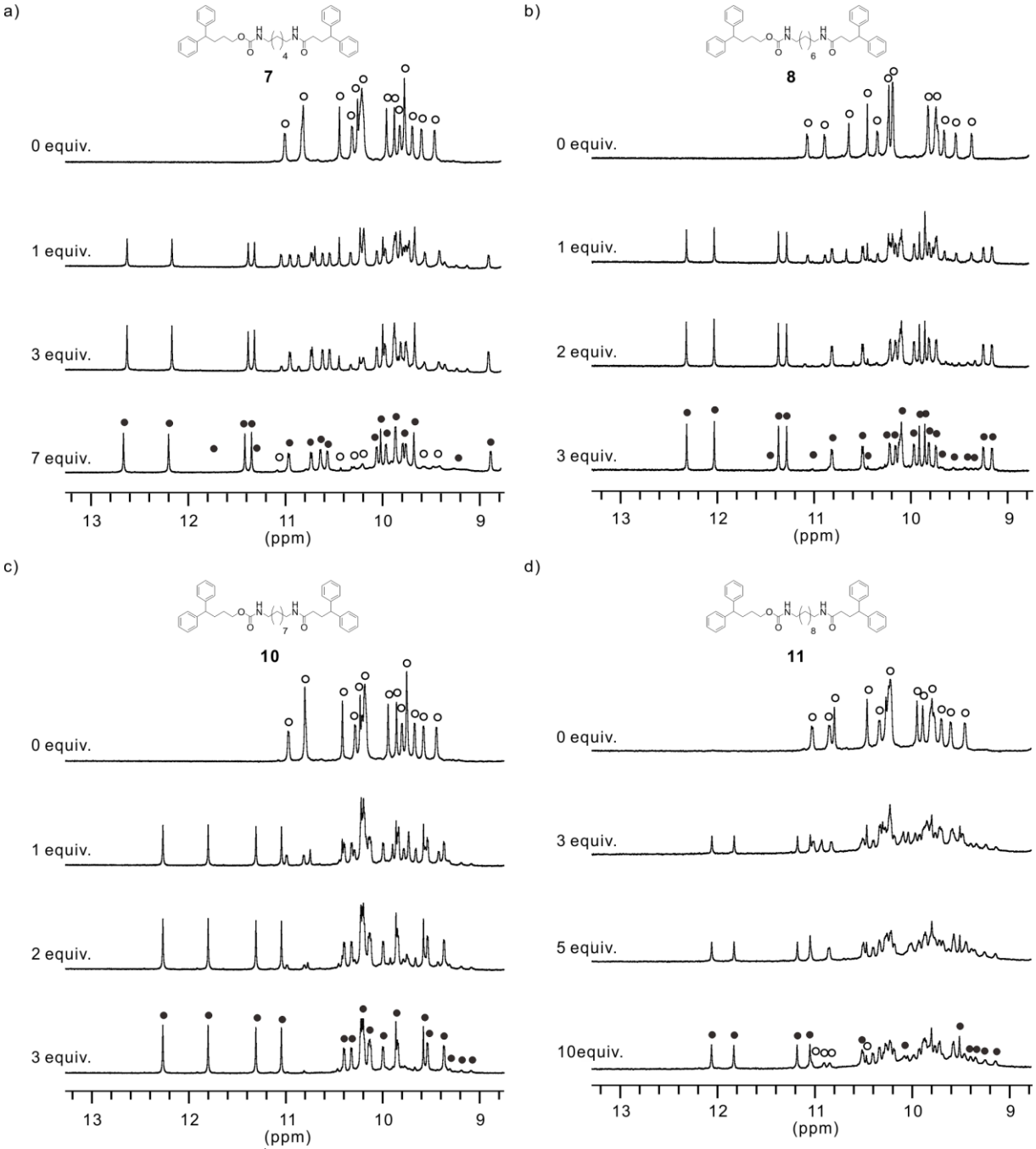

Figure 8. Representative ^{1}H NMR spectra of **4** in $CDCl_3$ at 298K titrated with various guests. a) 2 mM of **3** with rod **7**; b) 1 mM of **3** with rod **8**; c) 2 mM of **3** with rod **10**; d) 2 mM of **3** with rod **11**. Amide signals of the free single helix and foldaxane are marked with empty and black circles, respectively.

Table 1. Binding constants of foldamer **4** with different dumbbell-like asymmetrical molecules monitored by ^{1}H Nuclear Magnetic Resonance in $CDCl_3$.

6 (5 CH_2)	**7** (6 CH_2)	**8** (7 CH_2)	**9** (8 CH_2)	**10** (9 CH_2)	**11** (10 CH_2)	**12** (11 CH_2)
< 1	2 190 (± 10)	28 200 (± 200)	8 000 (± 100)	2 650 (± 50)	133 (± 14)	< 1

Single crystals were obtained by slow diffusion of hexane into a chlorobenzene solution of **4⊃8** at thermodynamic equilibrium. In agreement with the NMR study, the crystal structure unambiguously revealed the exclusive selectivity of $\mathbf{P_3}$ towards the carbamate group and $\mathbf{NP_2}$ towards the amide group. For both the $\mathbf{P_3}$ part and the $\mathbf{NP_2}$ part, the hydrogen bonds between the amide protons of 2,6-pyridinedicarboxamide unit and the carbonyl group of the rod are identical. Missing hydrogen bond between the **N** unit and amide group, along with the electrostatic repulsion between nitrogen atom of **N** unit and oxygen of the carbamate group, afforded the high selectivity.

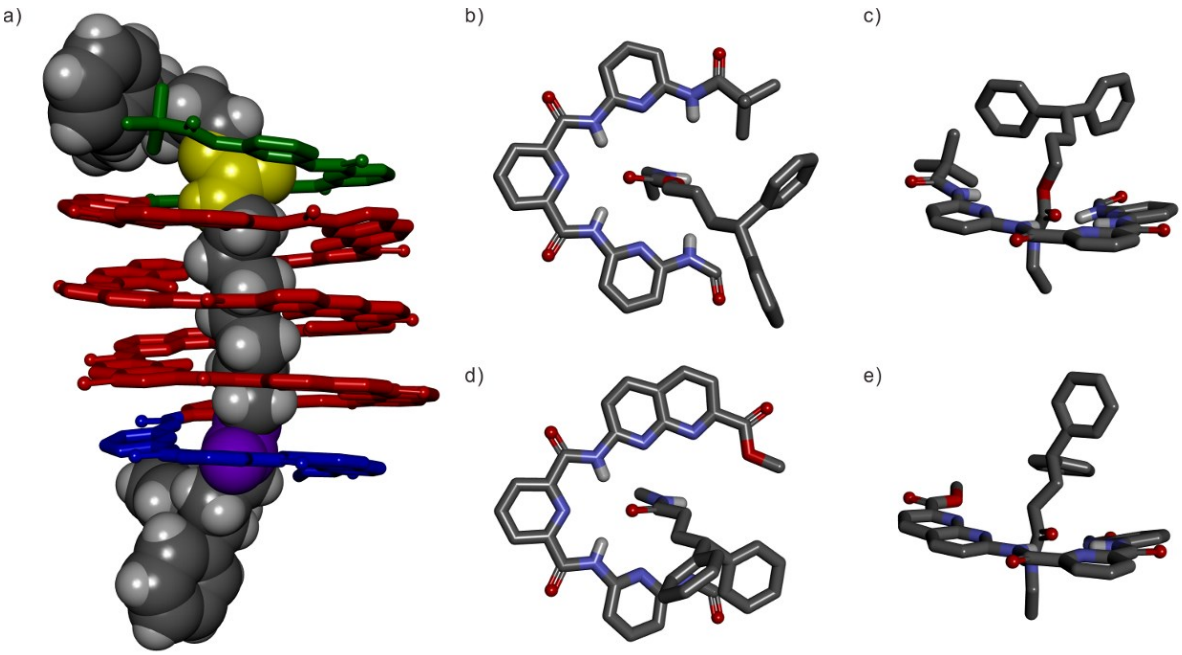

Figure 9. a) Side view of the crystal structure of **4⊃8**. The foldamer **4** is shown in tube representation, in which the terminal $\mathbf{P_3}$, $\mathbf{NP_2}$ and the central segments are colored in green, blue and red, respectively. The rod **8** is shown in CPK with the carbamate and amide group are colored in yellow and purple, respectively. b) Top view and c) side view of $\mathbf{P_3}$ of **4** binding to the carbamate group. d) Top view and e) side view of $\mathbf{NP_2}$ of **4** binding to the amide group. Side chains (O*i*Bu groups) and included solvent molecules have been removed for clarity.

3.3 The kinetics of the formation of the foldamer-guest complex

As described in chapter 3, depending on the termini bulkiness of the rod-like guest, foldamer **4** can bind to it via either an unfolding/refolding or a threading mechanism. Firstly, the kinetics of foldamer **4** toward guest **8,** a dumbbell rod-like guest was investigated. Since the diphenyl stoppers are too large to fit in the cavity of **4**, foldamer **4** can only bind to **8** through an unfolding/refolding process. As shown in Figure 10, before thermodynamic equilibrium is reached, the major signals correspond to the thermodynamic product, which can be termed as

the matching complex. A minor set of peaks appeared along with the matching complex. This new set of peaks can be assigned to the mismatching isomer of **4⊃8**, in which **P3** binds to the amide group and **NP2** binds to the carbamate group. The relative low intensity of this mismatching complex indicated the high kinetic selectivity of **4** toward the matching complex when folding onto rod **8**.

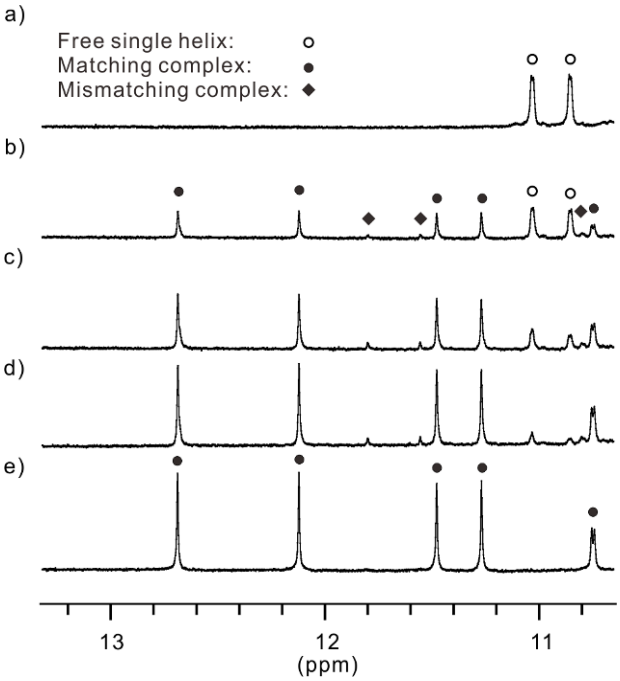

Figure 10. Part of the 400 MHz NMR spectrum of the amide region at 323K of **4** (1 mM) in $CDCl_3$: a) without guest; b-e) after addition of 3 equivalents of **4** at b) t = 5 min.; c) t = 20 min.; d) t = 60 min; e) at thermodynamic equilibrium. Amide signals of the free single helix **4**, **4⊃8** with matching binding and **4⊃8** with mismatching binding are marked with empty circles, black circles, and black diamonds, respectively.

Foldamer-guest complex can also form via threading along an unhindered chain. The threading kinetics with two rods embodying reversed arrangements of the carbamate and amide groups were monitored with ^{1}H NMR. PEG chain (MW = 750 g/mol) was appended at the entrance to let a time window long enough for an accurate monitoring of the matching/mismatching ratio.

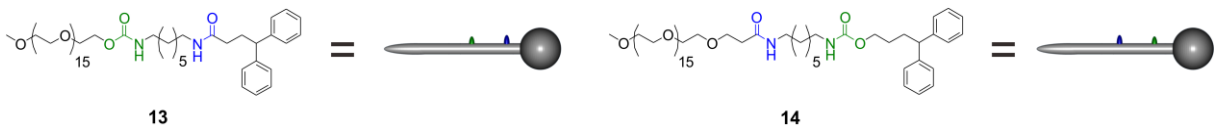

13 **14**

Figure 11. Molecular formulas and cartoon representation of rod **13** and **14**. Both rods possess an amide group (blue) and a carbamate group (green), linked by 1,7- diaminoheptane group.

When 3 equivalents of **13** were added to a solution of foldamer **4** at 10 °C, two set of new resonances appeared corresponding to the matching and mismatching complexes. Four minutes after the addition of **13**, the first NMR spectrum was acquired (Fig. 12b), and revealed that the mismatching complex concentration was 30% higher than the matching complex concentration. As time evolved, the mismatching complex reached its maximum concentration 10 minutes after the addition of **13**, with a ratio of approximately 1:1 against the matching complex. Then, the concentration of matching complex continued to increase, whilst the mismatching complex decreased slowly. When thermodynamic equilibrium was reached, a single set of signals remained, corresponding to the matching complex. This whole kinetic scenario indicated that the threading orientation of **4** is biased. The higher proportion of mismatching complex at the start of the experiment means that the mismatching complex formed faster, indicating the faster threading rate of the **P3** end compared to the **NP2** end.

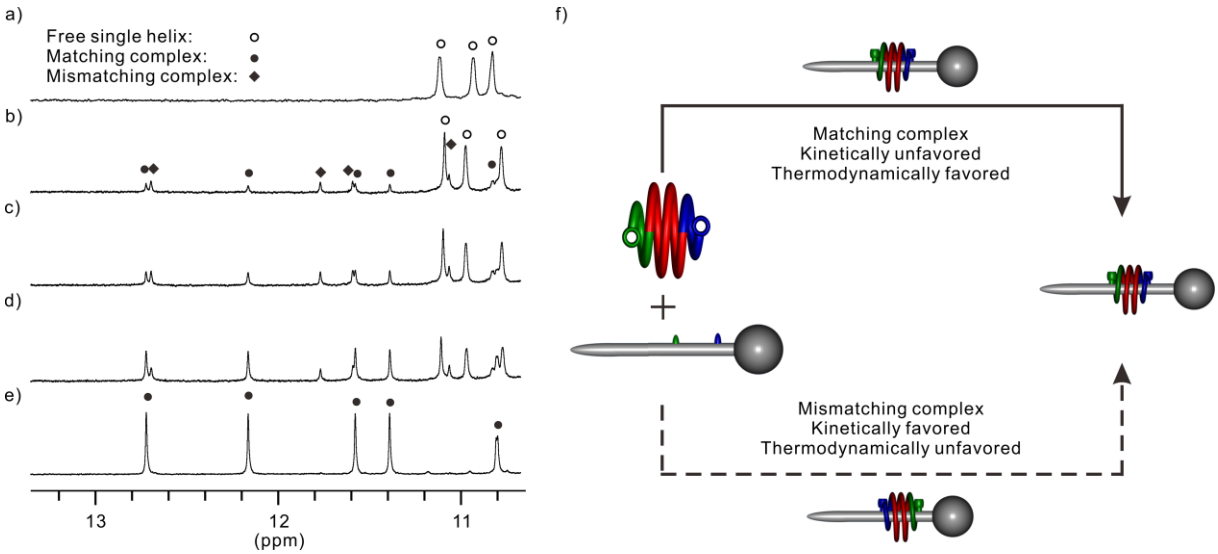

Figure 12. Part of the 400 MHz NMR spectrum of the amide region at 283K of **4** (1mM) in $CDCl_3$: a) without guest; b-e) after addition of 3 equivalents of **13** at b) t = 4 min.; c) t = 10 min.; d) t = 30 min; e) at thermodynamic equilibrium. Amide signals of the free single helix **4**, matching and mismatching complex of **4**⊃**13** are marked with empty circles, black circles, and black diamonds, respectively. f) Schematic representation of the threading process of **4** on to rod **13**.

The threading kinetic of rod **14** was also investigated. To our surprise, the threading of the **P3** end was even more favored comparing to the **NP2** end. As Figure 13b shows, a 3:1 ratio for matching complex vs mismatching complex was observed 10 minutes after addition of the guest. The inversion of the arrangement of the amide and the carbamate group did not reverse the ratio of the matching complex and the mismatching complex. An explanation based on the influence of the methoxy entrance is not sufficient. A polarization effect caused by the first amide/carbamate group of the binding station should also be envisaged.

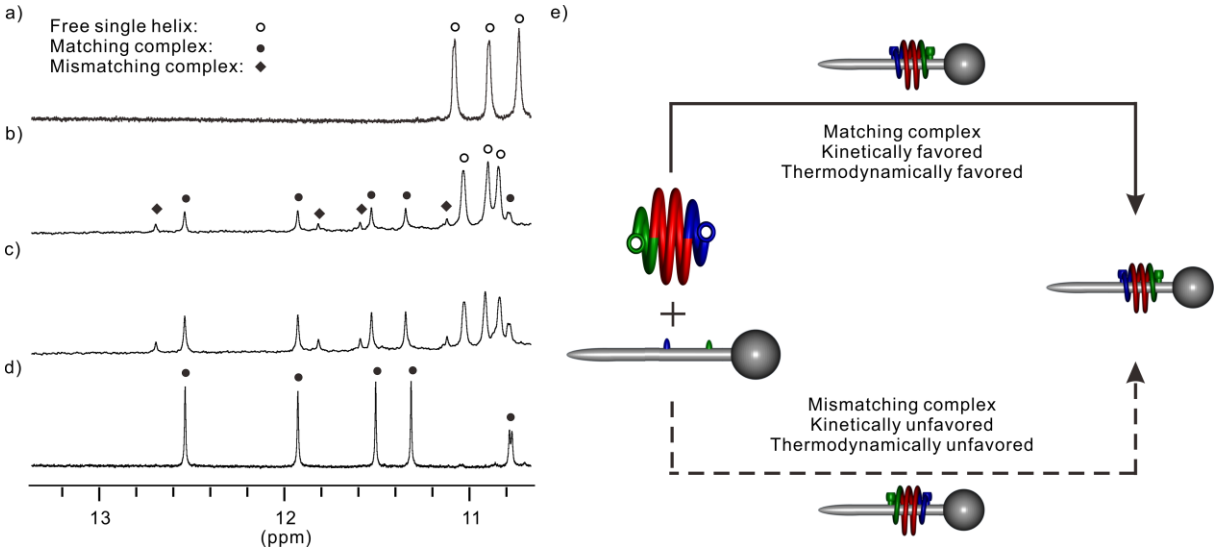

Figure 13. Part of the 400 MHz NMR spectrum of the amide region at 283K of **4** (1mM) in $CDCl_3$: a) without guest; b-e) after addition of 3 equivalents of **14** at b) t = 10 min.; c) t = 20 min.; d) at thermodynamic equilibrium. Amide signals of the free single helix **4**, matching and mismatching complex of **4**⊃**14** are marked with empty circles, black circles, and black diamonds, respectively. e) Schematic representation of the threading process of **4** on to rod **14**.

4. Conclusion

In conclusion, an asymmetrical foldamer with **P_3** and **NP_2** at the two termini was synthesized. This foldamer showed high selectivity toward asymmetrical guests, with **P_3** and **NP_2** binding to carbamate and amide group respectively. This resulted in the formation of only one thermodynamic product out of two potential isomeric complexes. Preliminary studies indicated that the threading of the foldamer onto linear rods can be polarized by the introduction of functional groups on the rod. Further investigations to understand and control this polarization effect are currently under progress.

5. Experimental part

5.1 Methods for NMR

NMR spectra were recorded on 3 different NMR spectrometers: (1) an Avance II NMR spectrometer (Bruker Biospin) with a vertical 7,05T narrow-bore/ultrashield magnet operating at 300 MHz for ^{1}H observation and 75 MHz for ^{13}C observation by means of a 5-mm direct BBO H/X probe with Z gradient capabilities; (2) an Avance 400 NMR spectrometer (Bruker Biospin) with a vertical 9.4T narrow-bore/ultrashield magnet operating at 400 MHz for ^{1}H observation by means of a 5-mm direct QNP $^{1}H/^{13}C/^{31}P/^{19}F$ probe with gradient capabilities; (3) a Bruker Avance II 500MHz spectrometer equipped with a 4mm HR-MAS ^{1}H-^{13}C probe. Chemical shifts are reported in parts per million (ppm, δ) relative to the ^{1}H residual signal of the deuterated solvent used. ^{1}H NMR splitting patterns with observed first-order coupling are designated as singlet (s), doublet (d), triplet (t), or quartet (q). Coupling constants (*J*) are reported in hertz. Data processing was performed with Topspin 2.0 software. Samples were not degassed. $CDCl_3$ from Eurisotop was used after filtration through an alumina pad followed by a distillation over calcium hydride.

^{1}H HR-MAS-NMR. ^{1}H NMR spectrum was recorded on a Bruker Avance II 500MHz spectrometer equipped with a 4mm HR-MAS 1H-13C probe. The sample was suspended in $CDCl_3$ and placed into a 4mm zirconia rotor (80µl volume). Sample was spun at 7kHz at room temperature. Spectrum was acquired with the use of a Carr-Purcell-Meiboon-Gill sequence[21,22] (1, 2), 32k data-points across a spectral width of 10kHz, 4s recycling delay, 256 scans, 3ms interpulse delay for a total spin echo period of 24ms (4 loops). A line-broadening apodization function of 0.3 Hz was applied to ^{1}H NMR free induction decays prior to Fourier transformation.

5.2 Methods for X-ray crystallography

X-Ray diffraction studies for **4⊃8** have been performed at the IECB X-ray facility (UMS 3033 – UMS001) on a Rigaku FRX rotating anode (2.9 kW). Data were collected at the copper kα wavelength with a partial chi goniometer. Phi-scans were performed and data recorded with a large Dectris Pilatus 6M detector. The Rigaku CrystalClear suite[23] was used to index and integrate the home source data with a multi-scan absorption correction. Data collected at the

21. S. Meiboom, D. Gill. Modified spin-echo method for measuring nuclear relaxation times. *Rev. Sci. Instr.* **1958**, *29*, 688-691.
22. E. L. Hahn. Spin echoes. *Phys. Rev.* **1950**, *80*, 580-594.
23. CrystalClear-SM Expert 2.1 (Rigaku, Jun 7th 2013) Software, Version 5.6.2.0, Tokyo, Japan.

synchrotron were processed with the XDS package[24]. The structure was solved with and Shelxt[25]. All structures were refined by full-matrix least-squares method on F^2 with Shelxl-2014[23]. SQUEEZE[26] procedure was employed for removing disordered solvent molecules that could not be reliably modeled. Big size of the structures, large volume fractions of disordered solvent molecules and side chains, small size of the crystals are main reason for rather moderate quality of the diffraction data and refinement statistics.

24. W. Kabsch, XDS. *Acta Cryst* **2010**, *D66*, 125–132.
25. G. M. Sheldrick, A short history of SHELX. *Acta Cryst.* **2008**, *A64*, 112–122.
26. A. L. Spek, SQUEEZE. *J. Appl. Cryst.* **2003**, *36*, 7–13.

5.3 Summary of X-Ray crystallographic data

Name	**4⊃8**
Formula	$C_{238}H_{222}F_{13}N_{40}O_{36}\cdot C_{40}H_{48}N_2O_3\cdot 3.87(C_6H_5Cl)\cdot 1.11(H_2O)$
M	5525.87 g/mol
Crystal system	Monoclinic
Space group	$P2_1/c$
a/Å	22.576 (11)
b/Å	32.40 (2)
c/Å	42.55 (2)
α/o	90 (2)
β/o	93.84 (4)
γ/o	90
U/Å^3	31056 (30)
T /*K*	100 (2)
Z	4, (Z'=1)
ρ/g cm^{-1}	1.181
size (mm)	0.15 × 0.04 × 0.03
λ/ Å	1.54178
μ/mm^{-1}	1.00
Absorption correction	Multi-scan
unique data	48503
parameters/restraints	3397/379
*R*1, *wR*2	0.2000, 0.3672
goodness of fit	1.79

5.4 Methods for chemical synthesis

All reactions were carried out under a dry nitrogen atmosphere. Commercial reagents were purchased from Sigma-Aldrich, Alfa-Aesar or TCI and were used without further purification unless otherwise specified. Tetrahydrofurane (THF) and dichloromethane (CH_2Cl_2) were dried over alumina columns; chloroform ($CHCl_3$), triethylamine (Et_3N) and diisopropylethylamine (DIEA) were distilled over calcium hydride (CaH_2) prior to use. Reactions were monitored by

thin layer chromatography (TLC) on Merck silica gel 60-F254 plates and observed under UV light. Column chromatography purifications were carried out on Merck GEDURAN Si60 (40-63 μm). ESI mass spectra were obtained from the Mass Spectrometry Laboratory at the European Institute of Chemistry and Biology (UMS 3033 - IECB), Pessac, France.

5.4.1 Synthesis of foldamer

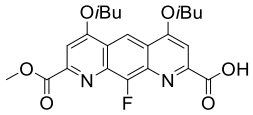

16

Compound 16. NaOH (210 mg, 5.25 mmol) in 10 mL H_2O was added quickly into a solution of compound **15** (2.0 g, 4.36 mmol) in a mixture of 1.4 L THF and 0.7 L H_2O at 0 ºC. The solution was stirred for 3 hours at 0 ºC, after which the solution was acidified with 5% citric acid. THF was removed under reduced pressure, and the aqueous phase was extracted with CH_2Cl_2 (3×300 mL). The organic phase was dried over $MgSO_4$, the solvent was removed to get the crude, which was purified by silica column chromatography eluting with AcOH/MeOH/DCM (1:1:96 to 1:9:90) to get the product as a yellow solid (1.1 g, 59% yield). ^{1}H NMR ($CDCl_3$, 300 MHz): δ 9.04 (d, *J*(H, H) = 2.3, 1H), 7.61 (s, 1H), 7.58 (s, 1H), 4.21-4.15 (m, 4H), 4.12 (s, 3H), 2.46-2.31 (m, 2H), 1.21 (d, *J*(H, H) = 1.9, 6H), 1.19 (d, *J*(H, H) = 1.9, 6H). ^{13}C NMR ($CDCl_3$, 100 MHz): δ 165.90, 164.54, 164.22, 163.36, 163.32, 155.04, 152.33, 151.95, 149.71, 136.48, 136.39, 134.63, 134.52, 122.75, 122.47, 111.62, 111.54, 100.11, 97.62, 76.02, 75.71, 53.74, 28.38, 28.32, 19.25, 19.19. HRMS (ESI): *m/z* calcd for $C_{23}H_{26}FN_2O_6$ $[M+H]^+$ 445.1769 found 445.1816.

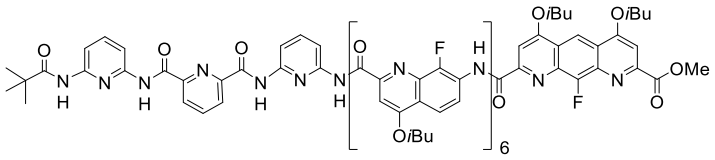

19

Compound 19. Under N_2 atmosphere, to a solution of compound **16** (140 mg, 0.34 mmol) in 3 mL dry CH_2Cl_2 was added oxalyl chloride (0.32 mL, 3.4 mmol) at room temperature. After stirring for 3 hours, the solvent was removed under vacuum to provide the acid chloride **17**.

Under N_2 atmosphere, a solution of the resulting acid chloride **17** in dry CH_2Cl_2 was added to a solution of compound **18** (340 mg, 0.18 mmol) and DIEA (0.12 mL, 0.72 mmol) in 3 mL dry CH_2Cl_2. The reaction was allowed to proceed overnight at room temperature. The crude was concentrated to dryness, and purified by silica column chromatography eluting with EtOAc/DCM (99:1 to 40:60) to get the product as a yellow solid (410mg, 95% yield). ^{1}H NMR (d_6-DMSO, 400 MHz, 313K): δ 11.56 (s, 1H), 11.03 (s, 1H), 10.47-10.28 (m, 3H), 10.14 (s, 1H), 10.10 (s, 1H), 9.90 (s, 2H), 8.82 (s, 1H), 8.24 (br, 1H), 7.94 (br, 1H), 7.94 (br, 1H), 7.88-6.31 (m, 27H), 4.38-3.65 (m, 19H), 2.40-2.13 (m, 8H), 1.40-1.06 (m, 48H), 0.32 (s, 9H). HRMS (ESI): *m/z* calcd for $C_{129}H_{124}F_7N_{21}O_{20}$ $[2M+2H]^{2+}$ 2421.9326 found 2421.9401.

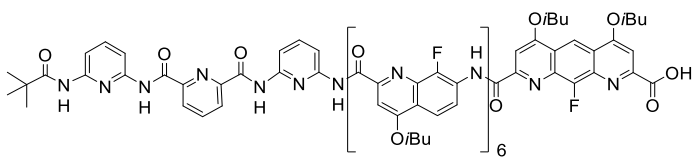

20

Compound 20. NaOH (34 mg, 0.85 mmol) in 4 mL H_2O was added dropwise into a solution of compound **19** (410 mg, 0.17 mmol) in 16 mL THF at room temperature. The solution was stirred for 3 hours at room temperature, after which the solution was diluted in to 200 mL CH_2Cl_2, acidified with 5% citric acid. The organic phase was dried over $MgSO_4$, the solvent was removed to get the product as a yellow solid with quantitative yield, which was used directly without further purification. Attempts to acquire NMR spectra failed due to its poor solubility in most organic solvents. HRMS (ESI): *m/z* calcd for $C_{256}H_{246}F_{14}N_{42}O_{40}$ $[2M+2H]^{2+}$ 2407.9170 found 2407.9268.

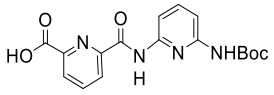

22

Compound 22. NaOH (7.0 g, 175 mmol) in 28 mL H_2O was added dropwise into a solution of compound **21**[27] (9.1 g, 24.6 mmol) in 280 mL THF at 0 ºC. After stirring for 30 minutes at 0 ºC, the reaction was proceeded for 3 hours further at room temperature. The solution was acidified with 5% citric acid, extracted with EtOAc (3×300 mL). The organic phase was dried over $MgSO_4$, the solvent was removed to get the the product as a white solid (8.5 g, 97% yield). ^{1}H NMR ($CDCl_3$, 300 MHz): δ 10.77 (s, 1H), 8.56 (dd, *J*(H, H) = 7.8, *J*(H, H) = 1.1, 1H), 8.45 (dd, *J*(H, H) = 7.8, *J*(H, H) = 1.1, 1H), 8.19-8.09 (m, 2H), 7.85-7.74 (m, 2H), 7.65 (br, 1H), 1.56 (s, 9H). ^{13}C NMR ($CDCl_3$, 75 MHz): δ 166.93, 162.08, 152.23, 150.44, 149.50, 149.03, 146.92, 141.67, 139.37, 128.08, 126.63, 109.18, 108.86, 81.63, 28.42. HRMS (ESI): *m/z* calcd for $C_{16}H_{24}O_3$ $[M+H]^+$ 264.1725 found 265.1804.

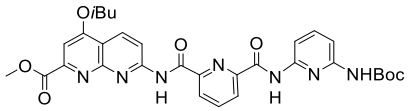

24

Compound 24. Under N_2 atmosphere, PyBOP (4 g, 1.5 eq) and DIEA (3.5 mL, 20.4 mmol) was added to a solution of compound **22** (1.8 g, 5.1 mmol) and compound **23** (1.6 g, 5.1 mmol) in 30 mL dry $CHCl_3$, and the mixture was heated at 45 ºC overnight. The crude was extracted with CH_2Cl_2/H_2O, the organic phase was dried over $MgSO_4$, the solvent was removed under reduced pressure. The product was collected by precipitation from MeOH as a white solid (3.1 g, 92% yield). ^{1}H NMR ($CDCl_3$, 300 MHz): δ 11.14 (s, 1H), 10.47 (s, 1H), 8.88 (d, *J*(H, H) = 9.1, 1H), 8.71 (d, *J*(H, H) =9.1, 1H), 8.62-8.53 (m, 2H), 8.19 (t, *J*(H, H) = 7.8, 1H), 8.15-8.07 (m, 2H), 7.82-7.73 (m, 2H), 7.57 (s, 1H), 4.10 (d, *J*(H, H) = 6.5, 2H), 4.06 (s, 3H), 2.42-2.24 (m, 1H), 1.58 (s, 9H), 1.17 (d, *J*(H, H) = 6.7, 6H). ^{13}C NMR ($CDCl_3$, 75 MHz): δ 165.44, 163.74, 162.72, 161.48, 154.68, 152.59, 151.85, 150.81, 149.18, 149.08, 148.23, 140.65, 139.56, 134.54, 126.38, 126.06, 115.84, 115.02, 108.54, 108.46, 101.39, 80.86, 75.78, 53.08, 28.35, 28.19, 19.23. HRMS (ESI): *m/z* calcd for $C_{31}H_{34}N_7O_7$ $[M+H]^+$ 616.2514 found 616.2508.

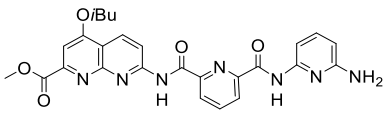

25

Compound 25. Trifluoroacetic acid (5 mL) was added dropwise to a solution of compound **24** (1 g, 1.6 mmol) in 10 mL dry CH_2Cl_2 under N_2 at room temperature. After stirring for 6 hours at room temperature, the crude was neutralized with saturated aqueous solution of $NaHCO_3$, while the product precipitated out. CH_2Cl_2 was removed under reduced pressure, the product was collected by filtration as a yellow solid (680 mg, 82% yield), which was used directly without further purification. ^{1}H NMR ($CDCl_3$, 300 MHz): δ 10.94 (s, 1H), 10.19 (s, 1H), 8.84 (d, *J*(H, H) = 9.1, 1H), 8.69 (d, *J*(H, H) =9.1, 1H), 8.60-8.50

27. D. O. Frimannsson, T. McCabe, W. Schmitt, M. Lawler, T. Gunnlaugsson. Synthesis and crystallographic analysis of short pyridine-based oligoamides as DNA-targeting supramolecular binders. *Supramol. Chem.* **2010**, *22*, 483-490.

(m, 2H), 8.17 (t, *J*(H, H) = 7.8, 1H), 7.77 (t, *J*(H, H) = 7.7, 1H), 7.58 (s, H), 7.53 (t, *J*(H, H) = 7.9, 1H), 6.33 (t, *J*(H, H) = 7.9, 1H), 4.66 (br, 2H), 4.09 (d, *J*(H, H) = 6.5, 2H), 4.06 (s, 3H), 2.41-2.24 (m, 1H), 1.16 (d, *J*(H, H) = 6.7, 6H). ^{13}C NMR ($CDCl_3$, 75 MHz): δ 163.73, 162.89, 161.42, 157.60, 152.16, 149.48, 148.44, 140.18, 139.64, 134.52, 126.46, 126.15, 115.97, 105.16, 103.82, 101.47, 75.87, 53.30, 28.32, 19.37. HRMS (ESI): *m/z* calcd for $C_{26}H_{26}N_7O_5$ $[M+H]^+$ 516.1990 found 516.1969.

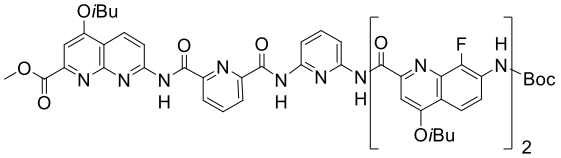

27

Compound 27. Under N_2 atmosphere, to a suspension of compound **25** (440 mg, 0.85 mmol) in 10 mL dry CH_2Cl_2 was added DIEA (0.58 mL, 3.4 mmol). A solution of $\mathbf{Q^F}$ dimer acid chloride (1.1 eq) in 10 mL dry CH_2Cl_2 was injected *via* a syringe, and the reaction was allowed to proceed overnight at room temperature. The crude was concentrated to dryness, and the product was collected by precipitation from MeOH as a white solid (910 mg, 94% yield). ^{1}H NMR ($CDCl_3$, 300 MHz): δ 11.14 (s, 1H), 10.93 (s, 1H), 10.52 (s, 1H), 10.33 (s, 1H), 8.84 (br, 2H), 8.60 (m, 2H), 8.47 (dd, *J*(H, H) = 7.0, *J*(H, H) = 2.0, 1H), 8.33-8.11 (m, 4H), 8.04-7.82 (m, 3H), 7.68-7.55 (m, 2H), 6.75-6.63 (m, 2H), 4.13 (d, *J*(H, H) = 6.5, 2H), 4.00 (br, 2H), 3.28-3.12 (m, 5H), 2.41-2.20 (m, 2H), 2.04-1.88 (m, 1H), 1.70 (s, 9H), 1.23-1.10 (m, 12H), 0.94 (d, *J*(H, H) = 6.7, 6H). ^{13}C NMR ($CDCl_3$, 75 MHz): δ 165.24, 163.07, 162.84, 162.54, 162.19, 161.94, 161.36, 154.91, 154.44, 152.47, 150.86, 150.48, 149.71, 149.57, 148.97, 148.32, 140.48, 139.17, 136.77, 133.33, 127.76, 127.66, 126.35, 125.82, 120.49, 119.20, 118.80, 118.19, 117.11, 116.79, 115.42, 114.07, 110.34, 109.94, 100.10, 97.35, 81.64, 75.57, 75.10, 74.95, 52.24, 31.08, 28.45, 28.32, 28.21, 27.98, 19.42, 19.24, 19.16. HRMS (ESI): *m/z* calcd for $C_{59}H_{60}F_2N_{11}O_{11}$ $[M+H]^+$ 1136.4436 found 1136.4431.

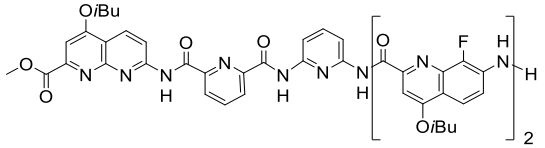

28

Compound 28. Trifluoroacetic acid (9 mL) was added dropwise to a solution of compound **27** (760 mg, 0.67 mmol) in 18 mL dry CH_2Cl_2 under N_2 at room temperature. After stirring for 6 hours at room temperature, the crude was neutralized with saturated aqueous solution of $NaHCO_3$, while the product precipitated out. CH_2Cl_2 was removed under reduced pressure, the product was collected by filtration as a yellow solid (570 mg, 83% yield), which was used directly without further purification. ^{1}H NMR (d_6-DMSO, 300 MHz): δ 12.04 (s, 1H), 11.82 (s, 1H), 10.60 (s, 1H), 10.24 (s, 1H), 8.56-8.39 (br, 2H), 8.38-8.17 (m, 4H), 8.10 (d, *J*(H, H) = 7.9, 1H), 8.05-7.85 (m, 2H), 7.75-7.47 (m, 3H), 7.26 (s, 1H), 7.04-6.90 (br, 1H), 6.48 (s, 1H), 5.24 (br, 2H), 4.23-4.07 (m, 4H), 3.00-2.86 (m, 3H), 2.35-2.16 (m, 2H), 1.93-1.77 (m, 1H), 1.18 (t, *J*(H, H) = 5.7, 12H), 0.90 (t, *J*(H, H) = 6.6, 6H). HRMS (ESI): *m/z* calcd for $C_{54}H_{52}F_2N_{11}O_9$ $[M+H]^+$ 1036.3912 found 1936.3922.

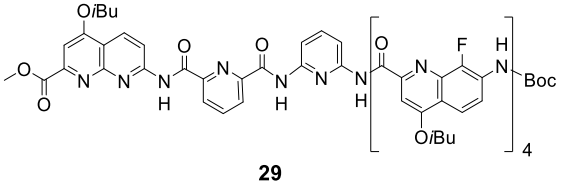

29

Compound 29. Under N_2 atmosphere, to a suspension of compound **28** (330 mg, 0.32 mmol) in 6 mL dry CH_2Cl_2 was added DIEA (0.22 mL, 1.28 mmol). A solution of $\mathbf{Q^F}$ dimer acid chloride (2 eq) in 6 mL dry CH_2Cl_2 was injected *via* a syringe, and the reaction was allowed to proceed overnight at room temperature. After removing the insoluble amine by filtration, the filtrate was concentrated to dryness,

and purified by purified by silica column chromatography eluting with EtOAc/DCM (99:1 to 50:50) to get the product as a white solid (270 mg, 51% yield). ^{1}H NMR (d_6-DMSO, 300 MHz): δ 11.85 (s, 1H), 11.67 (s, 1H), 10.83 (s, 1H), 10.13 (s, 1H), 9.99 (s, 2H), 9.65 (s, 1H), 8.49 (t, *J*(H, H) = 8.7, 1H), 8.12 (d, *J*(H, H) = 7.6, 1H), 8.04-7.92 (m, 2H), 7.83-7.73 (m, 2H), 7.71-7.52 (m, 5H), 7.51-7.36 (m, 5H), 7.33 (s, 1H), 7.14 (d, *J*(H, H) = 9.1, 1H), 6.90 (d, *J*(H, H) = 9.1, 1H), 6.77 (s, 1H), 6.49 (s, 1H), 6.28 (s, 1H), 4.44-3.88 (m, 10H), 2.82 (s, 3H), 2.46-2.30 (m, 5H), 1.40-1.20 (m, 24H), 1.67 (s, 9H), 0.65 (t, *J*(H, H) = 7.8, 6H). HRMS (ESI): *m/z* calcd for $C_{87}H_{85}F_4N_{15}O_{15}$ $[2M+2H]^{2+}$ 1655.6286 found 1655.6285.

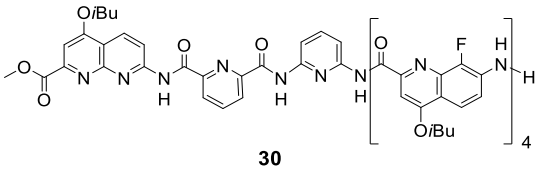

30

Compound 30. Trifluoroacetic acid (2 mL) was added dropwise to a solution of compound **29** (400 mg, 0.24 mmol) in 4 mL dry CH_2Cl_2 under N_2 at room temperature. After stirring for 6 hours at room temperature, the crude was dissolved in 100 mL CH_2Cl_2, washed three times with saturated solution of $NaHCO_3$, dried with $MgSO_4$. The solvent was removed under reduced pressure to get the product as a yellow solid (370 mg, 98% yield), which was used directly without further purification. ^{1}H NMR (d_6-DMSO, 300 MHz): δ 12.00 (s, 1H), 11.71 (s, 1H), 10.93 (s, 1H), 10.16 (s, 1H), 10.02 (s, 2H), 9.85 (s, 1H), 8.53 (dd, *J*(H, H) = 6.8, *J*(H, H) = 2.0, 1H), 8.16-8.08 (m, 1H), 8.01 (t, *J*(H, H) = 7.7, 1H), 7.90-7.81 (m, 1H), 7.81-7.63 (m, 4H), 7.58 (d, *J*(H, H) = 8.9, 1H), 7.53-7.41 (m, 2H), 7.39-7.19 (m, 4H), 7.18-7.09 (m, 2H), 7.04 (d, *J*(H, H) = 8.6, 1H), 6.79 (s, 1H), 6.56 (t, *J*(H, H) = 8.2, 1H), 6.13 (s, 1H), 4.40-3.87 (m, 12H), 3.09-3.00 (m, 3H), 2.45-2.22 (m, 5H), 1.41-1.18 (m, 24H), 0.65 (dd, *J*(H, H) = 7.6, *J*(H, H) = 6.5, 6H). HRMS (ESI): *m/z* calcd for $C_{164}H_{156}F_8N_{30}O_{26}$ $[2M+2H]^{2+}$ 1557.0851 found 1557.5901.

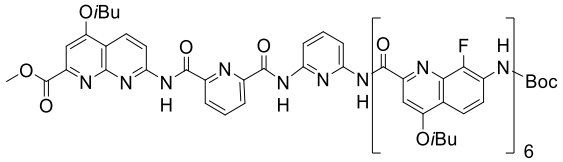

31

Compound 31. Under N_2 atmosphere, to compound **30** (370 mg, 0.24 mmol) in 3 mL dry CH_2Cl_2 was added DIEA (0.16 mL, 0.96 mmol). A solution of $\mathbf{Q^F}$ dimer acid chloride (1.2 eq) in 3 mL dry CH_2Cl_2 was injected *via* a syringe, and the reaction was allowed to proceed overnight at room temperature. The crude was concentrated to dryness, and the product was collected by precipitation from MeOH as a white solid (430 mg, 83% yield). ^{1}H NMR (d_6-DMSO, 300 MHz): δ 11.98 (s, 1H), 11.91 (s, 1H), 11.33 (s, 1H), 11.21 (s, 1H), 10.96-9.86 (br, 2H), 9.67 (s, 1H), 9.34 (s, 1H), 8.38 (t, *J*(H, H) = 7.7, 1H), 8.14-7.87 (m, 3H), 7.86-7.67 (m, 2H), 7.67-7.41 (m, 6H), 7.10-6.92 (m, 2H), 6.82 (s, 1H), 6.74 (d, *J*(H, H) = 8.6, 1H), 6.70 (s, 2H), 6.45 (d, *J*(H, H) = 8.9, 1H), 6.18 (s, 1H), 4.44-3.76 (m, 14H), 2.37-2.16 (m, 10H), 1.45-1.34 (m, 12H), 1.34-1.14 (m, 24H), 1.03 (s, 9H), 0.55 (t, *J*(H, H) = 6.6, 6H). HRMS (ESI): *m/z* calcd for $C_{230}H_{224}F_{12}N_{38}O_{38}$ $[2M+2H]^{2+}$ 2177.8314 found 2177.8341.

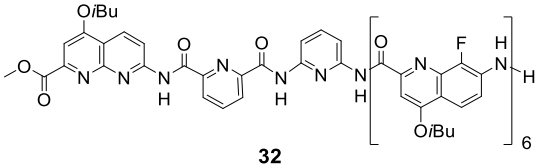

32

Compound 32. Trifluoroacetic acid (0.9 mL) was added dropwise to a solution of compound **31** (250 mg, 0.11 mmol) in 1.8 mL dry CH_2Cl_2 under N_2 at room temperature. After stirring for 6 hours at room temperature, the crude was dissolved in 100 mL CH_2Cl_2, washed three times with saturated solution of $NaHCO_3$, dried with $MgSO_4$. The solvent was removed under reduced pressure to get the product as a

yellow solid (220 mg, 96% yield), which was used directly without further purification. ^{1}H NMR (d_6-DMSO, 300 MHz): δ 11.95 (s, 1H), 11.91 (s, 1H), 10.41 (s, 1H), 10.17 (s, 1H), 10.13 (s, 1H), 9.94 (s, 1H), 9.71 (s, 1H), 9.32 (s, 1H), 8.31 (dd, *J*(H, H) = 6.8, *J*(H, H) = 2.0, 1H), 8.08 (dd, *J*(H, H) = 6.8, *J*(H, H) = 2.3, 1H), 8.02-7.92 (d, 7.9, 1H), 7.92-7.79 (m, 2H), 7.72-7.58 (m, 2H), 7.50-7.34 (m, 5H), 76.33-7.15 (m, 6H), 7.12-7.05 (m, 2H), 7.04-6.98 (m, 2H), 7.00 (d, *J*(H, H) = 8.5, 1H), 6.96 (s, 1H), 6.74 (s, 1H), 6.64 (d, *J*(H, H) = 9.0, 1H), 6.28 (t, *J*(H, H) = 8.1, 1H), 6.12 (s, 1H), 4.52 (br, 2H), 4.43-3.80 (m, 14H), 2.43-3.80 (m, 10H), 1.44-1.34 (m, 12H), 1.34-1.15 (m, 24H), 0.57 (t, *J*(H, H) = 6.6, 6H). HRMS (ESI): *m/z* calcd for $C_{220}H_{208}F_{12}N_{38}O_{34}$ $[2M+2H]^{2+}$ 2077.7790 found 2077.7842.

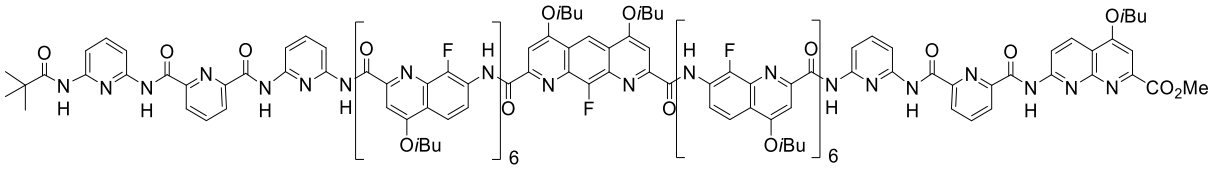

4

Compound 4. Under N_2 atmosphere, to a suspension of compound **20** (460 mg, 0.19 mmol) in 4 mL dry CH_2Cl_2 was added oxalyl chloride (0.18 mL, 1.9 mmol) at room temperature. Although the acid is not soluble, the activation proceeded well. After stirring for 3 hours, the solvent was removed under vacuum to provide the acid chloride.

A solution of compound **32** (200 mg, 0.10 mmol) and DIEA (0.07 mL, 0.40 mmol) in 4 mL dry $CHCl_3$ was added to a suspension of the acid chloride in 4 mL $CHCl_3$. The reaction was allowed to proceed overnight, after which the product was purified by resin extraction as a yellow solid (300 mg, 70% yield). ^{1}H NMR (d_6-DMSO, 400 MHz, 323K, single helix): δ 11.90 (s, 1H), 11.69 (s, 1H), 11.54 (s, 1H), 10.18 (s, 1H), 11.00 (s, 1H), 10.81 (s, 1H), 10.49 (s, 1H), 10.37 (s, 1H), 10.28 (s, 2H), 10.12 (s, 1H), 10.05 (s, 1H), 9.86 (s, 1H), 9.75 (s, 1H), 9.45 (s, 1H), 9.37 (s, 1H), 9.08 (s, 1H), 8.88 (s, 1H), 8.86-8.78 (m, 1H), 8.78-8.63 (m, 2H), 8.44-8.21 (m, 3H), 8.06-7.91 (m, 3H), 7.91-7.81 (m, 1H), 7.81-7.69 (m, 2H), 7.68-6.55 (m, 43H), 6.43-6.32 (m, 1H), 5.89 (s, 2H), 4.37-3.90 (m, 30H), 2.66 (s, 3H), 2.46-2.26 (m, 15H), 1.44-1.16 (m, 84H), 0.83 (dd, *J*(H, H) = 17.9, *J*(H, H) = 6.4, 6H), 0.31 (s, 9H). HRMS (ESI): *m/z* calcd for $C_{238}H_{225}F_{13}N_{40}O_{36}$ $[M+2H]^{2+}$ 2233.8427 found 2233.8437

5.4.2 Synthesis of dumbbell-like asymmetrical guests

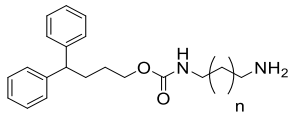

Compound 34 (n = 3). A solution of compound **33**[15] (390 mg, 1 mmol) in dry CH_2Cl_2 (10 mL) was added dropwise to a solution of 1,5-pentanediamine (510 mg, 5 mmol) and Et_3N (0.28 mL, 2 mmol) in dry CH_2Cl_2 (10 mL) at 0 °C over 30 min. The stirring was continued overnight at room temperature. The solution was washed 3 times with 1M NaOH solution (10 mL), dried over $MgSO_4$, and concentrated to dryness. The residue was purified by silica column chromatography eluting with MeOH/DCM/Et_3N (99:1:1 to 90:10:1) to get the product as a yellowish oil. This amine was used directly due to the low stability.

Compound 35, 36, 37, 38, and 39 were synthesized following similiar procedure.

Compound 35 (n = 4). Colorless oil, 80% yield. ^{1}H NMR ($CDCl_3$, 300 MHz): δ 7.31-7.27 (m, 2H), 7.27-7.13 (m, 8H), 4.60 (br, 1H), 4.05 (t, *J*(H, H) = 6.4, 2H), 3.90 (t, *J*(H, H) = 7.9, 1H), 3.14 (q, *J*(H, H) = 6.5, *J*(H, H) = 6.5, 2H), 2.69 (t, *J*(H, H) = 6.8, 2H), 2.16-2.05 (m, 2H) 1.65-1.27 (m, 12H). ^{13}C NMR ($CDCl_3$, 75 MHz): δ 156.77, 144.79, 128.52, 127.85, 126.25, 64.58, 51.00, 41.93, 40.91, 33.19, 31.96, 30.01, 27.69, 26.56, 26.52. HRMS (ESI): *m/z* calcd for $C_{23}H_{33}N_2O_2$ $[M+H]^+$ 369.2537 found 369.2542.

Compound 36 (n = 5). Colorless oil, 92% yield. ^{1}H NMR ($CDCl_3$, 300 MHz): δ 7.31-7.27 (m, 2H), 7.27-7.13 (m, 8H), 4.61 (br, 1H), 4.05 (t, *J*(H, H) = 6.4, 2H), 3.90 (t, *J*(H, H) = 7.9, 1H), 3.13 (q, *J*(H, H) = 6.5, *J*(H, H) = 6.5, 2H), 2.69 (t, *J*(H, H) = 6.9, 2H), 2.18-2.05 (m, 2H) 1.65-1.24 (m, 14H). ^{13}C NMR ($CDCl_3$, 75 MHz): δ 156.81, 144.88, 128.60, 127.94, 126.33, 64.70, 51.09, 42.12, 41.08, 33.31, 32.04, 30.08, 29.18, 27.77, 26.85, 26.80. HRMS (ESI): *m/z* calcd for $C_{24}H_{35}N_2O_2$ $[M+H]^+$ 383.2693 found 383.2706.

Compound 37 (n = 6). Colorless oil, 85% yield. ^{1}H NMR ($CDCl_3$, 300 MHz): δ 7.31-7.27 (m, 2H), 7.26-7.13 (m, 8H), 4.59 (br, 1H), 4.05 (t, *J*(H, H) = 6.3, 2H), 3.90 (t, *J*(H, H) = 7.7, 1H), 3.19-3.06 (m, 2H), 2.70 (t, *J*(H, H) = 7.0, 2H), 2.16-2.05 (m, 2H) 1.65-1.22 (m, 16H). ^{13}C NMR ($CDCl_3$, 75 MHz): δ 166.58, 156.60, 144.58, 128.29, 127.62, 126.01, 64.25, 53.34, 50.77, 46.05, 41.67, 40.76, 32.76, 31.74, 29.81, 29.15, 29.06, 27.49, 26.60, 26.52. HRMS (ESI): *m/z* calcd for $C_{25}H_{37}N_2O_2$ $[M+H]^+$ 397.2850 found 397.2848.

Compound 38 (n = 7). Colorless oil, 80% yield. ^{1}H NMR ($CDCl_3$, 300 MHz): δ 7.31-7.27 (m, 2H), 7.26-7.13 (m, 8H), 4.58 (br, 1H), 4.05 (t, *J*(H, H) = 6.4, 2H), 3.90 (t, *J*(H, H) = 7.8, 1H), 3.13 (q, *J*(H, H) = 6.5, *J*(H, H) = 6.5, 2H), 2.70 (t, *J*(H, H) = 7.0, 2H), 2.16-2.06 (m, 2H) 1.67-1.19 (m, 18H). ^{13}C NMR ($CDCl_3$, 75 MHz): δ 156.66, 144.67, 128.38, 127.71, 126.10, 64.38, 50.86, 41.77, 40.87, 32.85, 31.83, 29.90, 29.38, 29.26, 29.12, 27.57, 26.74, 26.64. HRMS (ESI): *m/z* calcd for $C_{26}H_{39}N_2O_2$ $[M+H]^+$ 411.3006 found 411.3000.

Compound 39 (n = 8). Colorless oil, 77% yield. ^{1}H NMR ($CDCl_3$, 300 MHz): δ 7.31-7.27 (m, 2H), 7.26-7.13 (m, 8H), 4.58 (br, 1H), 4.05 (t, *J*(H, H) = 6.3, 2H), 3.90 (t, *J*(H, H) = 7.8, 1H), 3.22-3.05 (m, 2H), 2.68 (t, *J*(H, H) = 6.9, 2H), 2.19-2.04 (m, 2H) 1.67-1.20 (m, 20H). ^{13}C NMR ($CDCl_3$, 75 MHz): δ166.30, 156.54, 144.47, 128.17, 127.51, 125.89, 64.07, 50.66, 41.83, 40.66, 33.30, 31.65, 30.61, 29.72, 29.28, 29.23, 29.02, 28.91, 27.40, 26.61, 26.49. HRMS (ESI): *m/z* calcd for $C_{27}H_{41}N_2O_2$ $[M+H]^+$ 425.3163 found 425.3160.

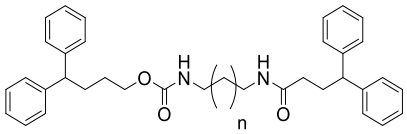

Compound 6 (n = 3). To a solution of compound **41** (240 mg, 1.0 mmol), EDC (380 mg, 2.0 mmol), and HOBt (380 mg, 2.0 mmol) in 10 mL dry $CHCl_3$ was added DIEA (1.32 mL, 8.0 mmol). After 20 minutes of activation at room temperature, compound **34** (350 mg, 1 mmol) in 10 mL dry $CHCl_3$ was added. The reaction was stirred overnight at room temperature. The crude was diluted into 200 mL CH_2Cl_2, washed with three times with saturated $NaHCO_3$ solution, dried over $MgSO_4$, and concentrated to dryness. The residue was purified by silica column chromatography eluting with EtOAc/DCM (99:1 to 80:20) to get the product as a colorless oil (460 mg, 80% yield). ^{1}H NMR ($CDCl_3$, 300 MHz): δ 7.31-7.27 (m, 4H), 7.25-7.13 (m, 16H), 5.30 (br, 1H), 4.62 (br, 1H), 4.02 (t, *J*(H, H) = 6.3, 2H), 3.96-3.84 (m, 2H), 3.25-3.06 (m, 4H), 2.40 (q, *J*(H, H) = 7.7, *J*(H, H) = 7.7, 2H), 2.16-2.03 (m, 4H) 1.62-1.55 (m, 2H), 1.52-1.40 (m, 4H), 1.38-1.22 (m, 2H). ^{13}C NMR ($CDCl_3$, 75 MHz): δ 172.64, 156.92, 144.87, 144.40, 128.66, 128.62, 128.01, 127.94, 126.46, 126.35, 64.76, 51.08, 50.73, 40.72, 39.35, 35.11, 32.03, 31.26, 29.77, 29.29, 27.76, 23.96. HRMS (ESI): *m/z* calcd for $C_{38}H_{45}N_2O_3$ $[M+H]^+$ 577.3425 found 577.3438.

Compound 7, 8, 9, 10, 11, and 12 were synthesized following similar procedure.

Compound 7 (n = 4). Colorless oil, 97% yield. ^{1}H NMR ($CDCl_3$, 300 MHz): δ 7.36-7.28 (m, 4H), 7.26-7.13 (m, 16H), 5.29 (br, 1H), 4.61 (br, 1H), 4.04 (t, *J*(H, H) = 6.3, 2H), 3.97-3.85 (m, 2H), 3.26-3.06 (m, 4H), 2.40 (q, *J*(H, H) = 7.7, *J*(H, H) = 7.7, 2H), 2.17-2.03 (m, 4H) 1.65-1.55 (m, 2H), 1.52-1.38 (m, 4H), 1.38-1.22 (m, 4H). ^{13}C NMR ($CDCl_3$, 75 MHz): δ 172.55, 156.86, 144.84, 144.39, 128.62, 128.58, 127.99, 127.91, 126.42, 126.31, 64.70, 51.06, 50.69, 40.74, 39.28, 35.08, 32.01, 31.27, 30.00, 29.60, 27.74, 26.39, 26.21. HRMS (ESI): *m/z* calcd for $C_{39}H_{47}N_2O_3$ $[M+H]^+$ 591.3581 found 591.3589.

Compound 8 (n = 5). Colorless oil, 92% yield. ^{1}H NMR ($CDCl_3$, 300 MHz): δ 7.32-7.27 (m, 4H), 7.25-7.13 (m, 16H), 5.23 (br, 1H), 4.58 (br, 1H), 4.04 (t, *J*(H, H) = 6.2, 2H), 3.96-3.85 (m, 2H), 3.24-3.07 (m, 4H), 2.40 (q, *J*(H, H) = 7.7, *J*(H, H) = 7.7, 2H), 2.16-2.05 (m, 4H) 1.64-1.55 (m, 2H), 1.51-1.37 (m, 4H), 1.34-1.27 (m, 6H). ^{13}C NMR ($CDCl_3$, 75 MHz): δ 172.49, 156.82, 144.87, 144.41, 128.65, 128.60, 128.01, 127.94, 126.45, 126.34, 64.70, 51.08, 50.70, 40.99, 39.50, 35.13, 32.04, 31.29, 30.03, 29.68, 28.93, 27.77, 26.86, 26.68. HRMS (ESI): *m/z* calcd for $C_{40}H_{49}N_2O_3$ $[M+H]^+$ 605.3738 found 605.3748.

Compound 9 (n = 6). Colorless oil, 67% yield. ^{1}H NMR ($CDCl_3$, 300 MHz): δ 7.32-7.27 (m, 4H), 7.25-7.13 (m, 16H), 5.22 (br, 1H), 4.58 (br, 1H), 4.05 (t, *J*(H, H) = 6.3, 2H), 3.96-3.85 (m, 2H), 3.24-3.06 (m, 4H), 2.40 (q, *J*(H, H) = 7.7, *J*(H, H) = 7.7, 2H), 2.17-2.05 (m, 4H) 1.65-1.55 (m, 2H), 1.51-1.37 (m, 4H), 1.35-1.21 (m, 8H). ^{13}C NMR ($CDCl_3$, 75 MHz): δ 172.48, 156.81, 144.87, 144.40, 128.64, 128.60, 128.01, 127.93, 126.44, 126.33, 64.69, 51.08, 50.69, 41.06, 39.57, 35.13, 32.03, 31.29, 30.08, 29.83, 29.73, 29.23, 27.76, 26.92, 26.74. HRMS (ESI): *m/z* calcd for $C_{41}H_{51}N_2O_3$ $[M+H]^+$ 619.3894 found 619.3903.

Compound 10 (n = 7). Colorless oil, 60% yield. ^{1}H NMR ($CDCl_3$, 300 MHz): δ 7.31-7.27 (m, 4H), 7.26-7.13 (m, 16H), 5.23 (br, 1H), 4.58 (br, 1H), 4.05 (t, *J*(H, H) = 6.4, 2H), 3.97-3.85 (m, 2H), 3.25-3.07 (m, 4H), 2.40 (q, *J*(H, H) = 7.7, *J*(H, H) = 7.7, 2H), 2.18-2.05 (m, 4H) 1.65-1.56 (m, 2H), 1.51-1.38 (m, 4H), 1.35-1.21 (m, 10H). ^{13}C NMR ($CDCl_3$, 75 MHz): δ 172.47, 156.80, 144.86, 144.40, 128.63, 128.58, 128.00, 127.92, 126.43, 126.32, 64.67, 51.07, 50.68, 41.07, 39.58, 35.11, 32.02, 31.29, 30.08, 29.72, 29.45, 29.24, 27.75, 26.95, 26.77. HRMS (ESI): *m/z* calcd for $C_{42}H_{53}N_2O_3$ $[M+H]^+$ 633.4051 found 633.4060.

Compound 11 (n = 8). Colorless oil, 53% yield. ^{1}H NMR ($CDCl_3$, 300 MHz): δ 7.32-7.27 (m, 4H), 7.26-7.13 (m, 16H), 5.22 (br, 1H), 4.58 (br, 1H), 4.05 (t, *J*(H, H) = 6.4, 2H), 3.98-3.85 (m, 2H), 3.25-3.06 (m, 4H), 2.40 (q, *J*(H, H) = 7.7, *J*(H, H) = 7.7, 2H), 2.16-2.05 (m, 4H) 1.64-1.56 (m, 2H), 1.51-1.38 (m, 4H), 1.32-1.22 (m, 12H). ^{13}C NMR ($CDCl_3$, 75 MHz): δ 172.47, 156.79, 144.85, 144.39, 128.62, 128.57, 127.99, 127.91, 126.41, 126.30, 64.64, 51.06, 50.67, 41.08, 39.59, 35.09, 32.01, 31.28, 30.09, 29.73, 29.49, 29.30, 27.74, 26.97, 26.79. HRMS (ESI): *m/z* calcd for $C_{43}H_{55}N_2O_3$ $[M+H]^+$ 647.4207 found 647.4219.

Compound 12 (n = 9). Colorless oil, 70% yield. ^{1}H NMR ($CDCl_3$, 300 MHz): δ 7.31-7.27 (m, 4H), 7.26-7.13 (m, 16H), 5.22 (br, 1H), 4.58 (br, 1H), 4.05 (t, *J*(H, H) = 6.4, 2H), 3.96-3.85 (m, 2H), 3.26-3.06 (m, 4H), 2.40 (q, *J*(H, H) = 7.7, *J*(H, H) = 7.7, 2H), 2.17-2.04 (m, 4H) 1.66-1.54 (m, 2H), 1.51-1.38 (m, 4H), 1.32-1.22 (m, 14H). ^{13}C NMR ($CDCl_3$, 75 MHz): δ 172.43, 156.76, 144.82, 144.37, 128.58, 128.54, 127.95, 127.88, 126.38, 126.27, 64.59, 51.02, 50.64, 41.06, 39.56, 35.04, 31.98, 31.25, 30.06, 29.71, 29.54, 29.32, 29.31, 27.72, 26.98, 26.79. HRMS (ESI): *m/z* calcd for $C_{44}H_{57}N_2O_3$ $[M+H]^+$ 661.4364 found 661.4379.

5.4.3 Synthesis of polyethylene glycol appended guests

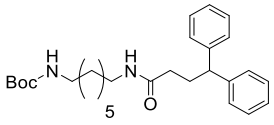

43

Compound 43. This compound was synthysized from Mono-Boc-1,7-diaminoheptane **42**[28] following similiar procedure as for cmopound **6**. Colorless oil, 81% yield. ^{1}H NMR ($CDCl_3$, 300 MHz): δ 7.31-

28. C. Dardonville, C. Fernandez-Fernandez, S.-L. Gibbons, G. J. Ryan, N. Jagerovic, A. M. Gabilondo, J. J. Meana, L. F. Callado. Synthesis and pharmacological studies of new hybrid derivatives of fentanyl active at the μ-opioid receptor and I 2–imidazoline binding sites. *Bioorg. Med. Chem.* **2006**, *14*, 6570-6580.

7.27 (m, 2H), 7.26-7.14 (m, 8H), 5.24 (br, 1H), 4.48 (br, 1H), 3.92 (t, *J*(H, H) = 7.9, 1H), 3.09 (t, *J*(H, H) = 6.6, *J*(H, H) = 6.6, 2H), 2.40 (t, *J*(H, H) = 7.7, *J*(H, H) = 7.7, 2H), 2.15-2.05 (m, 2H) 1.64-1.56 (m, 2H), 1.52-1.38 (m, 13H), 1.37-1.20 (m, 8H). ^{13}C NMR ($CDCl_3$, 75 MHz): δ172.51, 156.13, 144.40, 128.64, 128.01, 126.44, 50.70, 40.64, 39.54, 35.13, 31.30, 30.10, 29.68, 28.98, 28.56, 26.90, 26.74. HRMS (ESI): *m/z* calcd for $C_{28}H_{40}N_2O_3$ $[M+H]^+$ 452.3039 found 453.3103.

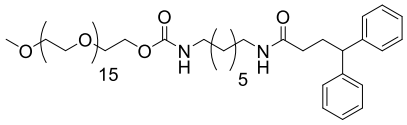

13

Compound 13. PEG (MW = 750 g/mol, 300 mg) and Et_3N (0.84 mL, 6 mmol) in 10 mL dry CH_2Cl_2 was added slowly to a solution of p-nitrophenyl chloroformate (600 mg, 3 mmol) in 10 mL dry CH_2Cl_2 at 0 °C. The solution was stirred overnight at room temperature to get the activated alcohol.
TFA (0.3 mL) was added slowly into a solution of compound **43** (210 mg, 1.2 mmol) in 1.5 mL CH_2Cl_2. After stirring for 6 hours at room temperature, the reaction mixture was diluted into 100 mL CH_2Cl_2, washed 3 times with saturated aqueous solution of $NaHCO_3$. The organic phase was dried over $MgSO_4$, concentrated to dryness to get the resulting amine, which was used directly without further purification. To a solution of the amine in 10 mL CH_2Cl_2 was added the solution of the above activated alcohol. The mixture was stirred for 20 hours at room temperature. Then the crude was diluted into 200 mL CH_2Cl_2, washed with three times with 1M NaOH solution, dried over $MgSO_4$, and concentrated to dryness. The residue was purified by silica column chromatography eluting with MeOH/DCM (99:1 to 90:10) to get the product as a colorless oil (220 mg, 48% yield). ^{1}H NMR ($CDCl_3$, 400 MHz): δ 7.30-7.27 (m, 2H), 7.25-7.14 (m, 8H), 5.30 (br, 1H), 4.82 (br, 1H), 4.20 (t, *J*(H, H) = 4.3, 2H), 3.92 (t, *J*(H, H) = 7.9, 1H), 3.75-3.52 (m, 56H), 3.38 (s, 3H), 3.23-3.10 (m, 4H), 2.40 (t, *J*(H, H) = 7.7, *J*(H, H) = 7.7, 2H), 2.10 (t, *J*(H, H) = 7.6, 2H), 1.52-1.39 (m, 4H), 1.35-1.22 (m, 8H). ^{13}C NMR ($CDCl_3$, 100 MHz): δ 172.53, 156.56, 144.41, 128.65, 128.01, 126.45, 72.07, 70.70, 70.65, 69.81, 63.95, 59.18, 50.70, 41.04, 39.52, 35.12, 31.28, 29.97, 29.68, 28.95, 26.88, 26.68. ESI-MS: Due to polydispersion of the PEG lengths, the compound has a distribution of molecular weights centered around 1188.7.

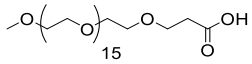

44

Compound 44. To a solution of PEG (MW = 750 g/mol, 5 g) in 3 mL dry THF was added NaH (12 mg, 0.3 mmol, 60% in oil), and the mixture was stirred at 50 °C for 30 min. After cooling down to room temperature, methyl acrylate (0.7 mL, 7.7 mmol) was added, and the reaction proceeded overnight. To this reaction mixture was added 7 mL THF and a solution of NaOH (1.2 g, 30 mmol) in 10 mL H_2O successively. The mixture was stirred for 5 hours further. The reaction was quenched by 5% citric acid, extracted with CH_2Cl_2, the organic phase was combined, dried over $MgSO_4$, and concentrated to dryness. The crude was purified by silica column chromatography eluting with AcOH/MeOH/DCM (1:1:98 to 1:19:80) to get the product as a colorless oil (2.4 g, 43% yield). ^{1}H NMR ($CDCl_3$, 400 MHz): δ 3.77 (t, *J*(H, H) = 6.1, 2H), 3.74-3.52 (m, 66H), 3.38 (s, 3H), 2.60 (t, *J*(H, H) = 6.1, 2H). ^{13}C NMR ($CDCl_3$, 100 MHz): δ 174.32, 71.94, 70.56, 70.43, 70.34, 66.81, 59.05, 35.21. ESI-MS: Due to polydispersion of the PEG lengths, the compound has a distribution of molecular weights centered around 851.5.

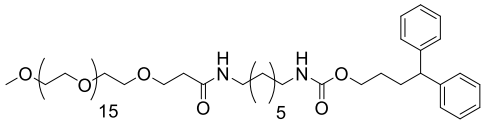

14

Compound 14. To a solution of compound **44** (500 mg), EDC (230 mg, 1.2 mmol), and HOBt (160 mg, 1.2 mmol) in 5 mL dry $CHCl_3$ was added DIEA (0.42 mL, 2.4 mmol). After 20 minutes of activation at

room temperature, compound **36** (462 mg, 1.2 mmol) was added. The reaction was stirred overnight at room temperature. The crude was diluted into 200 mL CH_2Cl_2, washed with three times with saturated $NaHCO_3$ solution, dried over $MgSO_4$, and concentrated to dryness. The residue was purified by silica column chromatography eluting with MeOH/DCM (1:99 to 15:85) to get the product as a colorless oil (600 mg, 83% yield). ^{1}H NMR ($CDCl_3$, 400 MHz): δ 7.30-7.27 (m, 2H), 7.25-7.14 (m, 8H), 6.43 (br, 1H), 4.67 (br, 1H), 4.05 (t, *J*(H, H) = 6.1, 2H), 3.90 (t, *J*(H, H) = 7.8, 1H), 3.71 (t, *J*(H, H) = 11.5, 2H), 3.68-3.52 (m, 66H), 3.38 (s, 3H), 3.26-3.07 (m, 4H), 2.45 (t, *J*(H, H) = 5.7, 2H), 2.10 (q, *J*(H, H) = 7.7, *J*(H, H) = 7.7, 2H), 1.58-1.53 (m, 2H), 1.51-1.43 (m, 4H), 1.34-1.26 (m, 8H). ^{13}C NMR ($CDCl_3$, 100 MHz): δ 171.60, 156.80, 144.84, 128.58, 127.91, 126.31, 72.04, 70.67, 70.62, 70.44, 70.32, 67.47, 64.64, 59.15, 51.05, 41.00, 39.39, 37.11, 32.01, 30.01, 29.62, 28.98, 27.74, 26.86, 26.73. ESI-MS: Due to polydispersion of the PEG lengths, the compound has a distribution of molecular weights centered around 1146.4.

CONCLUSION AND PERSPECTIVES

Biological machines are self-assemblies of folded biopolymers derived from a handful of amino acids and nucleotides. Fast local conformational changes rather than disassembling of the whole folded architecture ensures the operation of biomachinery with high efficiency and accuracy. Aromatic amide oligomers adopting a helical conformation with cylindrical cavity have been shown to bind to rod-like guests following two distinct pathways: when the extremities of the rod are hindered, the oligomer slowly unfolds and refolds around the guest; when one extremity is unhindered, the oligomer threads fast on to the guest. In this dissertation, such segregation of kinetic timescales of complex formation is exploited to manipulate supramolecular assemblies and to control directional motion.

Firstly, through unfolding-refolding, high fidelity self-assemblies of foldamers were translated from programmed multistation rods. Each station of the rod corresponded to a foldamer of defined chirality, length and single or double helicity. During the self-assembly process, the unfolding-refolding of foldamers allowed error correction to eliminate the thermodynamically unstable intermediates. This error correction process ensured the high fidelity production of unprecedented large abiotic folded architecture. The high fidelity and rigidity of this architecture allow the organization of various functional groups by attaching them to the foldamer backbone. It can be also envisaged that by connecting the assembled foldamers with covalent bond will yield a single molecular polymeric chains of high rigidity.

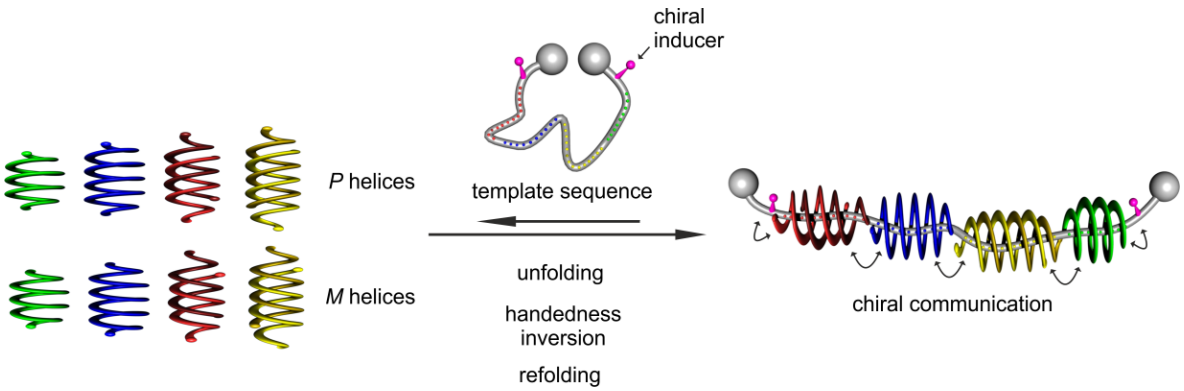

Secondly, unidirectional motion of an antiparallel double helix foldamer was investigated. The double helix could quickly thread onto the weak binder station through the unhindered entrance. By orchestrating the bulkiness of the spacer between the two stations, directional motion can be controlled to follow distinct kinetic pathways. When a linear spacer, either linear alkynes or oligo ethylene glycol, was installed, the double helix slides along the rod to reach

the thermodynamically favored strong binder station. When bulky molecules were used as spacer, this sliding process was blocked. However, thanks to the noncovalent nature of the complex, the double helix could unfold and refold onto the thermodynamically favored station.

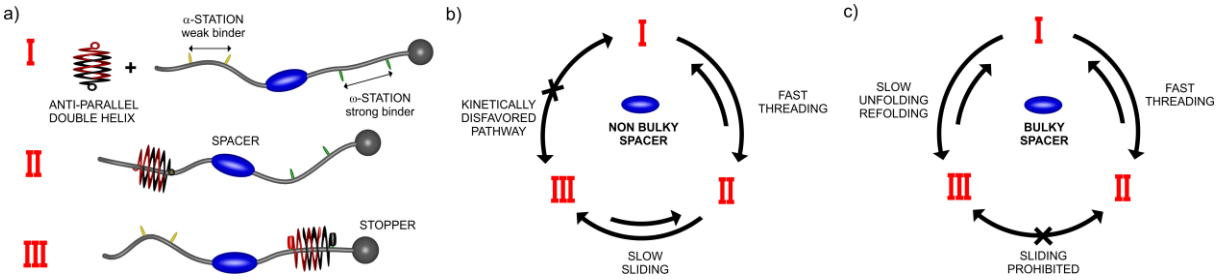

Thirdly, it was found that an asymmetrical foldamer with **P3** and **NP2** at each terminus can bind to a rod possessing carbamate and amide group at each extremity. Favored interactions of **P3** towards carbamate group and **NP2** towards amide group ensured the formation of only one thermodynamically stable complex. The threading kinetic data of this foldamer along polyethylene glycol appended rods indicated that the threading orientation of the foldamer was polarized by either the methoxy entrance or the first carbamate/amide group.

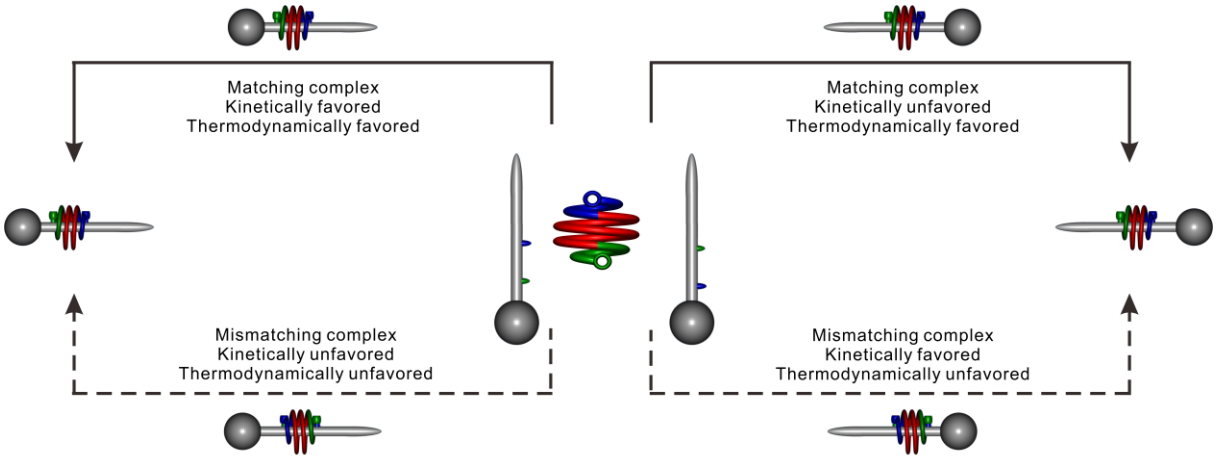

Although the investigations in this thesis are still preliminary comparing to biological machinery, perspectives can be drawn for foldamer based artificial molecular machines. When the threading orientation of asymmetrical foldamer can be fully polarized, a rod with two termini either favoring or disfavoring the threading of the foldamer can be designed. Only threading of one orientation of the foldamer from the favored terminus of the rod is kinetically feasible. Thanks to the high stability of its folded conformation, the foldamer can be appended with a catalytic group at the tail while the threading orientation remaining the same. As the foldamer slides directionally along the rod, catalytic reaction can be performed processively on the rod. The chemical changes of the rod caused by the catalytic reactions can prohibit backward

motion of the foldamer, driving the foldamer to move directionally along the rod to the other terminus. Then, the foldamer can slip out and thread on to the next rod to repeat its catalytic function. Moreover, the chiral information of the foldamer could also be transfered to the rod through the catalytic group.